

# Pentaphosphaferrocenes and Silver Salts as Building Blocks in the Self-Assembly of Discrete and Networked Spherical Supramolecules



DISSERTATION  
ZUR ERLANGUNG DES  
DOKTORGRADES DER NATURWISSENSCHAFTEN  
(DR. RER. NAT.)  
DER FAKULTÄT CHEMIE UND PHARMAZIE  
DER UNIVERSITÄT REGENSBURG

vorgelegt von  
**Barbara Hiltl**  
geb. Krämer  
aus Regensburg  
im Jahr 2018

---

Diese Arbeit wurde angeleitet von Prof. Dr. Manfred Scheer.

Das Promotionsgesuch wurde eingereicht am: Do, 29.08.2018

Tag der mündlichen Prüfung: Fr, 28.09.2018

Vorsitzender: Prof. Dr. Hubert Motschmann

Prüfungsausschuss: Prof. Dr. Manfred Scheer

Prof. Dr. Henri Brunner

Prof. Dr. Alkwin Slenczka



Universität Regensburg

## Eidesstattliche Erklärung

Ich erkläre hiermit an Eides statt, dass ich die vorliegende Arbeit mit dem Titel „*Pentaphosphaferrocenes and Silver Salts as Building Blocks in the Self-Assembly of Discrete and Networked Spherical Supramolecules*“ ohne unzulässige Hilfe Dritter und ohne Benutzung anderer als der angegebenen Hilfsmittel angefertigt habe; die aus anderen Quellen direkt oder indirekt übernommenen Daten und Konzepte sind unter Angabe des Literaturzitats gekennzeichnet.

---

Barbara Hiltl

---

This thesis was elaborated within the period from November 2014 until September 2018 in the Institute of Inorganic Chemistry at the University of Regensburg, under the supervision of Prof. Dr. Manfred Scheer.

**Results, which are not part of this work, have been published during this period:**

M. Elsayed Moussa, S. Evariste, B. Kraemer, R. Reau, M. Scheer, C. Lescop, *Angew. Chem., Int. Ed.* **2018**, *57*, 795-799.

C. Heindl, E. Peresypkina, A. V. Virovets, I. S. Bushmarinov, M. G. Medvedev, B. Kraemer, B. Dittrich, M. Scheer, *Angew. Chem., Int. Ed.* **2017**, *56*, 13237-13243.

F. Dielmann, E. V. Peresypkina, B. Kraemer, F. Hastreiter, B. P. Johnson, M. Zabel, C. Heindl, M. Scheer, *Angew. Chem., Int. Ed.* **2016**, *55*, 14833-14837.



*Lass die Moleküle rasen  
Was sie auch zusammenknobeln!  
Lass das Tüfteln, lass das Hobeln,  
heilig halte die Ekstasen!*

***Christian Morgenstern***



## Preface

A general introduction about the research topic of supramolecular spherical assemblies and coordination polymers based on  $P_n$  complexes is given in the beginning of this thesis (*Chapter I*), followed by the research objectives (*Chapter II*).

The following *Chapters III-VII* can be considered as self-contained and suitable for future publications. To ensure uniform design of this work, all chapters are subdivided into 'Introduction', 'Results and Discussion', 'Conclusion', 'Experimental Part', 'Author Contributions' and 'References'. Additionally, if some of the presented results have already been partly discussed in other theses, it is stated at the end of the respective chapters in the paragraph 'Author Contributions'.

Furthermore, all chapters have the same text settings and the numeration of compounds, figures, schemes and tables begins anew for reasons of future publishing. The depicted molecular structures may differ in their style.

*Chapter VIII* contains a thesis treasury, with separate results.

A comprehensive conclusion of this work is presented at the end of this thesis (*Chapter IX*).



# Table of Contents

<b>1.</b>	<b>Introduction</b>	<b>1</b>
1.1	Supramolecular Chemistry .....	1
1.2	Discrete Aggregates .....	2
1.2.1	Polyoxometalates and Clusters .....	2
1.2.2	Metal-Organic Polyhedra .....	2
1.2.3	Functionalized Aggregates .....	4
1.2.4	Organometallic Building Blocks .....	5
1.3	Arranging Discrete Assemblies to Networks .....	6
1.4	Supramolecular Chemistry Based on Polyphosphorus Complexes .....	7
<b>2.</b>	<b>Research Objectives</b> .....	<b>17</b>
<b>3.</b>	<b>Nano-Sized Spheres: Towards the first Ag/P<sub>n</sub> ligand based Self-Assembly Systems</b> .....	<b>18</b>
3.1	Introduction .....	19
3.2	Results and Discussion .....	21
3.3	Conclusion .....	30
3.4	Experimental Part .....	31
	General Remarks .....	31
	Synthesis of $\{[\text{Cp}^*\text{Fe}(\mu_4, \eta^{5:1:1:1}\text{-P}_5)]\{\text{Ag}(\text{SO}_3\text{CF}_3)\}_2\}_n$ ( <b>2</b> ) .....	32
	Synthesis of $[\text{Cp}^*\text{Fe}(\eta^5\text{-P}_5)]@[\{\text{Cp}^*\text{Fe}(\eta^5\text{-P}_5)\}_{12}\{\text{Ag}(\text{SO}_3\text{CF}_3)\}_x]$ ( $x \approx 10$ ) ( <b>3a</b> ) and $[\{\text{Cp}^*\text{Fe}(\eta^5\text{-P}_5)\} \cdot \text{tol}]@[\{\text{Cp}^*\text{Fe}(\eta^5\text{-P}_5)\}_{12}\{\text{Ag}(\text{SO}_3\text{CF}_3)\}_{20}]$ ( <b>3b</b> ) .....	32
	Synthesis of $[\text{Cp}^*\text{Fe}(\eta^5\text{-P}_5)]@[\{\text{Cp}^*\text{Fe}(\eta^5\text{-P}_5)\}_{12}\{\text{Ag}_{18}(\text{Ag}(\text{CH}_3\text{CN}))_8(\text{SO}_3\text{C}_7\text{H}_7)_{20}\}][\text{SO}_3\text{C}_7\text{H}_7]_6$ ( <b>4</b> ) .....	33
	Synthesis of $[\{\text{Cp}^{\text{Bn}}\text{Fe}(\eta^5\text{-P}_5)\}_{12}\{\text{Ag}(\text{CF}_3\text{SO}_3)\}_{20}]$ ( <b>5</b> ) .....	34
3.5	Crystallographic Details .....	35
3.6	Author Contributions .....	38
3.7	References .....	38
<b>4.</b>	<b>A Small Cationic Host-Guest Assembly and its Possible Curved Shell Precursor</b> .....	<b>42</b>
4.1	Introduction .....	43
4.2	Results and Discussion .....	44
4.3	Conclusion .....	48
4.4	Experimental Part .....	49
	General Remarks .....	49
	Synthesis of $[\{\text{Cp}^{\text{Bn}}\text{Fe}(\eta^{5:1:1}\text{-P}_5)\}\text{Ag}]_2[\text{SbF}_6]_2$ ( <b>2</b> ) .....	49

Synthesis of $[\{\text{Cp}^{\text{Bn}}\text{Fe}(\eta^5\text{-P}_5)\}_4\{\text{Ag}(\text{CN}(\text{C}_6\text{H}_4)\text{Cl})\}_5][\text{SbF}_6]_5 \cdot (\text{CH}_2\text{Cl}_2)$ ( <b>3</b> ).....	50
Synthesis of $[\text{SbF}_6]@[\{\text{Cp}^{\text{Bn}}\text{Fe}(\eta^5\text{-P}_5)\}_6\{\text{Ag}(\text{NC}(\text{C}_6\text{H}_4)\text{Cl})\}_{9.55}][\text{SbF}_6]_{8.55}$ ( <b>4</b> ) .....	50
NMR spectroscopy .....	51
4.5 Crystallographic Details .....	53
4.7 References.....	56
<b>5. Three-Component Self-Assembly: A Way to Overcome Simple Coordination Polymers in Favor of 3D Connected Spherical Supramolecular Aggregates .....</b>	<b>58</b>
5.1 Introduction .....	59
5.2 Results and Discussion.....	61
5.3 Conclusion .....	72
General Remarks .....	73
Synthesis of $[\{\text{Cp}^*\text{Fe}(\eta^{5:2:1}\text{-P}_5)\}_2\text{Ag}]_n[\text{SbF}_6]_n$ ( <b>2</b> ) .....	73
Synthesis of $[\{\text{Cp}^*\text{Fe}(\eta^{5:1:1}\text{-P}_5)\}\{\text{Ag}(\text{CH}_3\text{CN})_2\}]_2[\text{SbF}_6]_2$ ( <b>3</b> ).....	73
Synthesis of $[\{\text{Cp}^*\text{Fe}(\eta^5\text{-P}_5)\}\{\text{Ag}(\text{NC}(\text{CH}_2)_5\text{CN})\}]_2[\text{SbF}_6]_n$ ( <b>4a</b> ) .....	74
Synthesis of $[\{\text{Cp}^*\text{Fe}(\eta^5\text{-P}_5)\}_4\{\text{Ag}_4(\text{NC}(\text{CH}_2)_5\text{CN})_2\}]_n[\text{SbF}_6]_{4n}$ ( <b>4b</b> ) .....	75
Synthesis of $[\{\text{Cp}^*\text{Fe}(\eta^5\text{-P}_5)\}\{\text{Ag}(\text{NC}(\text{CH}_2)_6\text{CN})\}]_n[\text{SbF}_6]_n$ ( <b>5</b> ) .....	76
Synthesis of $[\text{SbF}_6]@[\{\text{Cp}^*\text{Fe}(\eta^5\text{-P}_5)\}_9\{\text{Ag}_{11}(\text{NC}(\text{CH}_2)_7\text{CN})_6\}]_n[\text{SbF}_6]_{10n}$ ( <b>6a</b> ) with $[\{\text{Cp}^*\text{Fe}(\eta^5\text{-P}_5)\}\{\text{Ag}(\text{NC}(\text{CH}_2)_7\text{CN})\}]_n[\text{SbF}_6]_n$ ( <b>6b</b> ) and $[\{\text{Cp}^*\text{Fe}(\eta^5\text{-P}_5)\}\{\text{Ag}_2(\text{NC}(\text{CH}_2)_7\text{CN})\}]_n[\text{SbF}_6]_{2n}$ ( <b>6c</b> ) .....	77
5.5 Crystallographic Details .....	78
5.6 Author Contributions.....	84
5.7 References.....	84
<b>6. Benefitting from Flexibility: A Versatile Approach to Linked and Close-Packed Spherical Host-Guest Assemblies.....</b>	<b>88</b>
6.1 Introduction .....	89
6.2 Results and Discussion.....	91
Self-Assembly of $\text{Cp}^*\text{Fe}(\eta^5\text{-P}_5)$ with $[\text{Cu}(\text{CH}_3\text{CN})_4]\text{BF}_4$ or $\text{Ag}[\text{Al}\{\text{OC}(\text{CF}_3)_3\}_4]$ and flexible dinitriles .....	91
Self-Assembly of $\text{Cp}^{\text{Bn}}\text{Fe}(\eta^5\text{-P}_5)$ and $\text{AgSbF}_6$ with flexible dinitriles .....	93
Self-Assembly of $\text{Cp}^*\text{Fe}(\eta^5\text{-P}_5)$ and $\text{AgSbF}_6$ with flexible dinitriles .....	95
6.3 Conclusion .....	101
6.4 Experimental Part.....	102
General Remarks .....	102
Synthesis of $[\{\text{Cp}^*\text{Fe}(\eta^5\text{-P}_5)\}\{\text{Cu}(\text{NC}(\text{CH}_2)_8\text{CN})\}]_n[\text{BF}_4]_n \cdot (\text{CH}_2\text{Cl}_2)_n$ ( <b>2</b> ) .....	103

Synthesis of $\{[\text{Cp}^*\text{Fe}(\eta^5\text{-P}_5)]\{\text{Ag}(\text{NC}(\text{CH}_2)_{10}\text{CN})\}\}_n[\text{Al}\{\text{OC}(\text{CF}_3)_3\}_4]_n$ ( <b>3</b> ) .....	104
Synthesis of $\{[\text{Cp}^{\text{Bn}}\text{Fe}(\eta^5\text{-P}_5)]\{\text{Ag}(\text{NC}(\text{CH}_2)_8\text{CN})\}\}_n[\text{SbF}_6]_n$ ( <b>4</b> ) .....	105
Synthesis of $\{[\text{Cp}^{\text{Bn}}\text{Fe}(\eta^5\text{-P}_5)]_2\{\text{Ag}_2(\text{NC}(\text{CH}_2)_{10}\text{CN})_{1.5}\}\}_n[\text{SbF}_6]_{2n}(\text{CH}_2\text{Cl}_2)_{0.5n}$ ( <b>5</b> ) .....	106
Synthesis of $[[\text{Cp}^*\text{Fe}(\eta^5\text{-P}_5)]@[\{\text{Cp}^*\text{Fe}(\eta^{5:1:1:1}\text{-P}_5)\}_{12}\{\text{Ag}_{12}(\text{NC}(\text{CH}_2)_8\text{CN})_6\}]]_n[\text{SbF}_6]_{12n}$ ( <b>6</b> ) .....	107
Synthesis of $[[\text{Cp}^*\text{Fe}(\eta^5\text{-P}_5)]@[\{\text{Cp}^*\text{Fe}(\eta^{5:1:1:1}\text{-P}_5)\}_{12}\{\text{Ag}_{12}(\text{NC}(\text{CH}_2)_9\text{CN})_6\}]]_n[\text{SbF}_6]_{12n}$ ( <b>7</b> ) .....	109
Synthesis of $[[\text{Cp}^*\text{Fe}(\eta^5\text{-P}_5)]@[\{\text{Cp}^*\text{Fe}(\eta^{5:1:1:1}\text{-P}_5)\}_{12}\{\text{Ag}_{12}(\text{NC}(\text{CH}_2)_{10}\text{CN})_6\}]]_n[\text{SbF}_6]_{12n}$ ( <b>8</b> ) and $[[\text{Cp}^*\text{Fe}(\eta^5\text{-P}_5)]_2\{\text{Ag}_2(\text{NC}(\text{CH}_2)_{10}\text{CN})\}]_n[\text{SbF}_6]_{2n}$ ( <b>9</b> ) .....	110
6.5 Crystallographic Details .....	111
6.6 Author Contributions .....	117
6.7 References .....	117
<b>7. Polymeric Supramolecular Assemblies: Encapsulation or Coordination of White Phosphorus</b> .....	120
7.1 Introduction .....	121
7.2 Results and Discussion .....	122
7.3 Conclusion .....	129
7.4 Experimental Part .....	131
General Remarks .....	131
Synthesis of $\{[\text{Cp}^*\text{Fe}(\eta^5\text{-P}_5)]_2\{\text{Ag}_2(\text{CH}_2\text{Cl}_2)\}\}_n[\text{SbF}_6]_{2n}$ ( <b>2</b> ) .....	131
Synthesis of $\{[\text{Cp}^*\text{Fe}(\eta^5\text{-P}_5)]_2\{\text{Ag}_2(\eta^2\text{-P}_4)_m(\text{CH}_2\text{Cl}_2)_{1-m}\}\}_n[\text{SbF}_6]_{2n}$ ( <b>3</b> ; $m = 0.75$ ( <b>3a</b> ), $0.67$ ( <b>3b</b> ), $1$ ( <b>3c</b> )) .....	132
Synthesis of $[\text{P}_4@[\{\text{Cp}^*\text{Fe}(\eta^5\text{-P}_5)]_9\{\text{Ag}_x(\text{NC}(\text{CH}_2)_{10}\text{CN})_y\}]]_n[\text{SbF}_6]_{11n}$ ( <b>4</b> ) .....	133
7.5 Crystallographic Details .....	134
7.6 Computational Details .....	139
7.7 Spectra .....	141
7.8 Author Contributions .....	144
7.9 References .....	144
<b>8. Thesis Treasury</b> .....	146
8.1 Three-component self-assembly of $[\text{Cp}^*\text{Fe}(\eta^5\text{-P}_5)]$ with $\text{AgSbF}_6$ and $\text{NC}(\text{C}_{14}\text{H}_{10})\text{CN}$ ( <b>L1</b> ) ....	146
8.2 Self-assembly of $[\text{Cp}^{\text{Bn}}\text{Fe}(\eta^5\text{-P}_5)]$ with $\text{AgSbF}_6$ in the presence of $\text{CH}_3\text{CN}$ .....	147
8.3 Self-assembly of $[\text{Cp}^{\text{Bn}}\text{Fe}(\eta^5\text{-P}_5)]$ with Ag salts of the huge weakly coordinating anions $[\text{Al}\{\text{OC}(\text{CF}_3)_3\}_4]^-$ and $[\text{AlF}(\text{OC}_{12}\text{F}_{15})_3]^-$ .....	149
8.4 Self-assembly of $[\text{Cp}^{\text{Bn}}\text{Fe}(\eta^5\text{-P}_5)]$ with $\text{AgSO}_3\text{C}_7\text{H}_7$ .....	150
8.5 Experimental Part .....	152

General Remarks .....	152
Synthesis of $\{[\text{Cp}^*\text{Fe}(\eta^5\text{-P}_5)]\{\text{Ag}(\text{C}_{16}\text{H}_{10}\text{N}_2)\}_2(\text{C}_7\text{H}_7)\}_n[\text{SbF}_6]_{2n}$ ( <b>2</b> ).....	152
Synthesis of $[\text{SbF}_6]@[(\text{Cp}^{\text{Bn}}\text{Fe}(\eta^5\text{-P}_5)_6(\text{AgCH}_3\text{CN})_{14})[\text{SbF}_6]_{13}]$ ( <b>3</b> ) .....	153
Synthesis of $\{[\text{Cp}^{\text{Bn}}\text{Fe}(\eta^5\text{-P}_5)]_2\{\text{Ag}(\text{Al}(\text{O}(\text{C}(\text{CF}_3)_3)_4)_3\} \cdot (\text{CH}_2\text{Cl}_2)$ ( <b>4a</b> ) and $\{[\text{Cp}^{\text{Bn}}\text{Fe}(\eta^5\text{-P}_5)]_2\{\text{Ag}(\text{Al}(\text{O}(\text{C}(\text{CF}_3)_3)_4)_3\} \cdot (\text{CH}_2\text{Cl}_2)_2$ ( <b>4b</b> ).....	154
Synthesis of $\{[\text{Cp}^{\text{Bn}}\text{Fe}(\eta^5\text{-P}_5)]_2\{\text{Ag}(\text{AlF}(\text{OC}_{12}\text{F}_{15})_3)\}_3\}_4$ ( <b>5</b> ) .....	154
Synthesis of $\{[\text{Cp}^{\text{Bn}}\text{Fe}(\eta^5\text{-P}_5)]_{12}\{\text{Ag}(\text{SO}_3\text{C}_7\text{H}_7)\}_{20-n}\}$ ( <b>6</b> ) .....	155
8.6 Crystallographic Details .....	157
8.7 Author Contributions.....	160
8.8 References.....	160
<b>9. Conclusion</b> .....	162
Ag salts of functionalized or weakly coordinating anions applied in the self-assembly with $[\text{Cp}^{\text{R}}\text{Fe}(\eta^5\text{-P}_5)]$ ( $\text{Cp}^{\text{R}} = \text{Cp}^*, \text{Cp}^{\text{Bn}}$ ) .....	162
Three-component self-assembly of $[\text{Cp}^{\text{R}}\text{Fe}(\eta^5\text{-P}_5)]$ ( $\text{Cp}^{\text{R}} = \text{Cp}^*, \text{Cp}^{\text{Bn}}$ ), coinage metal salts and dinitriles.....	167
Four-component self-assembly of $[\text{Cp}^{\text{R}}\text{Fe}(\eta^5\text{-P}_5)]$ ( $\text{Cp}^{\text{R}} = \text{Cp}^*, \text{Cp}^{\text{Bn}}$ ), $\text{AgSbF}_6$ , flexible dinitriles $\text{NC}(\text{CH}_2)_x\text{CN}$ and white phosphorus .....	171
<b>10. Appendices</b> .....	173
10.1 Alphabetic List of Abbreviations .....	173
10.2 List of Numbered Compounds.....	175
10.3 Acknowledgements .....	177







# 1. Introduction

## 1.1 Supramolecular Chemistry

Supramolecular Chemistry decisively leads to a deep understanding of the chemical processes and the underlying principles to the architectures of life. Its principles are reflected by the structure of the DNA, proteins or virus capsids, or the mechanisms of metabolism based on the “lock and key” model, stated by *E. Fischer* in 1894.<sup>1</sup> Nearly one century later, the Nobel prize for Chemistry in 1987 was awarded jointly to *Jean-Marie Lehn*, *Donald J. Cram* and *Charles Pedersen* “for their development and use of molecules with structure-specific interactions of high selectivity”.<sup>2</sup> Thereby, research on Supramolecular Chemistry and its subtopics began to thrive, and is of unbroken importance and interest until now.

Many phenomena occurring in the “chemistry beyond the molecule”<sup>3</sup> as self-organization, self-assembly and host-guest chemistry rely on weak interactions such as hydrogen bonds,  $\pi$ -interactions and van der Waals forces. The terms of self-organization and self-assembly are often mentioned without a precise definition and therefore mixed up. Considering different definitions stated before, in 2008 consistent concepts were explained by *Halley* and *Winkler*.<sup>4</sup> Thus, the term *self-assembly* should be reserved for a “set of components that are encoded with specific and directional information on how they should interact with other components”, including the products showing a thermodynamically favorable equilibrium and the processes certain reversibility. *Steed*, *Turner* and *Wallace* concretized this to “the spontaneous and reversible association of two or more components to form a larger, non-covalently bound aggregate”.<sup>5</sup> In contrast to this, *Lehn* suggested reserving *self-organization* to dynamic multi-stable systems.<sup>6</sup> To clearly distinguish host-guest chemistry from these concepts, this term is used for larger *host* molecules being able to enclose or wrap around a smaller *guest* molecule, *via* non-covalent interactions.<sup>5</sup>

As all these terms are used regardless of the nature of the used compounds, *Constable* established the phrase Metallosupramolecular chemistry.<sup>7</sup> This field generally comprises the arrangement of transition metal ions and polydentate donor ligands, arranged by the properties inherited by the building blocks. These cover the size and preferred coordination number of the metal ion, as well as the nature and the spatial arrangement of the donor atoms of the ligand.

## 1.2 Discrete Aggregates

### 1.2.1 Polyoxometalates and Clusters

OD polyoxometalates (POMs) are known for almost 200 years<sup>8</sup> and can be considered as missing links between atoms and nanoparticles or molecules and materials.<sup>9</sup> Furthermore, exhibiting sizes ranged from a few nano- to micrometres for functionalized derivatives,<sup>10</sup> they give access to size dimensions hard to reach by either top-down or bottom-up approaches.<sup>11</sup> As these compounds exhibit covalent bonds, they have to be distinguished from the definitions of Supramolecular Chemistry, yet they contribute to the comprehension of assembly mechanisms and structural motifs.

These discrete aggregates are defined by the structural motif of  $\text{MO}_6$  octahedra ( $\text{M} = \text{Mo}, \text{W}, \text{V}, \text{Mn} \dots$ ) that share vertices, edges or faces. Together, they form diversely shaped polyanions, whereas the most common structural type is known as the Keggin ion  $[(\text{XO}_4)(\text{M}_{12}\text{O}_{36})]^{n-}$  ( $\text{X} = \text{P}^{5+}, \text{Si}^{4+}, \text{B}^{3+} \dots$ ;  $\text{M} = \text{Mo}^{6+}, \text{W}^{6+}, \text{V}^{5+} \dots$ ).<sup>12</sup> Throughout the years this class of compounds and closely related fields proved versatility and a row of remarkable clusters were described. *Fenske et al.* showed that huge phosphine- or thiolate-protected Ag clusters are possible to form, up to the record holder with respect to atom number count  $[\text{Ag}_{490}\text{S}_{188}(\text{StC}_5\text{H}_{11})_{114}]$ .<sup>13</sup> With respect to size, *Müller et al.* succeeded in the formation of the POM  $[\text{H}_x\text{Mo}_{368}\text{O}_{1032}(\text{H}_2\text{O})_{240}(\text{SO}_4)_{48}]^{48-}$  ( $x \sim 16$ ) as the largest representative, exhibiting an outer diameter of 6 nm.<sup>14</sup> Most of these compounds show a metal core being protected from aggregation by thiolates, phosphines or alkynyls.<sup>15</sup> Besides these POMs, *Schnöckel* presented a pseudo-fullerene metalloid cluster  $[\text{Al}_{50}\text{Cp}^*_{12}]$ , containing a  $\text{Al}_{50}$  core with protecting  $\text{Cp}^*$  ligands.<sup>16</sup>

This intense research furnished various application possibilities. Thus, not only the physical properties of diverse POM derivatives, like luminescence, magnetism and electrochemical properties were tested with respect to catalysis, green-chemistry or high-density data storage, but also its biological effects were examined considering antibacterial activity and diverse medicinal applications.<sup>17</sup>

### 1.2.2 Metal-Organic Polyhedra

Metal-organic polyhedra (MOPs), however, show bonding situations, based on weak interactions. Some are large enough to offer free space for smaller guest molecules. Early examples of host-guest compounds are crown ethers, cryptands and calixarenes, which often selectively form aggregates with cations or small molecules, fitting into their voids. Whereas a row of weakly bound cages and capsules exist, with different parts held together by hydrogen bonds<sup>18</sup> or van der Waals

forces,<sup>19</sup> metallocupramolecular capsules and cages rely on the coordination of donor ligands towards metal ions.<sup>20</sup> Self-assembled aggregates have been intensely explored in recent years, as they promise exciting progresses in catalysis<sup>21</sup> or drug delivery.<sup>22</sup> They also can be used as storage containers,<sup>23</sup> reaction vessels<sup>24</sup> or molecular flasks<sup>25</sup> to stabilize labile small guest molecules or enable reactions under a protected environment. These supramolecules often show highly symmetric polyhedral scaffolds, similar to Archimedean or Platonic Solids. Thus, supramolecular tetrahedra<sup>26</sup>, cubes<sup>30-33</sup>, octahedra<sup>27</sup>, dodecahedra<sup>28</sup> and icosahedra<sup>29</sup> are reported. Their scaffold formation can be directed either by building blocks, forming the edges or faces of these polyhedra. Following the concepts of *Stang et al.*, this principle is illustrated in *Figure 1*. The precursor, which directs the self-assembly process shows a predefined geometry or preferred coordination environment, respectively. Examples for all four types  $M_8L_{12}$ ,<sup>30</sup>  $M_{12}L_8$ ,<sup>31</sup>  $M_{12}L_6$ <sup>32</sup> and  $M_6L_{12}$ <sup>33</sup> are known in the literature.

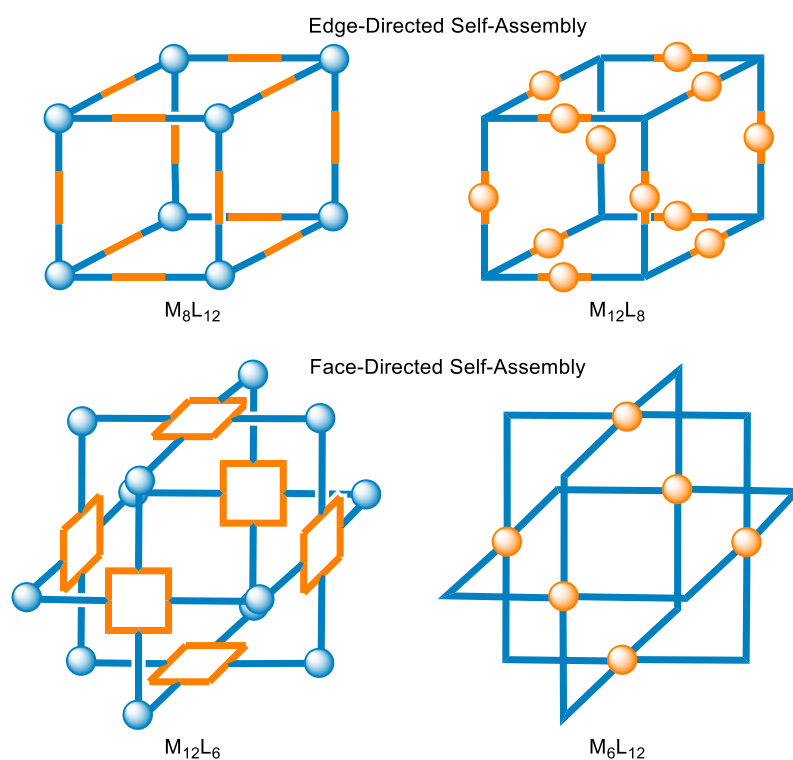


**Figure 1:** Edge- vs. Face-Directed Self-Assembly, illustrated by supramolecular cubes. Metal atoms are represented by spheres, ligands by lines. Building blocks marked in orange direct the self-assembly process.

Most of these cages are homoleptic, thus built up by one type of ligand coordinating to one type of metallic node. In contrast to that, *Ward et al.* shows a rare example of a three-component system by employing two different ligands – one edge-directing, one face-directing, according to the above described principle. By combining pyrazolyl-pyridine based tris-bidentate and bis-bidentate ligands

with  $\text{CdClO}_4$  a cuboctahedral  $\text{Cd}_{12}$  cage is formed (Figure 2).<sup>34</sup> The ligands in this compound show both, face- and edge-forming behavior.

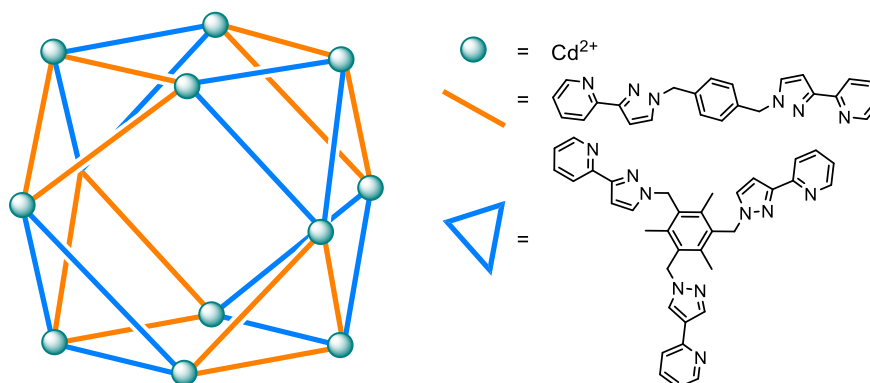


Figure 2: Cuboctahedral cage based on a three-component self-assembly by Ward et al.<sup>34</sup>

### 1.2.3 Functionalized Aggregates

The majority of applications of these cages is strongly linked to the shape and size of the inner void. But for a wider use of this class of compounds a functionalization of the inner void and/or the outer scaffold is indispensable. In this way, these polyhedra can interact in a predefined way with surfaces, tissues or enclosed guest molecules. As these supramolecular assemblies are built up relying on weak interactions, a post-synthetic functionalization is difficult, whereas a direct coupling of the ligand with the functional group, followed by the cage-building self-assembly, is most successful.<sup>35</sup> Thus, the use of designed functional building blocks in the self-assembly is established for both, endo- and exo-functionalization. The cage  $M_{12}L_{24}$  ( $M = \text{Pd}^{2+}$ ,  $L =$  bent pyridine based linker) of Fujita et al. was widely explored using these procedures.

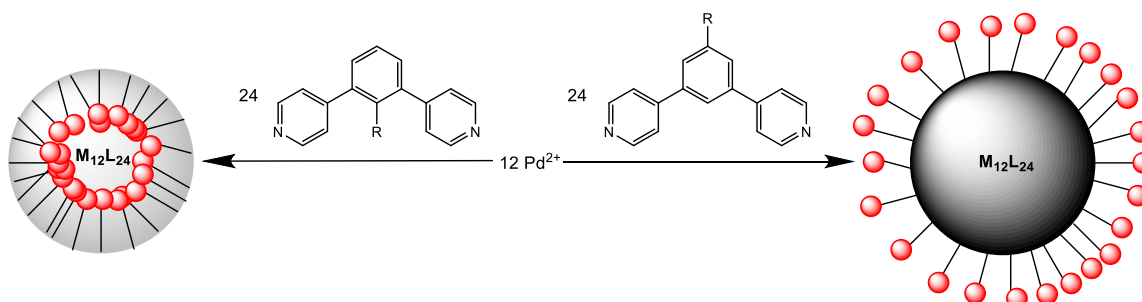


Figure 3: Endo- and exo-functionalization in the case of  $M_{12}L_{24}$ .<sup>36-39</sup>

By endo-functionalization of the ligands, azobenzene chromophores, peptides or coronenes were implemented, leading to a reversible guest uptake upon irradiation, voids of defined chirality or an increased solubility of  $\text{C}_{60}$ , respectively.<sup>36</sup> Also exo-functionalization can be used for applications. Thus, peptide-coated cages can be irreversibly immobilized on  $\text{TiO}_2$  surfaces or mimic DNA

compacting histones.<sup>37</sup> In addition, due to a dual functionalization of the spheres those can be utilized to enable the adhesion of proteins onto a  $\text{TiO}_2$  surface.<sup>38</sup> Another application of functionalized cages is the stimuli-responsive release of enclosed guests, as it is useful for directed drug or dye transport.<sup>39</sup>

### 1.2.4 Organometallic Building Blocks

Due to the extensive research on this field, cages based on various metal atoms as Co,<sup>40</sup> Pd,<sup>41</sup> Pt,<sup>42</sup> Cu,<sup>43</sup> Ag,<sup>44</sup> Zn<sup>45</sup> and Cd<sup>43c</sup> are known to date. Most of the used ligands are fully organic with N, O or S donor atoms, whereas metal-organic building blocks are more rarely employed. In *Figure 4* an overview of metal-organic building blocks for the use in the synthesis of supramolecular cage compounds is given. *Severin et al.* used on the one side  $[\text{Cp}^*\text{M}]$  fragments ( $\text{M} = \text{Ru}, \text{Rh}, \text{Ir}$ ) combined with organic linkers based on N and O donor atoms to build metallacycles (*Figure 4d*).<sup>46</sup> On the other side bipyridyl ligands based on a clathrochelate motif were used in the self-assembly with Pd atoms to obtain octahedral cages (*Figure 4a*).<sup>47</sup> *Clemmer et al.* also used a pyridyl-substituted cobaltocene derivative in combination with Pd atoms to construct a supramolecular cube (*Figure 4b*).<sup>48</sup> Contrarily, *Williams et al.* presented an extraordinary example with both building blocks being of organometallic nature: a fullerene-like sphere assembled from a pentapyrazole-substituted ferrocene as a ligand and a Rh paddle-wheel complex as a metallic node (*Figure 4c,e*).<sup>49</sup>

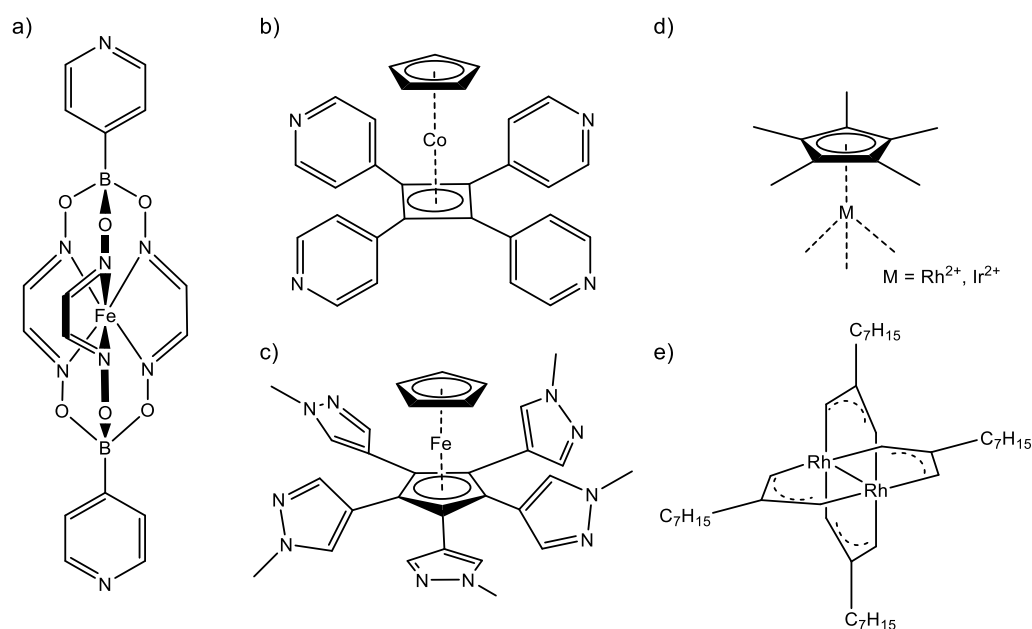


**Figure 4:** Selected metal-organic building blocks employed in supramolecular self-assembly. a) - c) are used as donor ligands, d) and e) as metallic nodes.

### 1.3 Arranging Discrete Assemblies to Networks

The idea of connecting these discrete MOPs to polymers, and therefore profit of the potential combination of characteristics of both classes of compounds, leads to Metal-Organic Frameworks (MOFs). Those are attracting remarkable attention for over twenty years, since *Yaghi* coined the term reporting on a 3D polymer built up by  $\text{Cu}^+$  and 4,4'-bipyridine.<sup>50</sup> Their application diversity ranges from crystalline sponges to absorb mainly small molecules,<sup>51</sup> gas storage<sup>52</sup> or sensing materials<sup>53</sup> and many more. In the original meaning this definition describes 1D - 3D mostly porous polymers with metal atoms as nodes and multitopic organic linkers. Those are most commonly based on N or O donating groups. But ongoing research produced manifold architectures of related classes of compounds: nodes can consist of clusters or MOPs as well, whereas the linkage possibilities vary from organic supramolecular aggregates to inorganic anions. Furthermore, this diversity allows direct and rational approach to reach the goal of connected supramolecular aggregates.<sup>54</sup>

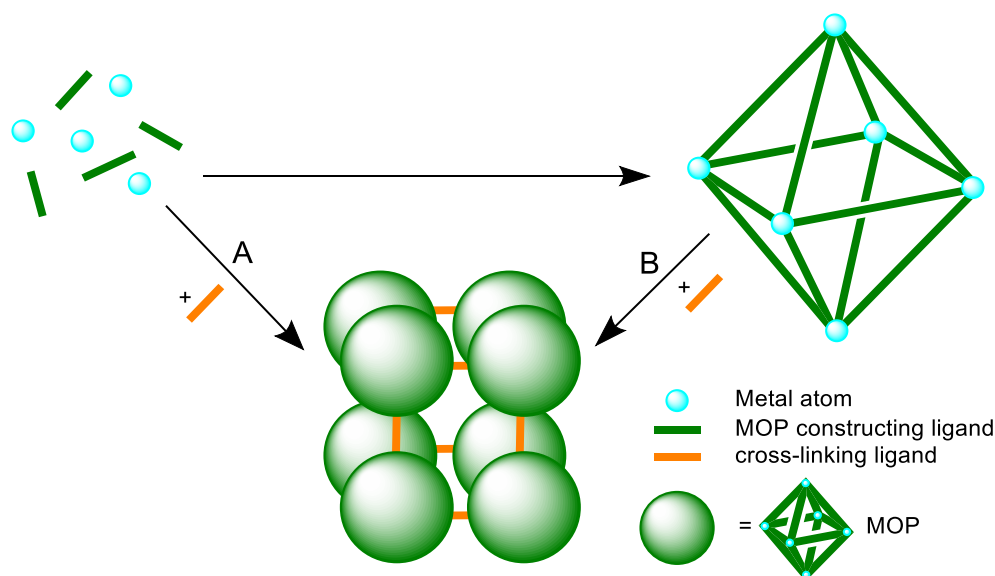


**Figure 5:** Different methods to obtain connected MOPs. **A:** three-component self-assembly and **B:** post-synthetic approach.

As mentioned before, the post-synthetic functionalization approach is difficult as supramolecular aggregates are based on weak interactions, and usually are not stable enough for subsequent reactions (method **B** in Figure 5). One remarkable exception is presented by *Choe et al.*, who synthesized the first MOF of post-synthetically covalently linked Zr-MOPs.<sup>55</sup> The latter are amine-capped and show remarkable water stability, while offering permanent porosity. By applying a condensation reaction with flexible ditopic acyl chloride linkers, these MOPs were successfully cross-linked, retaining their porosity and showing the potential of MOPs as building blocks for



further reactions. In addition, post-synthetically interlinked Cu-MOPs are presented by *Su et al.* and *Zhou et al.* respectively. They applied 4,4'-bipyridine as a linker coordinating towards Cu paddlewheel units acting as vertices of pre-synthesized MOPs to obtain 3D networks.<sup>56</sup>

A more commonly applied approach is the complete self-assembly of diverse building blocks (method **A** in *Figure 5*). Cu-MOPs as nodes in 3D MOFs can be obtained using self-assembly of a Cu salt with tetratopic ligands, inducing a linkage via the edges of the polyhedra.<sup>57</sup> However, motifs in MOFs that can be regarded as MOP analogies, are rather common. Instead of using an additional linking unit, *Fujita et al.* reported on a 3D MOF of vertex-sharing polyhedra of Co atoms and face-constructing tritopic pyridines (*Figure 6*).<sup>58</sup> Contrarily, *Ma et al.* and *Wright et al.* presented face-sharing polyhedra of Zn or Cd paddle-wheel complexes and functionalized porphyrines,<sup>59</sup> or Na atoms and pentatopic nitrile ligand.<sup>60</sup>

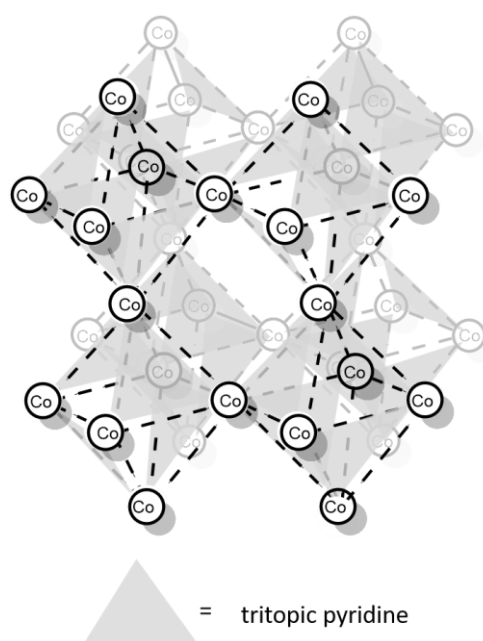


**Figure 6:** 3D MOF of vertex-sharing octahedra by *Fujita et al.*

## 1.4 Supramolecular Chemistry Based on Polyphosphorus Complexes

While all aforementioned organometallic complexes or organic electron donating ligands rely on N or O atoms, our group focuses on polyphosphorus ( $P_n$ ) complexes. Their reactivity is determined by the substituent-free P atoms, that are solely bound to other P or metal atoms. This influences the steric and electronic properties on the coordinating P atoms and enables a unique coordination chemistry.

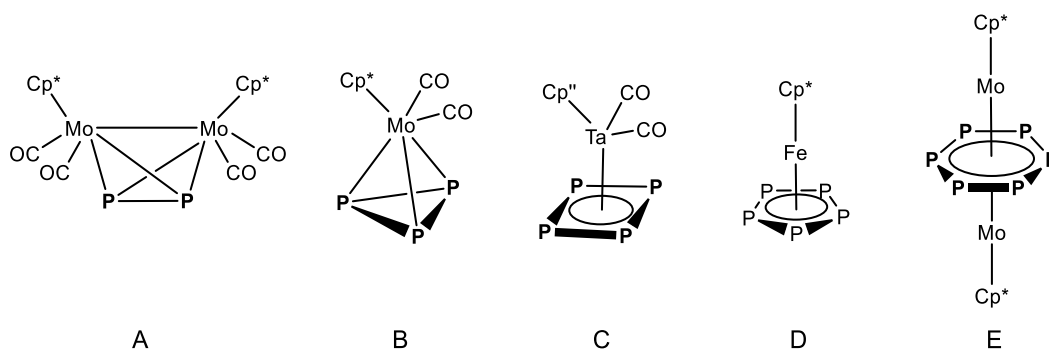


**Figure 7:** Selected  $P_n$  complexes:  $[Cp^*_2Mo_2(CO)_4(\mu,\eta^{2:2}-P_2)]$ ,<sup>61</sup>  $[Cp^*Mo(CO)_2(\eta^3-P_3)]$ ,<sup>61</sup>  $[Cp''Ta(CO)_2(\eta^4-P_4)]$ ,<sup>62</sup>  $[Cp^*Fe(\eta^5-P_5)]$ ,<sup>63</sup> and  $[(Cp^*Mo)_2(\mu,\eta^{6:6}-P_6)]$ .<sup>61</sup>

All  $P_n$  complexes shown in Figure 7 are easily synthesized by the thermolysis reaction of the respective carbonyl compound  $[Cp^*Mo(CO)_3]_2$ ,  $[Cp''Ta(CO)_4]$  or  $[Cp^*Fe(CO)_2]_2$  and white phosphorus ( $P_4$ ). While for **A**, **B** and **E** the Cp derivatives are known for a long time, for **D** this was only found out very recently.<sup>64</sup> Similar to **E**, the Cp derivative of **D** can only be synthesized by increasing the temperature of the thermolysis to 203°C, which is reached by using diisopropylbenzene as solvent. All known  $P_n$  complexes readily react with coinage metal salts in self-assembly reactions to form diverse metal-metalorganic polymeric frameworks (Figure 8).<sup>65</sup>

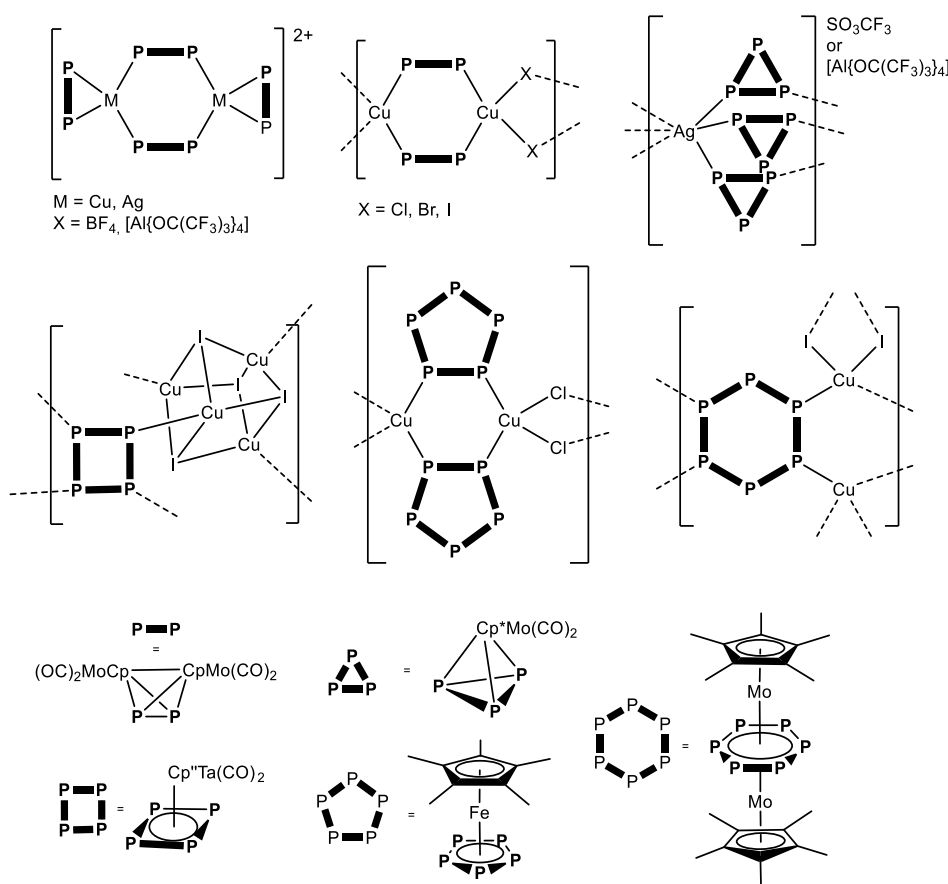


**Figure 8:** Selected polymeric compounds based on the  $P_n$  ligand complexes **A-E**.

Especially the coordination chemistry of  $[\text{Cp}^*_2\text{Mo}_2(\text{CO})_2(\mu, \eta^{2:2}\text{-P}_2)]$  was studied in detail. While with metal salts of weakly coordinating anions discrete dimeric compounds are formed, applying  $\text{AgNO}_3$  or  $\text{CuX}$  ( $\text{X} = \text{Cl}, \text{Br}, \text{I}$ ) and  $\text{CuX}_2$  the formation of 1D polymeric frameworks can be observed.<sup>66</sup> For the  $[\text{Al}\{\text{OC}(\text{CF}_3)_3\}_4]$  derivate of the dimeric dication a monomer/dimer equilibrium was proposed to exist in solution, based on NMR spectroscopic methods and DFT calculations.

The derivatives of the two cyclic  $\text{P}_n$  complexes  $[\text{Cp}^{\text{R}}\text{Ta}(\text{CO})_2(\eta^4\text{-P}_4)]$  ( $\text{Cp}^{\text{R}} = \text{Cp}''', \text{Cp}''$ ) and  $[\text{Cp}^{\text{R}}\text{Fe}(\eta^5\text{-P}_5)]$  ( $\text{Cp}^{\text{R}} = \text{Cp}^*, \text{Cp}^{\text{Et}}, \text{Cp}^{\text{Bn}}, \text{Cp}^{\text{BIG}}$ ) stand out of the row, as they not only form coordination polymers combined with coinage metal salts, but also enable the synthesis of unprecedented discrete supramolecules. By self-assembly reactions with  $\text{CuX}$  ( $\text{X} = \text{Cl}, \text{Br}, \text{I}$ ) various nano-sized spheres are built (*Figure 9*). Thus, the inorganic scaffold of the self-assembly product of  $[\text{Cp}^{\text{R}}\text{Ta}(\text{CO})_2(\eta^4\text{-P}_4)]$  with  $\text{CuCl}$  or  $\text{CuBr}$  consists of six *cyclo*- $\text{P}_4$  units and eight  $\text{CuX}$  fragments achieving a non-classical fullerene topology (*Figure 9a*). Switching to  $\text{CuI}$ , different spheres are formed, whereas one of them exhibits a peanut-shaped inorganic scaffold of ten *cyclo*- $\text{P}_4$  units and 14  $\text{CuI}$  fragments (*Figure 9b*). By employing  $[\text{Cp}^*\text{Fe}(\eta^5\text{-P}_5)]$  as a building block 80- and 90-vertex spheres with fullerene topology, as well as other scaffolds without fullerene topology are formed upon combining with  $\text{CuX}$ . Those can be selectively synthesized by applying different template molecules, which act as guests in the spheres of convenient inner void. Thus, guest molecules of different form, symmetry ( $\text{P}_4\text{S}_3$ ,<sup>67</sup>  $\text{P}_4$ ,<sup>68</sup>  $[\text{Cp}_2\text{Fe}]$ ,<sup>69,71</sup>  $[(\text{CpCr})_2(\mu, \eta^{5:5}\text{-As}_5)]$ ,<sup>69</sup>  $\text{C}_{60}$ ,<sup>70</sup>  $[\text{CpV}(\eta^7\text{-C}_7\text{H}_7)]$ <sup>67</sup>) or charge ( $[\text{CoCp}_2]^+$ )<sup>71</sup> could be incorporated. These self-assembly systems are very sensitive to subtle variations of stoichiometry, concentration or solvents used. Thus, at first only 1D and 2D polymers of  $[\text{Cp}^*\text{Fe}(\eta^5\text{-P}_5)]$  and  $\text{CuX}$  were found, before the first spherical compounds were observed upon using diluted solutions of the respective building blocks. Upon changing the stoichiometry of  $[\text{Cp}^*\text{Fe}(\eta^5\text{-P}_5)]$  and  $\text{CuX}$  from 1 : 2 (for 80- or 90-vertex spheres) to 2 : 1, a capsule is formed, consisting of two half shells, sticking together by weak dispersion forces between the inorganic half-shells and the two templated  $[\text{Cp}^*\text{Fe}(\eta^5\text{-P}_5)]$  ligands (*Figure 9d*).<sup>76</sup>

The building block pentaphosphaferrocene is very well tuneable concerning its steric demand in the organic cyclopentadienyl residue. Coming to the extreme,  $[\text{Cp}^{\text{BIG}}\text{Fe}(\eta^5\text{-P}_5)]$  has an diameter in the organic residue of  $\varnothing(\text{Cp in } [\text{Cp}^{\text{BIG}}\text{Fe}(\eta^5\text{-P}_5)]) = 18.57 \text{ \AA}$  (compared to  $\varnothing(\text{Cp in } [\text{Cp}^*\text{Fe}(\eta^5\text{-P}_5)]) = 8.29 \text{ \AA}$ ).<sup>72</sup> When reacted with  $\text{CuX}$  the building blocks assemble besides polymeric compounds to a spherical *I*- $\text{C}_{140}$  fullerene analogue inorganic scaffold, with incorporated  $\text{CuX}$  cluster.<sup>73</sup> Because of the limited solubility of both the  $[\text{Cp}^{\text{BIG}}\text{Fe}(\eta^5\text{-P}_5)]$  complex, as well as the  $\text{Cp}^*$  derivatives,  $[\text{Cp}^{\text{Bn}}\text{Fe}(\eta^5\text{-P}_5)]$  was involved in the synthesis of spheres. With respect to sterics, on the level of the  $\text{Cp}$  part this ligand does not differ much from  $\text{Cp}^*$  ( $\varnothing(\text{Cp in } [\text{Cp}^{\text{Bn}}\text{Fe}(\eta^5\text{-P}_5)]) = 8.34 \text{ \AA}$ ), but due to its  $\text{Bn}$  substituents it promises good solubility of the built products. Indeed, this system allows the

transformation of a porous 80-vertex sphere to a complete one and further to a novel tetrahedral shaped scaffold, depending on the stoichiometric ratios of the respective building blocks in solution (Figure 9e).<sup>77</sup>

Besides halides, triflate was involved in the self-assembly of  $\text{CuSO}_3\text{CF}_3$  with  $[\text{Cp}^{\text{Bn}}\text{Fe}(\eta^5\text{-P}_5)]$ . In this case the spherical scaffold consists of twelve *cyclo*- $\text{P}_5$  ligands, thirty positions for Cu atoms and twenty anions, coordinating in a tripodal way to scaffold building Cu atoms. For reasons of charge balance, only twenty positions for Cu are occupied to reach a “90-10”-vertex scaffold (Figure 9f).

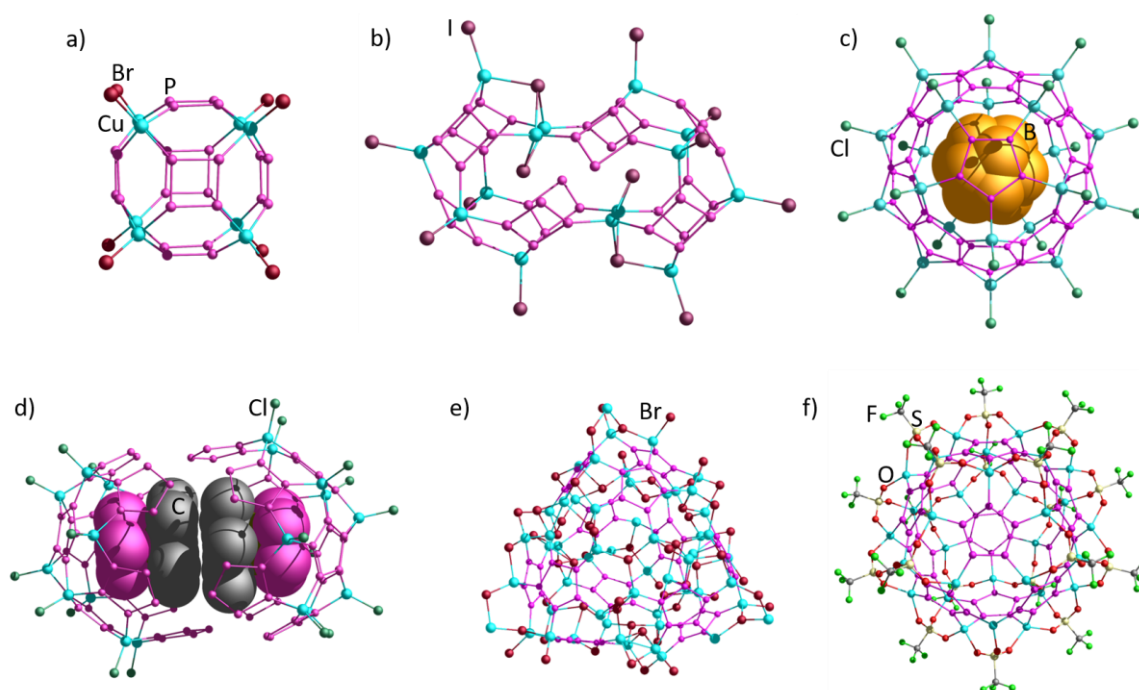


**Figure 9:** Selected spherical supramolecules based on  $[\text{Cp}^{\text{R}}\text{Ta}(\text{CO})_2(\eta^4\text{-P}_4)]$  and  $[\text{Cp}^{\text{R}}\text{Fe}(\eta^5\text{-P}_5)]$ : a)  $[\{\text{Cp}^{\text{'''}}\text{Ta}(\text{CO})_2(\eta^4\text{-P}_4)\}_6(\text{CuBr})_8]$ ,<sup>74</sup> b)  $[\{\text{Cp}^{\text{''}}\text{Ta}(\text{CO})_2(\mu\text{-I})_2(\mu^3\text{-I})_2\}]$ ,<sup>74</sup> c)  $(\text{C}_{2}\text{B}_{10}\text{H}_{12})@[\{\text{Cp}^{\text{*}}\text{Fe}(\eta^5\text{-P}_5)\}_{12}(\text{CuCl})_{20}]$ ,<sup>75</sup> d)  $[\text{Cp}^{\text{*}}\text{Fe}(\eta^5\text{-P}_5)]@[\{\text{Cp}^{\text{*}}\text{Fe}(\eta^5\text{-P}_5)\}_{12}(\text{CuCl})_{10}(\text{Cu}_2\text{Cl}_3)_5\{\text{Cu}(\text{CH}_3\text{CN})_2\}_5]$ ,<sup>76</sup> e)  $[\{\text{Cp}^{\text{Bn}}\text{Fe}(\eta^5\text{-P}_5)\}_{12}(\text{CuBr})_{51}(\text{CH}_3\text{CN})_8]$ ,<sup>77</sup> f)  $[\{\text{Cp}^{\text{Bn}}\text{Fe}(\eta^5\text{-P}_5)\}_{12}(\text{CuSO}_3\text{CF}_3)_{20}]$ .<sup>78</sup>  $[\text{Cp}^{\text{'''}}\text{Ta}]$ ,  $[\text{Cp}^{\text{R}}\text{Fe}]$  units, H atoms, solvent molecules and minor parts of disorder are omitted for clarity. Templates are depicted in space-filling model.

The  $[\{\text{Cp}^{\text{*}}\text{Mo}(\text{CO})_2\}_2(\mu, \eta^{2:2}\text{-P}_2)]$  ligand is the only one which was explored in a three component self-assembly with diverse N-donating organic ligands, so far.<sup>79</sup> (Figure 10) As our group found out very recently, the synthesis of hybrid coordination polymers is not restricted to the complete self-assembly, but due to the preorganization into the dimeric precursors the formation of 1D, 2D and 3D networks can be rationally planned and designed.<sup>80</sup> In this case the strong binding affinity of pyridine-based linker molecules towards Ag is used to partly or fully replace the  $\eta^2$ -coordinated  $[\text{Cp}^{\text{*}}_2\text{Mo}_2(\text{CO})_2(\mu, \eta^{2:2}\text{-P}_2)]$  ligands in the dimer  $[\text{Ag}_2\{\text{Cp}^{\text{*}}_2\text{Mo}_2(\text{CO})_2(\mu, \eta^{2:2}\text{-P}_2)\}_2][\text{BF}_4]_2$ .

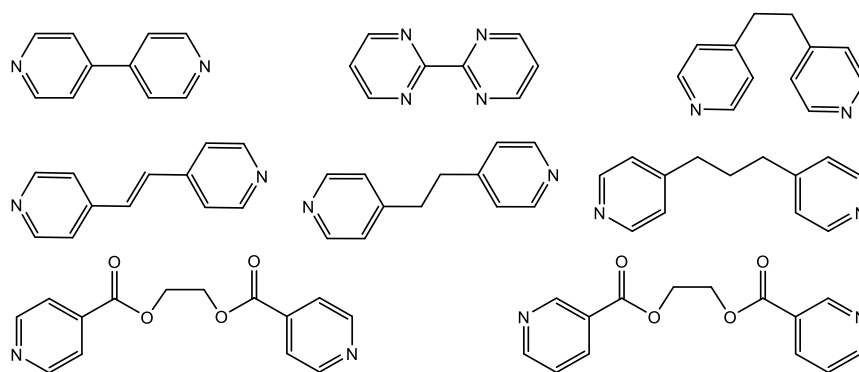


**Figure 10:** Potential organic linkers used in self-assembly reactions with  $[\{Cp^*Mo(CO)_2\}_2(\mu, \eta^{2:2}-P_2)]$  to obtain hybrid networks.<sup>79,80</sup>

## References

- <sup>1</sup> E. Fischer, *Berichte der Deutschen chemischen Gesellschaft zu Berlin* **1894**, 27, 2985-2993.
- <sup>2</sup> a) "The Nobel Prize in Chemistry 1987". *Nobelprize.org*. Nobel Media AB 2014. Web. 2 May 2018. [http://www.nobelprize.org/nobel\\_prizes/chemistry/laureates/1987/](http://www.nobelprize.org/nobel_prizes/chemistry/laureates/1987/); b) J. M. Lehn, *Angew. Chem.* **1988**, 100, 91-116; c) D. J. Cram, *Angew. Chem.* **1988**, 100, 1041-1052; d) C. J. Pedersen, *Angew. Chem.* **1988**, 100, 1053-1059.
- <sup>3</sup> J. M. Lehn, *Science* **1993**, 260, 1762-1763.
- <sup>4</sup> J. D. Halley, D. A. Winkler, *Complexity* **2008**, 14, 10-17.
- <sup>5</sup> J. W. Steed, D. R. Turner, K. J. Wallace, *Core Concepts in Supramolecular Chemistry and Nanochemistry*, John Wiley & Sons, Ltd, **2007**.
- <sup>6</sup> J. M. Lehn, *Supramolecular Chemistry*, Weinheim: New York **1995**.
- <sup>7</sup> E. C. Constable, *Pure Appl. Chem.* **1996**, 68, 253-260.
- <sup>8</sup> J. J. Berzelius, *Poggend. Ann. Phys. Chem.*, 1826, 6, p. 369.
- <sup>9</sup> a) I. Chakraborty, T. Pradeep, *Chem. Rev.* **2017**, 117, 8208-827; b) J. F. Corrigan, O. Fuhr, D. Fenske, *Adv. Mater.* **2009**, 21, 1867-1871.
- <sup>10</sup> D.-L. Long, R. Tsunashima, L. Cronin, *Angew. Chem., Int. Ed.* **2010**, 49, 1736-1758.
- <sup>11</sup> P. Gouzerh, M. Che, *Actual. Chim.* **2006**, 298, 9-22.
- <sup>12</sup> M. T. Pope, A. Mueller, *Angew. Chem.* **1991**, 103, 56-70
- <sup>13</sup> C. Anson, A. Eichhoefer, I. Issac, D. Fenske, O. Fuhr, P. Sevillano, C. Persau, D. Stalke, J. Zhang, *Angew. Chem., Int. Ed.* **2008**, 47, 1326-1331.
- <sup>14</sup> a) A. Mueller, B. Botar, S. K. Das, H. Boegge, M. Schmidtman, A. Merca, *Polyhedron* **2004**, 23, 2381-2385; b) A. Muller, E. Beckmann, H. Bogge, M. Schmidtman, A. Dress, *Angew Chem., Int. Ed.* **2002**, 41, 1162-1167.
- <sup>15</sup> a) C. Anson, A. Eichhoefer, I. Issac, D. Fenske, O. Fuhr, P. Sevillano, C. Persau, D. Stalke, J. Zhang,

- Angew. Chem., Int. Ed.* **2008**, *47*, 1326-1331, b) S. Bestgen, O. Fuhr, B. Breitung, V. S. Kiran Chakravadhanula, G. Guthausen, F. Hennrich, W. Yu, M. M. Kappes, P. W. Roesky, D. Fenske, *Chem. Sci.* **2017**, *8*, 2235-2240, c) B. Li, R.-W. Huang, J.-H. Qin, S.-Q. Zang, G.-G. Gao, H.-W. Hou, T. C. W. Mak, *Chem. Eur. J.* **2014**, *20*, 12416-12420, d) F. Gruber, M. Jansen, *Angew. Chem., Int. Ed.* **2010**, *49*, 4924-4926, e) L.-M. Zhang, T. C. W. Mak, *J. Am. Chem. Soc.* **2016**, *138*, 2909-2912, f) S. C. K. Hau, M. C. L. Yeung, V. W. W. Yam, T. C. W. Mak, *J. Am. Chem. Soc.* **2016**, *138*, 13732-13739.
- <sup>16</sup> J. Vollet, J. R. Hartig, H. Schnoeckel, *Angew. Chem., Int. Ed.* **2004**, *43*, 3186-3189.
- <sup>17</sup> a) A. Bijelic, M. Aureliano, A. Rompel, *Chem. Commun.* **2018**, *54*, 1153-1169; b) X. Chen, S.-T. Han, X. Chen, Y. Zhou, V. A. L. Roy, *Adv. Mater.* **2018**, *30*; c) A. Dolbecq, E. Dumas, C. R. Mayer, P. Mialane, *Chem. Rev.* **2010**, *110*, 6009-6048.
- <sup>18</sup> a) K. Tiefenbacher, D. Ajami, J. Rebek, Jr., *Angew. Chem., Int. Ed.* **2011**, *50*, 12003-12007; b) S. J. Park, O.-H. Kwon, K.-S. Lee, K. Yamaguchi, D.-J. Jang, J.-I. Hong, *Chem. Eur. J.* **2008**, *14*, 5353-5359; c) O. Ugono, K. T. Holman, *Chem. Commun.* **2006**, 2144-2146; c) S. J. Dalgarno, S. A. Tucker, D. B. Bassil, J. L. Atwood, *Science* **2005**, *309*, 2037-2039; d) L. R. MacGillivray, J. L. Atwood, *Nature* **1997**, *389*, 469-472.
- <sup>19</sup> a) W. Wei, W. Li, Z. Li, W. Su, M. Hong, *Chem. Eur. J.* **2013**, *19*, 469-473; b) G. S. Ananchenko, K. A. Udachin, M. Pojarova, A. Dubes, J. A. Ripmeester, S. Jebors, A. W. Coleman, *Cryst. Growth Des.* **2006**, *6*, 2141-2148; c) G. S. Ananchenko, K. A. Udachin, J. A. Ripmeester, T. Perrier, A. W. Coleman, *Chem. Eur. J.* **2006**, *12*, 2441-2447; d) G. S. Ananchenko, K. A. Udachin, A. Dubes, J. A. Ripmeester, T. Perrier, A. W. Coleman, *Angew. Chem., Int. Ed.* **2006**, *45*, 1585-1588.
- <sup>20</sup> a) T. R. Cook, P. J. Stang, *Chem. Rev.* **2015**, *115*, 7001-7045; b) S. J. Dalgarno, N. P. Power, J. L. Atwood, *Coord. Chem. Rev.* **2008**, *252*, 825-841.
- <sup>21</sup> a) S. H. A. M. Leenders, R. Gramage-Doria, B. de Bruin, J. N. H. Reek, *Chem. Soc. Rev.* **2015**, *44*, 433-448; b) C. J. Brown, F. D. Toste, R. G. Bergman, K. N. Raymond, *Chem. Rev.* **2015**, *115*, 3012-3035; c) C. J. Hastings, M. D. Pluth, R. G. Bergman, K. N. Raymond, *J. Am. Chem. Soc.* **2010**, *132*, 6938-6940.
- <sup>22</sup> a) N. Basilio, U. Pischel, *Chem. Eur. J.* **2016**, *22*, 15208-15211; b) N. Ahmad, H. A. Younus, A. H. Chughtai, F. Verpoort, *Chem. Soc. Rev.* **2015**, *44*, 9-25.
- <sup>23</sup> S. Zarra, D. M. Wood, D. A. Roberts, J. R. Nitschke, *Chem. Soc. Rev.* **2015**, *44*, 419-432.
- <sup>24</sup> a) K. Takaoka, M. Kawano, T. Ozeki, M. Fujita, *Chem Commun* **2006**, 1625-1627, b) Y. Inokuma, N. Kojima, T. Arai, M. Fujita, *J. Am. Chem. Soc.* **2011**, *133*, 19691-19693.
- <sup>25</sup> a) Y. Inokuma, M. Kawano, M. Fujita, *Nat. Chem.* **2011**, *3*, 349-358; b) M. Yoshizawa, J. K. Klosterman, M. Fujita, *Angew. Chem., Int. Ed.* **2009**, *48*, 3418-3438; c) P. Mal, B. Breiner, K. Rissanen, J. R. Nitschke, *Science* **2009**, *324*, 1697-1699; d) C. Schmuck, *Angew. Chem., Int. Ed.* **2007**, *46*, 5830-5833; e) S. Sato, J. Iida, K. Suzuki, M. Kawano, T. Ozeki, M. Fujita, *Science* **2006**, *313*, 1273-1276.

- 26 a) D. Yang, J. Zhao, L. Yu, X. Lin, W. Zhang, H. Ma, A. Gogoll, Z. Zhang, Y. Wang, X.-J. Yang, B. Wu, *J. Am. Chem. Soc.* **2017**, *139*, 5946-5951; b) D. Nam, J. Huh, J. Lee, J. H. Kwak, H. Y. Jeong, K. Choi, W. Choe, *Chem. Sci.* **2017**, *8*, 7765-7771.
- 27 M. Fujita, D. Oguro, M. Miyazawa, H. Oka, K. Yamaguchi, K. Ogura, *Nature* **1995**, *378*, 469-471.
- 28 D.-X. Zhang, H.-X. Zhang, H.-Y. Li, T. Wen, J. Zhang, *Cryst. Growth Des.* **2015**, *15*, 2433-2436.
- 29 a) M. Scheer, A. Schindler, C. Groeger, A. V. Virovets, E. V. Peresypkina, *Angew. Chem., Int. Ed.* **2009**, *48*, 5046-5049; b) T. Brasey, R. Scopelliti, K. Severin, *Chem. Commun.* **2006**, 3308-3310.
- 30 S. Roche, C. Haslam, S. L. Heath, J. A. Thomas, *Chem. Commun.* **1998**, 1681-1682.
- 31 a) J. M. Fowler, F. L. Thorp-Greenwood, S. L. Warriner, C. E. Willans, M. J. Hardie, *Chem. Commun.* **2016**, *52*, 8699-8702; b) B. F. Abrahams, S. J. Egan, R. Robson, *J. Am. Chem. Soc.* **1999**, *121*, 7172.
- 32 S. C. Johannessen, R. G. Brisbois, J. P. Fischer, P. A. Grieco, A. E. Counterman, D. E. Clemmer, *J. Am. Chem. Soc.* **2001**, *123*, 3818-3819.
- 33 K. Suzuki, M. Tominaga, M. Kawano, M. Fujita, *Chem. Commun.* **2009**, 1638-1640.
- 34 N. K. Al-Rasbi, I. S. Tidmarsh, S. P. Argent, H. Adams, L. P. Harding, M. D. Ward, *J. Am. Chem. Soc.* **2008**, *130*, 11641-11649.
- 35 J. Han, A. Schmidt, T. Zhang, H. Permentier, G. M. M. Groothuis, R. Bischoff, F. E. Kuehn, P. Horvatovich, A. Casini, *Chem. Commun.* **2017**, *53*, 1405-1408.
- 36 a) K. Suzuki, K. Takao, S. Sato, M. Fujita, *J. Am. Chem. Soc.* **2010**, *132*, 2544-2545; b) T. Murase, S. Sato, M. Fujita, *Angew. Chem., Int. Ed.* **2007**, *46*, 5133-5136; c) K. Suzuki, M. Kawano, S. Sato, M. Fujita, *J. Am. Chem. Soc.* **2007**, *129*, 10652-10653.
- 37 a) T. Kikuchi, S. Sato, D. Fujita, M. Fujita, *Chem. Sci.* **2014**, *5*, 3257-3260; b) M. Ikemi, T. Kikuchi, S. Matsumura, K. Shiba, S. Sato, M. Fujita, *Chem. Sci.* **2010**, *1*, 68-71.
- 38 S. Sato, M. Ikemi, T. Kikuchi, M. Fujita, S. Matsumura, K. Shiba, *J Am Chem Soc* **2015**, *137*, 12890-12896.
- 39 S. K. Samanta, J. Quigley, B. Vinciguerra, V. Briken, L. Isaacs, *J. Am. Chem. Soc.* **2017**, *139*, 9066-9074.
- 40 a) S. Matsuzaki, T. Arai, K. Ikemoto, Y. Inokuma, M. Fujita, *J. Am. Chem. Soc.* **2014**, *136*, 17899-17901, b) N. K. Al-Rasbi, I. S. Tidmarsh, S. P. Argent, H. Adams, L. P. Harding, M. D. Ward, *J. Am. Chem. Soc.* **2008**, *130*, 11641-11649.
- 41 a) T. Osuga, T. Murase, M. Fujita, *Angew. Chem., Int. Ed.* **2012**, *51*, 12199-12201, b) Y. Fang, T. Murase, S. Sato, M. Fujita, *J. Am. Chem. Soc.* **2013**, *135*, 613-615, c) K. Harris, D. Fujita, M. Fujita, *Chem. Commun.* **2013**, *49*, 6703-6712, d) Q.-F. Sun, J. Iwasa, D. Ogawa, Y. Ishido, S. Sato, T. Ozeki, Y. Sei, K. Yamaguchi, M. Fujita, *Science* **2010**, *328*, 1144-1147, e) M. Fujita, D. Oguro, M. Miyazawa, H. Oka, K. Yamaguchi, K. Ogura, *Nature* **1995**, *378*, 469-471.
- 42 S. Mukherjee, P. S. Mukherjee, *Chem. Commun.* **2014**, *50*, 2239-2248.
- 43 a) O. Oms, T. Jarrosson, L. H. Tong, A. Vaccaro, G. Bernardinelli, A. F. Williams, *Chem. Eur. J.* **2009**, *15*, 5012-5022, b) D.-X. Zhang, H.-X. Zhang, H.-Y. Li, T. Wen, J. Zhang, *Cryst. Growth Des.* **2015**, *15*,

- 2433-2436, c) N. K. Al-Rasbi, I. S. Tidmarsh, S. P. Argent, H. Adams, L. P. Harding, M. D. Ward, *J. Am. Chem. Soc.* **2008**, *130*, 11641-11649.
- 44 a) N. Giri, S. L. James, *Chem. Commun.* **2011**, *47*, 1458-1460, b) O. Oms, T. Jarrosson, L. H. Tong, A. Vaccaro, G. Bernardinelli, A. F. Williams, *Chem. Eur. J.* **2009**, *15*, 5012-5022,
- 45 D.-X. Zhang, H.-X. Zhang, H.-Y. Li, T. Wen, J. Zhang, *Cryst. Growth Des.* **2015**, *15*, 2433-2436.
- 46 a) C. Schouwey, M. Papmeyer, R. Scopelliti, K. Severin, *Dalton Trans* **2015**, *44*, 2252-2258; b) K. Severin, *Coord. Chem. Rev.* **2003**, *245*, 3-10.
- 47 a) M. D. Wise, J. J. Holstein, P. Pattison, C. Besnard, E. Solari, R. Scopelliti, G. Bricogne, K. Severin, *Chem. Sci.* **2015**, *6*, 1004-1010; b) T. Brasey, R. Scopelliti, K. Severin, *Chem. Commun.* **2006**, 3308-3310.
- 48 S. C. Johannessen, R. G. Brisbois, J. P. Fischer, P. A. Grieco, A. E. Counterman, D. E. Clemmer, *J. Am. Chem. Soc.* **2001**, *123*, 3818-3819.
- 49 a) L. H. Tong, L. Guenee, A. F. Williams, *Inorg. Chem.* **2011**, *50*, 2450-2457; b) O. Oms, T. Jarrosson, L. H. Tong, A. Vaccaro, G. Bernardinelli, A. F. Williams, *Chem. Eur. J.* **2009**, *15*, 5012-5022.
- 50 a) O. M. Yaghi, G. Li, H. Li, *Nature* **1995**, *378*, 703-706; b) O. M. Yaghi, H. Li, *J. Am. Chem. Soc.* **1995**, *117*, 10401-10402.
- 51 a) K. Rissanen, *Chem Soc Rev* **2017**, *46*, 2638-2648.; b) Y. Inokuma, S. Yoshioka, J. Ariyoshi, T. Arai, Y. Hitora, K. Takada, S. Matsunaga, K. Rissanen, M. Fujita, *Nature* **2013**, *495*, 461-466.
- 52 a) X. Yang, Q. Xu, *Cryst. Growth Des.* **2017**, *17*, 1450-1455; b) K. Sumida, D. L. Rogow, J. A. Mason, T. M. McDonald, E. D. Bloch, Z. R. Herm, T.-H. Bae, J. R. Long, *Chem. Rev.* **2012**, *112*, 724-781; c) M. P. Suh, H. J. Park, T. K. Prasad, D.-W. Lim, *Chem. Rev.* **2012**, *112*, 782-835; d) J.-R. Li, R. J. Kuppler, H.-C. Zhou, *Chem. Soc. Rev.* **2009**, *38*, 1477-1504.
- 53 a) G. Ji, J. Liu, X. Gao, W. Sun, J. Wang, S. Zhao, Z. Liu, *J. Mater. Chem. A* **2017**, *5*, 10200-10205; b) Y. Yu, J.-P. Ma, C.-W. Zhao, J. Yang, X.-M. Zhang, Q.-K. Liu, Y.-B. Dong, *Inorg. Chem.* **2015**, *54*, 11590-11592; c) L. E. Kreno, K. Leong, O. K. Farha, M. Allendorf, R. P. Van Duyne, J. T. Hupp, *Chem. Rev.* **2012**, *112*, 1105-1125.
- 54 a) J.-S. Qin, S. Yuan, Q. Wang, A. Alsalme, H.-C. Zhou, *J. Mater. Chem. A* **2017**, *5*, 4280-4291, b) J. J. I. V. Perry, J. A. Perman, M. J. Zaworotko, *Chem. Soc. Rev.* **2009**, *38*, 1400-1417.
- 55 D. Nam, J. Huh, J. Lee, J. H. Kwak, H. Y. Jeong, K. Choi, W. Choe, *Chem. Sci.* **2017**, *8*, 7765-7771.
- 56 a) H.-N. Wang, X. Meng, G.-S. Yang, X.-L. Wang, K.-Z. Shao, Z.-M. Su, C.-G. Wang, *Chem. Commun.* **2011**, *47*, 7128-7130.; b) J.-R. Li, D. J. Timmons, H.-C. Zhou, *J. Am. Chem. Soc.* **2009**, *131*, 6368-6369.
- 57 W. Lu, D. Yuan, T. A. Makal, Z. Wei, J.-R. Li, H.-C. Zhou, *Dalton Trans.* **2013**, *42*, 1708-1714.
- 58 a) S. Matsuzaki, T. Arai, K. Ikemoto, Y. Inokuma, M. Fujita, *J. Am. Chem. Soc.* **2014**, *136*, 17899-17901; b) Y. Inokuma, N. Kojima, T. Arai, M. Fujita, *J. Am. Chem. Soc.* **2011**, *133*, 19691-19693; c) Y. Inokuma, T. Arai, M. Fujita, *Nat. Chem.* **2010**, *2*, 780-783.



- 59 X.-S. Wang, M. Chrzanowski, W.-Y. Gao, L. Wojtas, Y.-S. Chen, M. J. Zaworotko, S. Ma, *Chem. Sci.* **2012**, *3*, 2823-2827.
- 60 J. Bacsá, R. J. Less, H. E. Skelton, Z. Soracevic, A. Steiner, T. C. Wilson, P. T. Wood, D. S. Wright, *Angew. Chem. Int. Ed.* **2011**, *50*, 8279-8282.
- 61 O. J. Scherer, H. Sitzmann, G. Wolmershaeuser, *Angew. Chem.* **1985**, *97*, 358-359.
- 62 O. J. Scherer, R. Winter, G. Wolmershaeuser, *Z. Anorg. Allg. Chem.* **1993**, *619*, 827-835.
- 63 O. J. Scherer, T. Brueck, *Angew. Chem.* **1987**, *99*, 59.
- 64 a) C. Heindl, *Dissertation* **2015**, b) M. Fleischmann, C. Heindl, M. Seidl, G. Balazs, A. V. Virovets, E. V. Peresyphkina, M. Tsunoda, F. P. Gabbai, M. Scheer, *Angew. Chem. Int. Ed.* **2012**, *51*, 9918-9921, c) O. J. Scherer, H. Sitzmann, G. Wolmershaeuser, *J. Organomet. Chem.* **1984**, *268*, C9-C12.
- 65 a) F. Dielmann, E. V. Peresyphkina, B. Kraemer, F. Hastreiter, B. P. Johnson, M. Zabel, C. Heindl, M. Scheer, *Angew. Chem. Int. Ed.* **2016**, *55*, 14833-14837; b) C. Heindl, E. V. Peresyphkina, D. Luedeker, G. Brunklaus, A. V. Virovets, M. Scheer, *Chem. Eur. J.* **2016**, *22*, 2599-2604; c) M. Fleischmann, S. Welsch, E. V. Peresyphkina, A. V. Virovets, M. Scheer, *Chem. Eur. J.* **2015**, *21*, 14332-14336; d) L. J. Gregoriades, B. K. Wegley, M. Sierka, E. Brunner, C. Groeger, E. V. Peresyphkina, A. V. Virovets, M. Zabel, M. Scheer, *Chem. Asian J.* **2009**, *4*, 1578-1587
- 66 a) M. Elsayed Moussa, M. Fleischmann, E. V. Peresyphkina, L. Duetsch, M. Seidl, G. Balazs, M. Scheer, *Eur. J. Inorg. Chem.* **2017**, *2017*, 3222-3226; b) M. Scheer, L. J. Gregoriades, M. Zabel, J. Bai, I. Krossing, G. Brunklaus, H. Eckert, *Chem. Eur. J.* **2008**, *14*, 282-295; c) M. Scheer, L. Gregoriades, J. Bai, M. Sierka, G. Brunklaus, H. Eckert, *Chem. Eur. J.* **2005**, *11*, 2163-2169; d) J. Bai, E. Leiner, M. Scheer, *Angew. Chem. Int. Ed.* **2002**, *41*, 783-786.
- 67 C. Heindl, *Dissertation* **2015**.
- 68 C. Schwarzmaier, A. Schindler, C. Heindl, S. Scheuermayer, E. V. Peresyphkina, A. V. Virovets, M. Neumeier, R. Gschwind, M. Scheer, *Angew. Chem. Int. Ed.* **2013**, *52*, 10896-10899.
- 69 A. Schindler, C. Heindl, G. Balazs, C. Groeger, A. V. Virovets, E. V. Peresyphkina, M. Scheer, *Chem. Eur. J.* **2012**, *18*, 829-835.
- 70 M. Scheer, A. Schindler, R. Merkle, B. P. Johnson, M. Linseis, R. Winter, C. E. Anson, A. V. Virovets, *J. Am. Chem. Soc.* **2007**, *129*, 13386-13387.
- 71 E. Peresyphkina, C. Heindl, A. Virovets, H. Brake, E. Maedl, M. Scheer, *Chem. Eur. J.* **2018**, *24*, 2503-2508.
- 72 The diameter on the level of the Cp residues were calculated as the distance of one methylene-C atom to the center of two opposing methylene-C atoms plus twice the van der Waals radius of C (170 pm from A. Bondi, *J. Phys. Chem.* **1964**, *68*, 441-451).
- 73 S. Heinl, E. Peresyphkina, J. Sutter, M. Scheer, *Angew. Chem. Int. Ed.* **2015**, *54*, 13431-13435.
- 74 F. Dielmann, E. V. Peresyphkina, B. Kraemer, F. Hastreiter, B. P. Johnson, M. Zabel, C. Heindl, M. Scheer, *Angew. Chem. Int. Ed.* **2016**, *55*, 14833-14837.

- <sup>75</sup> M. Scheer, A. Schindler, C. Groeger, A. V. Virovets, E. V. Peresypkina, *Angew. Chem. Int. Ed.* **2009**, *48*, 5046-5049.
- <sup>76</sup> S. Welsch, C. Groeger, M. Sierka, M. Scheer, *Angew. Chem. Int. Ed.* **2011**, *50*, 1435-1438.
- <sup>77</sup> F. Dielmann, M. Fleischmann, C. Heindl, E. V. Peresypkina, A. V. Virovets, R. M. Gschwind, M. Scheer, *Chem. Eur. J.* **2015**, *21*, 6208-6214.
- <sup>78</sup> C. Heindl, E. Peresypkina, A. V. Virovets, I. S. Bushmarinov, M. G. Medvedev, B. Kraemer, B. Dittrich, M. Scheer, *Angew. Chem. Int. Ed.* **2017**, *56*, 13237-13243.
- <sup>79</sup> a) M. Elsayed Moussa, B. Attenberger, M. Seidl, A. Schreiner, M. Scheer, *Eur. J. Inorg. Chem.* **2017**, *2017*, 5616-5620; b) M. Elsayed Moussa, B. Attenberger, E. V. Peresypkina, M. Fleischmann, G. Balazs, M. Scheer, *Chem. Commun.* **2016**, *52*, 10004-10007; c) B. Attenberger, E. V. Peresypkina, M. Scheer, *Inorg. Chem.* **2015**, *54*, 7021-7029; d) B. Attenberger, S. Welsch, M. Zabel, E. Peresypkina, M. Scheer, *Angew. Chem. Int. Ed.* **2011**, *50*, 11516-11519.
- <sup>80</sup> M. E. Moussa, M. Seidl, G. Balazs, M. Zabel, A. V. Virovets, B. Attenberger, A. Schreiner, M. Scheer, *Chem. Eur. J.* **2017**, *23*, 16199-16203.

## 2. Research Objectives

Up to now, the formation of spherical aggregates based on the self-assembly of  $[\text{Cp}^{\text{R}}\text{Fe}(\eta^5\text{-P}_5)]$  and coinage metal salts was restricted to  $\text{CuX}$  ( $\text{X} = \text{Cl}, \text{Br}, \text{I}$ ) or  $\text{CuBr}_2$ . One recently examined exception from this, is the use of  $\text{CuSO}_3\text{CF}_3$  along with  $[\text{Cp}^{\text{Bn}}\text{Fe}(\eta^5\text{-P}_5)]$  to construct a highly symmetric spherical scaffold, as it is described in the introductory part. This result opens the door to a so far unexplored field: the self-assembly of pentaphosphaferrocene derivatives with coinage metal salts of weakly coordinating anions. Moreover, due to the limited solubility of Ag halides in organic solvents, no spherical assemblies based on  $[\text{Cp}^{\text{R}}\text{Fe}(\eta^5\text{-P}_5)]$  and Ag salts are known so far. The use of weakly coordinating anions however, promises to extend this self-assembly approach from Cu to Ag salts. Thus, research objectives of this thesis are:

- Transferring synthetic approaches to obtain spherical supramolecules from Cu to Ag.
- Investigation of the coordination behaviour of  $[\text{Cp}^{\text{R}}\text{Fe}(\eta^5\text{-P}_5)]$  ( $\text{Cp}^{\text{R}} = \text{Cp}^*, \text{Cp}^{\text{Bn}}$ ) towards  $\text{AgSO}_3\text{CF}_3$ .
- Establishing the self-assembly approach of  $[\text{Cp}^{\text{R}}\text{Fe}(\eta^5\text{-P}_5)]$  together with Ag salts of weakly coordinating anions.

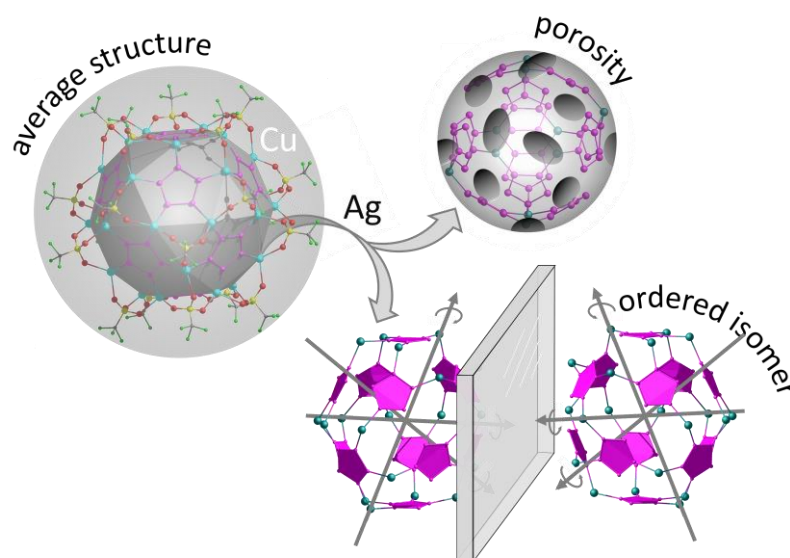
As the use of weakly coordinating anions would generate a free coordination site on the scaffold- or framework-building metal atom, the idea came to mind of applying a three-component self-assembly approach. With the  $\text{P}_n$  complex  $[\{\text{Cp}^*\text{Mo}(\text{CO})_2\}_2(\mu, \eta^{2:2}\text{-P}_2)]$ , this method involving Ag salts and organic linkers furnished astonishing results as outlined in the introductory part. Involving pentaphosphaferrocene, with its preference to build spherical scaffolds, could lead to novel frameworks of connected supramolecular aggregates. Furthermore, the property of these scaffolds to act as hosts for smaller molecules could be transferred from discrete supramolecules to polymeric compounds. Hence, a further objective of this work is:

- Investigating a three-component self-assembly approach involving  $[\text{Cp}^{\text{R}}\text{Fe}(\eta^5\text{-P}_5)]$  ( $\text{Cp}^{\text{R}} = \text{Cp}^*, \text{Cp}^{\text{Bn}}$ ), coinage metal salts of weakly coordinating anions and organic linkers.

### 3. Nano-Sized Spheres: Towards the first Ag/P<sub>n</sub> ligand based Self-Assembly Systems

B. Hiltl, E. Peresykina, C. Heini, A. V. Virovets, J. Hilgert, F. Hastreiter, W. Kremer, W. Tremel, R. Gschwind, M. Scheer

#### Graphical Abstract



#### Abstract:

Recently, the self-assembly system of pentaphosphaferrocenes  $[\text{Cp}^R\text{Fe}(\eta^5\text{-P}_5)]$  ( $\text{Cp}^R = \text{Cp}^*$ ,  $\text{Cp}^{\text{Bn}}$ ) and Cu halides, was successfully expanded by the use of  $\text{CuSO}_3\text{CF}_3$ . The functional anion  $\text{SO}_3\text{CF}_3^-$  showed its decisive scaffold building role in the formation of an unprecedented spherical supramolecule. Herein the effective transfer of this strategy from Cu- to Ag-based systems is demonstrated by using  $\text{AgSO}_3\text{CF}_3$  and  $\text{AgSO}_3\text{C}_7\text{H}_7$ . Due to the larger radii of the scaffold-building metal atoms, along with their different binding properties, these silver salts allowed together with  $[\text{Cp}^R\text{Fe}(\eta^5\text{-P}_5)]$  ( $\text{Cp}^R = \text{Cp}^*$  (**1a**),  $\text{Cp}^{\text{Bn}}$  (**1b**)), the formation of a series of unprecedented spherical host-guest aggregates. These show similarities as well as striking differences and novel structural features compared to Cu-containing spheres. Thus, the icosahedral  $[\text{Cp}^*\text{Fe}(\eta^5\text{-P}_5)]@[\{\text{Cp}^*\text{Fe}(\eta^5\text{-P}_5)\}_{12}(\text{AgSO}_3\text{CF}_3)_x]$  ( $x \approx 10$ ) (**3a**), resembling 80-vertex spheres, or the isomeric icosidodecahedral  $[\{\text{Cp}^*\text{Fe}(\eta^5\text{-P}_5)\}(\text{C}_7\text{H}_8)]@[\{\text{Cp}^*\text{Fe}(\eta^5\text{-P}_5)\}_{12}(\text{AgSO}_3\text{CF}_3)_{20}]$  (**3b**), as well as  $[\text{Cp}^*\text{Fe}(\eta^5\text{-P}_5)]@[\{\text{Cp}^*\text{Fe}(\eta^5\text{-P}_5)\}_{12}\{\text{Ag}_{18}(\text{Ag}(\text{CH}_3\text{CN}))_8(\text{SO}_3\text{C}_7\text{H}_7)_{20}\}[\text{SO}_3\text{C}_7\text{H}_7]_6]$  (**4**), and  $[\{\text{Cp}^{\text{Bn}}\text{Fe}(\eta^5\text{-P}_5)\}_{12}(\text{AgSO}_3\text{CF}_3)_{20}]$  (**5**) are synthesized and characterized. For the first time, the good stability of **5** in solution allowed the sample preparation for transmission electron microscopy and thus, the visualization of polyphosphorus-based spherical aggregates.

### 3.1 Introduction

In the past decades, diverse methods to create discrete spherical aggregates targeting different purposes have emerged from the fast-growing field of supramolecular chemistry. Regarding OD atomic precise clusters as a link between metal atoms and nanoparticles,<sup>1</sup> especially for Ag and Cu many different types are known, the metal core itself being protected from aggregation by thiolates, phosphines or alkynyls.<sup>2</sup> A compound with an Ag<sub>490</sub> core from the group of Fenske stands out from this vast class of compounds as the record holder with the highest metal atom count.<sup>15a</sup> Another class of discrete spheres aims at characteristics and applications, which go along with properties of hollow spheres being able to act as hosts for smaller molecules. Some of them are suitable as reaction vessels,<sup>3</sup> molecular container stabilizing labile compounds<sup>4</sup> or accelerators for catalytic reactions<sup>5</sup> by providing an adequate inner void. These self-assembled supramolecular aggregates often show highly symmetric polyhedral scaffolds, built up by various metal cations (Co,<sup>6</sup> Pd,<sup>7,8</sup> Pt,<sup>9</sup> Cu,<sup>40b,10</sup> Ag,<sup>43a,11</sup> Zn,<sup>12</sup> Cd<sup>40b</sup>) as vertices and mainly polytopic organic linkers as edges or faces. One example of this tremendous field is shown in *Figure 1a*. Notably, while there is a huge number of Pd-, Pt- and Cu- containing spherical supramolecular cages, the examples involving Ag<sup>+</sup> are still very rare in contrast to the abundance of Ag-containing spherical clusters without an accessible inner void. Recently, with an Ag<sub>180</sub> buckyball-like cage the group of Sun reported a combination of both classes, clusters with a protected metal core and self-assembled supramolecular spheres (*Figure 1b*). The Ag core is protected by iPrS<sup>-</sup> and SO<sub>3</sub>CH<sub>3</sub><sup>-</sup> and, in contrast to many cluster compounds, exhibits an icosahedral symmetry as well as an inner cavity like other cage compounds, which in this case is filled with solvent molecules.<sup>13</sup>

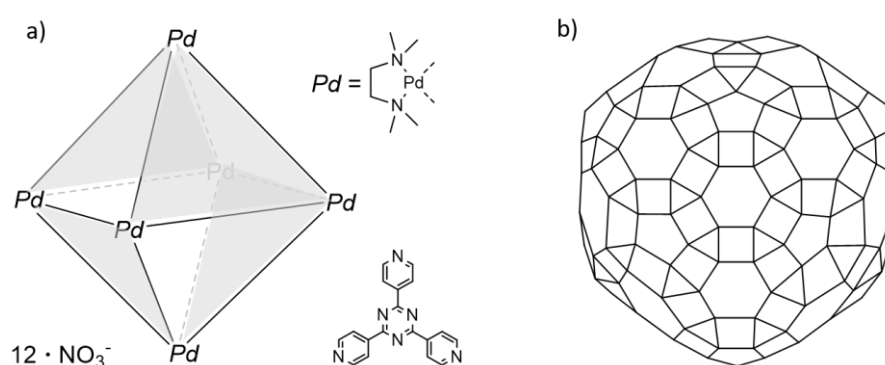


**Figure 1:** a) Discrete Pd<sup>2+</sup> containing cage molecule by Fujita et al.,<sup>41d</sup> b) schematic Ag...Ag connectivity of the Ag<sub>180</sub> core by Sun et al.<sup>13</sup>

Using the five-fold symmetric organometallic building block [Cp<sup>R</sup>Fe(η<sup>5</sup>-P<sub>5</sub>)] (**1**) in combination with Cu salts, in the past our group succeeded in synthesizing huge nano-scaled hollow self-assembled aggregates,<sup>14</sup> partly exhibiting fullerene-topology<sup>15</sup> and in characterizing them by X-ray

crystallography. With their inner cavity, they can act as versatile hosts for small guest molecules or stabilize labile molecules like P<sub>4</sub> and As<sub>4</sub>.<sup>16</sup>

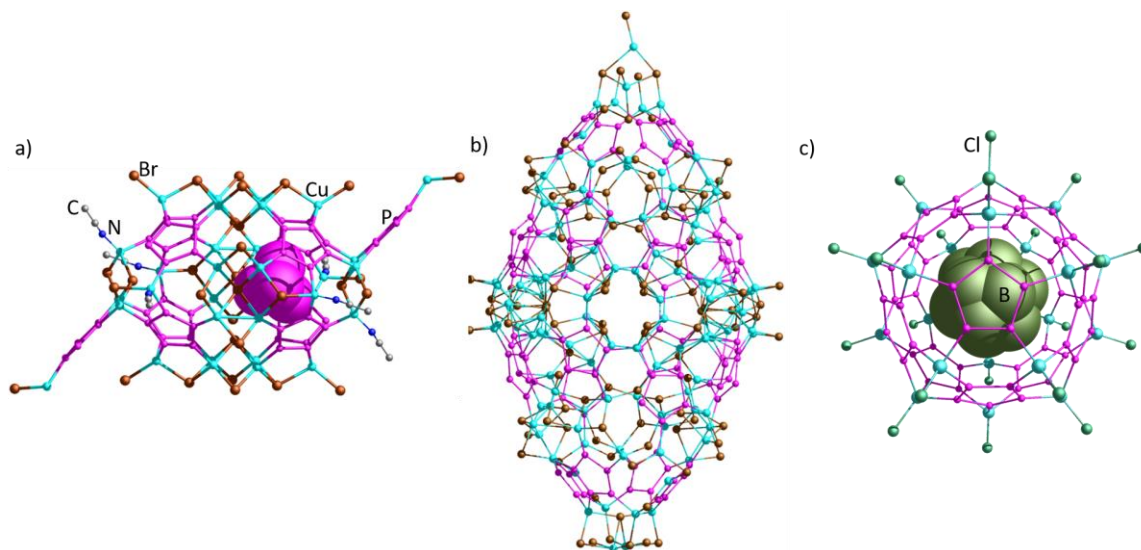
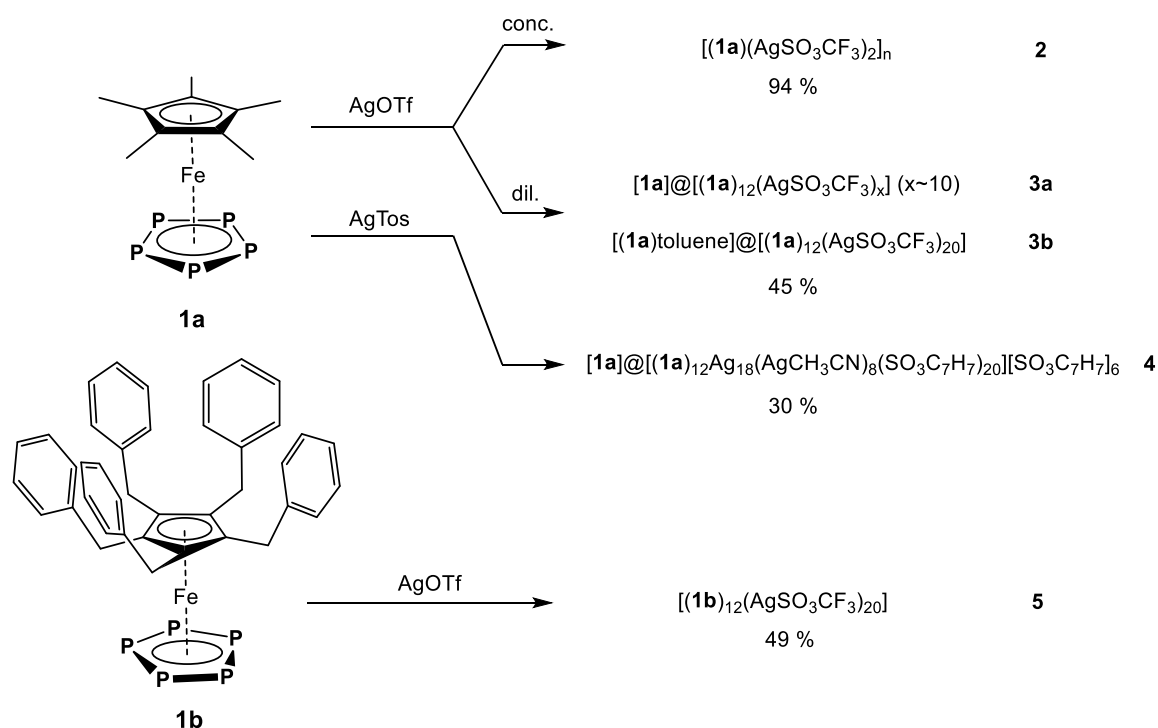


**Figure 2:** Selected discrete supramolecules based on **1**: a)  $P_4@[\{Cp^*Fe(\eta^5-P_5)\}_{10}Cu_{30}l_{30}(MeCN)_6]$ ,<sup>14d</sup> b)  $[\{Cp^{Bn}Fe(\eta^5-P_5)\}_{24}Cu_{96}Br_{96}]$ ,<sup>16b</sup> c)  $C_2B_{10}H_{12}@[\{Cp^*Fe(\eta^5-P_5)\}_{12}(CuCl)_{20}]$ <sup>15b</sup> with templates shown in space filling model.

The field of spherical compounds based on **1** was so far restricted to Cu as scaffold-building cations. Implementing other coinage metal cations like Ag<sup>+</sup> has not been successful until now, due to the poor solubility of the halide salts. Recently, we showed that also the use of functional anions like SO<sub>3</sub>CF<sub>3</sub><sup>−</sup> can result in self-assembled spheres by acting as an additional scaffold building block.<sup>17</sup> The use of this type of anion would offer well-soluble silver salts and therefore, the question arose if this approach would allow to involve Ag in spherical supramolecular scaffolds similarly to Cu, and how this change would affect the structural features of these assemblies. In the following, we report on the successful application of the soluble salts AgSO<sub>3</sub>CF<sub>3</sub> (AgOTf) and the bulkier AgSO<sub>3</sub>C<sub>7</sub>H<sub>7</sub> (AgTos) in the coordination chemistry of [Cp<sup>R</sup>Fe(η<sup>5</sup>-P<sub>5</sub>)] (Cp<sup>R</sup>= Cp\* (**1a**), Cp<sup>Bn</sup> (**1b**)) yielding in the self-assembly of the first Ag-containing spherical supramolecules based on P<sub>n</sub> ligands. Besides the characterization by X-ray crystallography, NMR spectroscopy and MS, the remarkable stability of some herein described spherical aggregates in solution enabled DOSY NMR spectroscopy and the sample preparation for investigation by transmission electron microscopy (TEM). Thus nano-scaled P<sub>n</sub>-containing supramolecules were visualised for the first time.

### 3.2 Results and Discussion

A solution of AgOTf or AgTos in CH<sub>2</sub>Cl<sub>2</sub> is carefully layered with a solution of **1a** in toluene. In the case of AgOTf, the formation of the supramolecular products is strongly dependent on the dilution of the reactants. When a minimum concentration of 0.04 mol/L of AgOTf and 0.016 mol/L of [Cp\*Fe(η<sup>5</sup>-P<sub>5</sub>)] is applied in the respective layers, the crystalline 2D polymer [{Cp\*Fe(μ<sub>4</sub>,η<sup>5:1:1:1</sup>-P<sub>5</sub>)}(AgSO<sub>3</sub>CF<sub>3</sub>)<sub>2</sub>]<sub>n</sub> (**2**) forms during the diffusion process. By diluting the respective reactant solutions by a minimum factor of 4, the crystallization of the isomeric supramolecules [Cp\*Fe(η<sup>5</sup>-P<sub>5</sub>)]@[{Cp\*Fe(η<sup>5</sup>-P<sub>5</sub>)}<sub>12</sub>(AgSO<sub>3</sub>CF<sub>3</sub>)<sub>x</sub>] (x ≈ 10) (**3a**) and [Cp\*Fe(η<sup>5</sup>-P<sub>5</sub>)](C<sub>7</sub>H<sub>8</sub>)@[{Cp\*Fe(η<sup>5</sup>-P<sub>5</sub>)}<sub>12</sub>(AgSO<sub>3</sub>CF<sub>3</sub>)<sub>20</sub>] (**3b**) is observed, whereas **3b** represents the main product. **3a** is only obtained sporadically, mainly co-crystallized with **3b** and its formation cannot be controlled objectively, regardless several attempts. The crystallization of **2** as minor byproduct was only observed sometimes and could be completely avoided by using even more diluted solutions in favor to the products **3a** and **b**. By using AgTos, the completely diffused reactant phases are layered with pentane for crystallization. After a few days, the formation of crystalline [Cp\*Fe(η<sup>5</sup>-P<sub>5</sub>)]@[{Cp\*Fe(η<sup>5</sup>-P<sub>5</sub>)}<sub>12</sub>Ag<sub>18</sub>(Ag(CH<sub>3</sub>CN))<sub>8</sub>(SO<sub>3</sub>C<sub>7</sub>H<sub>7</sub>)<sub>20</sub>][SO<sub>3</sub>C<sub>7</sub>H<sub>7</sub>]<sub>6</sub> (**4**) can be observed. On the other hand, the layering of **1b** with AgOTf fortunately always leads selectively to the formation of the discrete spherical supramolecule [{Cp<sup>Bn</sup>Fe(η<sup>5</sup>-P<sub>5</sub>)}<sub>12</sub>(AgSO<sub>3</sub>CF<sub>3</sub>)<sub>20</sub>] (**5**). All compounds were obtained in moderate to excellent crystalline yields and characterized by X-ray structure analysis.



**Scheme 1:** Reactions of **1a** and **1b** with AgOTf and AgTos.

In the 2D network **2** (Figure 3a) the *cyclo*-P<sub>5</sub> ligands show a 1,2,4-coordination mode to the Ag atoms, which in turn possess a tetrahedral environment (2 × O, 2 × P or 3 × O, 1 × P). The OTf<sup>-</sup> anions act in equal parts as μ<sub>2</sub>- or μ<sub>3</sub>-bridging ligands *via* coordination of two oxygen atoms to silver. Thereby, four-membered {Ag<sub>2</sub>O<sub>2</sub>}, six-membered {Ag<sub>2</sub>P<sub>4</sub>} and eight-membered {Ag<sub>2</sub>O<sub>4</sub>S<sub>2</sub>} rings are formed within the network. Noteworthy, toluene molecules are intercalated between the layers, explaining the rapid amorphization of crystalline **2** when removed from the mother liquor. The almost parallel arrangement (0.6°) and the short interplanar distance of toluene and the *cyclo*-P<sub>5</sub> ligands (3.43 Å) indicate π-π stacking interactions (Figure 3b).

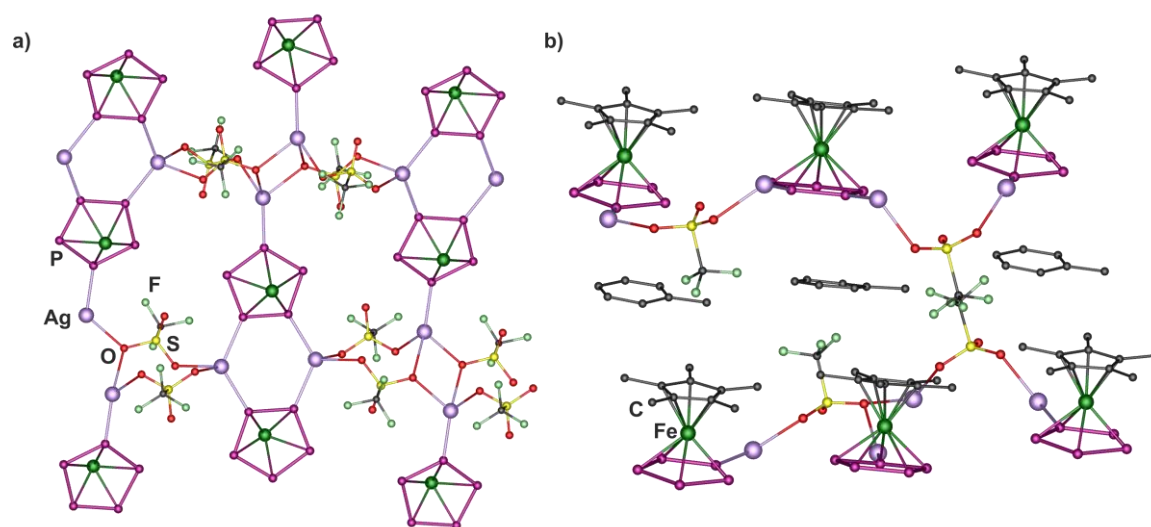


**Figure 3:** a) Section of the 2D network **2**; b) Illustration of the π-π-interaction between intercalated toluene molecules and the *cyclo*-P<sub>5</sub> ligands. Cp\* ligands and H atoms are partly omitted for clarity.

Compounds **3a** and **3b** both show discrete spherical host-guest assemblies. Their idealized frameworks are built up by 12 units of **1a**, 20 Ag<sup>+</sup> and 20 OTf<sup>-</sup>. However, the experimentally obtained composition of their scaffolds differs from the idealized one. In **3a**, this fact results from the partial occupancies of {AgOSO<sub>2</sub>CF<sub>3</sub>} units, leading to a tentative composition of the scaffold [{Cp\*Fe(η<sup>5</sup>-P<sub>5</sub>)}]<sub>12</sub>(AgSO<sub>3</sub>CF<sub>3</sub>)<sub>x</sub> (x ≈ 10). The ten positions, which are available, but not occupied by Ag<sup>+</sup>, according to the sum formula, cause 12-membered rings {Ag<sub>3</sub>P<sub>9</sub>} in the actual scaffold of **3a**. However, these ~ 10 Ag cations are disordered over 20 available positions, leading to different isomeric scaffolds. Thus, the coordination mode of the scaffold building ligands **1a** cannot be discussed in detail. One of the possible isomeric scaffolds is shown in Figure 4b, with 1,2-, 1,3- and 1,2,4-coordination modes of **1a**. However, all Ag atoms show a tetrahedral coordination environment of 3 × P and 1 × O atoms, resulting from the end-on coordination of the OTf<sup>-</sup> anions. In Figure 4a, the idealized scaffold with x = 20 is depicted with its incorporated guest **1a**, and the twelve *cyclo*-P<sub>5</sub> ligands situated at the vertices of an icosahedron. These structural characteristics underline the relation of **3a** to previously reported 80-vertex spheres, based on Cu halides.<sup>15b,18</sup> For



$[\{\text{Cp}^{\text{Bn}}\text{Fe}(\eta^5\text{-P}_5)\}_{12}(\text{CuBr})_{20-n}]$  was found that the CuX positions show partial occupancies, similar to **3a** ranging from  $n = 0 - 4.8$ . Thus the minimum of CuX content in a spherical 80-vertex observed by X-ray structure analysis was found to be 15 in the case of  $[\{\text{Cp}^{\text{Bn}}\text{Fe}(\eta^5\text{-P}_5)\}_{12}(\text{CuBr})_{20-n}]$ .<sup>18</sup> Therefore, the Ag-based **3a** featuring about 10 metal vacancies, represents the most porous 80-vertex host scaffold obtained so far.

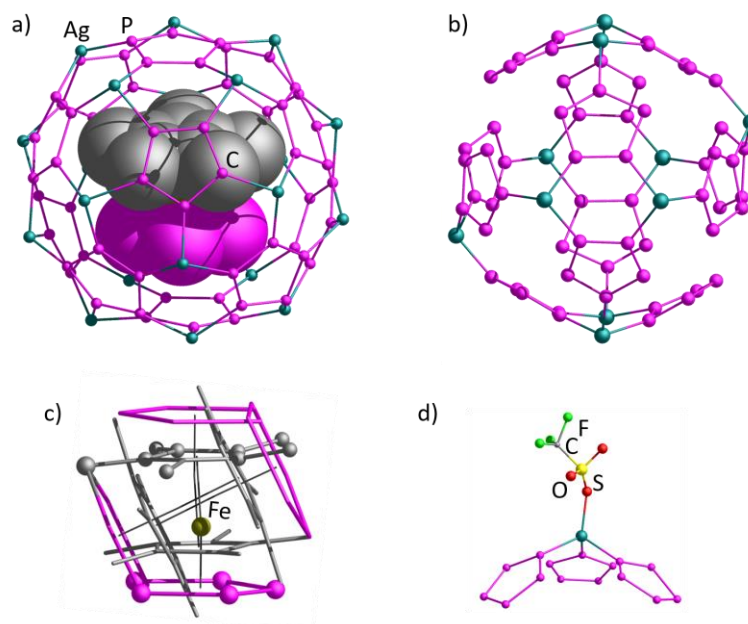


**Figure 4:** a) Idealized scaffold of **3a** with guest molecule **1a** shown in space-filling model, b) one possible isomeric scaffold (**1a**<sub>12</sub>Ag<sub>10</sub>) c) disordering of guest **1a** over four positions, d) end-on coordination mode of SO<sub>3</sub>CF<sub>3</sub><sup>-</sup>.

Compound **3b** with a sum formula of  $[\{\text{Cp}^*\text{Fe}(\eta^5\text{-P}_5)\}(\text{toluene})]@[\{\text{Cp}^*\text{Fe}(\eta^5\text{-P}_5)\}_{12}\{\text{Ag}(\text{SO}_3\text{CF}_3)\}_{20}]$  (**3b**) crystallizes with two crystallographically unique spherical supramolecules in the unit cell. Interestingly, one of them is ordered, whereas the other one shows disordering over at least three positions, with the major component amounting to about 85 - 86%, according to preliminary data. Gratifyingly, it generally represents the first example of a spherical supramolecule based on **1** and coinage metal salts mostly showing ordering in the solid state. Most previously reported compounds were refined as idealized or average structures and described as solid solutions of different isomers or similar molecules with varying metal content.<sup>13,19</sup> For instance in the scaffold of the recently presented isostructural Cu-containing compound  $[\{\text{Cp}^{\text{Bn}}\text{Fe}(\eta^5\text{-P}_5)\}_{12}(\text{CuSO}_3\text{CF}_3)_{20-n}]$  ( $n = 0.4$ ) the Cu<sup>+</sup> atoms are statistically distributed over 30 positions.<sup>17</sup> To specify the vacancies of Cu<sup>+</sup> and SO<sub>3</sub>CF<sub>3</sub><sup>-</sup>, this compound was described as a mixture of spheres with different values of  $n$  and thus different porosities. For the idealized complete sphere with  $n = 0$   $[\{\text{Cp}^{\text{Bn}}\text{Fe}(\eta^5\text{-P}_5)\}_{12}(\text{CuSO}_3\text{CF}_3)_{20}]$  the molecular structure of possible isomers was reconstructed to give four isomers of  $D_2$  and  $D_5$  point group symmetries, and DFT calculations were performed to optimize their

geometry and relative stability. The arrangement of the 12 *cyclo*-P<sub>5</sub> ligands in the ordered supramolecule of **3b** shows a distorted icosahedral symmetry  $I_h$  (Figure 5), similar to  $[\{\text{Cp}^{\text{Bn}}\text{Fe}(\eta^5\text{-P}_5)\}_{12}(\text{CuSO}_3\text{CF}_3)_{19,6}]$  and many further spheres based on **1**.<sup>14a,e;15a-b</sup> Ten of the ligands **1a** coordinate to Ag<sup>+</sup> in a 1,2,4-mode, whereas two coordinate in a 1,2,3,4-fashion (Figure 5b). The Ag<sup>+</sup> atoms in **3b** are all tetrahedrally coordinated by two P atoms of two different *cyclo*-P<sub>5</sub> ligands and two O atoms of different SO<sub>3</sub>CF<sub>3</sub> anions, whereas the latter act as  $\mu_2$ -bridging ligands. These features imply that the ordered scaffold of **3b** shows ten intrinsic 14-membered {Ag<sub>4</sub>P<sub>10</sub>} rings (Figure 5c) and possesses a similar structure of the inorganic scaffold as the  $D_2$  isomer of  $[\{\text{Cp}^{\text{Bn}}\text{Fe}(\eta^5\text{-P}_5)\}_{12}(\text{CuSO}_3\text{CF}_3)_{20}]$  theoretically reconstructed from an average structure. In contrast to the Cu-analogue, the inorganic scaffold of **3b** is remarkably distorted compared to the almost spherical supramolecules of  $[\{\text{Cp}^{\text{Bn}}\text{Fe}(\eta^5\text{-P}_5)\}_{12}(\text{CuSO}_3\text{CF}_3)_{19,6}]$ . This can be illustrated considering the 14-membered {P<sub>10</sub>M<sub>4</sub>} rings in **3b** and the  $D_2$  isomer of the Cu-containing compound (Figure 5c,d). In the Cu case the difference between non-valent intramolecular P...P contacts with and without Cu-bridges is only 0.2 Å, due to the short average Cu-P bond lengths of 2.16 Å, leading to a uniform architecture. In contrast to this, due to the larger covalent radius of Ag and therefore longer Ag-P bonds ( $d_{\text{av}}(\text{Ag-P}) = 2.46$  Å (**3b**)), the distances between Ag-bridged *cyclo*-P<sub>5</sub> ligands is about 0.6 Å longer than those non-valent contacts between two unbridged *cyclo*-P<sub>5</sub> ligands. This induces a distortion of the 14-membered rings and, as a consequence, the ellipsoidal-shaped inorganic scaffold of **3b**. The outer diameter of the supramolecule **3b** reaches 2.5 nm.<sup>20</sup>

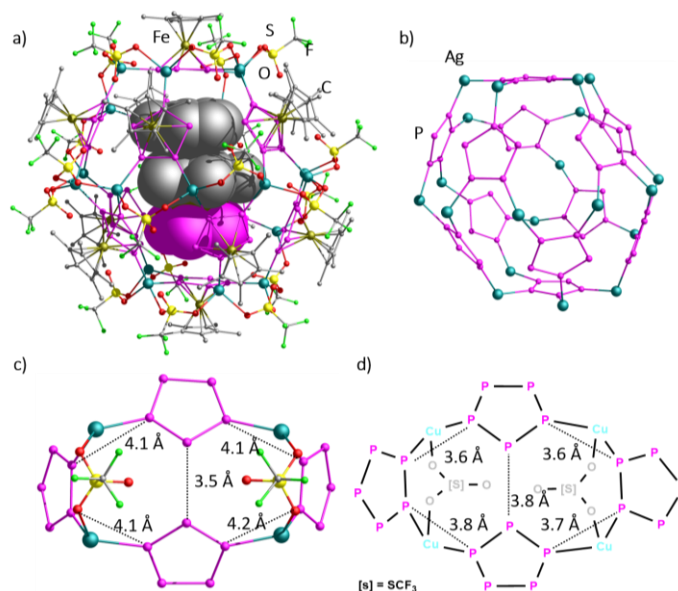


**Figure 5:** a) Supramolecule **3b** with guest molecules shown in space-filling style. H atoms and minor parts of disordered Cp\* and CF<sub>3</sub> groups are omitted for clarity; b) ellipsoidal scaffold Ag<sub>20</sub>P<sub>60</sub> of **3b**. 14-membered {M<sub>4</sub>P<sub>10</sub>} rings with bridging OTf and non-valent P...P contacts c) in the ordered molecule of **3b** (M = Ag) and d) in  $[\{\text{Cp}^{\text{Bn}}\text{Fe}(\eta^5\text{-P}_5)\}_{12}(\text{CuSO}_3\text{CF}_3)_{20}]$  optimized by DFT methods (M = Cu, schematic representation).<sup>17</sup>

The provided inner cavities of **3a** and **3b** with diameter of 8.1 Å (**3a**) and 10.4 Å (**3b**) are both occupied with one molecule of **1a**, showing a length of 7.0 Å.<sup>21</sup> In both cases the guest molecule is shifted from the center of the cavity, because of  $\pi$ -stacking interactions indicated by short interplanar distances of the *cyclo*-P<sub>5</sub> ligands of the guest and the host molecule (3.8 Å (**3b**)). For **3a**, no exact distances can be given due the fact that the scaffold is severely disordered, involving even molecules of **1a**. In the case of **3b**, the larger inner void fits an additional molecule of toluene (C<sub>7</sub>H<sub>8</sub>) between the Cp\* group of the guest and one of the *cyclo*-P<sub>5</sub> moieties of the host molecule (*Figure 5a*), stabilized by  $\pi$ - $\pi$  interactions to both sides ( $d(\text{P}_5^{\text{host}}\text{-toluene}) = 3.66 \text{ \AA}$ ,  $d(\text{Cp}^*\text{guest-toluene}) = 3.44 \text{ \AA}$ ). This represents the first supramolecular assembly found to be incorporated by spherical supramolecules based on P<sub>n</sub> complexes.

With AgTos, a bulkier sulfonyl anion was applied as a comparison to OTf. Upon combining the building blocks **1a** and AgTos, another supramolecular host-guest assembly **4** is formed, however possessing similar features as **3b** (*Figure 6*). The scaffold of **4** contains 12 units of **1a** and 26 Ag<sup>+</sup> atoms. Furthermore, 12 nine-membered {Ag<sub>2</sub>P<sub>6</sub>} rings and four 14-membered {Ag<sub>4</sub>P<sub>10</sub>} rings occur in the scaffold similar to that in **3b**. With only 20 Tos<sup>-</sup> coordinating in a maximum  $\mu^3$ -capping fashion towards the scaffold building Ag atoms, a 6-fold positively charged host-guest assembly  $[\text{Cp}^*\text{Fe}(\eta^5\text{-P}_5)]@[\{\text{Cp}^*\text{Fe}(\eta^5\text{-P}_5)\}_{12}\{\text{Ag}_{18}(\text{Ag}(\text{CH}_3\text{CN}))_8(\text{SO}_3\text{C}_7\text{H}_7)_{20}\}]^{6+}$  results. The charge is compensated by additional 6 Tos<sup>-</sup> anions of the outer sphere. Moreover, eight Ag<sup>+</sup> atoms of the scaffold are coordinated by additional CH<sub>3</sub>CN ligands. This leads to different coordination environments of Ag: either tetrahedral (18 Ag: 3  $\times$  P, 1  $\times$  O) or trigonal planar (8 Ag: 2  $\times$  P, 1  $\times$  O) with two additional long contacts to O atoms of neighboring Tos<sup>-</sup> anions (2.5 – 2.7 Å) increasing the coordination sphere to trigonal bipyramidal. The *cyclo*-P<sub>5</sub> ligands, however show 1,2,4-, 1,2,3,4- and 1,2,3,4,5-coordination modes towards scaffold building Ag atoms. Moreover, **4** incorporates one molecule **1a**, which is disordered over four positions and in each case orientated with its *cyclo*-P<sub>5</sub> ring towards one of the scaffold building ligands **1a**.

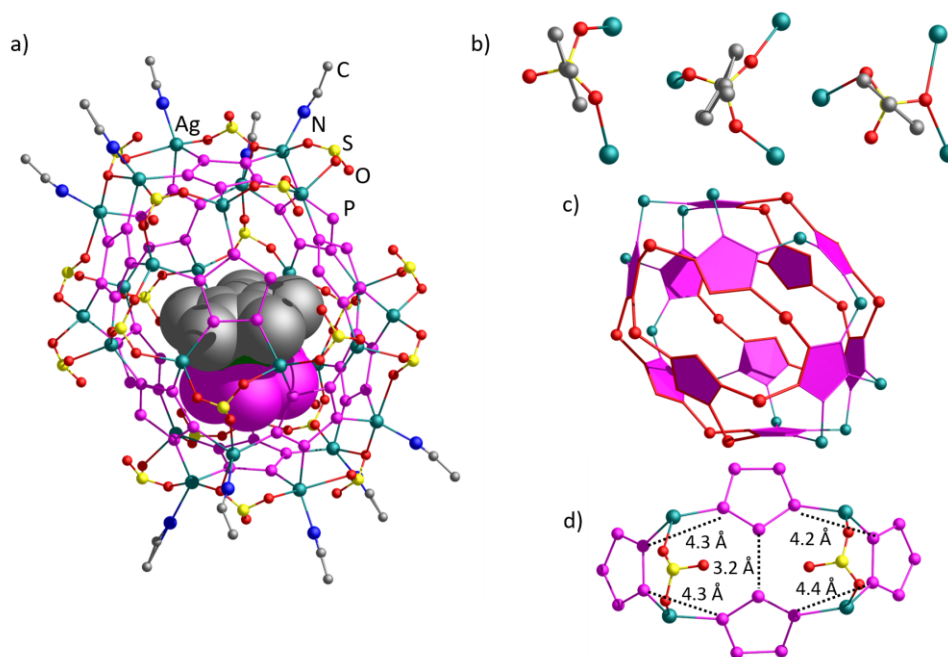


**Figure 6:** a) Supramolecule **4** with guest **1a** shown in space-filling model.  $[\text{Cp}^*\text{Fe}]$  and  $[\text{C}_7\text{H}_7]$  units are omitted for clarity, b) different coordination modes of  $\text{Tos}^-$  anions in **4**, c) inorganic scaffold of **4** with 14-membered  $\{\text{Ag}_4\text{P}_{10}\}$  rings highlighted in red, d) 14-membered  $\{\text{Ag}_4\text{P}_{10}\}$  rings with bridging  $\text{Tos}^-$  and non-valent  $\text{P}\cdots\text{P}$  contacts.

If all ten vacancies in **3a** are hypothetically occupied by  $\{\text{AgOSO}_2\text{CF}_3\}$  units, a 80-vertex sphere would result, analogue to the known icosahedral CuX-based 80 vertex spheres  $[(\mathbf{1})_{12}(\text{CuX})_{20}]$  (Figure 7a).<sup>15b,18</sup> However, if all  $\{\text{Ag}_4\text{P}_{10}\}$  rings of **3b** and **4** would be occupied with  $\text{Ag}^+$  atoms, a ten-fold positively charged imaginary scaffold results in both cases. This features 90 scaffold building atoms and thus underlines its structural similarity to the icosidodecahedral inorganic scaffold of the idealized Cu-containing compound  $[(\text{Cp}^{\text{Bn}}\text{Fe}(\eta^5\text{-P}_5))_{12}(\text{CuSO}_3\text{CF}_3)_{19,6}]$ .<sup>17</sup> To clearly distinguish this type from the known 80- and 90-vertex spheres, actual isomeric scaffolds of **3b** can be referred to as (90-10)-vertex spheres keeping in mind the 10 vacant positions, whereas the more distorted **4** shall be classified as (90-4)-vertex sphere.

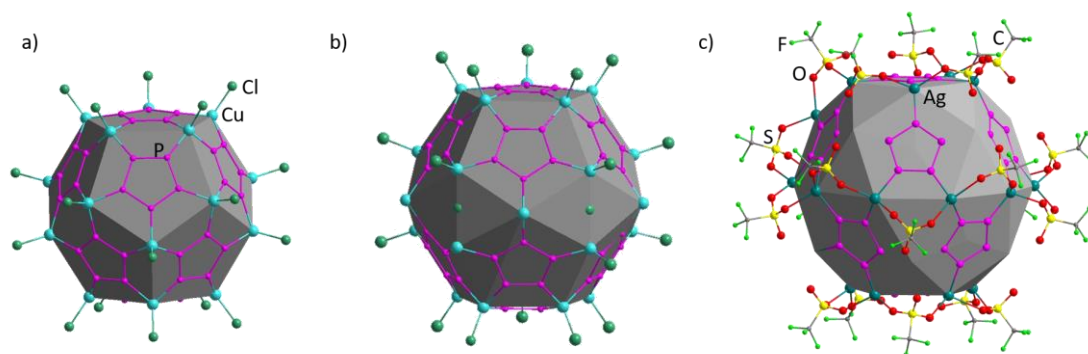


**Figure 7:** Scaffolds of a) icosahedral 80-vertex  $[(\text{Cp}^*\text{Fe}(\eta^5\text{-P}_5))_{12}(\text{CuCl})_{20}]$ ,<sup>15b</sup> b) 90-vertex  $[(\text{Cp}^*\text{Fe}(\eta^5\text{-P}_5))_{12}(\text{CuCl})_{25}(\text{CH}_3\text{CN})_{10}]$ ,<sup>15c</sup> c) (90-10)-vertex **3b** with inscribed icosidodecahedron of theoretical 10-fold positively charged scaffold.

The presence of **1a** as a guest in the inner voids of **3a,b** and **4** invites to compare these diverse, but related scaffolds. Moreover, the encapsulation of **1a** in **3a** is the first example of **1a** encapsulated in a sphere with an idealized 80-vertex scaffold. The earlier reported Cu-based 80-vertex spheres consisting of  $[(\text{Cp}^*\text{Fe}(\eta^5\text{-P}_5))_{12}(\text{CuX})_{20}]$  ( $\text{X} = \text{Cl}, \text{Br}$ ) with an inner diameter of 7.8 Å indeed act as hosts for a variety of small molecules.<sup>16</sup> However, besides the herein mentioned examples, the complex **1a** was only observed as a template in Cu-based 90-vertex spheres  $[(\text{Cp}^*\text{Fe}(\eta^5\text{-P}_5))_{12}(\text{CuX})_{25}(\text{CH}_3\text{CN})_{10}]$  ( $\text{X} = \text{Cl}, \text{Br}$ ) with larger inner diameter of 11.5 Å.<sup>14c</sup> The inclusion of **1a** into the vacant 80-vertex sphere **3a** is thus enabled on the one hand by the slightly larger Ag-P than Cu-P distances ( $d(\text{Ag-P}) = 2.5$  Å (**3a-b**),<sup>22</sup>  $d(\text{Cu-P}) = 2.3$  Å in  $[(\text{Cp}^*\text{Fe}(\eta^5\text{-P}_5))_{12}(\text{CuX})_{20}]$ ) but on the other hand by the intrinsic  $[\text{Ag}_3\text{P}_9]$  pores in the scaffold. Dimensions of reported guests and of inner voids for all spherical compounds based on **1a** discussed herein, along with selected previously reported host-guest assemblies are shown in Table 1.

**Table 1:** Size of the inner voids and of host molecules based on **1a** and templates of herein described compounds and formerly published ones (\* values can slightly vary from preliminary to final structural data).

	$d_{\text{av}}(\text{M-P}) / \text{\AA}$	dimension of inner void / $\text{\AA}^{[a]}$	dimension of templates min, max / $\text{\AA}^{[b]}$
idealized 80-vertex sphere <b>3a</b>	2.5 (Ag-P)*	8.2*	7.0, 9.3 ( <b>1a</b> )
80-vertex sphere $[(\text{Cp}^*\text{Fe}(\eta^5\text{-P}_5))_{12}(\text{CuBr})_{20}]^{16a}$	2.3 (Cu-P)	7.8	6.3, 7.8 ( $\text{Cp}_2\text{Fe}$ )
(90-10)-vertex sphere <b>3b</b>	2.5 (Ag-P)*	9.2 - 10.4*	10.2 ( <b>1a</b> -tol)* <sup>[c]</sup>
(90-4)-vertex sphere <b>4</b>	2.5 (Ag-P)*	10.9*	7.0, 9.3 ( <b>1a</b> )
90-vertex sphere $[(\text{Cp}^*\text{Fe}(\eta^5\text{-P}_5))_{12}(\text{CuBr})_{25}(\text{CH}_3\text{CN})_{10}]^{23}$	2.3 (Cu-P)	11.5	7.0, 9.3 ( <b>1a</b> )

[a] maximal distance or minimal/maximal distance between the centroids of opposing ligands **1** ( $\text{P}_5 \dots \text{P}_5$ ) minus twice the van der Waals radii of phosphorus, [b] minimal or maximal diametral interatomic distance of the non-spherical template molecules plus the corresponding van der Waals radii, [c] total length of supramolecular assembly plus the corresponding van der Waals radii

All compounds containing the Cp\* derivative **1a** (**2-4**) are insoluble in common solvents such as hexane, toluene, CH<sub>2</sub>Cl<sub>2</sub>, thf and Et<sub>2</sub>O. Only in CH<sub>3</sub>CN they are poorly soluble, though accompanied by partial fragmentation of the coordination network. Therefore, in the <sup>1</sup>H NMR spectra and <sup>31</sup>P{<sup>1</sup>H} NMR spectra of **2-4** in CD<sub>3</sub>CN, respectively, the only signals present can be assigned to the fragmented assemblies with **1a** coordinating to some extent to Ag atoms. However, mass spectrometric investigations reveal the presence of at least oligomeric moieties. For example, in the respective cationic ESI MS spectra of **3b** and **4** in CH<sub>3</sub>CN numerous peaks of pentaphosphaferrocene-containing fragments are observed. Thereby, the peaks with the highest mass at *m/z* = 2946.0 (**3b**) and 1425.0 (**4**) can be assigned to  $[\{\text{Cp}^*\text{Fe}(\eta^5\text{-P}_5)\}_3\text{Ag}_8(\text{SO}_3\text{CF}_3)_7]^+$  and  $[\{\text{Cp}^*\text{Fe}(\eta^5\text{-P}_5)\}_3\text{Ag}_2(\text{SO}_3\text{C}_7\text{H}_7)]^+$ , respectively.

The Cp<sup>Bn</sup> derivative **5** reveals many characteristics underlining its structural similarity with (90-10)-vertex **3b** and  $[\{\text{Cp}^{\text{Bn}}\text{Fe}(\eta^5\text{-P}_5)\}_{12}(\text{CuSO}_3\text{CF}_3)_{19.6}]$ .<sup>17</sup> Thus, the average structure exhibits an idealized icosidodecahedral symmetric shape, consisting of 12 *cyclo*-P<sub>5</sub> ligands, about 20 Ag<sup>+</sup> cations, disordered over 30 positions, and about 20 tripodal coordinating OTf (*Figure 8*). Hence, assumedly similar *D*<sub>2</sub> and *D*<sub>5</sub> isomers of **5** exist, like those reconstructed and optimized for the CuOTf-containing sphere and the *D*<sub>2</sub> isomer observed in the crystal structure of **3b**. Like discussed for **3b**, the actual scaffold of **5** is supposed to show an intrinsic ellipsoidal-shaped distortion, when compared to the Cu-based sphere. Due to the preliminary data and the average structure, this distortion could not be concretized, yet. The spherical framework of **5** provides an inner cavity with a diameter of about 9.8 Å, which is most likely filled with disordered CH<sub>2</sub>Cl<sub>2</sub> molecules.<sup>21</sup> Compared with the diameter of **3b** (cf. *Table 1*), that for **5** represents the mean value of the minimal and the maximal diameter of **3b**. This underlines the structural similarity of the scaffolds, with **3b** showing one isomeric and **5** the average scaffold. As **1b** is 0.5 nm larger in size than **1a**, the supramolecules in **5** reach outer diameters of 3.3 nm.<sup>20</sup>

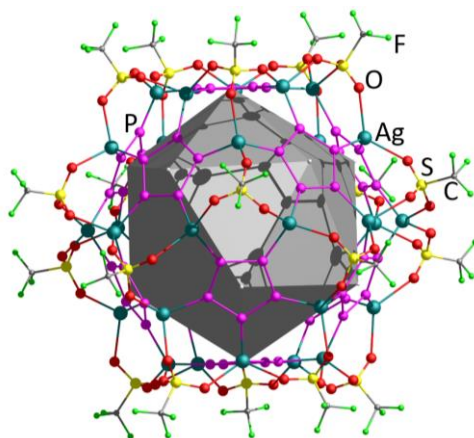


**Figure 8:** Average structure of the scaffold of **5** with inscribed icosidodecahedron.  $[\text{Cp}^{\text{Bn}}\text{Fe}]$  units are omitted for clarity.

The benzyl ligands of **1b** increase the solubility of supramolecular compounds remarkably. Thus, **5** shows a good solubility in CH<sub>2</sub>Cl<sub>2</sub>, toluene and thf, whereas upon solution in CH<sub>3</sub>CN or pyridine, fragmentation is observed. In the <sup>1</sup>H NMR spectra of **5** in CD<sub>2</sub>Cl<sub>2</sub>, a set of four broad signals corresponding to the methylene as well as to the aromatic protons (*o*-CH, *m*-CH and *p*-CH) for the Cp<sup>Bn</sup> ligand are observed ( $\delta$  = 4.21, 6.34, 6.75, 6.93 ppm). The good solubility allows the detection of broad signals in the <sup>31</sup>P{<sup>1</sup>H} NMR spectrum at room temperature at  $\delta$  = -40, 71, 138 ppm as well as a sharp singlet at  $\delta$  = 161 ppm for free **1b**. These signals do not change significantly upon cooling to 193 K. Similarly, in relation to free **1b**, up-field shifted broad signals, could also be observed in the <sup>31</sup>P{<sup>1</sup>H}-MAS NMR spectrum ( $\delta$  = -37.31 ( $\omega_{1/2}$  = 4228 Hz), 117.8 ( $\omega_{1/2}$  = 9388 Hz)). These different broad signals are reminiscent of the obtained spectra for porous 80-vertex derivatives [(**1b**)<sub>12</sub>(CuX)<sub>20-n</sub>] (X = Cl, Br; n ≤ 4.6), though the signals of **5** are distributed over a wider range and are shifted to higher fields.<sup>14e</sup> A comprehensive NMR study concerning these fullerene derivatives revealed that the broad signals can be attributed to different coordination modes of the *cyclo*-P<sub>5</sub> ligands resulting from different porosity.<sup>14e</sup> In the case of the idealized sphere in **5** one can assume that the same isomers with D<sub>2</sub> and D<sub>5</sub> symmetries are possible as for the similar Cu containing [{Cp<sup>Bn</sup>Fe( $\eta^5$ -P<sub>5</sub>)}<sub>12</sub>(CuSO<sub>3</sub>CF<sub>3</sub>)<sub>20</sub>]. Therefore, three different coordination modes of the *cyclo*-P<sub>5</sub> ligand towards the Ag<sup>+</sup> atoms are expected to be found in the mixture of these isomers in the crystalline phase, namely 1,2,4-, 1,2,3,4- (for D<sub>2</sub> isomer) and 1,2,3,4,5-coordination mode (specific only for D<sub>5</sub> isomer together with 1,2,3,4-mode)). Hence, the broad signals in the <sup>31</sup>P{<sup>1</sup>H} NMR spectrum of **5** might be interpreted analogously to the CuX-based sphere as overlapping signals of differently coordinating *cyclo*-P<sub>5</sub> ligands. The sharp signal of free complex **1b** at room temperature indicates that partly dissociation of the aggregates might have taken place in solution. Furthermore, diffusion ordered spectroscopy (DOSY) for **5** showed that the hydrodynamic radii, correlate well with those derived from the preliminary X-ray structure analysis (DOSY: d = 3.4 nm, solid state: d = 3.3 nm). In the cationic ESI MS spectra of **5** numerous peaks attributed to fragments containing pentaphosphaferrocene **1b**, Ag<sup>+</sup> and OTf<sup>-</sup> are detected. The largest peak is at m/z = 2331.6 attributed to the species [{Cp<sup>Bn</sup>Fe( $\eta^5$ -P<sub>5</sub>)}<sub>2</sub>Ag<sub>4</sub>(SO<sub>3</sub>CF<sub>3</sub>)<sub>3</sub>]<sup>+</sup>. Due to the stability of **5** in solution, confirmed by the DOSY experiments, this compound could also be examined by transmission electron microscopy (TEM). For this purpose, crystals of **5** were dissolved in CH<sub>2</sub>Cl<sub>2</sub> and dropped on a copper grid coated with amorphous carbon. The average diameter of the particles shown in *Figure 9* is 2.7 nm, whereas the expected maximal outer diameter measured from diametral opposed H...H is 3.3 nm. The difference can be explained by the fact that the lighter atoms H and C in the outer shell of the sphere are hardly visible due to the contrast to the grid. The inner scaffold based on the heaviest atoms Ag, S, Fe, P measures 2.3 nm.<sup>24</sup>

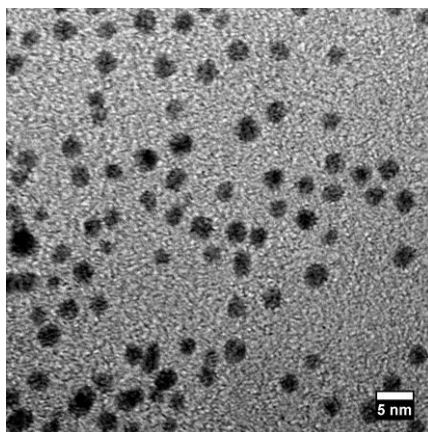


**Figure 9:** TEM record of **5**, dispersed in CH<sub>2</sub>Cl<sub>2</sub> on a Cu grid, coated with amorphous carbon and measured in vacuo on a FEI Tecnai G2 Spirit Twin transmission electron microscope with an acceleration voltage of 120 kV.

### 3.3 Conclusion

In summary, we have shown that the well-established coordination chemistry of [Cp<sup>R</sup>Fe(η<sup>5</sup>-P<sub>5</sub>)] towards Cu salts to form nano-sized spherical supramolecules can be successfully transferred to Ag<sup>+</sup>, furnishing intriguing insights into new spherical assemblies. This is enabled by using soluble silver salts as AgSO<sub>3</sub>CF<sub>3</sub> or AgSO<sub>3</sub>C<sub>7</sub>H<sub>7</sub>, which anions bear the possibility to act as an additional scaffold-constructing building block. Thus, besides spheres with a P<sub>60</sub>M<sub>20-n</sub> core (**3b**, **5**) showing an idealized (90-10)-vertex scaffold, also unprecedented but related spherical scaffolds P<sub>60</sub>Ag<sub>10</sub> (**3a**: idealized 80-vertex sphere) and P<sub>60</sub>Ag<sub>26</sub> (**4**: (90-4)-vertex sphere) are obtained. Moreover, the X-ray structure analysis of **3b** reveals a *D*<sub>2</sub> symmetric isomer resulting from the specific distribution of 20 Ag atoms over 30 positions in the scaffold. To this point, this isomer was only predicted from a Cu-containing average crystal structure implying sensible structural prerequisites, and optimized by DFT calculations. All scaffolds feature an inner void with diameters ranging from 8.2 Å (**3a**) to 9.8 Å (**5**) and act as host molecules for either one molecule **1a** (**3a**) or solvent molecules (**5**). In the case of **3a**, this is of particular interest, as it represents the first idealized 80-vertex sphere to incorporate the molecule **1a** itself. This is enabled by the longer Ag-P bond distances, compared to Cu-P, leading to a slightly larger scaffold in comparison to the Cu-based spherical supramolecules. The good solubility of **5**, together with the stability of the spheres in solution permitted diverse analytical methods. Thus, besides the size estimation by DOSY measurements, the visualisation of these exciting spherical aggregates by TEM methods succeeded for the first time.



### 3.4 Experimental Part

#### General Remarks

All reactions were performed under an inert atmosphere of dry nitrogen with standard vacuum, Schlenk and glove-box techniques. Solvents were purified, dried and degassed prior to use by standard procedures. [Cp\*Fe( $\eta^5$ -P<sub>5</sub>)]<sup>25</sup> and [Cp<sup>Bn</sup>Fe( $\eta^5$ -P<sub>5</sub>)]<sup>26</sup> were synthesized following reported procedures. Commercially available AgSO<sub>3</sub>CF<sub>3</sub>, 99.95% and AgSO<sub>3</sub>C<sub>7</sub>H<sub>7</sub>, 98% were used without further purification.

Solution NMR spectra were recorded on a Bruker Avance 300 or 400 spectrometer. The <sup>31</sup>P{<sup>1</sup>H} MAS spectrum was measured on a Bruker Avance 300 spectrometer. The DOSY spectra were recorded on an Avance III HD 600 (600.25 MHz) spectrometer equipped with a z gradient (53.5 Gauss/cm), 5 mm TCI cryo probe and BVT 3000 unit at 298 K. The NMR data was processed with the Bruker program TopSpin® 3.2 and the diffusion coefficient was calculated with the Bruker software T1/T2 relaxation package. For the calibration of the <sup>1</sup>H chemical shifts and for the temperature- and viscosity-correction of the diffusion coefficients, TMS (tetramethylsilane) was added. The <sup>1</sup>H-diffusion measurement was performed with the convection suppressing DSTE (double stimulated echo) pulse sequence, developed by *Mueller* and *Jerschow*<sup>27</sup> in a pseudo 2D mode. 120 dummy scans and 16 scans were used with a relaxation delay of 2 s. Sinusoidal shapes were used for the gradient and a linear gradient ramp with 20 or 5 increments between 5 and 95% of the maximum gradient strength was applied for the diffusion relevant gradients. For the homospoil gradients, -13.7, 20 and 17.13 G cm<sup>-1</sup> were applied. The length of the gradient pulse  $\delta$  was adjusted for every species in the sample to achieve appropriate signal attenuation curves, giving values for  $\delta$  of 2.0 ms for TMS and 3.4 or 3.6 ms for the supramolecules. A diffusion time  $\Delta$  of 45 ms was used.

The corresponding ESI-MS spectra were acquired on a ThermoQuest Finnigan MAT TSQ 7000 mass spectrometer.

CHN Elemental analyses were performed on a Vario EL III apparatus, whereas all other elements were determined by the Catalysis Research Center of the Technical University Munich by Photometry, Atomic Absorption Spectroscopy or Titrimetry. The storage and handling under air lead to the aggregation of water to the crystalline samples, due to the hygroscopic behavior of the -SO<sub>3</sub>CF<sub>3</sub> groups. Furthermore, the determination of Ag and Fe in one sample showed to be defective. Thus, these values show a large deviance with respect to calculated ones.

The Transmission electron microscopy (TEM) measurements were carried out on a FEI Tecnai G2 Spirit Twin transmission electron microscope equipped with a field emission gun and processed with an acceleration voltage of 120 kV. The machine is fitted with a LaB6 cathode and the pictures

were recorded with an Gatan US1000 CCD-camera (2k × 2k). The analysis of the pictures was done with the graphic software Fiji.<sup>28</sup> For the preparation of the samples were the nanoparticles dispersed in dichloromethane and 20 µL were dropped on copper grids coated with amorphous carbon.

### Synthesis of $[\{\text{Cp}^*\text{Fe}(\mu_4, \eta^{5:1:1:1}\text{-P}_5)\}\{\text{Ag}(\text{SO}_3\text{CF}_3)\}_2]_n$ (**2**)

In a Schlenk tube a solution of  $\text{Ag}(\text{SO}_3\text{CF}_3)$  (114 mg, 0.44 mmol) in  $\text{CH}_2\text{Cl}_2$  (10 mL) is carefully layered with a green solution of  $[\text{Cp}^*\text{Fe}(\eta^5\text{-P}_5)]$  (55 mg, 0.16 mmol) in toluene (11 mL). Thereby, the phase boundary turns yellow. During the diffusion process, the formation of small yellow plates of **2** below the phase boundary can be observed. After complete diffusion the mother liquor is decanted, the crystals are washed with hexane (3 × 10 mL) and dried *in vacuo*.

Analytical data of **2**:

**Yield:** 125 mg (0.15 mmol, 94% referred to  $[\text{Cp}^*\text{Fe}(\eta^5\text{-P}_5)]$ )

**Positive ion ESI-MS** ( $\text{CH}_3\text{CN}$ ):  $m/z$  (%) = 798.9  $[\{\text{Cp}^*\text{Fe}(\eta^5\text{-P}_5)\}_2\text{Ag}]^+$ , 493.9 (100)  $[\{\text{Cp}^*\text{Fe}(\eta^5\text{-P}_5)\}\text{Ag}(\text{CH}_3\text{CN})]^+$

**Negative ion ESI-MS** ( $\text{CH}_3\text{CN}$ ):  $m/z$  (%) = 404.7  $[\text{Ag}(\text{SO}_3\text{CF}_3)_2]^-$ , 148.7 (100)  $[\text{SO}_3\text{CF}_3]^-$

**Elemental analysis:** Calculated (%) for  $[\{\text{Cp}^*\text{Fe}(\eta^5\text{-P}_5)\}\{\text{Ag}(\text{CF}_3\text{SO}_3)\}_2]$  (860 g/mol): C 16.76, H 1.76, S 7.46; found: C 15.81, H 2.29, S 6.76.

### Synthesis of $[\text{Cp}^*\text{Fe}(\eta^5\text{-P}_5)]@[\{\text{Cp}^*\text{Fe}(\eta^5\text{-P}_5)\}_{12}\{\text{Ag}(\text{SO}_3\text{CF}_3)\}_x]$ ( $x \approx 10$ ) (**3a**) and $[\{\text{Cp}^*\text{Fe}(\eta^5\text{-P}_5)\}\cdot\text{tol}]@[\{\text{Cp}^*\text{Fe}(\eta^5\text{-P}_5)\}_{12}\{\text{Ag}(\text{SO}_3\text{CF}_3)\}_{20}]$ (**3b**)

In a thin Schlenk tube a solution of  $\text{Ag}(\text{SO}_3\text{CF}_3)$  (32 mg, 0.125 mmol) in  $\text{CH}_2\text{Cl}_2$  (12 mL) is carefully layered with a green solution of  $[\text{Cp}^*\text{Fe}(\eta^5\text{-P}_5)]$  (15 mg, 0.043 mmol) in toluene (12 mL). Thereby the phase boundary turns yellow. During the diffusion process, the formation of greenish brown rods of **3b** can be observed, though sometimes accompanied by the crystallization of a minor amount of brown prisms of isomeric **3a**. After complete diffusion, the mother liquor is decanted, the crystals are washed with hexane (3 × 5 mL) and dried *in vacuo*.

Analytical data of **3b**:

**Yield:** 15 mg (1.6 µmol, 45% referred to  $[\text{Cp}^*\text{Fe}(\eta^5\text{-P}_5)]$ )

**<sup>1</sup>H NMR** ( $\text{CD}_3\text{CN}$ ):  $\delta$  [ppm] = 1.46 (s,  $[\text{Cp}^*\text{Fe}(\eta^5\text{-P}_5)]$ ).

**<sup>31</sup>P{<sup>1</sup>H} NMR** ( $\text{CD}_3\text{CN}$ ):  $\delta$  [ppm] = 135.00 (s,  $[\text{Cp}^*\text{Fe}(\eta^5\text{-P}_5)]$ ).

<sup>19</sup>F{<sup>1</sup>H} NMR (CD<sub>3</sub>CN): δ [ppm] = -77.8 (s, br, (SO<sub>3</sub>CF<sub>3</sub>)<sup>-</sup>).

**Positive ion ESI-MS** (CH<sub>3</sub>CN): *m/z* (%) = 2946.0 [{Cp\*Fe(η<sup>5</sup>-P<sub>5</sub>)}<sub>3</sub>Ag<sub>8</sub>(SO<sub>3</sub>CF<sub>3</sub>)<sub>7</sub>]<sup>+</sup>, 2686.1 [{Cp\*Fe(η<sup>5</sup>-P<sub>5</sub>)}<sub>3</sub>Ag<sub>7</sub>(SO<sub>3</sub>CF<sub>3</sub>)<sub>6</sub>]<sup>+</sup>, 2430.2 [{Cp\*Fe(η<sup>5</sup>-P<sub>5</sub>)}<sub>3</sub>Ag<sub>6</sub>(SO<sub>3</sub>CF<sub>3</sub>)<sub>5</sub>]<sup>+</sup>, 2172.2 [{Cp\*Fe(η<sup>5</sup>-P<sub>5</sub>)}<sub>3</sub>Ag<sub>5</sub>(SO<sub>3</sub>CF<sub>3</sub>)<sub>4</sub>]<sup>+</sup>, 2172.6 [{Cp\*Fe(η<sup>5</sup>-P<sub>5</sub>)}<sub>3</sub>Ag<sub>4</sub>(SO<sub>3</sub>CF<sub>3</sub>)<sub>3</sub>]<sup>+</sup>, 2084.3 [{Cp\*Fe(η<sup>5</sup>-P<sub>5</sub>)}<sub>2</sub>Ag<sub>6</sub>(SO<sub>3</sub>CF<sub>3</sub>)<sub>5</sub>]<sup>+</sup>, 1916.6 [{Cp\*Fe(η<sup>5</sup>-P<sub>5</sub>)}<sub>3</sub>Ag<sub>4</sub>(SO<sub>3</sub>CF<sub>3</sub>)<sub>3</sub>]<sup>+</sup>, 1826.6 [{Cp\*Fe(η<sup>5</sup>-P<sub>5</sub>)}<sub>2</sub>Ag<sub>5</sub>(SO<sub>3</sub>CF<sub>3</sub>)<sub>4</sub>]<sup>+</sup>, 1660.7 [{Cp\*Fe(η<sup>5</sup>-P<sub>5</sub>)}<sub>3</sub>Ag<sub>3</sub>(SO<sub>3</sub>CF<sub>3</sub>)<sub>2</sub>]<sup>+</sup>, 1570.5 [{Cp\*Fe(η<sup>5</sup>-P<sub>5</sub>)}<sub>2</sub>Ag<sub>4</sub>(SO<sub>3</sub>CF<sub>3</sub>)<sub>3</sub>]<sup>+</sup>, 1312.7 [{Cp\*Fe(η<sup>5</sup>-P<sub>5</sub>)}<sub>2</sub>Ag<sub>3</sub>(SO<sub>3</sub>CF<sub>3</sub>)<sub>2</sub>]<sup>+</sup>, 1056.6 [{Cp\*Fe(η<sup>5</sup>-P<sub>5</sub>)}<sub>2</sub>Ag<sub>2</sub>(SO<sub>3</sub>CF<sub>3</sub>)<sub>1</sub>]<sup>+</sup>, 798.8 [{Cp\*Fe(η<sup>5</sup>-P<sub>5</sub>)}<sub>2</sub>Ag]<sup>+</sup>, 493.8 (100) [{Cp\*Fe(η<sup>5</sup>-P<sub>5</sub>)}Ag(CH<sub>3</sub>CN)]<sup>+</sup>, 452.8 [{Cp\*Fe(η<sup>5</sup>-P<sub>5</sub>)}Ag]<sup>+</sup>.

**Negative ion ESI-MS** (CH<sub>3</sub>CN): *m/z* (%) = 406.7 [Ag(SO<sub>3</sub>CF<sub>3</sub>)<sub>2</sub>]<sup>-</sup>, 360.7 [Cu(SO<sub>3</sub>CF<sub>3</sub>)<sub>2</sub>]<sup>-</sup>, 148.8 [SO<sub>3</sub>CF<sub>3</sub>]<sup>-</sup>.

**Elemental analysis:** Calculated (%) for [{Cp\*Fe(η<sup>5</sup>-P<sub>5</sub>)}<sub>13</sub>(AgCF<sub>3</sub>SO<sub>3</sub>)<sub>20</sub>(C<sub>7</sub>H<sub>7</sub>)(H<sub>2</sub>O)<sub>20</sub>] (10088.54 g/mol): C 18.69, H 2.43, S 6.36, Ag 21.38, Fe 7.20, O 12.69, P 18.03 ; found: C 17.9, H 2.15, S 7.01, Ag 21.4, Fe 6.47, O 12.08, P 18.03.

#### Synthesis of [Cp\*Fe(η<sup>5</sup>-P<sub>5</sub>)]@[{Cp\*Fe(η<sup>5</sup>-P<sub>5</sub>)}<sub>12</sub>{Ag<sub>18</sub>(Ag(CH<sub>3</sub>CN))<sub>8</sub>(SO<sub>3</sub>C<sub>7</sub>H<sub>7</sub>)<sub>20</sub>}] [SO<sub>3</sub>C<sub>7</sub>H<sub>7</sub>]<sub>6</sub> (**4**)

In a thin Schlenk tube to a solution of Ag(SO<sub>3</sub>C<sub>7</sub>H<sub>7</sub>) (40 mg, 0.15 mmol) in CH<sub>3</sub>CN (0.5 mL) was added CH<sub>2</sub>Cl<sub>2</sub> (8 mL). This solution is carefully layered with a green solution of [Cp\*Fe(η<sup>5</sup>-P<sub>5</sub>)] (18 mg, 0.05 mmol) in toluene/pentane (1:1, 8 mL). Thereby the phase boundary turns yellow. After diffusion, the red reaction mixture was filtered and once more layered with pentane. After one day, the formation of green-brown plates of **4** can be observed. After complete diffusion, the mother liquor is decanted, the crystals are washed with pentane (3 × 5 mL) and dried *in vacuo*.

Analytical data of **4**:

**Yield:** 10 mg (0.85 μmol, 22 % referred to [Cp\*Fe(η<sup>5</sup>-P<sub>5</sub>)])

<sup>1</sup>H NMR (CD<sub>2</sub>Cl<sub>2</sub>): δ [ppm] = 1.42 (s(br), 195 H, [Cp\*Fe(η<sup>5</sup>-P<sub>5</sub>)]), 1.96 (s(br), 30 H, CH<sub>3</sub>CN coord.), 2.32 (s(br), 78 H, [CH<sub>3</sub>C<sub>6</sub>H<sub>4</sub>SO<sub>3</sub>]<sup>-</sup>), 7.13 (s(br), 52 H, [CH<sub>3</sub>C<sub>6</sub>H<sub>4</sub>SO<sub>3</sub>]<sup>-</sup>), 7.69 (s(br), 52 H, [CH<sub>3</sub>C<sub>6</sub>H<sub>4</sub>SO<sub>3</sub>]<sup>-</sup>).

<sup>31</sup>P{<sup>1</sup>H} NMR (CD<sub>2</sub>Cl<sub>2</sub>): δ [ppm] = no signal found

<sup>19</sup>F{<sup>1</sup>H} NMR (CD<sub>2</sub>Cl<sub>2</sub>+): δ [ppm] = no signal found

**Positive ion ESI-MS** (CH<sub>3</sub>CN): *m/z* (%) = 1425.0 [{Cp\*Fe(η<sup>5</sup>-P<sub>5</sub>)}<sub>3</sub>Ag<sub>2</sub>(SO<sub>3</sub>C<sub>7</sub>H<sub>7</sub>)<sub>1</sub>]<sup>+</sup>, 1078.9 [{Cp\*Fe(η<sup>5</sup>-P<sub>5</sub>)}<sub>2</sub>Ag<sub>2</sub>(SO<sub>3</sub>C<sub>7</sub>H<sub>7</sub>)<sub>1</sub>]<sup>+</sup>, 798.99 (100) [{Cp\*Fe(η<sup>5</sup>-P<sub>5</sub>)}<sub>2</sub>Ag]<sup>+</sup>, 493.9 [{Cp\*Fe(η<sup>5</sup>-P<sub>5</sub>)}Ag(CH<sub>3</sub>CN)]<sup>+</sup>, 452.9 [{Cp\*Fe(η<sup>5</sup>-P<sub>5</sub>)}Ag]<sup>+</sup>, 267.03 [Ag(CH<sub>3</sub>CN)<sub>4</sub>]<sup>+</sup>, 190.9 [Ag(CH<sub>3</sub>CN)<sub>2</sub>]<sup>+</sup>

**Negative ion ESI-MS** (CH<sub>3</sub>CN): *m/z* (%) = 343 [(SO<sub>3</sub>HC<sub>7</sub>H<sub>7</sub>)(SO<sub>3</sub>C<sub>7</sub>H<sub>7</sub>)]<sup>-</sup>, 252.9 [(SO<sub>3</sub>C<sub>7</sub>H<sub>7</sub>)(CH<sub>3</sub>CN)<sub>2</sub>]<sup>-</sup>, 171.0 (100) [SO<sub>3</sub>C<sub>7</sub>H<sub>7</sub>]<sup>-</sup>

**Elemental analysis:** Calculated (%) for [{Cp\*Fe(η<sup>5</sup>-P<sub>5</sub>)}<sub>13</sub>{Ag(SO<sub>3</sub>C<sub>7</sub>H<sub>7</sub>)<sub>26</sub>}] (11753.0 g/mol): C 31.88, H 3.23, S 7.09; found: 29.19, H 3.84, S 7.07.

### Synthesis of $[\{\text{Cp}^{\text{Bn}}\text{Fe}(\eta^5\text{-P}_5)\}_{12}\{\text{Ag}(\text{CF}_3\text{SO}_3)\}_{20}]$ (**5**)

A solution of  $\text{AgCF}_3\text{SO}_3$  (14 mg, 0.055 mmol) in  $\text{CH}_2\text{Cl}_2$  (8 mL) is carefully layered with a green solution of  $[\text{Cp}^{\text{Bn}}\text{Fe}(\eta^5\text{-P}_5)]$  (20 mg, 0.028 mmol) in toluene (8 mL). After complete diffusion, the brownish solution is layered with hexane. A few hours later, the growth of deep red-brown crystals of **6** can be observed at the phase boundary. After complete diffusion, the mother liquor is decanted, the crystals are washed with hexane ( $3 \times 5$  mL) and dried *in vacuo*.

Analytical data of **5**:

**Yield:** 17 mg (1.1  $\mu\text{mol}$ , 49% referred to  $[\text{Cp}^{\text{Bn}}\text{Fe}(\eta^5\text{-P}_5)]$ )

**$^1\text{H}$  NMR** ( $\text{CD}_2\text{Cl}_2$ ):  $\delta$  [ppm] = 4.21 (m, br, 120H,  $\text{CH}_2$ ), 6.34 (m, br, 120H, *ortho*-CH), 6.75 (s, br, 120H, *meta*-CH), 6.93 (s, br, 60H, *para*-CH).

**$^{31}\text{P}\{^1\text{H}\}$  NMR** ( $\text{CD}_2\text{Cl}_2$ , 293 K):  $\delta$  [ppm] = 160.89 (s,  $\omega$  = 92 Hz,  $[\text{Cp}^{\text{Bn}}\text{Fe}(\eta^5\text{-P}_5)]$ ), 138.07 (s(br),  $\omega$  = 260 Hz,  $[\text{Cp}^{\text{Bn}}\text{Fe}(\eta^5\text{-P}_5)]$ ), 70.52 (s(br),  $\omega$  = 3010 Hz,  $[\text{Cp}^{\text{Bn}}\text{Fe}(\eta^5\text{-P}_5)]$ ), -40.33 (s(br),  $\omega$  = 7858 Hz,  $[\text{Cp}^{\text{Bn}}\text{Fe}(\eta^5\text{-P}_5)]$ )

**$^{31}\text{P}\{^1\text{H}\}$  NMR** ( $\text{CD}_2\text{Cl}_2$ , 193 K):  $\delta$  [ppm] = 161.32 (m(br),  $\omega$  = 1152 Hz,  $[\text{Cp}^{\text{Bn}}\text{Fe}(\eta^5\text{-P}_5)]$ ), 154.09 (s(br),  $\omega$  = 256 Hz,  $[\text{Cp}^{\text{Bn}}\text{Fe}(\eta^5\text{-P}_5)]$ ), 128.23 (m(br),  $\omega$  = 2262 Hz,  $[\text{Cp}^{\text{Bn}}\text{Fe}(\eta^5\text{-P}_5)]$ ), 69.80 (m(br),  $\omega$  = 4914 Hz,  $[\text{Cp}^{\text{Bn}}\text{Fe}(\eta^5\text{-P}_5)]$ ), -40.85 (m(br),  $\omega$  = 7500 Hz,  $[\text{Cp}^{\text{Bn}}\text{Fe}(\eta^5\text{-P}_5)]$ ).

**$^{31}\text{P}\{^1\text{H}\}$  MAS NMR:**  $\delta$  [ppm] = 117.80 (m(br),  $\omega$  = 9388 Hz,  $[\text{Cp}^{\text{Bn}}\text{Fe}(\eta^5\text{-P}_5)]$ ), -37.31 (m(br),  $\omega$  = 4228 Hz,  $[\text{Cp}^{\text{Bn}}\text{Fe}(\eta^5\text{-P}_5)]$ )

**$^{19}\text{F}\{^1\text{H}\}$  NMR** ( $\text{CD}_2\text{Cl}_2$ ):  $\delta$  [ppm] = -77.55 (s, br,  $(\text{CF}_3\text{SO}_3)^-$ ).

**DOSY:** dissolved starting materials:  $M$  = 3357 g/mol,  $d$  = 3.4 nm, dissolved crystal:  $M$  = 2613 g/mol,  $d$  = 3.0 nm; calculated for  $[\{\text{Cp}^{\text{Bn}}\text{Fe}(\eta^5\text{-P}_5)\}_{12}(\text{AgSO}_3\text{CF}_3)_{20}]$ :  $M$  = 13856 g/mol, 3.3 nm.

**Positive ion ESI-MS** ( $\text{CH}_2\text{Cl}_2/\text{CH}_3\text{CN}$ ):  $m/z$  (%) = 2331  $[\{\text{Cp}^{\text{Bn}}\text{Fe}(\eta^5\text{-P}_5)\}_2\text{Ag}_4(\text{SO}_3\text{CF}_3)_3]^+$ , 2075  $[\{\text{Cp}^{\text{Bn}}\text{Fe}(\eta^5\text{-P}_5)\}_2\text{Ag}_3(\text{SO}_3\text{CF}_3)_2]^+$ , 1817  $[\{\text{Cp}^{\text{Bn}}\text{Fe}(\eta^5\text{-P}_5)\}_2\text{Ag}_2\text{SO}_3\text{CF}_3]^+$ , 1561  $[\{\text{Cp}^{\text{Bn}}\text{Fe}(\eta^5\text{-P}_5)\}_2\text{Ag}]^+$ , 1091  $[\{\text{Cp}^{\text{Bn}}\text{Fe}(\eta^5\text{-P}_5)\}\text{Ag}_2\text{SO}_3\text{CF}_3]^+$ , 874  $[\{\text{Cp}^{\text{Bn}}\text{Fe}(\eta^5\text{-P}_5)\}\text{Ag}(\text{CH}_3\text{CN})]^+$ , 833 (100)  $[\{\text{Cp}^{\text{Bn}}\text{Fe}(\eta^5\text{-P}_5)\}\text{Ag}]^+$ , 531  $[\text{Cp}^{\text{Bn}}\text{O}]^+$ .

**Negative ion ESI-MS** ( $\text{CH}_2\text{Cl}_2/\text{CH}_3\text{CN}$ ):  $m/z$  (%) = 502  $[\text{Fe}(\text{SO}_3\text{CF}_3)_3]^-$ , 406  $[\text{Ag}(\text{SO}_3\text{CF}_3)_2]^-$ , 148 (100)  $[\text{SO}_3\text{CF}_3]^-$ .

**Elemental analysis:** Calculated (%) for  $[\{\text{Cp}^{\text{Bn}}\text{Fe}(\eta^5\text{-P}_5)\}_{12}(\text{AgSO}_3\text{CF}_3)_{20}(\text{H}_2\text{O})_{40}(\text{CH}_2\text{Cl}_2)_5]$  (15001.3 g/mol): C 40.43, H 3.43, S 4.28, Ag 14.38, Fe 4.47, O 10.67, P 12.39; found: C 40.33, H 2.97, S 4.75, Ag 18.20, Fe 4.19, O 10.66, P 12.39.

**TEM measurements:** measured diameter of selected aggregates /nm: 2.07, 2.10, 2.27, 2.33, 2.45, 2.54, 2.68, 2.74, 2.74, 2.74, 2.77, 2.77, 2.83, 2.89, 3.00, 3.06, 3.06, 3.18, 3.24, 2.33. Mean value: 2.7(3) nm; Expected diameter:  $\approx$  3.30 nm.

### 3.5 Crystallographic Details

Crystals of **2-5** were taken from a Schlenk flask under a stream of argon and immediately covered with perfluorinated Fomblin® mineral oil to prevent decomposition and a loss of solvent. The quickly chosen single crystals covered by a protective film of the oil were immediately placed into a stream of cold nitrogen ( $T = 90\text{ K}$ ) with the pre-centered goniometer head with CryoMount® and mounted on the goniometer of a diffractometer. Crystals of **3**, **4** and **5** were carefully selected, mounted on a magnetic holder with CryoMount®, checked for quality and stored into a Dewar vessel in liquid nitrogen using standard cryocrystallography tools. After a few weeks, they were transported to the DESY PETRA III synchrotron (Hamburg, Germany). Using standard procedures it was placed into a Dewar vessel filled with liquid nitrogen among other crystals. A robotic mounting/demounting was used for further manipulations in the P11 beamline hutch.<sup>29</sup>

The data for **2-5** were collected on an Agilent Technologies diffractometer equipped with a Titan<sup>S2</sup> CCD detector and a SuperNova Cu K $\alpha$  microfocus source  $\omega$  scans. Unfortunately, undesirable icing of the single crystals was observed during all experiments for supramolecules **3a**, **3b** and **4** performed in-house due to longer exposure times and low symmetry. For this reason, alternative datasets for X-ray diffraction experiment for **3 - 5** were collected at 80 K at the DESY PETRA III synchrotron (beamline P11). Data collection was performed by a shutterless 360°  $\phi$ -rotation at wavelength  $\lambda = 0.6199\text{ \AA}$  (20 keV). Data reduction for all crystal structures was performed with CrysAlis Pro software.<sup>30</sup> Analytical absorption correction for **2-5** measured in-house, was applied based on crystal faces; whereas for synchrotron diffraction experiments for a number of single crystals (**3-5**), an empirical absorption correction based on averaging of the equivalent reflections was used. Crystallographic data and further details (not listed for preliminary data for **3 - 5**) of the diffraction experiments are given in *Tables 2-4*.

The structures were solved by direct methods with *SHELXT*<sup>[31]</sup> and were refined by full-matrix least-squares method against  $F^2$  in anisotropic approximation using multiprocessor variable memory versions of *SHELXL* (2014-2015). All non-hydrogen atoms were refined anisotropically, while the hydrogen atoms were refined riding on pivot atoms. For **3a**, **3b**, **4** and **5**, the best datasets will be used for a final structure refinement after estimation of the data quality for several crystals measured in-house and at DESY synchrotron.

In **3a**, **4** and **5**, the inorganic scaffold is severely disordered over more than 2 close positions. The occupation factors for disordered heavy atoms were refined with fixed isotropic  $U_{\text{iso}}$  similar to the average  $U_{\text{iso}}$  (usually  $0.03 - 0.05\text{ \AA}^{-2}$ ) for the fully occupied heavy atoms in the corresponding structure. Despite relatively low quality factors, this work including interpretation of the isomeric compositions of the supramolecules is still in progress.

**Table 2:** Experimental details for compounds **2** and **3a** with preliminary data marked with (\*).

Crystal data	2 (final data)	3a (preliminary data)
Chemical formula	C <sub>12</sub> H <sub>15</sub> Ag <sub>2</sub> F <sub>6</sub> FeO <sub>6</sub> P <sub>5</sub> S <sub>2</sub> ·C <sub>7</sub> H <sub>8</sub>	C <sub>75</sub> H <sub>140</sub> Ag <sub>10</sub> F <sub>20</sub> Fe <sub>12</sub> O <sub>66</sub> P <sub>60</sub> S <sub>10</sub>
<i>M</i> <sub>r</sub> (g/mol)	951.97	6405.56
Crystal system, space group	monoclinic, <i>P</i> 2 <sub>1</sub> / <i>c</i>	monoclinic, <i>P</i> 2 <sub>1</sub> / <i>n</i>
Temperature (K)	123	90
<i>a</i> , <i>b</i> , <i>c</i> (Å)	11.0744(2), 18.3563(4), 15.3723(3)	24.2545 (3), 24.7264 (4), 24.3865 (4)
$\alpha$ , $\beta$ , $\gamma$ (°)	90, 97.712(2), 90	93.649 (1)
<i>V</i> (Å <sup>3</sup> )	3096.68(12)	14595.6 (4)
<i>Z</i>	4	2
<i>F</i> (000)	1864	6280 (*)
<i>D</i> <sub>x</sub> (Mg m <sup>-3</sup> )	2.042	1.458 (*)
Radiation type	Cu <i>K</i> α	Cu <i>K</i> α
μ (mm <sup>-1</sup> )	18.12	14.22
Crystal shape	plate	prism
Crystal colour	red	dark brown
Crystal size (mm)	0.24 × 0.16 × 0.01	0.37 × 0.28 × 0.23
Data collection		
Diffractometer	SuperNova, Titan <sup>S2</sup> diffractometer	
Absorption correction	gaussian	
<i>T</i> <sub>min</sub> , <i>T</i> <sub>max</sub>	0.045, 0.447	
No. of measured, independent and observed [ <i>I</i> > 2σ( <i>I</i> )] reflections	10748, 6012, 4541	
<i>R</i> <sub>int</sub>	0.0637	
(sin θ/λ) <sub>max</sub> (Å <sup>-1</sup> )	0.624	
Range of <i>h</i> , <i>k</i> , <i>l</i>	<i>h</i> = -11→13, <i>k</i> = -21→14, <i>l</i> = -18→18	
Refinement		
<i>R</i> [ <i>F</i> <sup>2</sup> > 2σ( <i>F</i> <sup>2</sup> )], <i>wR</i> ( <i>F</i> <sup>2</sup> ), <i>S</i>	0.0632, 0.166, 0.977	
No. of reflections	6012	
No. of parameters	376	
No. of restraints	0	
H-atom treatment	H-atom parameters constrained	
Δ <sub>max</sub> , Δ <sub>min</sub> (e Å <sup>-3</sup> )	2.820, -2.296	
Computer programs for <b>2</b> : <i>CrysAlisPRO</i> 1.171.37.34 (Rigaku OD), <i>SHELXS-97</i> (Sheldrick, 2008).		
Computer programs for <b>3a</b> : <i>SHELXL2014/7</i> (Sheldrick, 2014).		

**Table 3:** Experimental details for compounds **3b** and **4** with preliminary data marked with (\*).

Crystal data	<b>3b</b> (preliminary data)	<b>4</b> (preliminary data)
Chemical formula	C <sub>157</sub> H <sub>203</sub> Ag <sub>20</sub> F <sub>60</sub> Fe <sub>13</sub> O <sub>60</sub> P <sub>65</sub> S <sub>20</sub> (*)	C <sub>328</sub> H <sub>427</sub> Ag <sub>26</sub> Fe <sub>13</sub> N <sub>8</sub> O <sub>78</sub> P <sub>65</sub> S <sub>26</sub> (*)
<i>M<sub>r</sub></i> (g/mol)	9728.23 (*)	12107.65 (*)
Crystal system, space group	triclinic, <i>P</i> $\bar{1}$	monoclinic, <i>P</i> 2 <sub>1</sub> / <i>c</i>
Temperature (K)	89.9(4)	89.9(4)
<i>a</i> , <i>b</i> , <i>c</i> (Å)	26.6210(3), 37.4009(4) 46.1126(4)	22.5489(3), 44.7796(6) 27.2813(4)
$\alpha$ , $\beta$ , $\gamma$ (°)	84.3257(8), 82.8394(8) 86.8296(9)	90.0, 105.1595(14), 90.0
<i>V</i> (Å <sup>3</sup> )	45287.7(8)	26588.1(6)
<i>Z</i>	4	2
<i>F</i> (000)	21043 (*)	11912 (*)
<i>D<sub>x</sub></i> (Mg m <sup>-3</sup> )	1.573 (*)	1.508 (*)
Radiation type	Cu K $\alpha$ (*)	Cu K $\alpha$ (*)
$\mu$ (mm <sup>-1</sup> )	13.55 (*)	13.61 (*)
Crystal shape	prism	rod
Colour	brown	brown
Crystal size (mm)	0.296 × 0.137 × 0.076	0.117 × 0.048 × 0.032
<b>Refinement</b>		
<i>R</i> [ <i>F</i> <sup>2</sup> > 2 $\sigma$ ( <i>F</i> <sup>2</sup> )], <i>wR</i> ( <i>F</i> <sup>2</sup> ), <i>S</i>	0.0633, 0.1908, 1.030	0.0535, 0.1378, 0.901

**Table 4:** Experimental details for compounds **5** with preliminary data marked with (\*).

Crystal data	<b>5</b> (preliminary data)
Chemical formula	C <sub>500</sub> H <sub>420</sub> Ag <sub>20</sub> F <sub>60</sub> Fe <sub>12</sub> O <sub>60</sub> P <sub>60</sub> S <sub>20</sub> (*)
<i>M<sub>r</sub></i> (g/mol)	13856.01 (*)
Crystal system, space group	monoclinic, <i>C</i> 2/ <i>c</i>
Temperature (K)	90
<i>a</i> , <i>b</i> , <i>c</i> (Å)	46.5470(4), 32.1063(4), 91.7761(12)
$\alpha$ , $\beta$ , $\gamma$ (°)	90, 97.7119(10), 90
<i>V</i> (Å <sup>3</sup> )	135914(3)
<i>Z</i>	8
<i>F</i> (000)	> 57610 (*)
Radiation type	Cu K $\alpha$ (*)
$\mu$ (mm <sup>-1</sup> )	9.034 (*)
Crystal colour and shape	red prism
Crystal size (mm)	0.45 × 0.24 × 0.20
<b>Refinement</b>	
<i>R</i> [ <i>F</i> <sup>2</sup> > 2 $\sigma$ ( <i>F</i> <sup>2</sup> )], <i>wR</i> ( <i>F</i> <sup>2</sup> ), <i>S</i>	0.14

### 3.6 Author Contributions

- The synthesis and characterization of **2** were performed by Dr. C. Heindl.
- The synthesis and characterization of **3b** were performed by B. Hiltl and Dr. C. Heindl.
- The synthesis and characterization of the supramolecules **3a**, **4** and **5** were done by B. Hiltl.
- The synthesis and characterization of **2**, **3b** and **5** are also part of the dissertation thesis of Dr. C. Heindl (University of Regensburg, 2015).
- The synthesis and parts of the chemical characterization methods of **5** are also part of the master thesis of B. Hiltl (University of Regensburg, 2014).
- The manuscript (introduction, results and discussions, experimental part, conclusion; including figures and graphical abstract) was written by B. Hiltl. Figures of **2** were made by Dr. C. Heindl.
- The section 'crystallographic details' was written by Dr. E. Peresypkina
- All X-ray structure analysis were performed by Dr. E. Peresypkina and Dr. Sc. A. V. Virovets with Dr. C. Heindl (for **2**) and B. Hiltl (**3-5**). The X-ray structure analysis at synchrotron PETRA III (P11 beamline, DESY, Hamburg) for (**4-5**) was performed by Dr. E. Peresypkina and Dr. Sc. A. V. Virovets.
- MAS NMR investigation of **5** was performed by Prof. W. Kremer.
- DOSY measurements were performed by F. Hastreiter.
- TEM measurement was performed by J. Hilgert.

### 3.7 References

- <sup>1</sup> I. Chakraborty, T. Pradeep, *Chem. Rev.* **2017**, *117*, 8208-8271.
- <sup>2</sup> a) C. Anson, A. Eichhoefer, I. Issac, D. Fenske, O. Fuhr, P. Sevilano, C. Persau, D. Stalke, J. Zhang, *Angew. Chem., Int. Ed.* **2008**, *47*, 1326-1331, b) S. Bestgen, O. Fuhr, B. Breitung, V. S. Kiran Chakravadhanula, G. Guthausen, F. Hennrich, W. Yu, M. M. Kappes, P. W. Roesky, D. Fenske, *Chem. Sci.* **2017**, *8*, 2235-2240, c) B. Li, R.-W. Huang, J.-H. Qin, S.-Q. Zang, G.-G. Gao, H.-W. Hou, T. C. W. Mak, *Chem. Eur. J.* **2014**, *20*, 12416-12420, d) F. Gruber, M. Jansen, *Angew. Chem., Int. Ed.* **2010**, *49*, 4924-4926, e) L.-M. Zhang, T. C. W. Mak, *J. Am. Chem. Soc.* **2016**, *138*, 2909-2912, f) S. C. K. Hau, M. C. L. Yeung, V. W. W. Yam, T. C. W. Mak, *J. Am. Chem. Soc.* **2016**, *138*, 13732-13739.
- <sup>3</sup> a) K. Takaoka, M. Kawano, T. Ozeki, M. Fujita, *Chem Commun* **2006**, 1625-1627, b) Y. Inokuma, N. Kojima, T. Arai, M. Fujita, *J. Am. Chem. Soc.* **2011**, *133*, 19691-19693.
- <sup>4</sup> a) P. Mal, B. Breiner, K. Rissanen, J. R. Nitschke, *Science* **2009**, *324*, 1697-1699, b) S. Sato, J. Iida, K. Suzuki, M. Kawano, T. Ozeki, M. Fujita, *Science* **2006**, *313*, 1273-1276.



- 5 C. J. Hastings, M. D. Pluth, R. G. Bergman, K. N. Raymond, *J. Am. Chem. Soc.* **2010**, *132*, 6938-6940.
- 6 a) S. Matsuzaki, T. Arai, K. Ikemoto, Y. Inokuma, M. Fujita, *J. Am. Chem. Soc.* **2014**, *136*, 17899-17901,  
b) N. K. Al-Rasbi, I. S. Tidmarsh, S. P. Argent, H. Adams, L. P. Harding, M. D. Ward, *J. Am. Chem. Soc.*  
**2008**, *130*, 11641-11649.
- 7 a) T. Osuga, T. Murase, M. Fujita, *Angew. Chem., Int. Ed.* **2012**, *51*, 12199-12201, b) Y. Fang, T.  
Murase, S. Sato, M. Fujita, *J. Am. Chem. Soc.* **2013**, *135*, 613-615, c) Q.-F. Sun, J. Iwasa, D. Ogawa, Y.  
Ishido, S. Sato, T. Ozeki, Y. Sei, K. Yamaguchi, M. Fujita, *Science* **2010**, *328*, 1144-1147, d) M. Fujita,  
D. Oguro, M. Miyazawa, H. Oka, K. Yamaguchi, K. Ogura, *Nature* **1995**, *378*, 469-471.
- 8 K. Harris, D. Fujita, M. Fujita, *Chem. Commun.* **2013**, *49*, 6703-6712.
- 9 S. Mukherjee, P. S. Mukherjee, *Chem. Commun.* **2014**, *50*, 2239-2248.
- 10 a) O. Oms, T. Jarrosson, L. H. Tong, A. Vaccaro, G. Bernardinelli, A. F. Williams, *Chem. Eur. J.* **2009**,  
*15*, 5012-5022, b) D.-X. Zhang, H.-X. Zhang, H.-Y. Li, T. Wen, J. Zhang, *Cryst. Growth Des.* **2015**, *15*,  
2433-2436,
- 11 N. Giri, S. L. James, *Chem. Commun.* **2011**, *47*, 1458-1460.
- 12 D.-X. Zhang, H.-X. Zhang, H.-Y. Li, T. Wen, J. Zhang, *Cryst. Growth Des.* **2015**, *15*, 2433-2436.
- 13 Z. Wang, H.-F. Su, Y.-Z. Tan, S. Schein, S.-C. Lin, W. Liu, S.-A. Wang, W.-G. Wang, C.-H. Tung, D. Sun,  
L.-S. Zheng, *Proc. Natl. Acad. Sci. U. S. A.* **2017**, *114*, 12132-12137.
- 14 a) E. Peresypkina, C. Heindl, E. Madl, H. Brake, A. Virovets, M. Scheer, *Chemistry* **2017**, b) S. Welsch,  
C. Groeger, M. Sierka, M. Scheer, *Angew. Chem., Int. Ed.* **2011**, *50*, 1435-1438, c) M. Scheer, A.  
Schindler, J. Bai, B. P. Johnson, R. Merkle, R. Winter, A. V. Virovets, E. V. Peresypkina, V. A. Blatov,  
M. Sierka, H. Eckert, *Chem. Eur. J.* **2010**, *16*, 2092-2107, d) C. Heindl, E. V. Peresypkina, A. V. Virovets,  
W. Kremer, M. Scheer, *J. Am. Chem. Soc.* **2015**, *137*, 10938-10941, e) F. Dielmann, M. Fleischmann,  
C. Heindl, E. V. Peresypkina, A. V. Virovets, R. M. Gschwind, M. Scheer, *Chem. Eur. J.* **2015**, *21*, 6208-  
6214.
- 15 a) S. Heindl, E. Peresypkina, J. Sutter, M. Scheer, *Angew. Chem., Int. Ed.* **2015**, *54*, 13431-13435, b) M.  
Scheer, A. Schindler, C. Groeger, A. V. Virovets, E. V. Peresypkina, *Angew. Chem., Int. Ed.* **2009**, *48*,  
5046-5049, c) J. Bai, A. V. Virovets, M. Scheer, *Science* **2003**, *300*, 781-783.
- 16 a) A. Schindler, C. Heindl, G. Balazs, C. Groeger, A. V. Virovets, E. V. Peresypkina, M. Scheer, *Chem.*  
*Eur. J.* **2012**, *18*, 829-835, b) C. Schwarzmaier, A. Schindler, C. Heindl, S. Scheuermayer, E. V.  
Peresypkina, A. V. Virovets, M. Neumeier, R. Gschwind, M. Scheer, *Angew. Chem., Int. Ed.* **2013**, *52*,  
10896-10899.
- 17 C. Heindl, E. Peresypkina, A. V. Virovets, I. S. Bushmarinov, M. G. Medvedev, B. Kraemer, B. Dittrich,  
M. Scheer, *Angew. Chem., Int. Ed.* **2017**, *56*, 13237-13243.
- 18 F. Dielmann, M. Fleischmann, C. Heindl, E. V. Peresypkina, A. V. Virovets, R. M. Gschwind, M. Scheer,  
*Chem. Eur. J.* **2015**, *21*, 6208-6214.

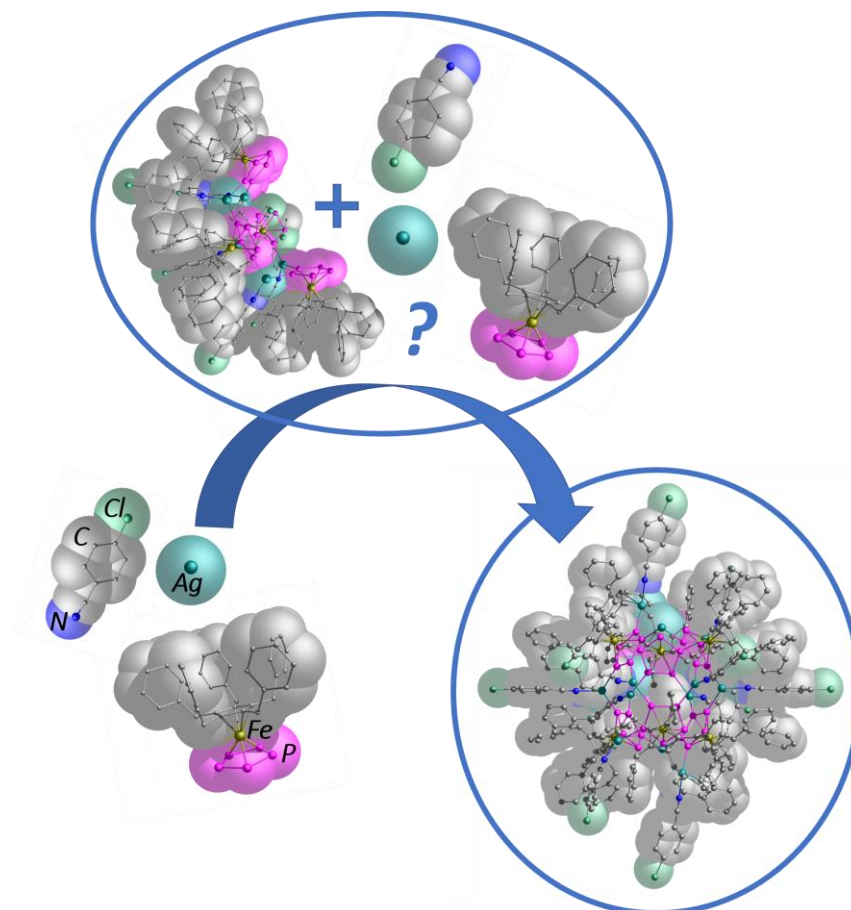
- 19 a) S. Heintl, E. Peresyphkina, J. Sutter, M. Scheer, *Angew. Chem., Int. Ed.* **2015**, 54, 13431-13435; b) F. Dielmann, M. Fleischmann, C. Heindl, E. V. Peresyphkina, A. V. Virovets, R. M. Gschwind, M. Scheer, *Chem. Eur. J.* **2015**, 21, 6208-6214; c) F. Dielmann, C. Heindl, F. Hastreiter, E. V. Peresyphkina, A. V. Virovets, R. M. Gschwind, M. Scheer, *Angew. Chem., Int. Ed.* **2014**, 53, 13605-13608.
- 20 The outer diameter were calculated from the sum of the maximum distance of two H atoms of **1** and two times the van-der-Waals radius of H.
- 21 The inner diameter were calculated from difference of the distance of centroids of two opposite cyclo-P<sub>5</sub> ligands and two times the van-der-Waals radius of P.
- 22 values can slightly vary from preliminary to final data
- 23 M. Scheer, J. Bai, B. P. Johnson, R. Merkle, A. V. Virovets, C. E. Anson, *Eur. J. Inorg. Chem.* **2005**, 4023-4026.
- 24 Maximal distance of two opposing S atoms plus twice the van der Waals radius of S (180 pm from A. Bondi, *J. Phys. Chem.* **1964**, 68, 3, 441–451).
- 25 M. Detzel, G. Friedrich, O. J. Scherer and G. Wolmershäuser, *Angew. Chem. Int. Ed.* **1995**, 34, 1321.
- 26 F. Dielmann, R. Merkle, S. Heintl, M. Scheer, *Z. Naturforsch.* **2009**, 64, 3.
- 27 a) A. Jerschow, N. Müller, *J. Magn. Reson.* **1997**, 125, 372-375. b) C. S. Johnson, *Prog. Nucl. Magn. Reson. Spectrosc.* **1999**, 34, 203-256; c) W. S. Price, *Concepts Magn. Reson.* 1998, 10, 197-237; d) E. O. Stejskal, J. E. Tanner, *The Journal of Chemical Physics* **1965**, 42, 288-292.
- 28 a) C. T. Rueden, J. Schindelin, M. C. Hiner, et al. *BMC Bioinformatics* **2017**, 18, 529; b) C. A. Schneider, W. S. Rasband, K. W. Eliceiri, *Nature methods* **2012**, 9, 7, 671-675; c) J. Schindelin, I. Arganda-Carreras, E. Frise, et al. *Nature methods* **2012**, 9, 7, 676-682.
- 29 A. Burkhardt, T. Pakendorf, B. Reime, et al, *Eur. Phys. J. Plus* **2016**, 131, 56-64.
- 30 CrysAlisPro., different versions (Rigaku OD).
- 31 G. M. Sheldrick, *Acta Cryst. sect. C* **2015**, C71, 3.



## 4. A Small Cationic Host-Guest Assembly and its Possible Curved Shell Precursor

B. Hiltl, E. Peresypkina, A. V. Virovets, M. Scheer

### Graphical Abstract



### Abstract:

Using a three-component self-assembly approach, involving  $[\text{Cp}^{\text{Bn}}\text{Fe}(\eta^5\text{-P}_5)]$  (**1**),  $\text{AgSbF}_6$  and a benzonitrile, the smallest so far obtained spherical supramolecular aggregate, based on pentaphosphaferrocenes  $[\text{SbF}_6]@[\{\text{Cp}^{\text{Bn}}\text{Fe}(\eta^5\text{-P}_5)\}_6\{\text{Ag}(\text{NC}(\text{C}_6\text{H}_4)\text{Cl})\}_{9.55}][\text{SbF}_6]_{8.55}$  (**4**) is achieved. All free coordination sites on the scaffold-building Ag atoms are saturated by benzonitrile ligands and one non-coordinating counter anion is encapsulated inside the cavity of the cationic sphere. Moreover, by sensibly selecting the reaction conditions of this highly condition-sensitive self-assembly system, it was possible to access and structurally characterize the potential pentanuclear intermediate complex  $[\{\text{Cp}^{\text{Bn}}\text{Fe}(\eta^5\text{-P}_5)\}_4\{\text{Ag}(\text{NC}(\text{C}_6\text{H}_4)\text{Cl})\}_5][\text{SbF}_6]_5 \cdot (\text{CH}_2\text{Cl}_2)$  (**3**) for the first time.

## 4.1 Introduction

Diverse supramolecular host aggregates and capsules are accessible by self-assembly processes and can be exploited for various applications including, among others, catalysis<sup>1</sup> and drug delivery<sup>2</sup>. Some important aspects concerning the rational design of applicable assemblies, that have to be considered, are the solubility, stability in solution and the size of the inner void, which is available for guest uptake. Additionally, functionalization of the outer scaffold of the host attracts special interest as it can enable the aggregates to specifically interact with certain surfaces<sup>3</sup> or body tissues.<sup>4</sup> While fullerenes can easily be covalently functionalized by using organic reaction pathways,<sup>5</sup> this does not apply for most self-assembled supramolecular cage compounds as they rely on weaker interactions: coordinative<sup>6</sup> or hydrogen bonding,<sup>7</sup> as well as van der Waals interactions.<sup>8</sup> By functionalizing and varying the separate building blocks *Fujita et al.* was able to synthesize diverse *endo*- and *exo*-functionalized supramolecular cage compounds, all based on Pd<sub>12</sub>L<sub>24</sub> scaffolds (L = bent pyridine based linker).<sup>9</sup>

Our group succeeded in accessing various nano-sized spherical aggregates, which consist of the polyphosphorus complex [Cp<sup>R</sup>Fe(η<sup>5</sup>-P<sub>5</sub>)] (Cp<sup>R</sup> = Cp<sup>Bn</sup> (**1**)) and coinage metal salts (*Figure 1*).<sup>10,11,12</sup> Some of these supramolecular scaffolds act as hosts for diverse small guests and stabilize labile molecules as P<sub>4</sub> or As<sub>4</sub> (*Figure 1c,d*).<sup>13,14</sup>

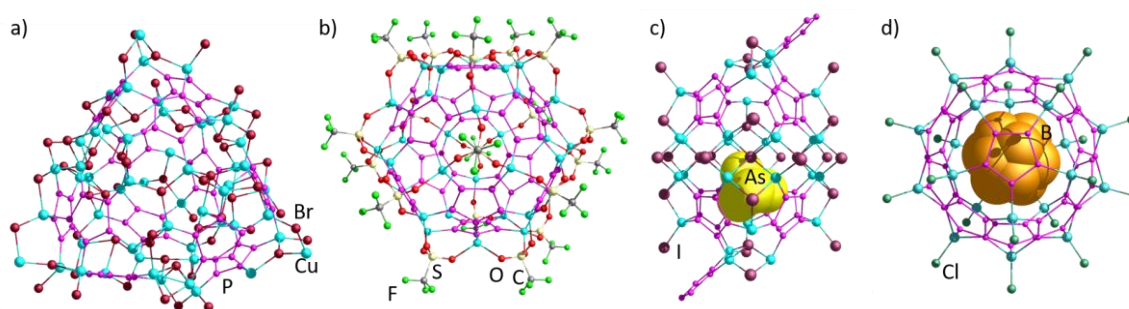


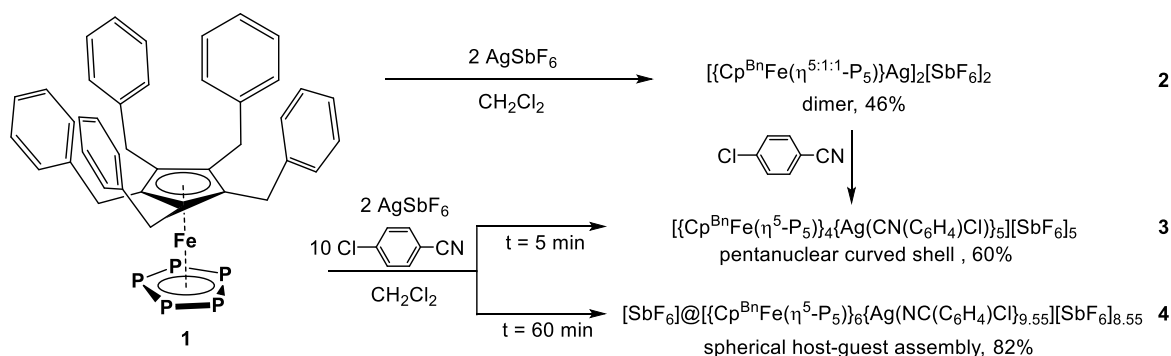
**Figure 1:** Selected spherical supramolecules based on [Cp<sup>R</sup>Fe(η<sup>5</sup>-P<sub>5</sub>)]: a) [{Cp<sup>Bn</sup>Fe(η<sup>5</sup>-P<sub>5</sub>)}]<sub>12</sub>(CuBr)<sub>51</sub>(CH<sub>3</sub>CN)<sub>8</sub>,<sup>11</sup> b) [{Cp<sup>Bn</sup>Fe(η<sup>5</sup>-P<sub>5</sub>)}]<sub>12</sub>{Cu(CF<sub>3</sub>SO<sub>3</sub>)}<sub>19.6</sub>,<sup>12</sup> c) As<sub>4</sub>@[{Cp<sup>\*</sup>Fe(η<sup>5</sup>-P<sub>5</sub>)}]<sub>10</sub>(CuI)<sub>30</sub>(CH<sub>3</sub>CN)<sub>6</sub>,<sup>13</sup> d) o-C<sub>2</sub>B<sub>10</sub>H<sub>12</sub>@[{Cp<sup>\*</sup>Fe(η<sup>5</sup>-P<sub>5</sub>)}]<sub>12</sub>(CuCl)<sub>20</sub>.<sup>14</sup> [Cp<sup>R</sup>Fe] fragments, H atoms, solvent molecules and CH<sub>3</sub>CN ligands are omitted for clarity.

As the use of the functional anions SO<sub>3</sub>CF<sub>3</sub><sup>-</sup> and SO<sub>3</sub>C<sub>7</sub>H<sub>7</sub><sup>-</sup> in *Chapter III* showed, the formation of diverse neutral and cationic Ag-based spherical assemblies is enabled with [Cp<sup>R</sup>Fe(η<sup>5</sup>-P<sub>5</sub>)] (Cp<sup>R</sup> = Cp<sup>\*</sup>, Cp<sup>Bn</sup> (**1**)). When the bulkier Cp<sup>Bn</sup> ligand is involved, the formed aggregates exhibit an enhanced solubility due to the benzyl residues at the Cp ligand and show remarkable stability in solution, proved by DOSY NMR spectroscopy and TEM (cf. *Chapter III*). Following these results, the question arose, whether the surface of the nano-sized spheres could be rationally functionalized? This

property is strongly related to the coordination environment of the scaffold-building metal cations. So far, in all obtained supramolecules, based on polyphosphorus complexes, the Cu or Ag cations were coordinatively saturated by halide or triflate anions. Further functionalization of these supramolecules by other ligands or linkers is prevented, due to the strong binding affinity of these anions towards the metal cations. However, free coordination sites on the metal atoms can be induced by the use of silver salts of weaker coordinating anions, like  $\text{AgSbF}_6$ . However, would such an approach result in spheres, exhibiting a multiply positively charged scaffold? To answer this question, a three-component self-assembly process was studied, involving besides  $[\text{Cp}^{\text{Bn}}\text{Fe}(\eta^5\text{-P}_5)]$  (**1**) and  $\text{AgSbF}_6$ , the potential ligand  $\text{NC}(\text{C}_6\text{H}_4)\text{Cl}$  to stabilize expected free coordination sites on the scaffold-building Ag atoms.

## 4.2 Results and Discussion

To gain a general knowledge on the coordination behaviour of **1** and  $\text{AgSbF}_6$ , a solution of  $\text{AgSbF}_6$  in  $\text{CH}_2\text{Cl}_2$  was slowly dropped to a solution of **1** in  $\text{CH}_2\text{Cl}_2$  and stirred for 1h. After layering with pentane the formation of the green crystalline product **2** can be observed at the phase boundary (Scheme 1). To saturate the Ag atoms,  $\text{Cl}(\text{C}_6\text{H}_4)\text{CN}$  was added as a third component either directly to the reaction solution of **2** or together with **1** in an otherwise analogous reaction. By distinguishing between a stirring time of 5 min or 1h, and different crystallization methods **3** and **4** can be obtained selectively after layering the respective solutions with hexane. All compounds were isolated in reasonable crystalline yields.



**Scheme 1:** Reaction of **1** and  $\text{AgSbF}_6$  and in the presence of  $\text{Cl}(\text{C}_6\text{H}_4)\text{CN}$  as an additional ligand.

The X-ray structure analysis of single crystals of **2** reveals a dimeric complex  $[\{\text{Cp}^{\text{Bn}}\text{Fe}(\eta^5\text{-P}_5)\}\text{Ag}_2][\text{SbF}_6]_2$  (Figure 2). The *cyclo*- $\text{P}_5$  ligands bridge two Ag atoms in a 1,3-fashion. The latter ones in turn are surrounded by two P atoms of the two ligands **1**, and one  $\text{SbF}_6^-$  anion with an elongated Ag-F contact of 2.87 Å. Additionally, one Bn residue of a coordinating ligand **1** interacts with the Ag atom to form a  $\pi$ -contact with a distance of 2.53 Å.<sup>15</sup> The coordination environment of the Ag atoms is therefore pseudo-tetrahedral. Due to the Bn residues of the *cyclo*- $\text{P}_5$  ligands, compound **2** is well

soluble in  $\text{CH}_2\text{Cl}_2$ , toluene or benzene, but insoluble in hexane or pentane. In the  $^1\text{H}$  NMR spectrum in  $\text{C}_6\text{D}_6$  the expected signals for the Bn residues are visible, whereas the  $^{31}\text{P}\{^1\text{H}\}$  NMR spectrum shows a signal at 147.87 ppm, which can be assigned to the P atoms of **1**, though shifted with respect to free **1** (161 ppm).<sup>18</sup> The fact, that only one signal is visible in the  $^{31}\{^1\text{H}\}$  NMR spectrum, indicates a dynamic behavior of the dimeric units of **2** in solution. In the positive-ion ESI MS spectrum in a solvent mixture of  $\text{CH}_2\text{Cl}_2/\text{CH}_3\text{CN}$ , the highest mass peak at  $m/z = 1563.75$  can be attributed to the fragment  $[\{\text{Cp}^{\text{Bn}}\text{Fe}(\eta^5\text{-P}_5)\}_2\text{Ag}]^+$ .

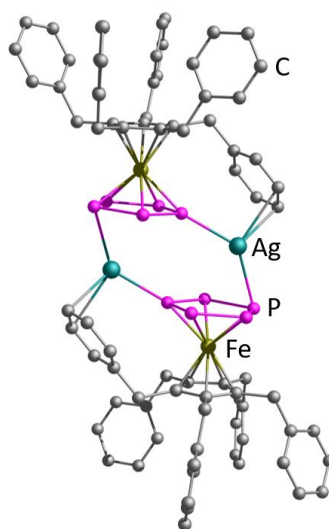


**Figure 2:** Cationic part of dimeric structure of **2**. H atoms are omitted for clarity.

To offer a suitable ligand for saturating the Ag atoms, benzonitrile  $\text{NC}(\text{C}_6\text{H}_4)\text{Cl}$  was chosen, as nitriles are a versatile and easy accessible class of organic compounds, that can be pre-designed to stabilize the scaffold-building Ag atoms, or to introduce functional groups to the supramolecules. Thus, the self-assembly was extended by this third component, leading to a very sensitive system. In this way, compounds **3** and **4** are obtained, whereas the selectivity of the reaction strongly depends on the procedure. Applying short reaction times ( $< 30$  min) and quick crystallization, or a concentrated solution of the reactants, leads to the formation of crystalline **3**. Its X-ray structural analysis reveals a curved shell of four ligands **1** connected by five  $[\text{Ag}\{\text{NC}(\text{C}_6\text{H}_4)\text{Cl}\}]^+$  units (Figure 3), to give two  $\{\text{Ag}_3\text{P}_6\}$  rings. The two ligands **1** on the side-tips coordinate Ag atoms in a 1,2-fashion, whereas the middle two *cyclo*- $\text{P}_5$  ligands show a 1,2,3-coordination mode. The latter ones possess a trigonal coordination environment, formed by two ligands **1** and one ligand  $\text{NC}(\text{C}_6\text{H}_4)\text{Cl}$ .

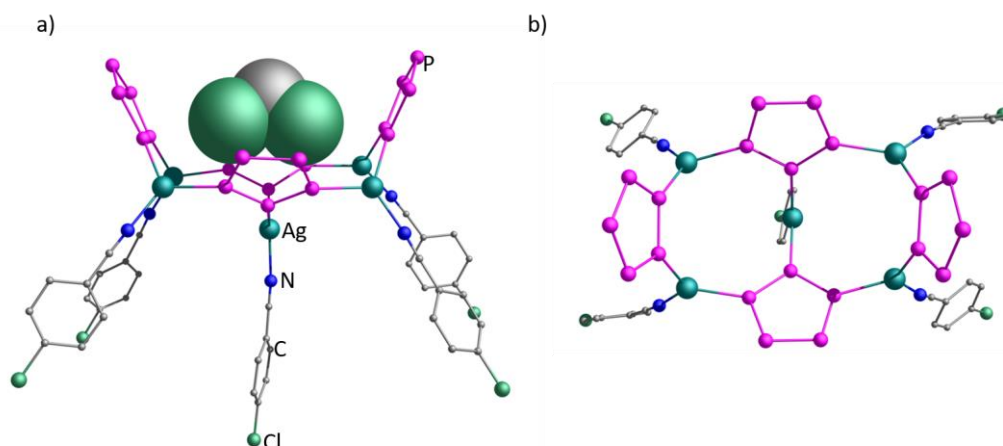


**Figure 3:** Cationic curved shell structure of **3** a) side view with intercalated  $\text{CH}_2\text{Cl}_2$  molecule shown in space-filling model, b) top view.  $[\text{Cp}^{\text{Bn}}\text{Fe}]$  fragments and H atoms are omitted for clarity.

Remarkably, stirring the reaction mixture for at least 1 h, involving crystallization methods with a weaker gradient of the polarity of the phases, such as applying layering of toluene/pentane (1 : 1)/ $\text{CH}_2\text{Cl}_2$  instead of hexane/ $\text{CH}_2\text{Cl}_2$ , or higher diluted solutions, a small supramolecular host-guest assembly  $[\text{SbF}_6]@[\{\text{Cp}^{\text{Bn}}\text{Fe}(\eta^5\text{-P}_5)\}_6\{\text{Ag}(\text{NC}(\text{C}_6\text{H}_4)\text{Cl})\}_{9.55}][\text{SbF}_6]_{8.55}$  (**4**) crystallizes in almost quantitative yields. According to the X-ray structural analysis of **4** the spherical inorganic scaffold of the host is formed by six ligands **1** in an distorted trigonal anti-prismatic arrangement which are connected by  $[\text{Ag}\{\text{NC}(\text{C}_6\text{H}_4)\text{Cl}\}]^+$  fragments (Figure 4b). The ideal scaffold would provide 14 accessible positions for Ag atoms, most of which are only partly occupied, resulting in an overall Ag content of 9.55 Ag. This implies that this cationic scaffold can be described as a solid solution of different scaffolds with different Ag content. Thus, for example a mixture of 45%  $[(\mathbf{1})_6(\text{Ag})_9]$  and 55%  $[(\mathbf{1})_6(\text{Ag})_{10}]$  would lead to the above obtained sum formula. Considering the above mentioned scaffold  $[(\mathbf{1})_6(\text{Ag})_{10}]$ , including the 10 positions of Ag atoms with major occupancies, which has at least 55% content in the solid solution, four ligands **1** coordinate in a 1,2,3- and two ligands a 1,2,4-mode towards the Ag atoms. Eight of the ten considered Ag atoms show a trigonal coordination environment of two ligands **1** and one benzonitrile ligand. However, two Ag atoms reveal a pseudo-tetrahedral coordination of one *cyclo*- $\text{P}_5$  ring of **1**, one benzonitrile, one  $\text{SbF}_6^-$  anion and one bent Bn residue (Figure 4a). One  $\text{SbF}_6^-$  anion with a diameter of  $6.96 \text{ \AA}^{16}$  acts as a template for the scaffold and fits into the inner void, with all F atoms pointing towards  $\{\text{Ag}_3\text{P}_6\}$  rings or between two ligands **1**. All remaining anions are located in the outer sphere, two of them form elongated Ag-F contacts of  $2.70 \text{ \AA}$ . Due to the long benzonitrile ligands coordinated to the Ag atoms and the bulky  $\text{Cp}^{\text{Bn}}$  residues, the supramolecular assembly **4** reaches a size of  $3.5 \text{ nm}^{17}$ .

Astonishingly, the structural motif of **3** can be found in the inorganic scaffold of **4**, if minor occupied Ag positions are considered as well (Figure 4c). Furthermore, this pentanuclear moiety  $[(\mathbf{1})_4\text{Ag}_5]$  is



reminiscent of parts in other known spherical supramolecules, as  $[\text{Cp}^*\text{Fe}(\eta^5\text{-P}_5)]@[\{\text{Cp}^*\text{Fe}(\eta^5\text{-P}_5)\}_{12}\{\text{Ag}_{18}(\text{Ag}(\text{CH}_3\text{CN}))_8(\text{SO}_3\text{C}_7\text{H}_7)_{20}\}][\text{SO}_3\text{C}_7\text{H}_7]_6$  and the idealized structures of  $[\text{Cp}^*\text{Fe}(\eta^5\text{-P}_5)](\text{C}_7\text{H}_8)@[\{\text{Cp}^*\text{Fe}(\eta^5\text{-P}_5)\}_{12}(\text{AgSO}_3\text{CF}_3)_{20}]$ ,  $[\{\text{Cp}^{\text{Bn}}\text{Fe}(\eta^5\text{-P}_5)\}_{12}(\text{AgSO}_3\text{CF}_3)_{20}]$  (cf. *Chapter III*) and  $[\{\text{Cp}^{\text{Bn}}\text{Fe}(\eta^5\text{-P}_5)\}_{12}(\text{CuSO}_3\text{CF}_3)_{19.6}]$ .<sup>12</sup> Therefore, the pentanuclear complex **3** can be regarded as a possible intermediate towards spherical supramolecular assemblies, that can be formed in this highly labile self-assembly system.

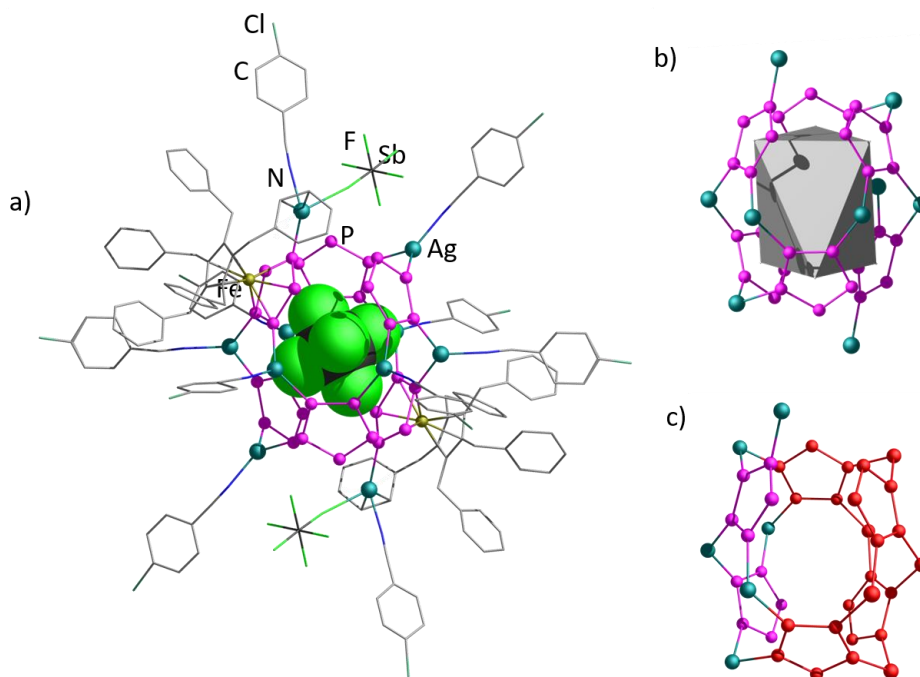


**Figure 4:** a) Cationic spherical structure of **4** with guest depicted in space-filling model, b) inorganic scaffold with inscribed trigonal antiprism, c) pentanuclear motif of **3** marked in red in the scaffold of **4**.

The good solubility of the crystalline compounds **3** and **4** allowed  $^{31}\text{P}\{^1\text{H}\}$  NMR studies at different temperatures. At room temperature two sharp signals appear at 104 and 147 ppm (for **3**) and 104 and 140 ppm (for **4**). Subsequent measurements of the solution of **4** after one and eight days showed that the signal at 140 ppm becomes sharper and slightly shifts towards lower fields to reach 157.22 ppm with  $\omega_{1/2} = 100$  Hz after eight days (cf. *Figure 7* in *Experimental Part*). This indicates that **4** is not stable in solution over a long time, and the coordination of the *cyclo*- $\text{P}_5$  ligand decreases as the free complex **1** shows a chemical shift of 161 ppm in the  $^{31}\text{P}\{^1\text{H}\}$  NMR spectrum.<sup>18</sup> This instability of both **3** and **4** in solution unfortunately impeded successful kinetic NMR experiments, monitoring their formation. However, characteristic signals for **3** and **4** can be obtained, when the crystals are dissolved at low temperatures. The  $^{31}\text{P}\{^1\text{H}\}$  NMR spectra show different signal sets, which can be most likely attributed to the different coordination modes of the *cyclo*- $\text{P}_5$  ligands (cf. *Figure 5* for **3** and *Figure 6* for **4** in *Experimental Part*). For **4**, two broad signal at -47 ppm and 83 ppm can be observed, reminding of previously reported sets of signals assigned to the scaffold-

building P atoms of different coordination modes of **1** in spherical supramolecules (cf. *Chapter III*).<sup>11</sup> This underlines a stability of the spherical scaffolds in solution at low temperatures. In the positive-ion ESI MS spectrum, measured from a CH<sub>2</sub>Cl<sub>2</sub>/CH<sub>3</sub>CN solution, the largest peaks can be attributed to  $m/z = 2248.3$  [ $\{\text{Cp}^{\text{Bn}}\text{Fe}(\eta^5\text{-P}_5)\}_2\text{Ag}_3(\text{SbF}_6)_2$ ]<sup>+</sup> (for **3**) and  $m/z = 1904.82$  [ $\{\text{Cp}^{\text{Bn}}\text{Fe}(\eta^5\text{-P}_5)\}_2\text{Ag}_2(\text{SbF}_6)$ ]<sup>+</sup> (for **4**).

### 4.3 Conclusion

Whereas in *Chapter III* the Ag-based self-assembly of [ $\text{Cp}^{\text{Bn}}\text{Fe}(\eta^5\text{-P}_5)$ ] (**1**) with AgSO<sub>3</sub>CF<sub>3</sub> was reported, this field was herein extended to the use of the weaker coordinating SbF<sub>6</sub><sup>−</sup> as a counter-anion, in order to obtain free coordination sites on the scaffold-building Ag atoms. Thus, from the two-component self-assembly of **1** and AgSbF<sub>6</sub> a dimeric complex [ $\{\text{Cp}^{\text{Bn}}\text{Fe}(\eta^5\text{-P}_5)\}\text{Ag}_2$ ][SbF<sub>6</sub>]<sub>2</sub> (**2**) was obtained, in which the additional coordination site on the Ag atoms is occupied by the benzyl residues of **1**. Furthermore, a third component CN(C<sub>6</sub>H<sub>4</sub>)Cl was added in order to saturate the established free coordination sites at the Ag atoms. Hereby, a curved shell-shaped complex [ $\{\text{Cp}^{\text{Bn}}\text{Fe}(\eta^5\text{-P}_5)\}_4\{\text{Ag}(\text{CN}(\text{C}_6\text{H}_4)\text{Cl})\}_5$ ][SbF<sub>6</sub>]<sub>5</sub>·(CH<sub>2</sub>Cl<sub>2</sub>) (**3**) and trigonal antiprismatic cationic supramolecule [SbF<sub>6</sub>]<sub>6</sub>@ $[\{\text{Cp}^{\text{Bn}}\text{Fe}(\eta^5\text{-P}_5)\}_6\{\text{Ag}(\text{NC}(\text{C}_6\text{H}_4)\text{Cl})\}_{9.55}]^{8.55+}$  (**4**) in obtained, with these benzonitrile ligands saturating the free coordination sites on the scaffold-building Ag atoms, together with bent benzyl residues of **1**. As the three-component system shows a strong sensitivity to the applied reaction conditions, compounds **3** and **4** can be synthesized selectively by strictly distinguishing the procedures regarding reaction times and crystallization methods. The cationic supramolecule **4** stands out of the row of so far known spherical assemblies by offering the smallest scaffold, based on only six pentaphosphaferrocene units, but also due to its multiple positive charge and the ability to encapsulate a small anion. Moreover, the successful use of nitriles as a third component in the self-assembly seems to be a decisive step towards functionalized spherical aggregates.

## 4.4 Experimental Part

### General Remarks

All reactions were performed under an inert atmosphere of dry nitrogen with standard vacuum, Schlenk and glove-box techniques. Solvents were purified, dried and degassed prior to use by standard procedures.  $[\text{Cp}^{\text{Bn}}\text{Fe}(\eta^5\text{-P}_5)]$  was synthesized following reported procedures.<sup>18</sup> Commercially available chemicals ( $\text{AgSbF}_6$ ,  $\text{CN}(\text{C}_6\text{H}_4)\text{Cl}$ ) were used without further purification. Solution NMR spectra were recorded on a Bruker Avance 300 or 400 spectrometer. The  $^{31}\text{P}\{^1\text{H}\}$  MAS spectrum was measured on a Bruker Avance 300. The corresponding ESI-MS spectra were acquired on a ThermoQuest Finnigan MAT TSQ 7000 mass spectrometer. CHN elemental analyses were performed on a Vario EL III apparatus, whereas all other elements were determined by the Catalysis Research Center of the Technical University Munich by photometry, atomic absorption spectroscopy or titrimetry.

### Synthesis of $[\{\text{Cp}^{\text{Bn}}\text{Fe}(\eta^{5:1:1}\text{-P}_5)\}\text{Ag}]_2[\text{SbF}_6]_2$ (**2**)

A solution of **1** (30 mg, 0.04 mmol) in  $\text{CH}_2\text{Cl}_2$  (2 mL) was dropped to a solution of  $\text{AgSbF}_6$  (14 mg, 0.04 mmol) in  $\text{CH}_2\text{Cl}_2$  (3 mL). After stirring for 1 h at r.t. the resulting red solution was layered with pentane. The formation of dark green prisms of **2** can be observed at the phase boundary after several hours. After complete diffusion, the mother liquor is decanted, the crystals are washed with hexane ( $3 \times 10$  mL) and dried *in vacuo*.

Analytical data of **2**:

**Yield:** 20 mg (0.009 mmol, 47 % referred to  $[\text{Cp}^{\text{Bn}}\text{Fe}(\eta^5\text{-P}_5)]$ ).

**$^1\text{H}$  NMR** ( $\text{C}_6\text{D}_6$ ):  $\delta$  [ppm] = 3.77 (s (br), 20 H,  $\text{CH}_2$ ,  $[\text{Cp}^{\text{Bn}}\text{Fe}(\eta^5\text{-P}_5)]$ ), 4.27 (s, 2 H,  $\text{CH}_2\text{Cl}_2$ ), 6.39 (d, 20 H, o-CH,  $[\text{Cp}^{\text{Bn}}\text{Fe}(\eta^5\text{-P}_5)]$ ), 6.67 (t, 20 H, m-CH,  $[\text{Cp}^{\text{Bn}}\text{Fe}(\eta^5\text{-P}_5)]$ ), 6.73 (t, 10 H, p-CH,  $[\text{Cp}^{\text{Bn}}\text{Fe}(\eta^5\text{-P}_5)]$ ).

**$^{31}\text{P}\{^1\text{H}\}$  NMR** ( $\text{C}_6\text{D}_6$ ):  $\delta$  [ppm] = 147.87 (s (br),  $[\text{Cp}^{\text{Bn}}\text{Fe}(\eta^5\text{-P}_5)]$ ).

**$^{19}\text{F}$  NMR** ( $\text{C}_6\text{D}_6$ ):  $\delta$  [ppm] = -112 (s (br),  $\text{SbF}_6^-$ ).

**Positive ion ESI-MS** ( $\text{CH}_2\text{Cl}_2/\text{CH}_3\text{CN}$ ):  $m/z$  (%) = 1563.75  $[\{\text{Cp}^{\text{Bn}}\text{Fe}(\eta^5\text{-P}_5)\}_2\text{Ag}]^+$ , 877.54  $[\{\text{Cp}^{\text{Bn}}\text{Fe}(\eta^5\text{-P}_5)\}\text{Ag}(\text{CH}_3\text{CN})]^+$ , 834.44 (100)  $[\{\text{Cp}^{\text{Bn}}\text{Fe}(\eta^5\text{-P}_5)\}\text{Ag}]^+$ , 191.29  $[\text{Ag}(\text{CH}_3\text{CN})_2]^+$ .

**Negative ion ESI-MS** ( $\text{CH}_2\text{Cl}_2/\text{CH}_3\text{CN}$ ):  $m/z$  (%) = 234.52  $[\text{SbF}_6]^-$ .

**Elemental analysis:** Calculated (%) for  $[\{\text{Cp}^{\text{Bn}}\text{Fe}(\eta^5\text{-P}_5)\}\text{Ag}]_2[\text{SbF}_6]_2 \cdot (\text{CH}_2\text{Cl}_2)_2$  (g/mol): C 42.64, H 3.23; found: C 42.73, H 3.35.

### Synthesis of $[\{\text{Cp}^{\text{Bn}}\text{Fe}(\eta^5\text{-P}_5)\}_4\{\text{Ag}(\text{CN}(\text{C}_6\text{H}_4)\text{Cl})\}_5][\text{SbF}_6]_5 \cdot (\text{CH}_2\text{Cl}_2)$ (**3**)

A mixture of **1** (30 mg, 0.04 mmol) and  $\text{Cl}(\text{C}_6\text{H}_4)\text{CN}$  (55 mg, 0.4) in  $\text{CH}_2\text{Cl}_2$  (5 mL) was dropped to a solution of  $\text{AgSbF}_6$  (15 mg, 0.04 mmol) in  $\text{CH}_2\text{Cl}_2$  (5 mL), stirred for 5 min and layered with pentane or hexane. In an alternative procedure a solution of **1** in hexane is layered over a mixture of  $\text{AgSbF}_6$  and  $\text{Cl}(\text{C}_6\text{H}_4)\text{CN}$  in  $\text{CH}_2\text{Cl}_2$ . In both cases, the growth of green rods of **3** can be observed at the phase boundary after one day. After complete diffusion, the mother liquor is decanted, the crystals are washed with hexane ( $3 \times 5$  mL) and dried *in vacuo*.

Analytical data of **3**:

**Yield:** 26 mg (0.005 mmol, 60 % referred to  $[\text{Cp}^{\text{Bn}}\text{Fe}(\eta^5\text{-P}_5)]$ )

$^1\text{H}$  NMR ( $\text{C}_6\text{D}_6$ ):  $\delta$  [ppm] = 3.95 (m(br), 40 H,  $\text{CH}_2$  (**1b**)), 4.25 (2H,  $\text{CH}_2\text{Cl}_2$ ), 6.44 (m(br), 40H, *ortho*-CH (**1b**)), 6.48 (m, 10H,  $\text{Cl}(\text{C}_6\text{H}_4)\text{CN}$ ), 6.64 (t, 40 H, *meta*-CH (**1b**)), 6.70 (d, 20H, *para*-CH (**1b**)), 6.76 (m, 10H,  $\text{Cl-C}_6\text{H}_4\text{-CN}$ ).

$^{31}\text{P}\{^1\text{H}\}$  NMR ( $\text{CD}_2\text{Cl}_2$ , 293 K):  $\delta$  [ppm] = 104.03 (s,  $\omega$  = 1170 Hz,  $[\text{Cp}^{\text{Bn}}\text{Fe}(\eta^5\text{-P}_5)]$ ), 146.56 (s,  $\omega$  = 578 Hz,  $[\text{Cp}^{\text{Bn}}\text{Fe}(\eta^5\text{-P}_5)]$ ).

$^{31}\text{P}\{^1\text{H}\}$  NMR ( $\text{CD}_2\text{Cl}_2$ , 193 K):  $\delta$  [ppm] = 104.20 (m(br)), 151.30 (m(br)).

$^{19}\text{F}$  NMR ( $\text{C}_6\text{D}_6$ ):  $\delta$  [ppm] = -113.9  $[\text{SbF}_6]^-$ .

**Positive ion ESI-MS** ( $\text{CH}_2\text{Cl}_2/\text{CH}_3\text{CN}$ ):  $m/z$  (%) = 2248.3  $[\{\text{Cp}^{\text{Bn}}\text{Fe}(\eta^5\text{-P}_5)\}_2\text{Ag}_3(\text{SbF}_6)_2]^+$ , 1904.6  $[\{\text{Cp}^{\text{Bn}}\text{Fe}(\eta^5\text{-P}_5)\}_2\text{Ag}_2(\text{SbF}_6)]^+$ , 1218.9  $[\{\text{Cp}^{\text{Bn}}\text{Fe}(\eta^5\text{-P}_5)\}\text{Ag}_2(\text{SbF}_6)(\text{CH}_3\text{CN})]^+$ , 1176.7  $[\{\text{Cp}^{\text{Bn}}\text{Fe}(\eta^5\text{-P}_5)\}\text{Ag}_2(\text{SbF}_6)]^+$ , 971.9  $[\{\text{Cp}^{\text{Bn}}\text{Fe}(\eta^5\text{-P}_5)\}\text{Ag}(\text{NC}(\text{C}_6\text{H}_4)\text{Cl})]^+$ , 875.4  $[\{\text{Cp}^{\text{Bn}}\text{Fe}(\eta^5\text{-P}_5)\}\text{Ag}(\text{CH}_3\text{CN})]^+$ , 832.9 (100)  $[\{\text{Cp}^{\text{Bn}}\text{Fe}(\eta^5\text{-P}_5)\}\text{Ag}]^+$ , 382.9  $[\text{Ag}(\text{NC}(\text{C}_6\text{H}_4)\text{Cl})_2]^+$ , 286.9  $[\text{Ag}(\text{CH}_3\text{CN})(\text{CN}(\text{C}_6\text{H}_4)\text{Cl})]^+$ , 245.9  $[\text{Ag}(\text{NC}(\text{C}_6\text{H}_4)\text{Cl})]^+$ , 190.9  $[\text{Ag}(\text{CH}_3\text{CN})_2]^+$ .

**Negative ion ESI-MS** ( $\text{CH}_2\text{Cl}_2/\text{CH}_3\text{CN}$ ):  $m/z$  (%) = 234.7 (100)  $[\text{SbF}_6]^-$ .

**Elemental analysis:** Calculated (%) for  $[\{\text{Cp}^{\text{Bn}}\text{Fe}(\eta^5\text{-P}_5)\}_4\{\text{Ag}(\text{CN}(\text{C}_6\text{H}_4)\text{Cl})\}_5][\text{SbF}_6]_5 \cdot (\text{CH}_2\text{Cl}_2)$  (5396.56 g/mol): C 43.64, H 3.03, N 1.30 ; found: C 42.73, H 3.14, N 1.14.

### Synthesis of $[\text{SbF}_6]@[\{\text{Cp}^{\text{Bn}}\text{Fe}(\eta^5\text{-P}_5)\}_6\{\text{Ag}(\text{NC}(\text{C}_6\text{H}_4)\text{Cl})\}_{9.55}][\text{SbF}_6]_{8.55}$ (**4**)

A mixture of **1** (30 mg, 0.04 mmol) and  $\text{Cl}(\text{C}_6\text{H}_4)\text{CN}$  (55 mg, 0.4 mmol) in  $\text{CH}_2\text{Cl}_2$  (5 mL) was dropped to a solution of  $\text{AgSbF}_6$  (15 mg, 0.04 mmol) in  $\text{CH}_2\text{Cl}_2$  (5 mL), stirred at least for 1h min and layered with pentane or hexane. In an alternative procedure a mixture of **1** (30 mg, 0.04 mmol) and  $\text{Cl}(\text{C}_6\text{H}_4)\text{CN}$  (55 mg, 0.4 mmol) in an solvent mixture of toluene/pentane (1 : 1, 8 mL) was layered on a solution of  $\text{AgSbF}_6$  in  $\text{CH}_2\text{Cl}_2$  (8 mL). After complete diffusion, the reaction mixture was layered once more with hexane. The growth of red blocks of **4** can be observed in both procedures at the phase boundary after one day. After complete diffusion, the mother liquor is decanted, the crystals are washed with hexane ( $3 \times 5$  mL) and dried *in vacuo*.

Analytical data of **4**:

**Yield:** 49 mg (0.0055 mmol, 82 % referred to  $[\text{Cp}^{\text{Bn}}\text{Fe}(\eta^5\text{-P}_5)]$ )

**$^1\text{H}$  NMR** ( $\text{CD}_2\text{Cl}_2$ ):  $\delta$  [ppm] = 3.60 (s, br, 60H,  $\text{CH}_2(\mathbf{1b})$ ), 6.35 (m, br, 60H, *ortho*-CH (**1b**)), 6.87 (s, br, 60H, *meta*-CH (**1b**)), 7.00 (s, br, 30H, *para*-CH (**1b**)), 7.37 - 7.43 (m, 40H, Cl- $\text{C}_6\text{H}_4$ -CN).

**$^{31}\text{P}\{^1\text{H}\}$  NMR** ( $\text{CD}_2\text{Cl}_2$ , 293 K):  $\delta$  [ppm] = 104.46 (s), 140.33 (s).

**$^{31}\text{P}\{^1\text{H}\}$  NMR** ( $\text{CD}_2\text{Cl}_2$ , 193 K):  $\delta$  [ppm] = -46.58 (m(br),  $\omega_{1/2}$  = 6000 Hz), 83.24 (m(br),  $\omega_{1/2}$  = 7000 Hz).

**Positive ion ESI-MS** ( $\text{CH}_2\text{Cl}_2/\text{CH}_3\text{CN}$ ):  $m/z$  (%) = 1904.82  $[\{\text{Cp}^{\text{Bn}}\text{Fe}(\eta^5\text{-P}_5)\}_2\text{Ag}_2(\text{SbF}_6)]^+$ , 832.90 (100)  $[\{\text{Cp}^{\text{Bn}}\text{Fe}(\eta^5\text{-P}_5)\}\text{Ag}]^+$ .

**Negative ion ESI-MS** ( $\text{CH}_2\text{Cl}_2/\text{CH}_3\text{CN}$ ):  $m/z$  (%) = 234.90  $[\text{SbF}_6]^-$ .

**Elemental analysis:** Calculated (%) for  $[\text{SbF}_6]@[\{\text{Cp}^{\text{Bn}}\text{Fe}(\eta^5\text{-P}_5)\}_6\{\text{Ag}(\text{NC}(\text{C}_6\text{H}_4)\text{Cl})\}_{10}][\text{SbF}_6]_{10}$  (9170.39 g/mol): C 40.60, H 2.75, N 1.53, Ag 11.76, Fe 3.65, Cl 3.87, P 10.13; found: C 38.93, H 2.74, N 1.72, Ag 11.80, Fe 3.30, Cl 3.61, P 9.38.

NMR spectroscopy

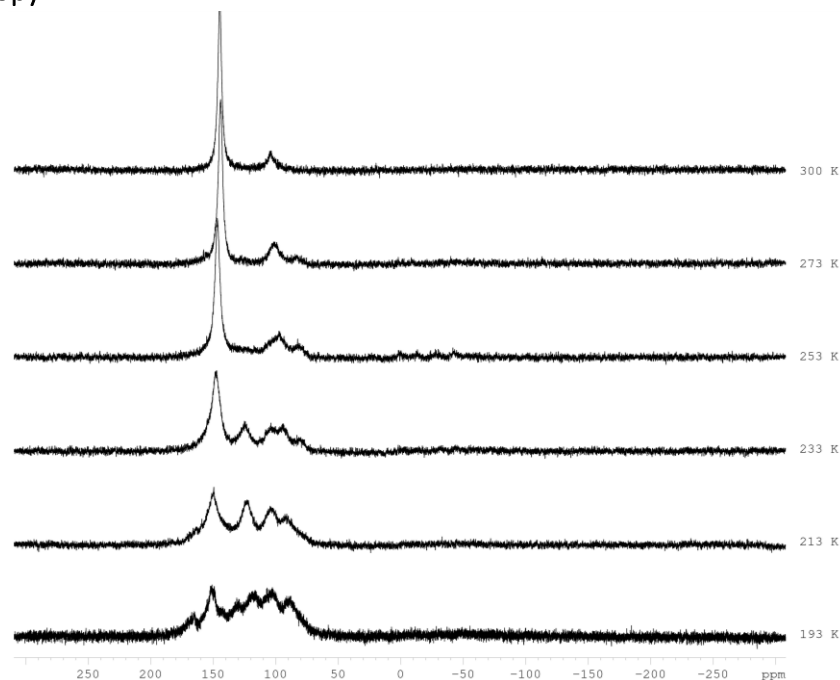


**Figure 5:**  $^{31}\text{P}\{^1\text{H}\}$  NMR spectrum of **3** in  $\text{CD}_2\text{Cl}_2$  at variable temperatures.

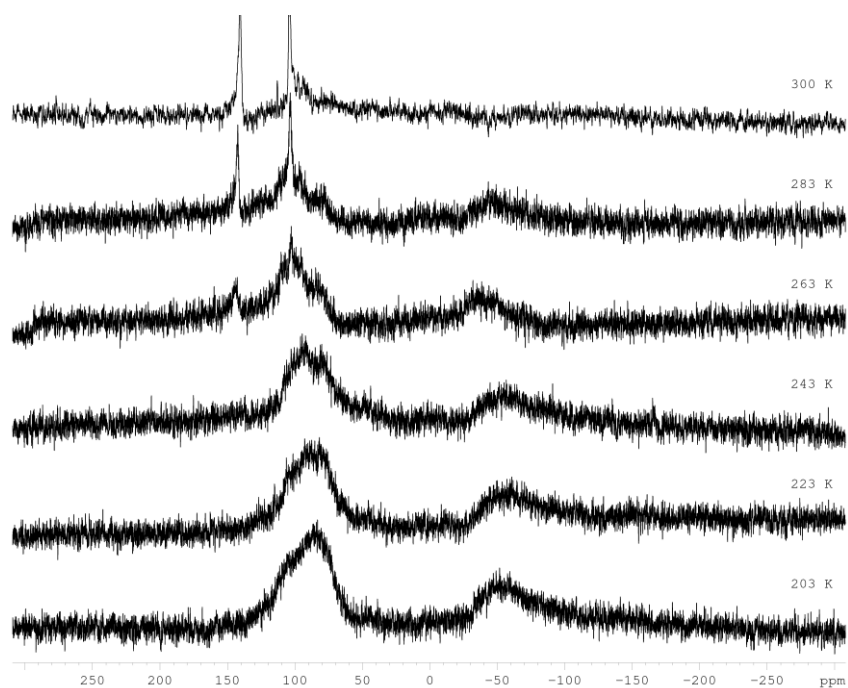


Figure 6:  $^{31}\text{P}\{^1\text{H}\}$  NMR spectrum of **4** in  $\text{CD}_2\text{Cl}_2$  at variable temperatures.

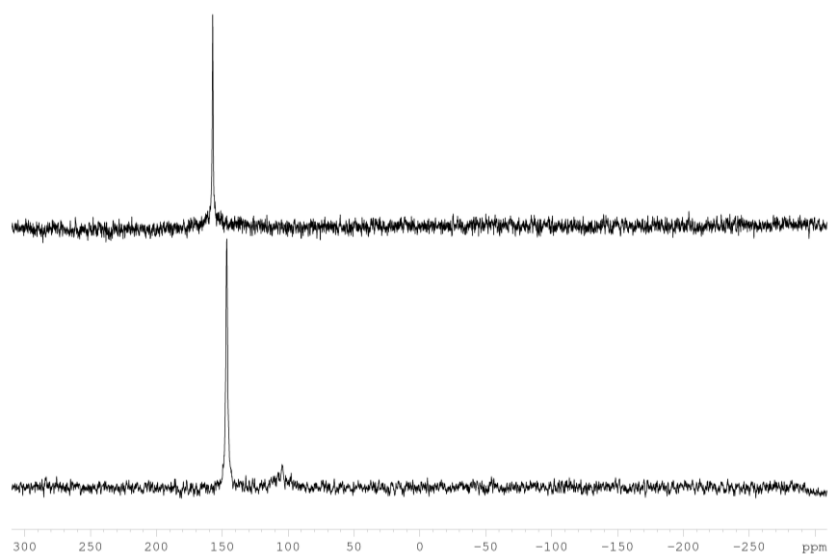


Figure 7:  $^{31}\text{P}\{^1\text{H}\}$  NMR spectrum of crystals of **4** in  $\text{CD}_2\text{Cl}_2$  after 24 h in solution (bottom) and after one week in solution (top). No precipitate or colour change was observed.

## 4.5 Crystallographic Details

Crystals of **2-4** were taken from a Schlenk flask under a stream of argon and immediately covered with perfluorinated Fomblin® mineral oil to prevent both, decomposition and a loss of solvent. The quickly chosen single crystals covered by a drop of the oil were directly placed into a stream of cold nitrogen with the pre-centered goniometer head with CryoMount® and attached to the goniometer of a diffractometer. Crystals of **3** and **4** were carefully selected, mounted on a magnetic holder, checked for quality and placed into a Dewar vessel in liquid nitrogen using standard cryocrystallography tools. After a few weeks, they were transported to the DESY PETRA III synchrotron (Hamburg, Germany). Using standard procedures, it was placed into a vessel filled with liquid nitrogen among other crystals. A robotic mounting/demounting was used for further manipulations in the P11 beamline hutch.<sup>19</sup>

The data for **2-4** were collected on an Agilent Technologies diffractometer equipped with a Titan<sup>52</sup> CCD detector and a SuperNova Cu K $\alpha$  microfocus source  $\omega$  scans. Alternative datasets for X-ray diffraction experiment for **3** and **4** were collected at 80 K at the DESY PETRA III synchrotron (beamline P11) using robotic mounting. Data collection was performed by a shutterless 360°  $\phi$ -rotation at wavelength  $\lambda = 0.6199 \text{ \AA}$  (20 keV). Data reduction for all crystal structures was performed with CrysAlis software.<sup>20</sup> Analytical absorption correction for **2-4** measured in-house, was applied based on crystal faces; whereas for synchrotron diffraction experiments (**3**, **4**), an empirical absorption correction using equivalent reflections was used. Crystallographic data and further details of the diffraction experiments are given in *Tables 1-2* (not listed for preliminary data for **3** and **4**).

The structures were solved by direct methods with *SHELXT*<sup>[21]</sup> and were refined by full-matrix least-squares method against  $F^2$  in anisotropic approximation using multiprocessor variable memory versions of *SHELXL* (2014-2015). All non-hydrogen atoms were refined anisotropically, whereas the hydrogen atoms were refined riding on pivot atoms. For **3** and **4**, the best datasets will be used for a final structure refinement after estimation of the data quality for several crystals measured in-house and at DESY synchrotron. In **3** and **4**, the  $\text{SbF}_6^-$  counter-anions are disordered over two or more close positions. The occupation factors for disordered positions of Sb atoms (and some Ag atoms of the inorganic scaffold in **4**) atoms were refined with fixed isotropic  $U_{\text{iso}}$  similar to the average  $U_{\text{iso}}$  (usually 0.025 - 0.035  $\text{\AA}^2$ ) for the fully occupied heavy atoms in the corresponding structure. For **4**, the disorder is so severe, that for minor disordered positions of the  $\text{SbF}_6^-$  counter-anions, not all fluorine atoms were located from the difference Fourier map. In case of small

occupancy for a certain disorder component, F atoms were refined isotropically. This work is still in progress.

**Table 1:** Experimental details for compounds **2**.

Crystal data	<b>2</b> (final data)
Chemical formula	C <sub>80</sub> H <sub>70</sub> Ag <sub>2</sub> Fe <sub>2</sub> P <sub>10</sub> ·2(F <sub>6</sub> Sb)·2(CH <sub>2</sub> Cl <sub>2</sub> )
<i>M<sub>r</sub></i> (g/mol)	2309.85
Crystal system, space group	Monoclinic, <i>P</i> 2 <sub>1</sub> / <i>c</i>
Temperature (K)	123
<i>a</i> , <i>b</i> , <i>c</i> (Å)	20.34757(15), 10.97815(8), 19.23413(15)
$\alpha$ , $\beta$ , $\gamma$ (°)	90, 96.8959(7), 90
<i>V</i> (Å <sup>3</sup> )	4265.41(6)
<i>Z</i>	2
<i>F</i> (000)	2280
<i>D<sub>x</sub></i> (Mg m <sup>-3</sup> )	1.798
Radiation type	Cu K $\alpha$
$\mu$ (mm <sup>-1</sup> )	14.74
Crystal shape	prism
Colour	clear dark green
Crystal size (mm)	0.20 × 0.10 × 0.08
Data collection	
Diffractometer	Xcalibur, Atlas <sup>S2</sup> , Gemini ultra
Absorption correction	Analytical
<i>T<sub>min</sub></i> , <i>T<sub>max</sub></i>	0.201, 0.446
No. of measured, independent and observed [ <i>I</i> > 2 $\sigma$ ( <i>I</i> )] reflections	27466, 7486, 6522
<i>R<sub>int</sub></i>	0.027
(sin $\theta$ /λ) <sub>max</sub> (Å <sup>-1</sup> )	0.596
Range of <i>h</i> , <i>k</i> , <i>l</i>	<i>h</i> = -19 → 24, <i>k</i> = -12 → 13, <i>l</i> = -22 → 22
Refinement	
<i>R</i> [ <i>F</i> <sup>2</sup> > 2 $\sigma$ ( <i>F</i> <sup>2</sup> )], <i>wR</i> ( <i>F</i> <sup>2</sup> ), <i>S</i>	0.022, 0.053, 1.03
No. of reflections	7486
No. of parameters	514
No. of restraints	0
H-atom treatment	H-atom parameters constrained
$\Delta$ <sub>max</sub> , $\Delta$ <sub>min</sub> (e Å <sup>-3</sup> )	0.58, -0.67
Computer programs for compound <b>2</b> : <i>CrysAlis PRO</i> 1.171.38.41 (Rigaku OD, 2015), <i>SHELXT2014</i> (Sheldrick, 2014), <i>SHELXL2014/7</i> (Sheldrick, 2014).	



**Table 2:** Experimental details for compounds **3** and **4**.

Crystal data	<b>3</b> (preliminary data)	<b>4</b> (preliminary data)
Chemical formula	$[(C_{40}H_{35}FeP_5)_4\{Ag(CN(C_6H_4)Cl)\}_5][SbF_6]_5 \cdot (CH_2Cl_2)$	$C_{314}H_{238}N_{10}F_{57.3}P_{30}Cl_{12}Fe_6Ag_{9.55}Sb_{9.55}$
$M_r$	5191.32	8917.61
Crystal system, space group	orthorhombic, $P2_12_12_1$	monoclinic, $P\bar{1}$
Temperature (K)	89.9(4)	91.15
$a, b, c$ (Å)	23.8845(3), 26.1568(2), 34.3516(3)	20.1153(2), 23.2010(3), 24.0639(2)
$\alpha, \beta, \gamma$ (°)	90, 90, 90	98.4345(10), 112.9969(11), 112.8523(12)
$V$ (Å <sup>3</sup> )	21460.9(4)	8917.62(18)
$Z$	4	1
$F(000)$	10216.0	4472.9
$D_x$ (Mg m <sup>-3</sup> )	1.607	1.702
Radiation type	Cu $K\alpha$	Cu $K\alpha$
$\mu$ (mm <sup>-1</sup> )	13.17	14.41
Crystal shape	rod	plate
Colour	brown	brown
Crystal size (mm)	0.11 × 0.07 × 0.05	0.17 × 0.10 × 0.06
<b>Refinement</b>		
$R[F^2 > 2\sigma(F^2)], wR(F^2), S$	0.0683, 0.2122, 1.048	

## 4.6 Author Contributions

- The synthesis and characterization of all compounds were performed by B. Hiltl.
- The manuscript (introduction, results and discussions, experimental part, conclusion; including figures and graphical abstract) was written by B. Hiltl.
- The section ‘crystallographic details’ was written by Dr. E. Peresypkina
- All X-ray structural analysis was performed by Dr. E. Peresypkina and Dr. Sc. A. V. Virovets with B. Hiltl.

## 4.7 References

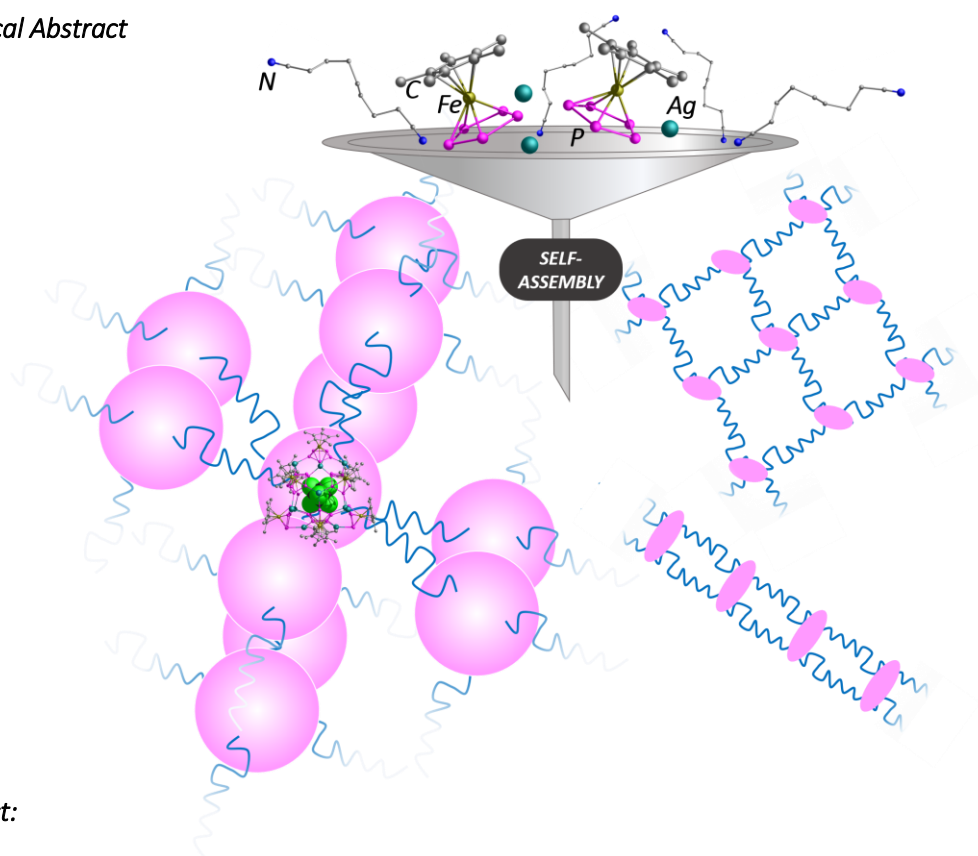
- <sup>1</sup> a) C. J. Brown, F. D. Toste, R. G. Bergman, K. N. Raymond, *Chem. Rev.* **2015**, *115*, 3012-3035; b) S. H. A. M. Leenders, R. Gramage-Doria, B. de Bruin, J. N. H. Reek, *Chem. Soc. Rev.* **2015**, *44*, 433-448; c) P. Howlader, P. Das, E. Zangrando, P. S. Mukherjee, *J. Am. Chem. Soc.* **2016**, *138*, 1668-1676.
- <sup>2</sup> a) N. Ahmad, H. A. Younus, A. H. Chughtai, F. Verpoort, *Chem. Soc. Rev.* **2015**, *44*, 9-25; b) N. Basilio, U. Pischel, *Chem. Eur. J.* **2016**, *22*, 15208-15211; M. J. Webber, R. Langer, *Chem. Soc. Rev.* **2017**, *46*, 6600-6620.
- <sup>3</sup> M. Ikemi, T. Kikuchi, S. Matsumura, K. Shiba, S. Sato, M. Fujita, *Chem. Sci.* **2010**, *1*, 68-71.
- <sup>4</sup> S. Sato, Y. Yoshimasa, D. Fujita, M. Yagi-Utsumi, T. Yamaguchi, K. Kato, M. Fujita, *Angew. Chem., Int. Ed.* **2015**, *54*, 8435-8439.
- <sup>5</sup> a) F. Diederich, *Pure Appl. Chem.* **1997**, *69*, 395-400; b) Y. Nakamura, S.-i. Kato, *Chem. Rec.* **2011**, *11*, 77-94; c) G.-W. Wang, *Top. Organomet. Chem.* **2016**, *55*, 119-136.
- <sup>6</sup> a) D. Fujita, Y. Ueda, S. Sato, N. Mizuno, T. Kumasaka, M. Fujita, *Nature* **2016**, *540*, 563-566; b) T. R. Cook, P. J. Stang, *Chem. Rev.* **2015**, *115*, 7001-7045; S. Mukherjee, P. S. Mukherjee, *Chem. Commun.* **2014**, *50*, 2239-2248; d) A. Schindler, C. Heindl, G. Balazs, C. Groeger, A. V. Virovets, E. V. Peresypkina, M. Scheer, *Chem. Eur. J.* **2012**, *18*, 829-835; e) L. H. Tong, L. Guenee, A. F. Williams, *Inorg. Chem.* **2011**, *50*, 2450-2457.
- <sup>7</sup> a) D. Ajami, J. Rebek, Jr., *Nat. Chem.* **2009**, *1*, 87-90; b) S. J. Park, O.-H. Kwon, K.-S. Lee, K. Yamaguchi, D.-J. Jang, J.-I. Hong, *Chem. Eur. J.* **2008**, *14*, 5353-5359; c) L. R. MacGillivray, J. L. Atwood, *Nature* **1997**, *389*, 469-472.
- <sup>8</sup> a) W. Wei, W. Li, Z. Li, W. Su, M. Hong, *Chem. Eur. J.* **2013**, *19*, 469-473; b) G. S. Ananchenko, K. A. Udachin, J. A. Ripmeester, T. Perrier, A. W. Coleman, *Chem. Eur. J.* **2006**, *12*, 2441-2447; c) S. Welsch, C. Groeger, M. Sierka, M. Scheer, *Angew. Chem., Int. Ed.* **2011**, *50*, 1435-1438.
- <sup>9</sup> a) M. Tominaga, K. Suzuki, T. Murase, M. Fujita, *J. Am. Chem. Soc.* **2005**, *127*, 11950-11951; b) K. Harris, Q.-F. Sun, S. Sato, M. Fujita, *J. Am. Chem. Soc.* **2013**, *135*, 12497-12499; c) T. Kikuchi, S. Sato,

- D. Fujita, M. Fujita, *Chem. Sci.* **2014**, *5*, 3257-3260; d) S. Sato, M. Ikemi, T. Kikuchi, M. Fujita, S. Matsumura, K. Shiba, *J Am Chem Soc* **2015**, *137*, 12890-12896.
- 10 a) J. Bai, A. V. Virovets, M. Scheer, *Science* **2003**, *300*, 781-783; b) M. Scheer, A. Schindler, R. Merkle, B. P. Johnson, M. Linseis, R. Winter, C. E. Anson, A. V. Virovets, *J. Am. Chem. Soc.* **2007**, *129*, 13386-13387; c) C. Heindl, E. V. Peresypkina, A. V. Virovets, W. Kremer, M. Scheer, *J. Am. Chem. Soc.* **2015**, *137*, 10938-10941; d) S. Heindl, E. Peresypkina, J. Sutter, M. Scheer, *Angew. Chem., Int. Ed.* **2015**, *54*, 13431-13435.
- 11 F. Dielmann, M. Fleischmann, C. Heindl, E. V. Peresypkina, A. V. Virovets, R. M. Gschwind, M. Scheer, *Chem. Eur. J.* **2015**, *21*, 6208-6214.
- 12 C. Heindl, E. Peresypkina, A. V. Virovets, I. S. Bushmarinov, M. G. Medvedev, B. Kraemer, B. Dittrich, M. Scheer, *Angew. Chem., Int. Ed.* **2017**, *56*, 13237-13243.
- 13 C. Schwarzmaier, A. Schindler, C. Heindl, S. Scheuermayer, E. V. Peresypkina, A. V. Virovets, M. Neumeier, R. Gschwind, M. Scheer, *Angew. Chem., Int. Ed.* **2013**, *52*, 10896-10899.
- 14 a) M. Scheer, A. Schindler, C. Groeger, A. V. Virovets, E. V. Peresypkina, *Angew. Chem., Int. Ed.* **2009**, *48*, 5046-5049; b) A. Schindler, C. Heindl, G. Balazs, C. Groeger, A. V. Virovets, E. V. Peresypkina, M. Scheer, *Chem. Eur. J.* **2012**, *18*, 829-835.
- 15 The distance of the  $\pi$ -contact was measured as the distance between the Ag atom and the center of the interacting bond.
- 16 The diameter was calculated considering the maximum distance between two F atoms plus twice the van der Waals radius of F (147 pm from A. Bondi, *J. Phys. Chem.* **1964**, *68*, 441-451).
- 17 The outer diameter of **4** was calculated as the maximum distance between two opposing Cl atoms of benzonitrile ligands plus two times the van der Waals radius of Cl (175 pm from A. Bondi, *J. Phys. Chem.* **1964**, *68*, 441-451).
- 18 F. Dielmann, R. Merkle, S. Heindl, M. Scheer, *Z. Naturforsch.* **2009**, *64*, 3.
- 19 A. Burkhardt, T. Pakendorf, B. Reime, et al, *Eur. Phys. J. Plus* **2016**, *131*, 56-64.
- 20 CrysAlisPro., different versions (Rigaku OD).
- 21 G. M. Sheldrick, *Acta Cryst. sect. C* **2015**, *C71*, 3.

## 5. Three-Component Self-Assembly: A Way to Overcome Simple Coordination Polymers in Favor of 3D Connected Spherical Supramolecular Aggregates

B. Hiltl, E. Peresyphkina, A. V. Virovets, K. Grill, W. Kremer, M. Scheer

### Graphical Abstract



### Abstract:

The dependency of the length of fully flexible aliphatic dinitriles  $\text{NC}(\text{CH}_2)_x\text{CN}$  ( $x = 5 - 7$ ) to form either coordination polymers or 3D linked supramolecular spheres with  $[\text{Cp}^*\text{Fe}(\eta^5\text{-P}_5)]$  (**1**) and  $\text{AgSbF}_6$  is reported. By one-pot self-assembly reactions we obtained diverse 1D, 2D and 3D coordination polymers, containing all three components. Furthermore,  $x = 7$  was experimentally found to be necessary for the formation of the supramolecular assemblies  $[\{\text{Cp}^*\text{Fe}(\eta^5\text{-P}_5)\}_9\text{Ag}_{11}]$ , linked by  $\text{NC}(\text{CH}_2)_7\text{CN}$  to a first unprecedented 3D network of nano-sized supramolecules as nodes. These novel polycationic host scaffolds exhibit a capped tetragonal anti-prismatic form and encapsulate one  $\text{SbF}_6^-$  anion as a guest. By coordination of the nitrile groups of the linkers towards the Ag atoms a 10-connected network with the supramolecular nodes is formed.

## 5.1 Introduction

Supramolecular chemistry relies on weak interactions, such as hydrogen bonding,  $\pi$ - $\pi$  stacking and van der Waals interactions, and enables molecular recognition effects and self-assembly.<sup>1</sup> Thus, the synthesis of self-assembled products is decisively dependent on the exact abundance by the reaction conditions. Small variations of stoichiometry, solvents or concentration may cause drastic changes in the structure of the resulting supramolecular architectures.<sup>2</sup> To create a rational design approach towards supramolecular motifs through self-assembly, these crucial aspects have to be considered and addressed thoroughly.

*Fujita et al.* synthesized  $M_{12}L_{24}$  and  $M_{24}L_{48}$  structures, consisting of  $Pd^{2+}$  and a rigid bent dipyrindine linker, showing either cuboctahedral or rhombicuboctahedral scaffolds.<sup>3</sup> A selective synthesis of these structural motifs was enabled by the rational prediction and experimental proof of the influence of the angle of the bent linker (*Figure 1a*).<sup>4</sup> Usually, rigid aromatic system containing linkers, like those used by *Fujita*, are used in Supramolecular Chemistry, enabling both a synthetic fine-tuning of the structural characteristics of the spacer and a good predictability of its behavior, due to a predefined geometry. However, leaving self-assembling systems enough flexibility, fully aliphatic linkers can induce unprecedented properties and structural motifs in their assemblies.<sup>6</sup> Nevertheless, only very few coordination compounds involving these ligands are known.<sup>5</sup> *Lescop et al.*, however, used flexible aliphatic linkers and showed on the system of a preassembled bimetallic clip with  $NC(CH_2)_xCN$  ( $x = 3 - 10, 12$ ) the distinctive influence of the linker length on the architectures of the obtained coordination products (*Figure 1c*).<sup>6</sup> On the one hand, shorter linkers lead to 1D zig-zag polymers, maximizing the distances between the bulky clips. On the other hand, with increasing length of the linker, the coordination products form metallacycles or, reaching the maximal size of  $x = 12$ , a 1D polymer in the solid state aggregating to pairs of separate strands driven by London dispersion forces of the interacting aliphatic chains.

Based on the discovery of metallosupramolecular spheres built up by 12  $[Cp^*Fe(\eta^5-P_5)]$  (**1**) ligands and  $CuX$  fragments ( $X = Cl^-, Br^-$ ), analogues to  $C_{80}$  fullerene topology,<sup>7</sup> our group also investigated the impact of variations in the nature of the building blocks. Changes from  $Cu^I$  to  $Cu^{II}$ , from  $X$  to  $SO_3CF_3^-$  or variation of the templates were proved to affect the architectures of the inorganic scaffolds drastically.<sup>8</sup> Exemplarily, the steric increase of the  $Cp^R$  residue of **1** from  $Cp^*$  to  $Cp^{BIG}$  ( $C_5(4-nBuC_6H_4)_5$ ) was exploited to effect an expansion of the spherical scaffold from a topologically  $I_h-C_{80}$  fullerene-analogous  $\{[Cp^*Fe(\eta^5-P_5)]_{12}(CuX)_{20}\}$  to an  $I-C_{140}$  analogous scaffold  $\{[Cp^{BIG}Fe(\eta^5-P_5)]_{12}(CuBr)_{92}\}$  (*Figure 1b*).<sup>9</sup>

**60 | V - Three-Component Self-Assembly:**  
**A Way to Overcome Simple Coordination Polymers in Favor**  
**of 3D Connected Spherical Supramolecular Aggregates**

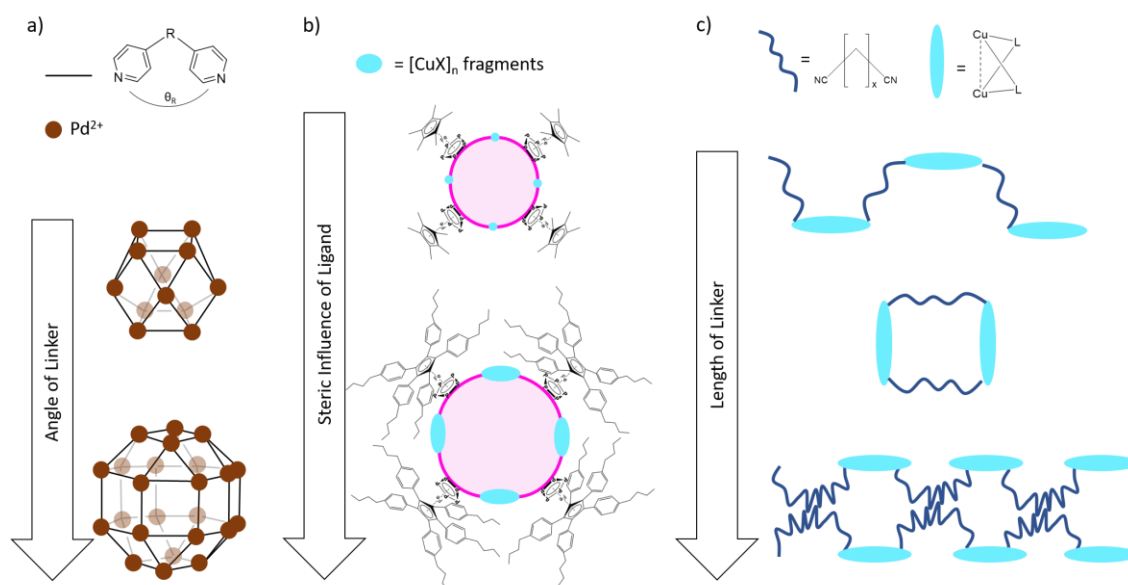


**Figure 1:** Selected factors controlling the architecture of self-assembled products: a) the bending angle of the linker<sup>3,4</sup> or b) the steric properties of a ligand,<sup>9</sup> c) the length of the linker.<sup>6</sup>

Besides **1**,  $[\{\text{Cp}^*\text{Mo}(\text{CO})_2\}_2(\mu, \eta^{2:2}\text{-P}_2)]$  was examined, proving to be a suitable building block in three-component self-assembly processes to form diverse coordination polymers, upon combining it with coinage metal salts of weakly coordinating anions and organic N donor linkers.<sup>10</sup> Therefore, the question arises, if a combination of these previously considered approaches is possible: The formation of spherical supramolecular assemblies, based on **1** and coinage metal ions, and the three-component self-assembly method, implementing a long flexible linking unit. If this approach is successful, the possibilities resulting are of great interest: Do linked spherical scaffolds assemble with the supramolecules acting as nodes in a network or are the molecular building blocks react to give nD polymeric frameworks? Thus it could be possible to overcome the simple formation of multidimensional polymers of small molecular building blocks by the assembly of spherical supramolecular aggregates, which are interconnected by bidentate linkers. To interconnect the potential scaffold building metal cations a long linking unit is needed. The possibilities that arise from the flexibility of the connecting part encouraged us to extend the system of **1** and coinage metal salt by flexible ditopic nitrile linkers  $\text{NC}(\text{CH}_2)_x\text{CN}$ , systematically exploring the influence of the length of the aliphatic backbone  $x = 5 - 7$  on the architecture and dimensionality of the resulting supramolecular assemblies. Herein, we describe for the first time a detailed study on the self-assembly of this three-component system, in dependency on the length of the linking unit. For this purpose, free coordination sites at the metal atoms of the spherical scaffolds are required. Hence, the application of  $\text{AgSbF}_6$  besides **1** came to mind, with  $\text{SbF}_6^-$  acting as a weakly coordinating anion and thus most likely leaving coordination sites at the Ag atoms available to additional linkers.

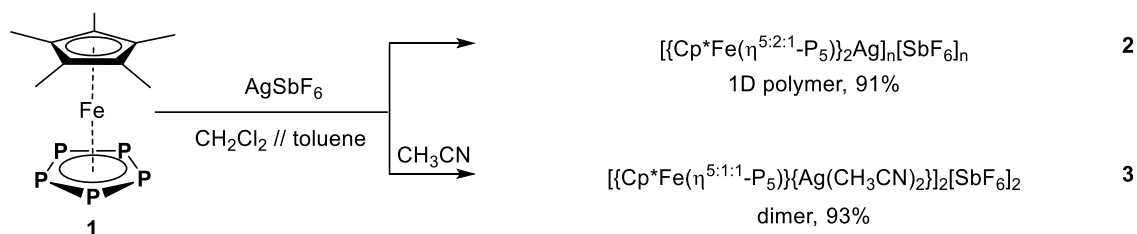
To prove the feasibility of this concept, the coordination chemistry of **1** and AgSbF<sub>6</sub> had to be investigated in a two-component way, using solvents with and without coordinating behavior.

## 5.2 Results and Discussion

To obtain the compounds discussed herein, one general reaction procedure was applied, with only small variations. A solution of  $\text{AgSbF}_6$  in  $\text{CH}_2\text{Cl}_2$  was first layered with a mixture of  $\text{CH}_2\text{Cl}_2$  and toluene (2:1), to prevent the formation of powder, and then with a layer of **1** in toluene.

## Two-Component Self-Assembly of **1** and AgSbF<sub>6</sub>

For a general examination of the coordination chemistry of **1** with AgSbF<sub>6</sub>, different solvents were applied. Using non-coordinating CH<sub>2</sub>Cl<sub>2</sub> / toluene for the layering, after one day [ $\text{Cp}^*\text{Fe}(\eta^{5:2:1}\text{-P}_5)\text{Ag}$ ]<sub>n</sub>[SbF<sub>6</sub>]<sub>n</sub> (**2**) forms at the phase boundary with no byproducts observed. (*Scheme 2*) By changing the solvent of the Ag-containing layer to a mixture of CH<sub>2</sub>Cl<sub>2</sub> and CH<sub>3</sub>CN (2:1), a dimeric compound [ $\text{Cp}^*\text{Fe}(\eta^{5:1:1}\text{-P}_5)\{\text{Ag}(\text{CH}_3\text{CN})_2\}_2$ ][SbF<sub>6</sub>]<sub>2</sub> (**3**) forms after layering the fully diffused reaction solution with *n*-pentane. The formations of compounds **2** and **3** are observed independent on the applied stoichiometric ratio of **1** and AgSbF<sub>6</sub> and can be isolated in excellent crystalline yields.



**Scheme 1:** Reactions of **1** with AgSbF<sub>6</sub> in different solvents.

X-ray structure analysis of crystalline **2** revealed a 1D polymeric structure (*Figure 2a*). The *cyclo*-P<sub>5</sub> ligands coordinate in a 1,2,3-mode to Ag atoms and act additionally as bridging ligands between two Ag atoms with one end-on and one side-on coordination mode per ligand **1**. The Ag atoms in turn are pseudo-tetrahedrally coordinated by six P atoms of four *cyclo*-P<sub>5</sub> ligands. This reveals a similar cationic part to that of the known 1D polymer [Ag{Cp\*Fe( $\eta^{5:2:1}$ -P<sub>5</sub>)}]<sub>2</sub>[Al{OC(CF<sub>3</sub>)<sub>3</sub>}]<sub>n</sub>.<sup>11</sup> Though being much smaller ( $d(\text{SbF}_6^-) = 6.69 \text{ \AA}$ ,  $d([\text{Al}\{\text{OC}(\text{CF}_3)_3\}_4]^-) = 12.46 \text{ \AA}$ )<sup>12</sup> the weakly coordinating nature of SbF<sub>6</sub><sup>-</sup> leads to a similar arrangement of the building blocks in the solid state. Like the [Al{OC(CF<sub>3</sub>)<sub>3</sub>}]<sup>-</sup>-containing compound, **2** is moderately soluble in CH<sub>2</sub>Cl<sub>2</sub>. In the <sup>1</sup>H NMR

spectrum of **2** the signal corresponding to the Cp\* ligand is visible, whereas the  $^{31}\text{P}\{^1\text{H}\}$  NMR spectrum shows a singlet at 152 ppm. After performing theoretical studies and low temperature NMR spectroscopy in the case of  $[\text{Ag}\{\text{Cp}^*\text{Fe}(\eta^{5:2:1}\text{-P}_5)\}_2]_n[\text{Al}\{\text{OC}(\text{CF}_3)_3\}_4]_n$ , this singlet was assigned to the monocation  $[\{\text{Cp}^*\text{Fe}(\eta^5\text{-P}_5)\}_2\text{Ag}]^+$ . This fragment is also observed in the ESI MS spectrum for compound **2** as the largest fragment at  $m/z = 798.9$ . These results underline both, the structural similarity as well as an analogous behavior in solution.

By adding  $\text{CH}_3\text{CN}$  as a coordinating solvent to the system of **1** and  $\text{AgSbF}_6$ , the reaction leads to the dimeric complex **3**, which structure was also investigated by X-ray structure analysis. The *cyclo*- $\text{P}_5$  ligands of **1** are coordinating in a 1,2-fashion towards Ag atoms, which are coordinatively saturated each by two  $\text{CH}_3\text{CN}$  ligands (*Figure 2b*). Together with the ligands **1**, they form a six-membered ring  $\{\text{Ag}_2\text{P}_4\}$ . This motif is well known in the architecture of coordination compounds based on **1** and Cu salts.<sup>13</sup> For instance, the 80-vertex spheres  $[\{\text{Cp}^*\text{Fe}(\eta^5\text{-P}_5)\}_{12}(\text{CuX})_{20-x}]$  consist of such six-membered rings between the five-membered rings of the ligand **1** and thus, according to the isolated pentagon rule, reach fullerene topology.<sup>14</sup> In the solid state, these dimeric units of **3** are stacked together, most likely stabilized by weak  $\pi$ - $\pi$  interactions between almost parallel aromatic *cyclo*- $\text{P}_5$  rings (deviation  $0.16^\circ$ ) indicated by interplanar distances of  $3.65 \text{ \AA}$  (*Figure 2c*). Though **3** is hardly soluble in  $\text{CH}_2\text{Cl}_2$ , it dissolves readily in  $\text{CH}_3\text{CN}$ . In the  $^1\text{H}$  NMR spectrum of **3** in  $\text{CD}_3\text{CN}$  signals corresponding to the Cp\* residue and the  $\text{CH}_3\text{CN}$  ligands are visible, whereas in the  $^{31}\text{P}\{^1\text{H}\}$  NMR spectrum one singlet at 140.8 ppm can be attributed to the P atoms of **1**. As just one singlet is visible, most likely dynamic behaviour of the Ag-**1** coordination contacts occur in solution similar to the cases of **2** and  $[\text{Ag}\{\text{Cp}^*\text{Fe}(\eta^{5:2:1}\text{-P}_5)\}_2]_n[\text{Al}\{\text{OC}(\text{CF}_3)_3\}_4]_n$ . In the ESI MS spectrum the largest detected signal at  $m/z = 2869.1$  can be attributed to  $[\{\text{Cp}^*\text{Fe}(\eta^5\text{-P}_5)\}_5\text{Ag}_4(\text{SbF}_6)_3]^+$  as an aggregate of several dimeric units in the gas phase.



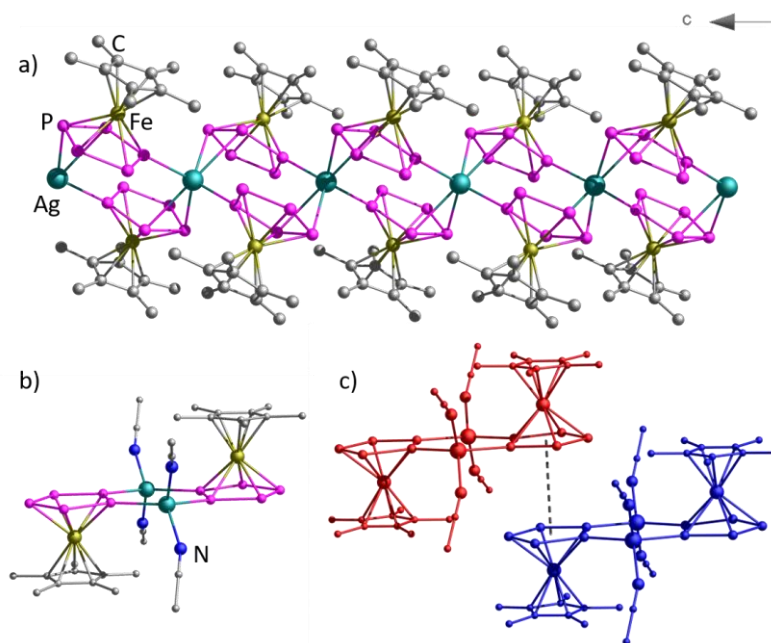
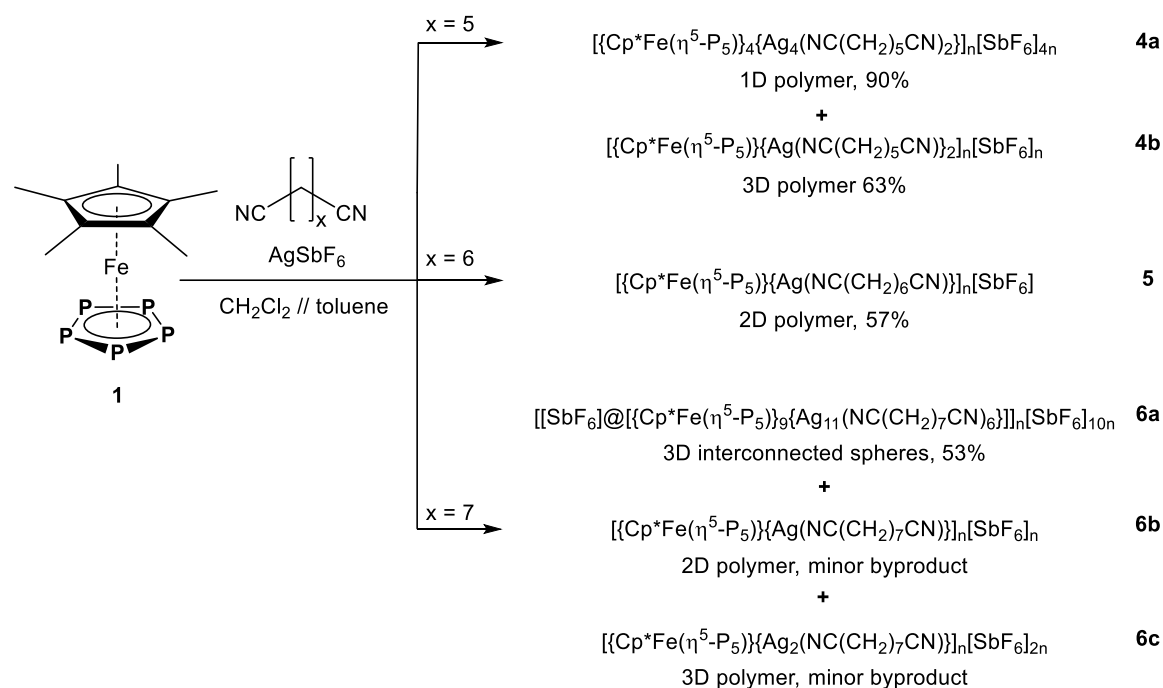


**Figure 2:** Structure of the cationic part of a) 1D polymeric **2**, b) dimeric unit of **3**. c)  $\pi$ - $\pi$  stacking interactions of  $P_5 \cdots P_5$  of the dimeric units in solid state (black dashed line). H atoms are omitted for clarity.

### Three-Component Self-Assembly of **1**, $\text{AgSbF}_6$ and Flexible Dinitriles $\text{NC}(\text{CH}_2)_x\text{CN}$ ( $x = 5 - 7$ )

Applying the three-component self-assembly approach involving the dinitrile  $\text{NC}(\text{CH}_2)_x\text{CN}$  the concentration of the starting materials was reduced to 2 mmol/L in the respective layers to minimize the formation of **2** as a byproduct. For all cases, the linker was added in a 10-fold excess with respect to **1**. Furthermore, a decisive part in the synthetic procedure is to combine the nitrile and the *cyclo*- $P_5$  complex in the first part, as flexible aliphatic dinitriles readily react with  $\text{Ag}^+$  to give insoluble polymeric products.<sup>15</sup> Furthermore, this was additionally ensured by using an excess of the dinitrile. Using the shortest dinitrile discussed in the scope of this study,  $\text{NC}(\text{CH}_2)_5\text{CN}$ , a 1D  $[\{\text{Cp}^*\text{Fe}(\eta^5\text{-P}_5)\}_4\{\text{Ag}_4(\text{NC}(\text{CH}_2)_5\text{CN})_2\}]_n[\text{SbF}_6]_{4n}$  (**4a**) and a 3D polymeric compound  $[\{\text{Cp}^*\text{Fe}(\eta^5\text{-P}_5)\}\{\text{Ag}(\text{NC}(\text{CH}_2)_5\text{CN})\}_2]_n[\text{SbF}_6]_n$  (**4b**) are obtained, depending on the stoichiometric ratios applied. Employing **1** and  $\text{AgSbF}_6$  in a ratio of 1 : 2 (**4a**) and 1 : 1 (**4b**), crystalline yields of 90% (**4a**) and 63% (**4b**) are obtained. Extending the linking unit to  $x = 6$ , a 2D polymer  $[\{\text{Cp}^*\text{Fe}(\eta^5\text{-P}_5)\}\{\text{Ag}(\text{NC}(\text{CH}_2)_6\text{CN})\}]_n[\text{SbF}_6]_n$  (**5**) is formed selectively, independent on the stoichiometric ratio of **1** and  $\text{AgSbF}_6$ , with a reasonable crystalline yield of 57%. Going further to  $x = 7$ , the system becomes versatile enough to form the first representative of an unprecedented class of compounds: a 3D interconnected polymer of novel spherical aggregates acting as nodes in  $[\text{SbF}_6]@[\{\text{Cp}^*\text{Fe}(\eta^5\text{-P}_5)\}_9\{\text{Ag}_{11}(\text{NC}(\text{CH}_2)_7\text{CN})_6\}]_n[\text{SbF}_6]_{10n}$  (**6a**). The formation of this product is accompanied by the minor appearance of a 2D  $[\{\text{Cp}^*\text{Fe}(\eta^5\text{-P}_5)\}\{\text{Ag}(\text{NC}(\text{CH}_2)_7\text{CN})\}]_n[\text{SbF}_6]_n$  (**6b**) and a

3D coordination polymer  $[\{\text{Cp}^*\text{Fe}(\eta^5\text{-P}_5)\}\{\text{Ag}_2(\text{NC}(\text{CH}_2)_7\text{CN})\}]_n[\text{SbF}_6]_{2n}$  (**6c**). Though **6c** differs in the stoichiometric ratio in the coordination compound from the main product **6a**, both, **6b** and **6c** could not be synthesized and isolated selectively by applying different stoichiometric ratios of the starting materials or concentration of the respective layers. By manual selection from the green polyhedra of **6b** and green plates of **6c**, brown plates of compound **6a** could be isolated in reasonable yields.



**Scheme 2:** One-pot self-assembly reactions of **1** with  $\text{AgSbF}_6$  and flexible dinitriles  $\text{NC}(\text{CH}_2)_x\text{CN}$  ( $x = 5 - 7$ ).

The 1D polymer **4a** is built up in a ladder-like way by tetrameric units  $[\{\text{Cp}^*\text{Fe}(\eta^5\text{-P}_5)\}_4\text{Ag}_4]^{4+}$  (Figure 3a,b). Two of the *cyclo*- $\text{P}_5$  ligands coordinate to Ag atoms in a 1,2-mode. The two bridging ligands show a  $\sigma$ -coordination in a 1,3-fashion towards Ag atoms ( $d(\text{Ag-P}) = 2.47 \text{ \AA}$  and  $2.54 \text{ \AA}$ ) and additionally two longer contacts to the opposing Ag atom, similar to an asymmetric  $\pi$ -coordination (Figure 3b). The  $\text{Ag}\cdots\text{P}$  interatomic distances for the latter amount to  $2.80 \text{ \AA}$  and  $3.08 \text{ \AA}$  and are in a comparable range with the  $\pi$ -coordination of **1** to Ag atoms in  $[\{\text{Cp}^*\text{Fe}(\eta^5\text{-P}_5)\}_2\text{Ag}]_n[\text{Al}\{\text{OC}(\text{CF}_3)_3\}_4]_n$  ( $d(\text{Ag}\cdots\text{P}) = 2.80$  and  $2.81 \text{ \AA}$ ).<sup>16</sup> The two Ag atoms, which are  $\sigma$ -coordinated by two ligands **1** and one nitrile group of a linker, show a trigonal coordination environment, whereas the two Ag atoms involved in the asymmetric  $\pi$ -coordination show a distorted pseudo-tetrahedral coordination of three ligands **1** and one nitrile group of a linker. The individual 1D strands are aligned in the solid state in a way that two *cyclo*- $\text{P}_5$  ligands of different tetrameric units reveal short intermolecular contacts, most likely stabilized by  $\pi$ - $\pi$  stacking interactions (Figure 3c). The *cyclo*- $\text{P}_5$  ligands are

perfectly parallel and slightly slipped with respect to each other. The interplanar distance  $3.62 \text{ \AA}$ <sup>17</sup> is comparable to recently reported ones.<sup>18</sup>

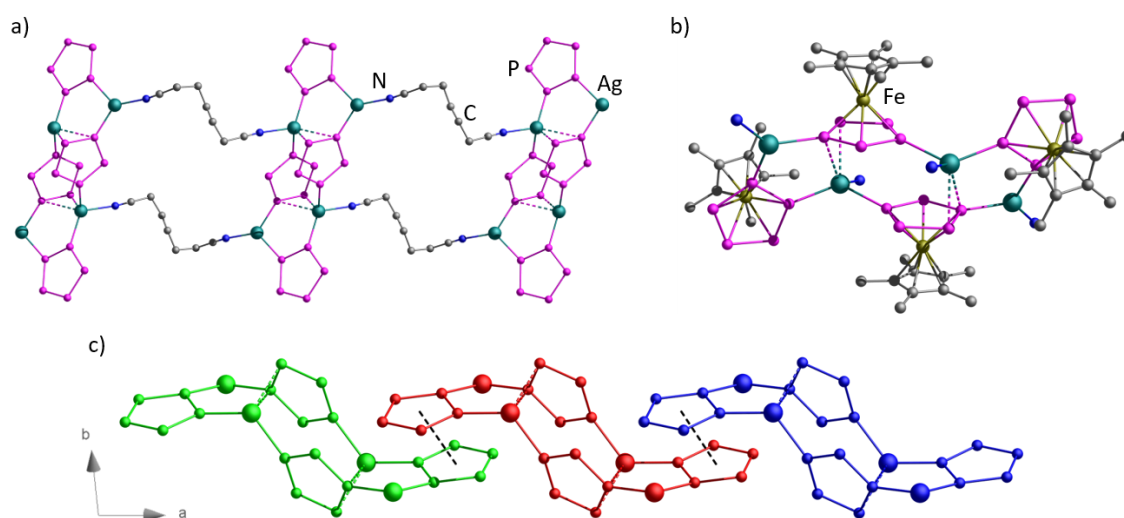


**Figure 3:** a) Section of the cationic part of 1D ladder-like structure of **4a**, b) tetrameric node: Asymmetric  $\pi$ -coordination contacts Ag-P (dashed bonds), c)  $\pi$ - $\pi$  stacking of the tetrameric nodes with  $P_5 \cdots P_5$  contacts shown as black dashed lines.  $[\text{Cp}^*\text{Fe}]$  units and H atoms are partly omitted for clarity.

The 3D network **4b** can formally be considered as parallel 1D strands  $[(\text{Cp}^*\text{Fe}(\eta^5\text{-P}_5))\text{Ag}_2]_n$ , which are interconnected by dinitriles (Figure 4a,b). These strands are built up by *cyclo*- $\text{P}_5$  ligands, coordinating in a 1,2,3,4-mode towards the Ag atoms, which are in turn tetrahedrally coordinated by two ligands **1** and two dinitrile linkers (Figure 4c). The two linkers at each Ag atom connect the 1D strand to two neighboring ones. In this way, each 1D strand is connected to four others. All  $\text{SbF}_6^-$  anions are non-coordinating and located between the 1D strands.

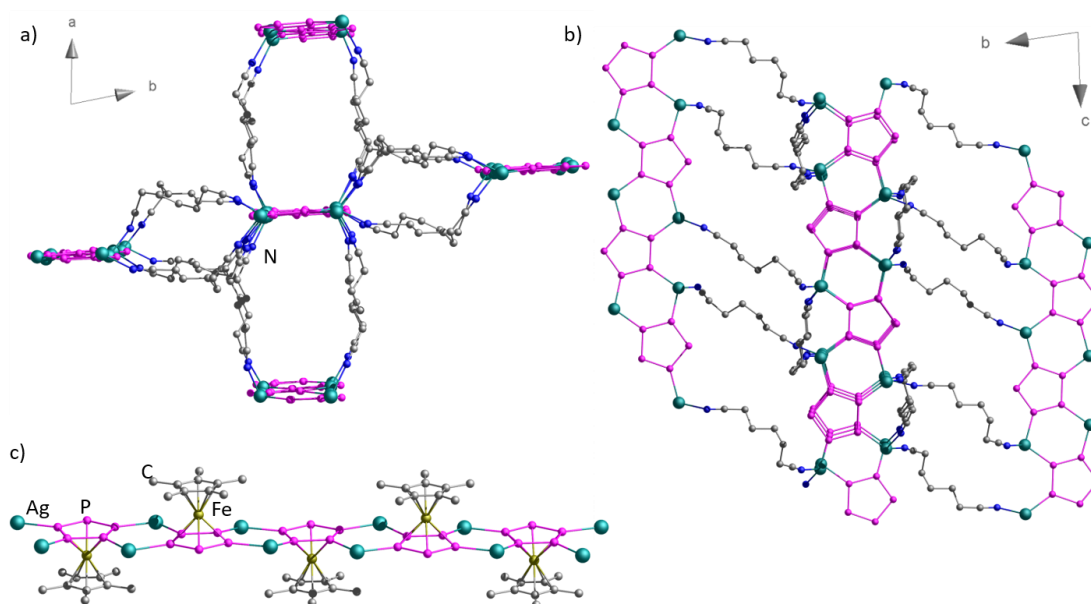


**Figure 4:** Section of the 3D cationic structure of **4b** along a) the c-axis and b) the a-axis. c) 1D strand  $[(\text{Cp}^*\text{Fe}(\eta^5\text{-P}_5)\text{Ag}_2)]^{2n+}$  as a substructure of **4b**. H atoms and partly  $[\text{Cp}^*\text{Fe}]$  units are partly omitted for clarity.

As all herein discussed polymeric compounds based on **1**, AgSbF<sub>6</sub> and flexible dinitriles, both compounds **4a** and **4b** are insoluble in common solvents as CH<sub>2</sub>Cl<sub>2</sub> or toluene, but undergo partial fragmentation upon dissolving them in CH<sub>3</sub>CN or pyridine. To enable characterization in solution by NMR and MS spectroscopy, all polymers were first fragmented by adding pyridine or CH<sub>3</sub>CN. In the <sup>1</sup>H NMR spectra of compounds **4** in CD<sub>2</sub>Cl<sub>2</sub>/pyridine the respective ratio of **1** : NC(CH<sub>2</sub>)<sub>5</sub>CN can be observed with the integral intensities of 2 : 1 (**4a**) and 1 : 2 (**4b**), whereas signals for the ligand **1** can be observed in the <sup>31</sup>P{<sup>1</sup>H} NMR spectra at 143.3 ppm (**4a**) and 139.8 ppm (**4b**). These signals are still upfield shifted compared to the signal of the free complex **1** (153 ppm),<sup>19</sup> which can be explained by incomplete fragmentation of the network. In the positive- as in the negative-ion ESI MS spectra signals are observed, which can be assigned to various oligomeric fragments. For **4a** the largest are  $m/z = 2522.0$  corresponding to  $[\{\text{Cp}^*\text{Fe}(\eta^5\text{-P}_5)\}_4\text{Ag}_4(\text{SbF}_6)_3]^+$  and  $m/z = 2647.9$  to  $[\{\text{Cp}^*\text{Fe}(\eta^5\text{-P}_5)\}_4\text{Ag}_3(\text{SbF}_6)_4]^-$ , whereas the cation represents the node of the 1D ladder-like polymer. For **4b**  $m/z = 2418.2$   $[\{\text{Cp}^*\text{Fe}(\eta^5\text{-P}_5)\}_3\text{Ag}_4(\text{SbF}_6)_3(\text{NC}(\text{CH}_2)_5\text{CN})_2]^+$  and  $m/z = 2772$   $[\{\text{Cp}^*\text{Fe}(\eta^5\text{-P}_5)\}_4\text{Ag}_3(\text{SbF}_6)_4(\text{NC}(\text{CH}_2)_5\text{CN})]^-$  can be assigned. However, the largest fragments containing all three building blocks can be attributed to  $m/z = 2077$  as  $[\{\text{Cp}^*\text{Fe}(\eta^5\text{-P}_5)\}_3\text{Ag}_3(\text{SbF}_6)_2(\text{NC}(\text{CH}_2)_5\text{CN})_2]^+$  and  $m/z = 2426$  as  $[\{\text{Cp}^*\text{Fe}(\eta^5\text{-P}_5)\}_3\text{Ag}_3(\text{SbF}_6)_4(\text{NC}(\text{CH}_2)_5\text{CN})]^-$  for **4a**.

Applying the nitrile with  $x = 6$  to the reaction mixture crystalline product **5** is formed, which the X-ray structure analysis shows a 2D polymer. It is built up by dimeric units of  $[\{\text{Cp}^*\text{Fe}(\eta^5\text{-P}_5)\}_2\text{Ag}_2]^{2+}$  as nodes, which are connected to each other via the flexible linker molecules, forming a square net with the quadrangular meshes between the dimeric nodes (Figure 5a). Each *cyclo*-P<sub>5</sub> ligand coordinates in a 1,2 mode towards Ag atoms, which are in turn tetrahedrally coordinated by two nitrile groups of different linkers and two ligands **1**. A similar framework is also featured by **6b**, which is a byproduct of the self-assembly of **1**, AgSbF<sub>6</sub> and the dinitrile with  $x = 7$  (Figure 5b). In contrast to **5**, the dimeric units of one quadrangular mesh in **6b** are not parallel, but show a twisted arrangement. The layers in **5** and **6b** are  $\pi$ - $\pi$  stacked in the solid state to give interplanar contacts and angles between the *cyclo*-P<sub>5</sub> ligands which amount to 3.63 Å (**5**) and 3.74 Å (**6b**)<sup>17</sup> with 0.38° (**5**), 0° (**6b**). As **6b** could not be synthesized and isolated selectively, except for X-ray structure analysis no analytical methods for a chemical characterization could be performed. For **5** in the <sup>1</sup>H NMR and <sup>13</sup>C NMR spectra of the partially fragmented compound the expected signals for ligand **1** and the linker could be observed in a stoichiometric ratio of 1 : 1. In the positive- and negative-ion ESI MS spectra the largest fragments at  $m/z = 2522.0$  and  $m/z = 2647.9$  can be attributed to  $[\{\text{Cp}^*\text{Fe}(\eta^5\text{-P}_5)\}_4\text{Ag}_4(\text{SbF}_6)_3]^+$  and  $[\{\text{Cp}^*\text{Fe}(\eta^5\text{-P}_5)\}_4\text{Ag}_3(\text{SbF}_6)_4]^-$ , whereas the largest fragments in the

positive ESI MS spectrum containing all three building blocks can be attributed to  $m/z = 1622.4$   $[\{\text{Cp}^*\text{Fe}(\eta^5\text{-P}_5)\}_2\text{Ag}_3(\text{SbF}_6)_2(\text{NC}(\text{CH}_2)_6\text{CN})]^+$ .

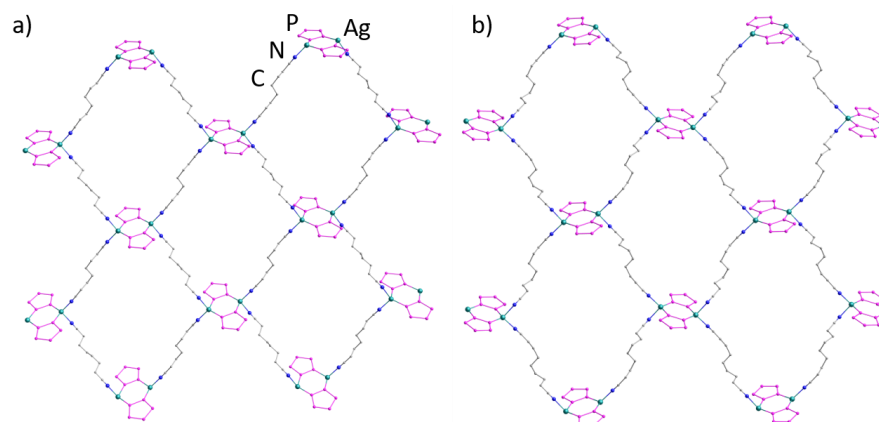


**Figure 5:** Sections of the cationic 2D polymeric frameworks a) **5** and b) **6b**.  $[\text{Cp}^*\text{Fe}]$  units and H atoms are omitted for clarity.

Besides **6b**, the 3D framework **6c** crystallizes as a second minor byproduct (Figure 6a). The network can formally be subdivided into 1D strands  $[\{\text{Cp}^*\text{Fe}(\eta^5\text{-P}_5)\}\text{Ag}_2]_n^{2n+}$  connected by dinitriles. The strands are similar to those in **4b** and the *cyclo*- $\text{P}_5$  ligands are coordinating in a 1,2,3,4-mode to Ag atoms (cf. Figure 4 and Figure 6b,c). These Ag atoms are each tetrahedrally coordinated by two moieties **1** and two nitrile groups of different linkers. One linker per Ag atom interconnects the 1D strands, whereas the other flexible dinitrile acts as a chelating bidentate ligand within the same strand. The linked strands are perpendicular to each other and therefore are connected to  $n$  other polymeric strands on each side, whereas neighboring parallel strands are isolated from each other by counter anions  $\text{SbF}_6^-$  (Figure 6a). Similar to **6b**, this compound could not be synthesized and isolated selectively and no further chemical characterization could be performed.

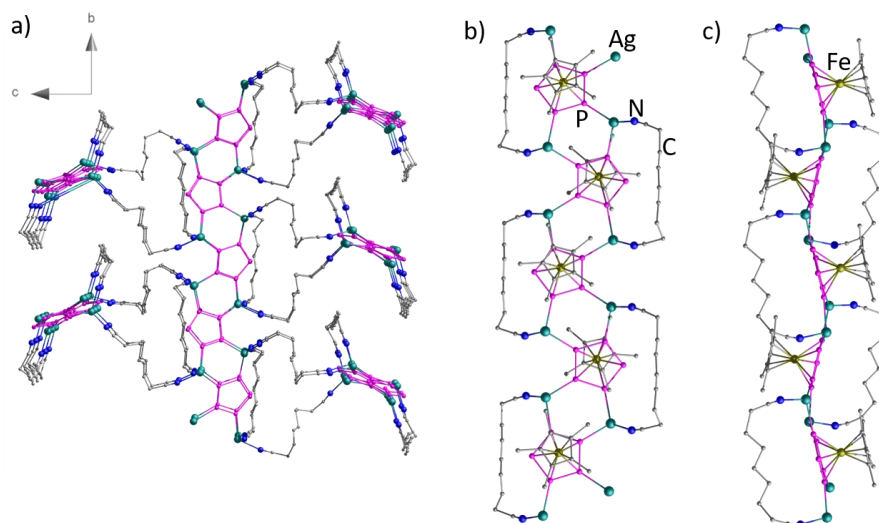


**Figure 6:** a) Section of the cationic 3D polymeric structure of **6c**. b) Top and c) side view of the 1D strands.  $[\text{Cp}^*\text{Fe}]$  units, H atoms, and minor positions of disordered linker molecules are omitted for clarity.

Compound **6a** represents the main product of the one-pot self-assembly of **1**, AgSbF<sub>6</sub> and NC(CH<sub>2</sub>)<sub>7</sub>CN and was characterized by X-ray structure analysis. It reveals the representative of a novel class of 3D frameworks of supramolecular spherical aggregates based on a polyphosphorus ligand. Spherical cationic scaffolds of [Cp\*Fe(η<sup>5</sup>-P<sub>5</sub>)<sub>9</sub>Ag<sub>11</sub>]<sup>11+</sup> act as nodes for the first time. The cationic supramolecules possess an unprecedented C<sub>5</sub> symmetric shape and act as hosts for one SbF<sub>6</sub><sup>-</sup> counter-anion, respectively (*Figure 7*). The centroids of the *cyclo*-P<sub>5</sub> ligands form a distorted capped tetragonal antiprism (*Figure 8e*). The *cyclo*-P<sub>5</sub> ligands show four different coordination modes towards Ag atoms: η<sup>5:1:1:1:1</sup> (2 times, yellow in *Figure 8a,b*), η<sup>5:1:1:1:1</sup> (2 times, orange), η<sup>5:1:1:1:1</sup> (2 times, green), η<sup>5:2:1:1</sup> (3 times, blue), whereas one of the latter forms the cap of the tetragonal antiprism. The Ag-P bond lengths for the σ-coordination lie in an expected range of 2.40 - 2.61 Å, whereas Ag-P bond lengths for the π-coordination amount to 2.72 – 2.88 Å.<sup>16</sup> The Ag atoms reveal tetrahedral or pseudo-tetrahedral coordination environments: 8 Ag atoms are tetrahedrally coordinated by either 3 × **1** and 1 × dinitrile (*Figure 8c,d*, red), or 2 × **1**, 1 × dinitrile, 1 × η<sup>2</sup>-coordinating dinitrile (turquoise). The other 3 Ag atoms pseudo-tetrahedrally coordinated by either 3 × **1** and 1 × dinitrile (green), or 3 × **1** and 1 × SbF<sub>6</sub><sup>-</sup> (yellow). The bond lengths Ag-N for the common end-on coordination modes of the dinitriles lie in a range of 2.186(7) - 2.344(6) Å, whereas the Ag-N bonds for the less common η<sup>2</sup>-coordination are significantly elongated to 2.9474(88) Å and 3.2004(89) Å, but still comparable to those known from the literature (2.93 Å)<sup>20</sup>.

The outer diameter of the spherical assembly amounts to 22.08 Å<sup>21</sup> and is therefore slightly smaller than that of the smallest known spherical assembly based on **1** so far, the 80-vertex scaffold [Cp\*Fe(η<sup>5</sup>-P<sub>5</sub>)<sub>12</sub>(CuX)<sub>20</sub>] (X = Cl, Br) with 2.29 nm. The non-spherical void can accommodate well the SbF<sub>6</sub><sup>-</sup> counter-anion with the maximum dimension of 6.69 Å.<sup>12</sup> The anion is ordered due to its special orientation in the void; two apical F atoms are directed towards scaffold-building Ag atoms forming the Ag...F contacts of 3.58 Å (*Figure 7a,b*, grey dashed lines).

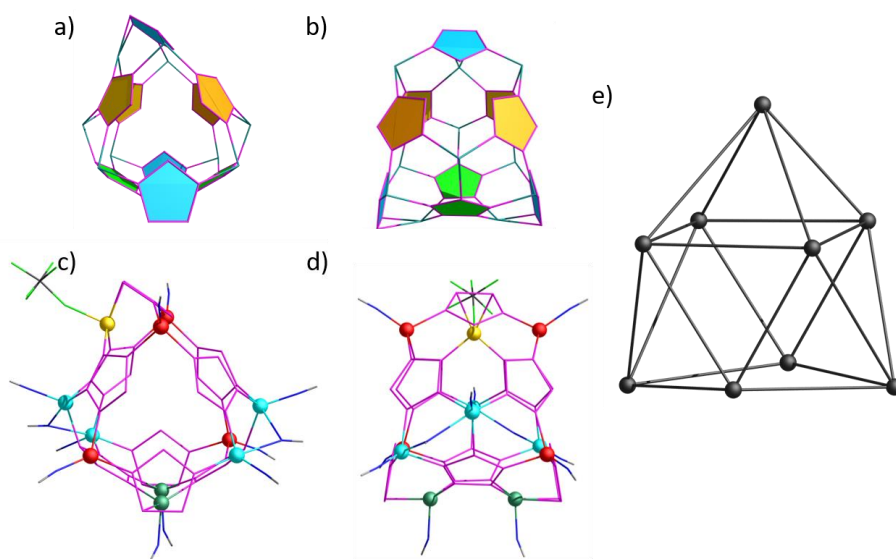
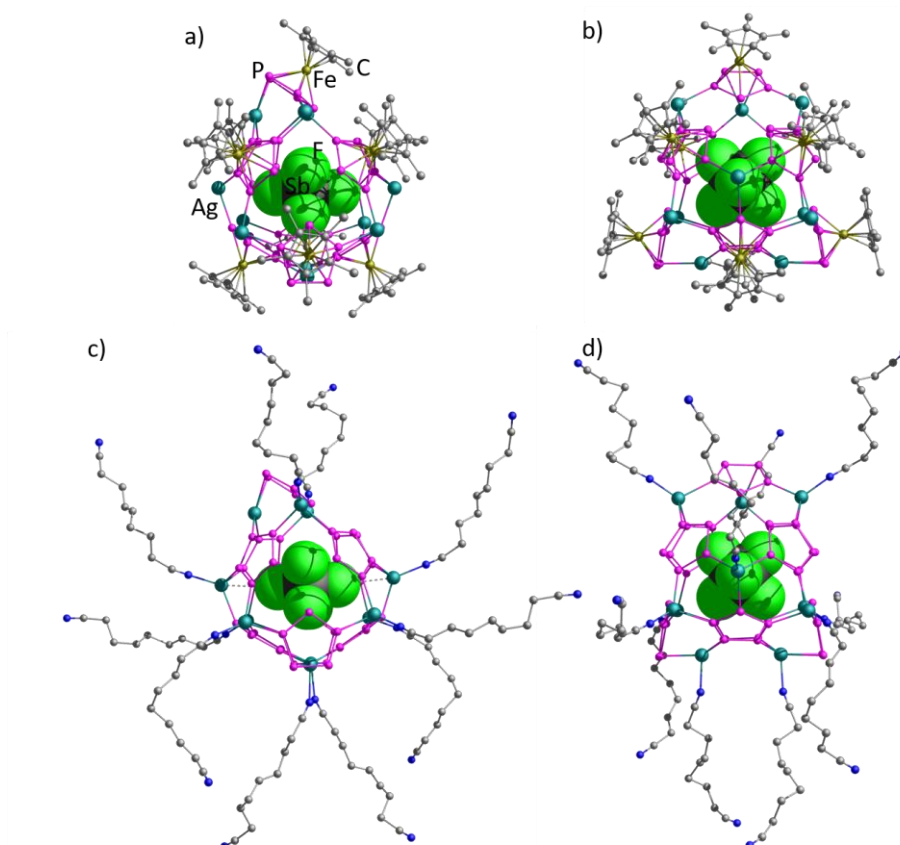


**Figure 8:** Supramolecular node in **6a**. a) and b) cyclo- $P_5$  ligands and c) and d) Ag atoms, highlighted with respect to their different coordination environments, e) distorted capped tetragonal antiprism formed by centroids of the cyclo- $P_5$  ligands. [Cp\*Fe] units, H atoms, and linkers are partly omitted for clarity. Only major positions of disordered structural fragments are shown.

**70 | V - Three-Component Self-Assembly:**  
**A Way to Overcome Simple Coordination Polymers in Favor**  
**of 3D Connected Spherical Supramolecular Aggregates**

Each supramolecular node in **6a** is linked to ten others *via* twelve dinitrile ligands (*Figure 9a*). To eight of them (four nodes on top and bottom in *Figure 9a*) it is connected by one dinitrile linker, which coordinates with both nitrile groups in an end-on fashion to two Ag atoms of different scaffolds. To two of the neighbouring spheres (on the sides in *Figure 9a* and highlighted in *Figure 9b*) the central scaffold is connected by two dinitrile linkers in a pairwise manner. Thus, one  $\eta^2$ -coordination to two neighbouring Ag atoms of one sphere is observed per linker (*Figure 9b*). The spherical supramolecules form a 10-connected network, which was assigned using TOPOSPro<sup>22</sup> to a **bcu-x-10-Fmmm** topology spheres (*Figure 9c*).<sup>23</sup> At the same time, the centroids of the supramolecules are arranged according to a well-known *bcc* packing.

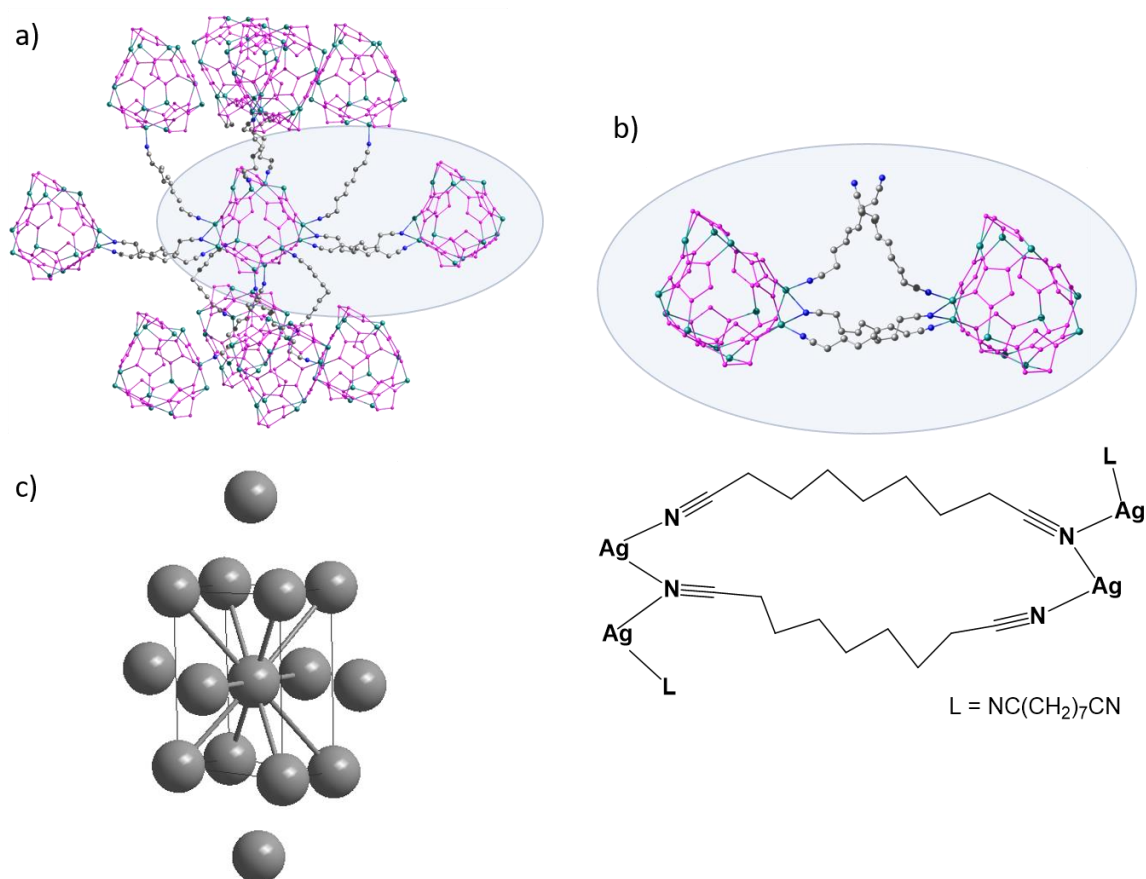


**Figure 9:** a) Section of the cationic 3D polymeric structure of interconnected spheres in **6a**, b) detail of pairwise connected spheres by  $\eta^2$ -coordination mode of the dinitriles, c) **bcu-x-10-Fmmm** net of the supramolecular nodes (grey lines) within *bcc* packing of the centroids. [Cp\*Fe] units, H atoms and disordered parts of linker are omitted for clarity.

The polymer of linked spheres **6a** is insoluble in solvents as hexane, toluene,  $\text{CH}_2\text{Cl}_2$ , thf and  $\text{Et}_2\text{O}$ . Only in  $\text{CH}_3\text{CN}$  or pyridine, it dissolves readily to give a deep red solution, though accompanied by fragmentation of the coordination network and supramolecular nodes. Therefore, in the  $^1\text{H}$  NMR and in the  $^{13}\text{C}$  NMR spectrum in  $\text{CD}_2\text{Cl}_2$ /pyridine, only signals corresponding to free **1** and the



dinitrile linker molecule are visible, whereas in the  $^{31}\text{P}\{^1\text{H}\}$  spectrum a signal at 151.53 ppm can be assigned to the P atoms of free **1**. However, the  $^{31}\text{P}\{^1\text{H}\}$  MAS NMR of **6a** shows a broad signal at 134 ppm (Figure 10). In the positive-ion ESI MS spectrum oligomeric fragments can be detected, whereas the largest signal at  $m/z = 2522.1$  can be assigned to  $[\{\text{Cp}^*\text{Fe}(\eta^5\text{-P}_5)\}_5\text{Ag}_3(\text{SbF}_6)_2]^+$ . The largest three-component fragment can be assigned to  $m/z = 1636.6$  as  $[\{\text{Cp}^*\text{Fe}(\eta^5\text{-P}_5)\}_2\text{Ag}_3(\text{SbF}_6)_2(\text{NC}(\text{CH}_2)_7\text{CN})]^+$ .

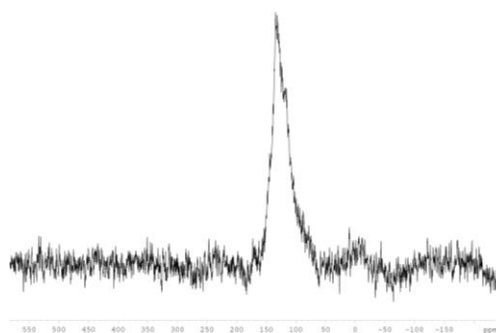


Figure 10:  $^{31}\text{P}\{^1\text{H}\}$  MAS-NMR spectrum of **6a**.

### Comparison of Coordination Products and Influence of the Linking Unit on the Resulting Architectures

The results of the variation in linker length in the three-component self-assembly of **1**,  $\text{AgSbF}_6$  and  $\text{NC}(\text{CH}_2)_x\text{CN}$  ( $x = 5 - 7$ ) show a clear trend: Chain lengths of  $x = 5$  and 6 in the aliphatic backbone of the dinitrile linking molecule  $\text{NC}(\text{CH}_2)_x\text{CN}$  leads the self-assembly of **1** and  $\text{AgSbF}_6$  to yield 1D, 2D and 3D polymeric compounds. The nodes in these frameworks consist of di-, tetra-nuclear assemblies or infinite strands based on  $[(\textbf{1})_x\text{Ag}_y]]^{y+}$  and are connected *via* the linkers (**4a-5**, **6b-c**). Only  $x = 7$  first enables the self-assembly system to form unique spherical aggregates as interconnected nodes in **6a** (Table 1).

Table 1: Comparison of **4a-6c** considering different structural aspects.

	dimensionality	node	$\text{NC}(\text{CH}_2)_x\text{CN}$	coordination of $\text{cyclo-P}_5$ towards Ag	coordination environment of Ag
<b>4a</b>	1D	$[(\textbf{1})_4\text{Ag}_4]^{4+}$	$x = 5$	$\eta^{1:1}(1,2)$ , $\eta^{2:1}(1,2,4)$	pseudo-tetrahedral, tetrahedral
<b>4b</b>	3D	$[(\textbf{1})\text{Ag}_2]_n^{2n+}$ (1D)	$x = 5$	$\eta^{1:1:1:1}(1,2,3,4)$	tetrahedral
<b>5</b>	2D	$[(\textbf{1})_2\text{Ag}_2]^{2+}$	$x = 6$	$\eta^{1:1}(1,2)$	tetrahedral
<b>6a</b>	3D	$[(\textbf{1})_9\text{Ag}_{11}]^{11+}$	$x = 7$	$\eta^{1:1:1}(1,2,4)$ , $\eta^{1:1:1:1}(1,2,3,4)$ , $\eta^{1:1:1:1:1}(1,2,3,4,5)$ , $\eta^{2:1:1}(1,2,3,4)$	pseudo-tetrahedral, tetrahedral
<b>6b</b>	2D	$[(\textbf{1})_2\text{Ag}_2]^{2+}$	$x = 7$	$\eta^{1:1}(1,2)$	tetrahedral
<b>6c</b>	3D	$[(\textbf{1})\{\text{Ag}_2(\text{NC}(\text{CH}_2)_7\text{CN})\}]_n^{2n+}$ (1D)	$x = 7$	$\eta^{1:1:1:1}(1,2,3,4)$	tetrahedral

Due to the flexibility of the aliphatic backbone in the dinitriles, the maximum length is strongly dependent on its conformation. The estimated maximum length of  $\text{NC}(\text{CH}_2)_x\text{CN}$  in a linear conformation and the lengths of folded conformations observed in the coordination products is given in Table 2. **4b** and **6c** both can be subdivided to interconnected 1D strands  $[(1)\text{Ag}_2]_n^{2n+}$  and thus, the length of the crosslinking dinitriles are with 8.06 - 8.37 Å (**4b**) and 8.76 Å (**6c**) similar, though differing in the length of the aliphatic backbone by two  $\text{CH}_2$  groups. Furthermore, **5** and **6b** both showing similar 2D networks, reveal comparable lengths of the dinitriles in the coordination products reaching 10.43 Å (**5**) and 10.66 Å (**6b**). Moreover, the possible borderline for the formation of interconnected scaffolds at linker length of  $x = 7$  can be explained by the fact that six of ten linkers per supramolecular node in **6a** are slightly longer (10.82 Å) than the theoretical reachable length of 10.73 Å of the previous shorter linker with  $x = 6$  in a linear conformation.

**Table 2:** Comparison of maximal length of the dinitriles to that in coordination products **4-6**.

$\text{NC}(\text{CH}_2)_x\text{CN}$	maximal length <sup>[a]</sup> / Å	length in coordination product <sup>[b]</sup> / Å
$x = 5$	9.28	7.59 ( <b>4a</b> , 1D)
		8.06, 8.37 ( <b>4b</b> , 3D)
$x = 6$	10.73	10.43 ( <b>5</b> , 2D)
$x = 7$	11.76	8.95 (x2), 9.01 (x2), 10.82 (x6) ( <b>6a</b> , 3D)
		10.66 ( <b>6b</b> , 2D)
		8.54, 8.76 ( <b>6c</b> , 3D)

[a] the maximal length was estimated with Chem3D 17.0 for a linear conformation of the backbone chain.

[b] the length in products is the maximal distance between the N atoms of one linker in the crystal structure.

### 5.3 Conclusion

By using with  $\text{SbF}_6^-$  a weakly coordinating anion in the coordination chemistry of **1** and  $\text{Ag}^+$  for the first time, free coordination sites on the Ag atom were generated, being available for the coordination by linkers. Thereby, we have presented a detailed study on the three-component self-assembly of these building blocks together with flexible linkers  $\text{NC}(\text{CH}_2)_x\text{CN}$  ( $x = 5 - 7$ ). The variability of conformations and therefore adjustable lengths of linking units lead together with different coordination modes of the nitrile groups to the formation of diverse nodes and coordination polymers. Thus, we succeeded in the construction of a 3D polymeric framework, built up by nano-sized spherical aggregates, besides various 1D, 2D and 3D coordination polymers. Starting with  $\text{NC}(\text{CH}_2)_x\text{CN}$  ( $x = 5, 6$ ) the 1D, 2D and 3D coordination polymers **4a**, **4b** and **5** were synthesized and characterized. With  $x = 7$  the system is flexible enough to build 2D (**6b**) and 3D (**6c**) polymeric networks, as well as the first representative of novel spherical host scaffolds interconnected to a 3D coordination polymer of **6a**. The supramolecular nodes in **6a** feature 10-connected network by dinitrile linkers, while individual spherical supramolecular nodes are packed in the distorted body-centered cubic packing. .

## 5.4 Experimental Part

### General Remarks

All reactions were performed under an inert atmosphere of dry nitrogen with standard vacuum, Schlenk and glove-box techniques. Solvents were purified, dried and degassed prior to use by standard procedures.  $[\text{Cp}^*\text{Fe}(\eta^5\text{-P}_5)]^{24}$  and were synthesized following reported procedures. Commercially available chemicals ( $\text{AgSbF}_6$ ,  $\text{NC}(\text{CH}_2)_x\text{CN}$  ( $x = 5, 6, 7, 8, 10$ )) were used without further purification. Solution NMR spectra were recorded on a Bruker Avance 300 or 400 spectrometer. The  $^{31}\text{P}\{^1\text{H}\}$  MAS spectrum was measured on a Bruker Avance 300. The corresponding ESI-MS spectra were acquired on a ThermoQuest Finnigan MAT TSQ 7000 mass spectrometer. CHN Elemental analyses were performed on a Vario EL III apparatus.

### Synthesis of $[\{\text{Cp}^*\text{Fe}(\eta^{5:2:1}\text{-P}_5)\}_2\text{Ag}]_n[\text{SbF}_6]_n$ (**2**)

In a Schlenk tube a solution of  $\text{AgSbF}_6$  (28 mg, 0.08 mmol) in  $\text{CH}_2\text{Cl}_2$  (8 mL) is carefully layered with a green solution of  $[\text{Cp}^*\text{Fe}(\eta^5\text{-P}_5)]$  (14 mg, 0.04 mmol) in toluene (8 mL). Thereby, the phase boundary turns turbid. After a few days, the formation of dark brown laths of **2** at the phase boundary can be observed. After complete diffusion, the mother liquor is decanted, the crystals are washed with hexane ( $3 \times 10$  mL) and dried *in vacuo*.

Analytical data of **2**:

**Yield:** 19 mg (0.018 mmol, 91% referred to  $[\text{Cp}^*\text{Fe}(\eta^5\text{-P}_5)]$ )

$^1\text{H}$  NMR ( $\text{CD}_2\text{Cl}_2$ ):  $\delta$  [ppm] = 1.39 (s,  $[\text{Cp}^*\text{Fe}(\eta^5\text{-P}_5)]$ ).

$^{31}\text{P}\{^1\text{H}\}$  NMR ( $\text{CD}_2\text{Cl}_2$ ):  $\delta$  [ppm] = 152 (s,  $[\text{Cp}^*\text{Fe}(\eta^5\text{-P}_5)]$ ).

**Positive ion ESI-MS** ( $\text{CH}_2\text{Cl}_2/\text{CH}_3\text{CN}$ ):  $m/z$  (%) = 798.9 (100)  $[\{\text{Cp}^*\text{Fe}(\eta^5\text{-P}_5)\}_2\text{Ag}]^+$ , 345.9  $[\text{Cp}^*\text{Fe}(\eta^5\text{-P}_5)]^+$ .

**Negative ion ESI-MS** ( $\text{CH}_2\text{Cl}_2/\text{CH}_3\text{CN}$ ):  $m/z$  (%) = 762.7  $[(\text{SbF}_6)_3\text{Fe}]^-$ , 546.7  $[(\text{SbF}_6)_2\text{FeF}]^-$ , 234.7 (100)  $[\text{SbF}_6]^-$ .

**Elemental analysis:** Calculated (%) for  $[\{\text{Cp}^*\text{Fe}(\eta^5\text{-P}_5)\}_2\{\text{AgSbF}_6\}(\text{CH}_2\text{Cl}_2)_4]$  (1375.23 g/mol): C 20.96, H 2.79; found: C 20.43, H 2.71.

### Synthesis of $[\{\text{Cp}^*\text{Fe}(\eta^{5:1:1}\text{-P}_5)\}\{\text{Ag}(\text{CH}_3\text{CN})_2\}]_2[\text{SbF}_6]_2$ (**3**)

In a Schlenk tube a solution of  $\text{AgSbF}_6$  (54 mg, 0.15 mmol) in a solvent mixture of  $\text{CH}_3\text{CN}/\text{CH}_2\text{Cl}_2$  (4 mL, 1:1) is carefully layered with a green solution of  $[\text{Cp}^*\text{Fe}(\eta^5\text{-P}_5)]$  (28 mg, 0.08 mmol) in toluene (5 mL). Thereby, the phase boundary turns turbid. After a few days, the formation of green plates

## 74 | V - Three-Component Self-Assembly: A Way to Overcome Simple Coordination Polymers in Favor of 3D Connected Spherical Supramolecular Aggregates

---

of **3** at the phase boundary can be observed. After complete diffusion, the colorless mother liquor is decanted, the crystals are washed with hexane (3 × 10 mL) and dried *in vacuo*.

Analytical data of **3**:

**Yield:** 57 mg (0.0372 mmol, 93% referred to [Cp\*Fe( $\eta^5$ -P<sub>5</sub>)])

**<sup>1</sup>H NMR** (CD<sub>3</sub>CN):  $\delta$  [ppm] = 1.45 (s, 15H, [Cp\*Fe( $\eta^5$ -P<sub>5</sub>)]), 1.96 (s, 6H, CH<sub>3</sub>CN).

**<sup>31</sup>P{<sup>1</sup>H} NMR** (CD<sub>3</sub>CN):  $\delta$  [ppm] = 140.80 (s, [Cp\*Fe( $\eta^5$ -P<sub>5</sub>)]).

**<sup>19</sup>F NMR** (CD<sub>3</sub>CN):  $\delta$  [ppm] = -122.71 (octet, Sb<sup>123</sup>F<sub>6</sub>), -122.70 (sextet, Sb<sup>121</sup>F<sub>6</sub>).

**Positive ion ESI-MS** (CH<sub>3</sub>CN):  $m/z$  (%) = 2869.1 [{Cp\*Fe( $\eta^5$ -P<sub>5</sub>)}<sub>5</sub>Ag<sub>4</sub>(SbF<sub>6</sub>)<sub>3</sub>]<sup>+</sup>, 2525.1 [{Cp\*Fe( $\eta^5$ -P<sub>5</sub>)}<sub>4</sub>Ag<sub>4</sub>(SbF<sub>6</sub>)<sub>3</sub>]<sup>+</sup>, 2217.6 [{Cp\*Fe( $\eta^5$ -P<sub>5</sub>)}<sub>4</sub>Ag<sub>3</sub>(SbF<sub>6</sub>)<sub>2</sub>(CH<sub>3</sub>CN)]<sup>+</sup>, 2178.9 [{Cp\*Fe( $\eta^5$ -P<sub>5</sub>)}<sub>4</sub>Ag<sub>3</sub>(SbF<sub>6</sub>)<sub>2</sub>]<sup>+</sup>, 1873.9 [{Cp\*Fe( $\eta^5$ -P<sub>5</sub>)}<sub>3</sub>Ag<sub>3</sub>(SbF<sub>6</sub>)<sub>2</sub>(CH<sub>3</sub>CN)]<sup>+</sup>, 1834.8 [{Cp\*Fe( $\eta^5$ -P<sub>5</sub>)}<sub>3</sub>Ag<sub>3</sub>(SbF<sub>6</sub>)<sub>2</sub>]<sup>+</sup>, 1568.7 [{Cp\*Fe( $\eta^5$ -P<sub>5</sub>)}<sub>3</sub>Ag<sub>2</sub>(SbF<sub>6</sub>)(CH<sub>3</sub>CN)]<sup>+</sup>, 1527.4 [{Cp\*Fe( $\eta^5$ -P<sub>5</sub>)}<sub>3</sub>Ag<sub>2</sub>(SbF<sub>6</sub>)(CH<sub>3</sub>CN)]<sup>+</sup>, 1488.8 [{Cp\*Fe( $\eta^5$ -P<sub>5</sub>)}<sub>3</sub>Ag<sub>2</sub>(SbF<sub>6</sub>)]<sup>+</sup>, 1219.5 [{Cp\*Fe( $\eta^5$ -P<sub>5</sub>)}<sub>2</sub>Ag<sub>2</sub>(SbF<sub>6</sub>)(CH<sub>3</sub>CN)]<sup>+</sup>, 1183.7 [{Cp\*Fe( $\eta^5$ -P<sub>5</sub>)}<sub>2</sub>Ag<sub>2</sub>(SbF<sub>6</sub>)(CH<sub>3</sub>CN)]<sup>+</sup>, 1142.9 [{Cp\*Fe( $\eta^5$ -P<sub>5</sub>)}<sub>2</sub>Ag<sub>2</sub>(SbF<sub>6</sub>)]<sup>+</sup>, 798.8 [{Cp\*Fe( $\eta^5$ -P<sub>5</sub>)}<sub>2</sub>Ag]<sup>+</sup>, 493.7 (100) [{Cp\*Fe( $\eta^5$ -P<sub>5</sub>)}Ag(CH<sub>3</sub>CN)]<sup>+</sup>, 453.8 [{Cp\*Fe( $\eta^5$ -P<sub>5</sub>)}Ag]<sup>+</sup>.

**Negative ion ESI-MS** (CH<sub>3</sub>CN):  $m/z$  (%) = 234.7 (100) [SbF<sub>6</sub>]<sup>-</sup>.

**Elemental analysis:** Calculated (%) for [{Cp\*Fe( $\eta^5$ -P<sub>5</sub>)}{Ag(CH<sub>3</sub>CN)<sub>2</sub>}(SbF<sub>6</sub>)<sub>2</sub>] (1543.32 g/mol): C 21.79, H 2.74, N 3.63; found: C 21.87, H 2.82, N 3.73.

### Synthesis of [{Cp\*Fe( $\eta^5$ -P<sub>5</sub>)}{Ag(NC(CH<sub>2</sub>)<sub>5</sub>CN)}<sub>2</sub>]<sub>n</sub>[SbF<sub>6</sub>]<sub>n</sub> (**4a**)

In a Schlenk tube a solution of AgSbF<sub>6</sub> (35 mg, 0.1 mmol) in CH<sub>2</sub>Cl<sub>2</sub> (25 mL) is carefully layered first with a solvent mixture of CH<sub>2</sub>Cl<sub>2</sub>/toluene (10 mL, 2:1) and then with a green solution of [Cp\*Fe( $\eta^5$ -P<sub>5</sub>)] (18 mg, 0.05 mmol) and NC(CH<sub>2</sub>)<sub>5</sub>CN (1 mL, 0.4 M in CH<sub>2</sub>Cl<sub>2</sub>) in toluene (25 mL). After a few hours, the phase boundary turns yellow and after one day, the formation of red rods of **4a** at the phase boundary can be observed. After complete diffusion, the light green mother liquor is decanted, the crystals are washed with CH<sub>2</sub>Cl<sub>2</sub> (3 × 10 mL) and dried *in vacuo*.

Analytical data of **4a**:

**Yield:** 57 mg (0.045 mmol, 90% based on [Cp\*Fe( $\eta^5$ -P<sub>5</sub>)]).

**<sup>1</sup>H NMR** (pyridine/CD<sub>2</sub>Cl<sub>2</sub>):  $\delta$  [ppm] = 1.46 (15H, [Cp\*Fe( $\eta^5$ -P<sub>5</sub>)]), 1.62 (4H, C-3, NC(CH<sub>2</sub>)<sub>5</sub>CN), 1.72 (8H, C-2/C-4, NC(CH<sub>2</sub>)<sub>5</sub>CN), 2.41 (8H, C-1/C-5, NC(CH<sub>2</sub>)<sub>5</sub>CN), 7.54 (m,  $\beta$ -H, pyridine), 7.83 (m,  $\gamma$ -H, pyridine), 8.72 (m,  $\alpha$ -H, pyridine).

**<sup>13</sup>C NMR** (pyridine/CD<sub>2</sub>Cl<sub>2</sub>):  $\delta$  [ppm] = 10.65 [Cp\*Fe( $\eta^5$ -P<sub>5</sub>)], 24.71 (NC(CH<sub>2</sub>)<sub>5</sub>CN), 27.75 (NC(CH<sub>2</sub>)<sub>5</sub>CN), no other signals were detected.

**<sup>31</sup>P{<sup>1</sup>H} NMR** (pyridine/CD<sub>2</sub>Cl<sub>2</sub>):  $\delta$  [ppm] = 139.78 ([Cp\*Fe( $\eta^5$ -P<sub>5</sub>)).

**<sup>19</sup>F NMR** (pyridine/CD<sub>2</sub>Cl<sub>2</sub>): no signal was detected.

**Positive ion ESI-MS** (CH<sub>2</sub>Cl<sub>2</sub>/CH<sub>3</sub>CN (1:1)):  $m/z$  (%) = 2418.2  
 [{Cp\*Fe( $\eta^5$ -P<sub>5</sub>)}<sub>3</sub>Ag<sub>4</sub>(SbF<sub>6</sub>)<sub>3</sub>(NC(CH<sub>2</sub>)<sub>5</sub>CN)<sub>2</sub>]<sup>+</sup>, 2074.3 [{Cp\*Fe( $\eta^5$ -P<sub>5</sub>)}<sub>3</sub>Ag<sub>3</sub>(SbF<sub>6</sub>)<sub>2</sub>(NC(CH<sub>2</sub>)<sub>5</sub>CN)<sub>2</sub>]<sup>+</sup>, 1955  
 [{Cp\*Fe( $\eta^5$ -P<sub>5</sub>)}<sub>3</sub>Ag<sub>3</sub>(SbF<sub>6</sub>)<sub>2</sub>(NC(CH<sub>2</sub>)<sub>5</sub>CN)]<sup>+</sup>, 1832.3 [{Cp\*Fe( $\eta^5$ -P<sub>5</sub>)}<sub>3</sub>Ag<sub>3</sub>(SbF<sub>6</sub>)<sub>2</sub>]<sup>+</sup>, 1731  
 [{Cp\*Fe( $\eta^5$ -P<sub>5</sub>)}<sub>2</sub>Ag<sub>3</sub>(SbF<sub>6</sub>)<sub>2</sub>(NC(CH<sub>2</sub>)<sub>5</sub>CN)<sub>2</sub>]<sup>+</sup>, 1608.4 [{Cp\*Fe( $\eta^5$ -P<sub>5</sub>)}<sub>2</sub>Ag<sub>3</sub>(SbF<sub>6</sub>)<sub>2</sub>(NC(CH<sub>2</sub>)<sub>5</sub>CN)]<sup>+</sup>,  
 1384.6 [{Cp\*Fe( $\eta^5$ -P<sub>5</sub>)}<sub>2</sub>Ag<sub>2</sub>(SbF<sub>6</sub>)(NC(CH<sub>2</sub>)<sub>5</sub>CN)<sub>2</sub>]<sup>+</sup>, 1265 [{Cp\*Fe( $\eta^5$ -P<sub>5</sub>)}<sub>2</sub>Ag<sub>2</sub>(SbF<sub>6</sub>)(NC(CH<sub>2</sub>)<sub>5</sub>CN)]<sup>+</sup>,  
 1142.5 [{Cp\*Fe( $\eta^5$ -P<sub>5</sub>)}<sub>2</sub>Ag<sub>2</sub>(SbF<sub>6</sub>)]<sup>+</sup>, 918.7 [{Cp\*Fe( $\eta^5$ -P<sub>5</sub>)}Ag<sub>2</sub>(SbF<sub>6</sub>)(NC(CH<sub>2</sub>)<sub>5</sub>CN)]<sup>+</sup>, 798.7  
 [{Cp\*Fe( $\eta^5$ -P<sub>5</sub>)}<sub>2</sub>Ag]<sup>+</sup>, 493.9 (100) [{Cp\*Fe( $\eta^5$ -P<sub>5</sub>)}Ag(CH<sub>3</sub>CN)]<sup>+</sup>, 452.8 [(Cp\*Fe( $\eta^5$ -P<sub>5</sub>))Ag]<sup>+</sup>.

**Negative ion ESI-MS** (CH<sub>2</sub>Cl<sub>2</sub>/CH<sub>3</sub>CN (1:1)):  $m/z$  (%) = 2772 [{Cp\*Fe( $\eta^5$ -P<sub>5</sub>)}<sub>4</sub>Ag<sub>3</sub>(SbF<sub>6</sub>)<sub>4</sub>(NC(CH<sub>2</sub>)<sub>5</sub>CN)]<sup>-</sup>,  
 2647.9 [{Cp\*Fe( $\eta^5$ -P<sub>5</sub>)}<sub>4</sub>Ag<sub>3</sub>(SbF<sub>6</sub>)<sub>4</sub>]<sup>+</sup>, 2544.0 [{Cp\*Fe( $\eta^5$ -P<sub>5</sub>)}<sub>3</sub>Ag<sub>3</sub>(SbF<sub>6</sub>)<sub>4</sub>(NC(CH<sub>2</sub>)<sub>5</sub>CN)<sub>2</sub>]<sup>-</sup>, 2426  
 [{Cp\*Fe( $\eta^5$ -P<sub>5</sub>)}<sub>3</sub>Ag<sub>3</sub>(SbF<sub>6</sub>)<sub>4</sub>(NC(CH<sub>2</sub>)<sub>5</sub>CN)]<sup>-</sup>, 2299.9 [{Cp\*Fe( $\eta^5$ -P<sub>5</sub>)}<sub>3</sub>Ag<sub>3</sub>(SbF<sub>6</sub>)<sub>4</sub>]<sup>-</sup>, 2078.1  
 [{Cp\*Fe( $\eta^5$ -P<sub>5</sub>)}<sub>3</sub>Ag<sub>2</sub>(SbF<sub>6</sub>)<sub>3</sub>(NC(CH<sub>2</sub>)<sub>5</sub>CN)]<sup>-</sup>, 1958.1 [{Cp\*Fe( $\eta^5$ -P<sub>5</sub>)}<sub>3</sub>Ag<sub>2</sub>(SbF<sub>6</sub>)<sub>3</sub>]<sup>-</sup>, 1612.2  
 [(Cp\*Fe( $\eta^5$ -P<sub>5</sub>))<sub>2</sub>Ag<sub>2</sub>(SbF<sub>6</sub>)<sub>3</sub>]<sup>-</sup>, 234.9 (100) [SbF<sub>6</sub>]<sup>-</sup>.

**Elemental analysis:** Calculated (%) for [{Cp\*Fe( $\eta^5$ -P<sub>5</sub>)}(AgSbF<sub>6</sub>)<sub>2</sub>(NC(CH<sub>2</sub>)<sub>5</sub>CN)<sub>2</sub>] (3002.56 g/mol):  
 C 22.56, H 2.76, N 4.39; found: C 21.75, H 2.85, N 4.07.

**IR:**  $\tilde{\nu}$ /cm<sup>-1</sup> = 2930 (vw), 2266 (w), 1615 (vw), 1462 (w), 1418 (w), 1375 (w), 1016 (w), 651 (s).

### Synthesis of [{Cp\*Fe( $\eta^5$ -P<sub>5</sub>)}<sub>4</sub>{Ag<sub>4</sub>(NC(CH<sub>2</sub>)<sub>5</sub>CN)<sub>2</sub>}]<sub>n</sub>[SbF<sub>6</sub>]<sub>4n</sub> (**4b**)

In a Schlenk tube a solution of AgSbF<sub>6</sub> (18 mg, 0.05 mmol) in CH<sub>2</sub>Cl<sub>2</sub> (25 mL) is carefully layered first with a solvent mixture of CH<sub>2</sub>Cl<sub>2</sub>/toluene (10 mL, 2:1) and then with a green solution of [Cp\*Fe( $\eta^5$ -P<sub>5</sub>)] (18 mg, 0.05 mmol) and NC(CH<sub>2</sub>)<sub>5</sub>CN (1 mL, 0.4 M in CH<sub>2</sub>Cl<sub>2</sub>) in toluene (25 mL). After a few hours, the phase boundary turns yellow and after one day, the formation of green rods of **4b** at the phase boundary was observed. After complete diffusion, the light green mother liquor is decanted, the crystals are washed with CH<sub>2</sub>Cl<sub>2</sub> (3 x 10 mL) and dried *in vacuo*.

Analytical data of **4b**:

**Yield:** 47 mg (0.016 mmol, 63 % based on [Cp\*Fe( $\eta^5$ -P<sub>5</sub>)])

**<sup>1</sup>H NMR** (pyridine/CD<sub>2</sub>Cl<sub>2</sub>):  $\delta$  [ppm] = 1.45 (s, 30H, [Cp(CH<sub>3</sub>)<sub>5</sub>Fe( $\eta^5$ -P<sub>5</sub>)]), 1.60 (m, 2H, C-4, NC(CH<sub>2</sub>)<sub>5</sub>CN), 1.69 (m, 4H, C-3/C-5, NC(CH<sub>2</sub>)<sub>5</sub>CN), 2.38 (t, 4H, C-2/C-6, NC(CH<sub>2</sub>)<sub>5</sub>CN), 7.45 (m,  $\beta$ -H, pyridine), 7.85 (m,  $\gamma$ -H, pyridine), 8.57 (m,  $\alpha$ -H, pyridine).

**<sup>13</sup>C NMR** (pyridine/CD<sub>2</sub>Cl<sub>2</sub>):  $\delta$  [ppm] = 10.69 ([Cp(CH<sub>3</sub>)<sub>5</sub>Fe( $\eta^5$ -P<sub>5</sub>)]), 93.04 ([C(CH<sub>3</sub>)<sub>5</sub>Fe( $\eta^5$ -P<sub>5</sub>)]), 124.7 ( $\beta$ -C, pyridine), 137.81 ( $\gamma$ -C, pyridine), 149.31 ( $\alpha$ -C, pyridine).

**<sup>31</sup>P{<sup>1</sup>H} NMR** (pyridine/CD<sub>2</sub>Cl<sub>2</sub>):  $\delta$  [ppm] = 143.46 (s, [Cp\*Fe( $\eta^5$ -P<sub>5</sub>)]).

**<sup>19</sup>F NMR** (pyridine/CD<sub>2</sub>Cl<sub>2</sub>): no signal was detected.

**Positive ion ESI-MS** (CH<sub>2</sub>Cl<sub>2</sub>/CH<sub>3</sub>CN (1:1)): *m/z* (%) = 2522.0 [{Cp\*Fe(η<sup>5</sup>-P<sub>5</sub>)}<sub>4</sub>Ag<sub>4</sub>(SbF<sub>6</sub>)<sub>3</sub>]<sup>+</sup>, 2178.2 [{Cp\*Fe(η<sup>5</sup>-P<sub>5</sub>)}<sub>4</sub>Ag<sub>3</sub>(SbF<sub>6</sub>)<sub>2</sub>]<sup>+</sup>, 2176 [{Cp\*Fe(η<sup>5</sup>-P<sub>5</sub>)}<sub>3</sub>Ag<sub>4</sub>(SbF<sub>6</sub>)<sub>3</sub>]<sup>+</sup>, 2077 [{Cp\*Fe(η<sup>5</sup>-P<sub>5</sub>)}<sub>3</sub>Ag<sub>3</sub>(SbF<sub>6</sub>)<sub>2</sub>(NC(CH<sub>2</sub>)<sub>5</sub>CN)]<sup>+</sup>, 1955 [{Cp\*Fe(η<sup>5</sup>-P<sub>5</sub>)}<sub>3</sub>Ag<sub>3</sub>(SbF<sub>6</sub>)<sub>2</sub>(NC(CH<sub>2</sub>)<sub>5</sub>CN)]<sup>+</sup>, 1832.3 [{Cp\*Fe(η<sup>5</sup>-P<sub>5</sub>)}<sub>3</sub>Ag<sub>3</sub>(SbF<sub>6</sub>)<sub>2</sub>]<sup>+</sup>, 1608.4 [{Cp\*Fe(η<sup>5</sup>-P<sub>5</sub>)}<sub>2</sub>Ag<sub>3</sub>(SbF<sub>6</sub>)<sub>2</sub>(NC(CH<sub>2</sub>)<sub>5</sub>CN)]<sup>+</sup>, 1387 [{Cp\*Fe(η<sup>5</sup>-P<sub>5</sub>)}<sub>2</sub>Ag<sub>2</sub>(SbF<sub>6</sub>)(NC(CH<sub>2</sub>)<sub>5</sub>CN)]<sup>+</sup>, 1265 [{Cp\*Fe(η<sup>5</sup>-P<sub>5</sub>)}<sub>2</sub>Ag<sub>2</sub>(SbF<sub>6</sub>)(NC(CH<sub>2</sub>)<sub>5</sub>CN)]<sup>+</sup>, 1142.5 [{Cp\*Fe(η<sup>5</sup>-P<sub>5</sub>)}<sub>2</sub>Ag<sub>2</sub>(SbF<sub>6</sub>)]<sup>+</sup>, 918.7 [{Cp\*Fe(η<sup>5</sup>-P<sub>5</sub>)}Ag<sub>2</sub>(SbF<sub>6</sub>)(NC(CH<sub>2</sub>)<sub>5</sub>CN)]<sup>+</sup>, 798.7 [{Cp\*Fe(η<sup>5</sup>-P<sub>5</sub>)}<sub>2</sub>Ag]<sup>+</sup>, 493.9 (100) [{Cp\*Fe(η<sup>5</sup>-P<sub>5</sub>)}Ag(CH<sub>3</sub>CN)]<sup>+</sup>, 452.8 [{Cp\*Fe(η<sup>5</sup>-P<sub>5</sub>)}Ag]<sup>+</sup>.

**Negative ion ESI-MS** (CH<sub>2</sub>Cl<sub>2</sub>/CH<sub>3</sub>CN (1:1)): *m/z* (%) = 2647.9 [{Cp\*Fe(η<sup>5</sup>-P<sub>5</sub>)}<sub>4</sub>Ag<sub>3</sub>(SbF<sub>6</sub>)<sub>4</sub>]<sup>-</sup>, 2426 [{Cp\*Fe(η<sup>5</sup>-P<sub>5</sub>)}<sub>3</sub>Ag<sub>3</sub>(SbF<sub>6</sub>)<sub>4</sub>(NC(CH<sub>2</sub>)<sub>5</sub>CN)]<sup>-</sup>, 2301.9 [{Cp\*Fe(η<sup>5</sup>-P<sub>5</sub>)}<sub>3</sub>Ag<sub>3</sub>(SbF<sub>6</sub>)<sub>4</sub>]<sup>-</sup>, 2078.1 [{Cp\*Fe(η<sup>5</sup>-P<sub>5</sub>)}<sub>3</sub>Ag<sub>2</sub>(SbF<sub>6</sub>)<sub>3</sub>(NC(CH<sub>2</sub>)<sub>5</sub>CN)]<sup>-</sup>, 1958.1 [{Cp\*Fe(η<sup>5</sup>-P<sub>5</sub>)}<sub>3</sub>Ag<sub>2</sub>(SbF<sub>6</sub>)<sub>3</sub>]<sup>-</sup>, 1739.2 [{Cp\*Fe(η<sup>5</sup>-P<sub>5</sub>)}<sub>2</sub>Ag<sub>2</sub>(SbF<sub>6</sub>)<sub>3</sub>(NC(CH<sub>2</sub>)<sub>5</sub>CN)]<sup>-</sup>, 1612.2 [{Cp\*Fe(η<sup>5</sup>-P<sub>5</sub>)}<sub>2</sub>Ag<sub>2</sub>(SbF<sub>6</sub>)<sub>3</sub>]<sup>-</sup>, 234.9 (100) [SbF<sub>6</sub>]<sup>-</sup>.

**Elemental analysis:** Calculated (%) for [{Cp\*Fe(η<sup>5</sup>-P<sub>5</sub>)}<sub>4</sub>(AgSbF<sub>6</sub>)<sub>4</sub>(NC(CH<sub>2</sub>)<sub>5</sub>CN)<sub>2</sub>] (4280.07 g/mol): C 21.6, H 2.69, N 1.87; found: C 21.49, H 2.82, N 1.58.

**IR:**  $\tilde{\nu}$ /cm<sup>-1</sup> = 2964 (vw), 2274 (vw), 1478 (w), 1425 (w), 1378 (w), 1020 (w), 655 (s).

### Synthesis of [{Cp\*Fe(η<sup>5</sup>-P<sub>5</sub>)}{Ag(NC(CH<sub>2</sub>)<sub>6</sub>CN)}]<sub>n</sub>[SbF<sub>6</sub>]<sub>n</sub> (**5**)

In a Schlenk tube a solution of AgSbF<sub>6</sub> (14 mg, 0.04 mmol) in CH<sub>2</sub>Cl<sub>2</sub> (15 mL) is carefully layered with a green solution of [Cp\*Fe(η<sup>5</sup>-P<sub>5</sub>)] (14 mg, 0.04 mmol) and NC(CH<sub>2</sub>)<sub>6</sub>CN (1 mL, 0.4 mmol, 0.4 M in CH<sub>2</sub>Cl<sub>2</sub>) in toluene (15 mL). Thereby, the phase boundary turns yellow. After a few days, the formation of green-brown prismatic crystals of **3** at the phase boundary was observed. After complete diffusion, the light green mother liquor is decanted, the crystals are washed with hexane (3 x 10 mL) and dried *in vacuo*.

Analytical data of **5**:

**Yield:** 19 mg (0.023 mmol, 57% based on [Cp\*Fe(η<sup>5</sup>-P<sub>5</sub>)]).

**<sup>1</sup>H NMR** (CD<sub>2</sub>Cl<sub>2</sub>/pyridine):  $\delta$  [ppm] = 1.43 (s, 15H, [Cp(CH<sub>3</sub>)<sub>5</sub>Fe(η<sup>5</sup>-P<sub>5</sub>)]), 1.47 (m, 4H, NC(CH<sub>2</sub>)<sub>6</sub>CN), 1.66 (m, 4H, NC(CH<sub>2</sub>)<sub>6</sub>CN), 2.36 (t, 4H, NC(CH<sub>2</sub>)<sub>6</sub>CN).

**<sup>13</sup>C NMR** (CD<sub>2</sub>Cl<sub>2</sub>/pyridine):  $\delta$  [ppm] = 10.66 ([Cp(CH<sub>3</sub>)<sub>5</sub>Fe(η<sup>5</sup>-P<sub>5</sub>)]), 16.98 (C-2, NC(CH<sub>2</sub>)<sub>6</sub>CN), 25.13 (C-3, NC(CH<sub>2</sub>)<sub>6</sub>CN), 27.86 (C-4, NC(CH<sub>2</sub>)<sub>6</sub>CN), 149.75 (NC(CH<sub>2</sub>)<sub>6</sub>CN).

**<sup>31</sup>P{<sup>1</sup>H} NMR** (CD<sub>2</sub>Cl<sub>2</sub>/pyridine):  $\delta$  [ppm] = 141.20 (s, [Cp\*Fe(η<sup>5</sup>-P<sub>5</sub>)]).

**<sup>19</sup>F NMR** (CD<sub>2</sub>Cl<sub>2</sub>/pyridine): no signal was detected.

**Positive ion ESI-MS** (CH<sub>2</sub>Cl<sub>2</sub>/CH<sub>3</sub>CN (1:1)): *m/z* (%) = 2522.0 [{Cp\*Fe(η<sup>5</sup>-P<sub>5</sub>)}<sub>4</sub>Ag<sub>4</sub>(SbF<sub>6</sub>)<sub>3</sub>]<sup>+</sup>, 2178.2 [{Cp\*Fe(η<sup>5</sup>-P<sub>5</sub>)}<sub>4</sub>Ag<sub>3</sub>(SbF<sub>6</sub>)<sub>2</sub>]<sup>+</sup>, 2176 [{Cp\*Fe(η<sup>5</sup>-P<sub>5</sub>)}<sub>3</sub>Ag<sub>4</sub>(SbF<sub>6</sub>)<sub>3</sub>]<sup>+</sup>, 1832.3 [{Cp\*Fe(η<sup>5</sup>-P<sub>5</sub>)}<sub>3</sub>Ag<sub>3</sub>(SbF<sub>6</sub>)<sub>2</sub>]<sup>+</sup>,

1622.4  $[\{\text{Cp}^*\text{Fe}(\eta^5\text{-P}_5)\}_2\text{Ag}_3(\text{SbF}_6)_2(\text{NC}(\text{CH}_2)_6\text{CN})]^+$ , 1412.6  $[\{\text{Cp}^*\text{Fe}(\eta^5\text{-P}_5)\}_2\text{Ag}_2(\text{SbF}_6)(\text{NC}(\text{CH}_2)_6\text{CN})_2]^+$ , 1278.6  $[\{\text{Cp}^*\text{Fe}(\eta^5\text{-P}_5)\}_2\text{Ag}_2(\text{SbF}_6)(\text{NC}(\text{CH}_2)_6\text{CN})]^+$ , 1142.5  $[\{\text{Cp}^*\text{Fe}(\eta^5\text{-P}_5)\}_2\text{Ag}_2(\text{SbF}_6)]^+$ , 932.7  $[\{\text{Cp}^*\text{Fe}(\eta^5\text{-P}_5)\}\text{Ag}_2(\text{SbF}_6)(\text{NC}(\text{CH}_2)_6\text{CN})]^+$ , 798.7  $[\{\text{Cp}^*\text{Fe}(\eta^5\text{-P}_5)\}_2\text{Ag}]^+$ , 493.9 (100)  $[\{\text{Cp}^*\text{Fe}(\eta^5\text{-P}_5)\}\text{Ag}(\text{CH}_3\text{CN})]^+$ , 452.8  $[\{\text{Cp}^*\text{Fe}(\eta^5\text{-P}_5)\}\text{Ag}]^+$ .

**Negative ion ESI-MS** ( $\text{CH}_2\text{Cl}_2/\text{CH}_3\text{CN}$  (1:1)):  $m/z$  (%) = 2647.9  $[\{\text{Cp}^*\text{Fe}(\eta^5\text{-P}_5)\}_4\text{Ag}_3(\text{SbF}_6)_4]^-$ , 1613.0  $[\{\text{Cp}^*\text{Fe}(\eta^5\text{-P}_5)\}_2\text{Ag}_2(\text{SbF}_6)_3]^-$ , 234.9 (100)  $[\text{SbF}_6]^-$ .

**Elemental analysis:** Calculated (%) for  $[\{\text{Cp}^*\text{Fe}(\eta^5\text{-P}_5)\}(\text{AgSbF}_6)(\text{NC}(\text{CH}_2)_6\text{CN})]$  (825.75 g/mol): C 26.18, H 3.30, N 3.39; found: C 25.50, H 3.22, N 3.27.

**IR:**  $\tilde{\nu}/\text{cm}^{-1}$  = 2929 (vw), 2273 (vw), 1476 (w), 1379 (w), 1020 (w), 656 (s).

**Synthesis of  $[\{\text{SbF}_6\}@\{\{\text{Cp}^*\text{Fe}(\eta^5\text{-P}_5)\}_9\{\text{Ag}_{11}(\text{NC}(\text{CH}_2)_7\text{CN})_6\}}]_n[\text{SbF}_6]_{10n}$  (6a) with  $[\{\text{Cp}^*\text{Fe}(\eta^5\text{-P}_5)\}\{\text{Ag}(\text{NC}(\text{CH}_2)_7\text{CN})\}]_n[\text{SbF}_6]_n$  (6b) and  $[\{\text{Cp}^*\text{Fe}(\eta^5\text{-P}_5)\}\{\text{Ag}_2(\text{NC}(\text{CH}_2)_7\text{CN})\}]_n[\text{SbF}_6]_{2n}$  (6c)**

In a Schlenk tube a solution of  $\text{AgSbF}_6$  (14 mg, 0.04 mmol) in  $\text{CH}_2\text{Cl}_2$  (25 mL) is carefully layered first with a solvent mixture of  $\text{CH}_2\text{Cl}_2$ /toluene (10 mL, 2:1) and then with a green solution of  $[\text{Cp}^*\text{Fe}(\eta^5\text{-P}_5)]$  (14 mg, 0.04 mmol) and  $\text{NC}(\text{CH}_2)_7\text{CN}$  (1 mL, 0.04 mmol, 0.4 M in  $\text{CH}_2\text{Cl}_2$ ) in toluene (25 mL). After a few hours, the phase boundary turns yellow and after one day, the formation of brown plates of **6a** at the phase boundary was observed. Furthermore a few green polyhedra of **6b** and green plates of **6c** appear at the phase boundary. After complete diffusion, the light yellow mother liquor is decanted, the crystals are washed with  $\text{CH}_2\text{Cl}_2$  (3 x 10 mL) and dried *in vacuo*. **6a** was isolated by manually separating the crystals from those of **6b** and **6c**.

Analytical data of **6a**:

**Yield:** 15 mg (0.0019 mmol, 53% based on  $[\text{Cp}^*\text{Fe}(\eta^5\text{-P}_5)]$ ).

**$^1\text{H}$  NMR** (pyridine/ $\text{CD}_2\text{Cl}_2$ ):  $\delta$  [ppm] = 1.38 (2H, C-4,  $\text{NC}(\text{CH}_2)_7\text{CN}$ ), 1.46 (4H, C-3/C-5,  $\text{NC}(\text{CH}_2)_7\text{CN}$ ), 1.65 (4H, C-2/C-6,  $\text{NC}(\text{CH}_2)_7\text{CN}$ ), 2.34 (t, 4H, C-1/C-7,  $\text{NC}(\text{CH}_2)_7\text{CN}$ ), 7.56 (m,  $\beta$ -H, pyridine), 7.97 (m,  $\gamma$ -H, pyridine), 8.67 (m,  $\alpha$ -H, pyridine), no signal was found for the  $\text{Cp}^*$  residue.

**$^{13}\text{C}$  NMR** (pyridine/ $\text{CD}_2\text{Cl}_2$ ):  $\delta$  [ppm] = 16.99 (C-1/C-7,  $\text{NC}(\text{CH}_2)_7\text{CN}$ ), 25.26 (C-2/C-6,  $\text{NC}(\text{CH}_2)_7\text{CN}$ ), 27.96 (C-4,  $\text{NC}(\text{CH}_2)_7\text{CN}$ ), 28.34 (C-3/C-5,  $\text{NC}(\text{CH}_2)_7\text{CN}$ ), 119.78 ( $\text{NC}(\text{CH}_2)_7\text{CN}$ ), 125.09 ( $\beta$ -C, pyridine), 139.23 ( $\gamma$ -C, pyridine), 147.50 ( $\alpha$ -C, pyridine), no signal was found for the  $\text{Cp}^*$  residue.

**$^{31}\text{P}\{^1\text{H}\}$  NMR** (pyridine/ $\text{CD}_2\text{Cl}_2$ ):  $\delta$  [ppm] = 151.53 ( $[\text{Cp}^*\text{Fe}(\eta^5\text{-P}_5)]$ ).

**$^{31}\text{P}$  MAS NMR:**  $\delta$  [ppm] = 134.27 (m(br),  $\omega_{1/2}$  = 3483 Hz,  $[\text{Cp}^*\text{Fe}(\eta^5\text{-P}_5)]$ ).

**$^{19}\text{F}$  NMR** (pyridine/ $\text{CD}_2\text{Cl}_2$ ): no signal was detected.

**Positive ion ESI-MS** ( $\text{CH}_3\text{CN}$ ):  $m/z$  (%) = 2522.06  $[\{\text{Cp}^*\text{Fe}(\eta^5\text{-P}_5)\}_5\text{Ag}_3(\text{SbF}_6)_2]^+$ , 2178.28  $[\{\text{Cp}^*\text{Fe}(\eta^5\text{-P}_5)\}_4\text{Ag}_3(\text{SbF}_6)_2]^+$ , 1832.44  $[\{\text{Cp}^*\text{Fe}(\eta^5\text{-P}_5)\}_3\text{Ag}_3(\text{SbF}_6)_2]^+$ , 1636.64  $[\{\text{Cp}^*\text{Fe}(\eta^5\text{-P}_5)\}_2\text{Ag}_3(\text{SbF}_6)_2(\text{NC}(\text{CH}_2)_7\text{CN})]^+$ , 1292.75  $[\{\text{Cp}^*\text{Fe}(\eta^5\text{-P}_5)\}_2\text{Ag}_2(\text{SbF}_6)(\text{NC}(\text{CH}_2)_7\text{CN})]^+$ , 1178.94  $[\{\text{Cp}^*\text{Fe}(\eta^5\text{-P}_5)\}_2\text{Ag}_2(\text{SbF}_6)(\text{CH}_3\text{CN})]^+$ , 1142.58  $[\{\text{Cp}^*\text{Fe}(\eta^5\text{-P}_5)\}_2\text{Ag}_2(\text{SbF}_6)]^+$ , 946.74  $[\{\text{Cp}^*\text{Fe}(\eta^5\text{-P}_5)\}\text{Ag}_2(\text{SbF}_6)(\text{NC}(\text{CH}_2)_7\text{CN})]^+$ , 798.77  $[\{\text{Cp}^*\text{Fe}(\eta^5\text{-P}_5)\}_2\text{Ag}]^+$ , 603.03  $[\{\text{Cp}^*\text{Fe}(\eta^5\text{-P}_5)\}\text{Ag}(\text{NC}(\text{CH}_2)_7\text{CN})]^+$ , 493.97 (100)  $[\{\text{Cp}^*\text{Fe}(\eta^5\text{-P}_5)\}\text{Ag}(\text{CH}_3\text{CN})]^+$ , 452.94  $[\{\text{Cp}^*\text{Fe}(\eta^5\text{-P}_5)\}\text{Ag}]^+$ .

**Negative ion ESI-MS** ( $\text{CH}_3\text{CN}$ ):  $m/z$  (%) = 234.9 (100)  $[\text{SbF}_6]^-$ .

**Elemental analysis:** Calculated (%) for  $[[[\text{SbF}_6]@\{\{\text{Cp}^*\text{Fe}(\eta^5\text{-P}_5)\}_9\{\text{Ag}_{11}(\text{NC}(\text{CH}_2)_7\text{CN})_6\}\}]_n[\text{SbF}_6]_{10n}$  (7794.56 g/mol): C 22.19, H 2.83, N 2.16; found: C 22.47, H 3.17, N 2.30.

**IR:**  $\tilde{\nu}/\text{cm}^{-1}$  = 3626 (vw), 2942 (vw), 2358 (vw), 2270 (vw), 1476 (vw), 1423 (vw), 1378 (vw), 655 (vs).

## 5.5 Crystallographic Details

Crystals of **4a-6b** were taken from a Schlenk flask under a stream of argon and immediately covered with perfluorinated Fomblin® mineral oil to prevent both, decomposition and a loss of solvent. The quickly chosen single crystals covered by a drop of the oil were directly placed into a stream of cold nitrogen with the pre-centered goniometer head with CryoMount® and attached to the goniometer of a diffractometer. The crystal of **6c** was carefully selected, mounted on a magnetic holder, checked for quality and placed into a dewar vessel in liquid nitrogen using standard cryocrystallography tools. After a few weeks it was taken to the DESY PETRA III synchrotron. Using standard procedures it was placed into a vessel filled with liquid nitrogen among other crystals. A robotic mounting/demounting was used for further manipulations in the P11 beamline hutch.<sup>25</sup>

The data for **4a-6b** were collected on an Agilent Technologies diffractometer equipped with a Titan<sup>S2</sup> CCD detector and a SuperNova Cu K $\alpha$  microfocus source using either 1° (**4a**, **4b**, **5**, **6b**) or 0.5° (**6c**)  $\omega$  scans depending on the unit cell constants. X-ray diffraction experiment for **6c** was measured at 80 K at the DESY PETRA III synchrotron (beamline P11) using robotic mounting.<sup>25</sup> Data collection was performed by 360°  $\phi$ -rotation with 0.2° scan width and exposure 0.12 s per frame at wavelength  $\lambda$  = 0.6199 Å (20 keV). Data reduction for all crystal structures was performed with XDS<sup>26</sup> or CrysAlis software.<sup>27</sup> Analytical absorption correction for **4a-6b**, was applied based on crystal faces; whereas for **6c** empirical absorption correction using equivalent reflections was used. Crystallographic data and further details of the diffraction experiments are given in *Tables 3-6*.



The structures were solved by direct methods with *SHELXT*<sup>[28]</sup> and were refined by full-matrix least-squares method against  $F^2$  in anisotropic approximation using multiprocessor variable memory versions of *SHELXL* (2014-2015). The model received for **6c** from a preliminary X-ray experiment at an in-house diffractometer was used to refine the structure. All non-hydrogen atoms were refined anisotropically, while the hydrogen atoms were refined riding on pivot atoms.

In **4b**, **6a**, and **6b** the  $\text{SbF}_6^-$  counter-anions are disordered over two or more close positions. The occupation factors for disordered positions of Sb atoms were refined with fixed isotropic  $U_{\text{iso}}$  similar to the average  $U_{\text{iso}}$  (usually 0.025-0.035  $\text{\AA}^{-2}$ ) for the fully occupied heavy atoms in the corresponding structure. For **6a** and **6b**, the disorder is so severe, that for minor disordered positions of the  $\text{SbF}_6^-$  counter-anions, not all fluorine atoms were located from the difference Fourier map. For the same reason, the fluorine atoms in very close positions were refined using restraint a.d.p. parameters. In case of small occupancy for a certain disorder component, F atoms were refined isotropically.

The flexible linker molecules also showed a strong tendency for disorder. In **4b**, **6a**, **6b** the dinitrile molecules were disordered typically over two close positions with different occupancies. Their molecular site occupancy factors (equal s.o.f.'s for all atoms of a molecule) were refined using the FVAR instruction of SHELX with isotropic displacement parameters fixed at  $U_{\text{iso}} = 0.05 \text{ \AA}^{-2}$ . The resulting occupancies were fixed and the C and N atoms with occupancies of more than 0.5 were refined in anisotropic approximation. Some minor positions of the linker molecules were refined with restraint geometry. The restraints were removed at the final stage of the refinement when possible. The disorder of the solvent molecules  $\text{CH}_2\text{Cl}_2$  was treated in a similar way.

**80 | V - Three-Component Self-Assembly:**  
**A Way to Overcome Simple Coordination Polymers in Favor**  
**of 3D Connected Spherical Supramolecular Aggregates**

**Table 3:** Experimental details for compounds **2** and **3**.

Crystal data	<b>2</b>	<b>3</b>
Chemical formula	(C <sub>20</sub> H <sub>30</sub> AgFe <sub>2</sub> P <sub>10</sub> ) <sup>+</sup> ·(SbF <sub>6</sub> ) <sup>-</sup>	C <sub>28</sub> H <sub>42</sub> Ag <sub>2</sub> Fe <sub>2</sub> N <sub>4</sub> P <sub>10</sub> ·2(SbF <sub>6</sub> )
<i>M<sub>r</sub></i>	1035.46	1543.29
Crystal system, space group	Monoclinic, <i>C2/c</i>	Triclinic, <i>P</i> $\bar{1}$
Temperature (K)	80	123
<i>a</i> , <i>b</i> , <i>c</i> (Å)	26.73026 (13), 11.20485 (4), 10.94534 (6)	8.3225 (2), 12.2260 (3), 14.1342 (4)
$\alpha$ , $\beta$ , $\gamma$ (°)	90.0027 (4)	100.321 (2), 106.292 (2), 109.233 (2)
<i>V</i> (Å <sup>3</sup> )	3278.22 (3)	1243.48 (6)
<i>Z</i>	4	1
<i>F</i> (000)	2016	744
<i>D<sub>x</sub></i> (Mg m <sup>-3</sup> )	2.098	2.061
Radiation type	Synchrotron, $\lambda$ = 0.6199 Å	Cu <i>K</i> α
$\mu$ (mm <sup>-1</sup> )	1.93	23.01
Crystal shape	Lath	Plate
Colour	Dark brown	Clear green
Crystal size (mm)	0.15 × 0.10 × 0.05	0.23 × 0.11 × 0.06
<b>Data collection</b>		
Diffractometer	Synchrotron, beamline P11 at DESY Petra III, DECTRIS PILATUS M6	Xcalibur, Atlas <sup>S2</sup> , Gemini ultra
Absorption correction	Multi-scan	Analytical
<i>T<sub>min</sub></i> , <i>T<sub>max</sub></i>	0.312, 1.000	0.068, 0.367
No. of measured, independent and observed [ <i>I</i> > 2σ( <i>I</i> )] reflections	33178, 6355, 6272	17665, 4370, 3894
<i>R<sub>int</sub></i>	0.045	0.038
(sin $\theta/\lambda$ ) <sub>max</sub> (Å <sup>-1</sup> )	0.839	0.596
Range of <i>h</i> , <i>k</i> , <i>l</i>	<i>h</i> = -39 → 39, <i>k</i> = -16 → 16, <i>l</i> = -15 → 13	<i>h</i> = -9 → 9, <i>k</i> = -14 → 14, <i>l</i> = -16 → 16
<b>Refinement</b>		
<i>R</i> [ <i>F</i> <sup>2</sup> > 2σ( <i>F</i> <sup>2</sup> )], <i>wR</i> ( <i>F</i> <sup>2</sup> ), <i>S</i>	0.036, 0.097, 1.06	0.021, 0.050, 0.96
No. of reflections	6355	4370
No. of parameters	190	278
No. of restraints	0	0
H-atom treatment	H-atom parameters constrained	H-atom parameters constrained
$\Delta$ <sub>max</sub> , $\Delta$ <sub>min</sub> (e Å <sup>-3</sup> )	2.32, -4.85	0.48, -0.71
Computer programs for <b>2</b> : XDS, (Kabsch, 2010), CrysAlis PRO 1.171.39.37b (Rigaku OD, 2017), SHELXT2014/7 (Sheldrick, 2014), SHELXL2014/7 (Sheldrick, 2014).		
Computer programs for <b>3</b> : CrysAlis PRO 1.171.38.41 (Rigaku OD, 2015), SHELXT2014 (Sheldrick, 2014), SHELXL2014/7 (Sheldrick, 2014).		

**Table 4:** Experimental details for compounds **4a** and **4b**.

Crystal data	<b>4a</b>	<b>4b</b>
Chemical formula	C <sub>27.50</sub> H <sub>41</sub> Ag <sub>2</sub> ClF <sub>12</sub> Fe <sub>2</sub> N <sub>2</sub> P <sub>10</sub> Sb <sub>2</sub>	C <sub>25.50</sub> H <sub>38</sub> Ag <sub>2</sub> Cl <sub>3</sub> F <sub>12</sub> FeN <sub>4</sub> P <sub>5</sub> Sb <sub>2</sub>
<i>M</i> <sub>r</sub>	1543.71	1404.89
Crystal system, space group	triclinic, <i>P</i> $\bar{1}$	triclinic, <i>P</i> $\bar{1}$
Temperature (K)	123	123
<i>a</i> , <i>b</i> , <i>c</i> (Å)	12.3068 (5), 14.2078 (7), 15.5935 (8)	11.9353 (3), 15.1268 (4), 26.2100 (6)
$\alpha$ , $\beta$ , $\gamma$ (°)	67.494 (5), 72.042 (4), 88.491 (4)	82.699 (2), 84.780 (2), 76.923 (2)
<i>V</i> (Å <sup>3</sup> )	2383.1 (2)	4562.4 (2)
<i>Z</i>	2	4
<i>F</i> (000)	1486	2700
<i>D</i> <sub>x</sub> (Mg m <sup>-3</sup> )	2.151	2.045
Radiation type	Cu K $\alpha$	Cu K $\alpha$
$\mu$ (mm <sup>-1</sup> )	24.401	22.489
Crystal shape	rod	rod
Colour	red	green
Crystal size (mm)	0.248 × 0.065 × 0.020	0.697 × 0.153 × 0.060
Data collection		
Diffractometer	SuperNova, Titan <sup>S2</sup>	SuperNova, Titan <sup>S2</sup>
Absorption correction	Gaussian	Gaussian
<i>T</i> <sub>min</sub> , <i>T</i> <sub>max</sub>	0.128, 0.652	0.029, 0.371
No. of measured, independent and observed [ <i>I</i> > 2 $\sigma$ ( <i>I</i> )] reflections	17537, 9354, 7209	33255, 17920, 12304,
<i>R</i> <sub>int</sub>	0.0393	0.0587
(sin $\theta$ /λ) <sub>max</sub> (Å <sup>-1</sup> )	0.625	0.624
Range of <i>h</i> , <i>k</i> , <i>l</i>	<i>h</i> = -15 → 12, <i>k</i> = -16 → 17, <i>l</i> = -19 → 18	<i>h</i> = -13 → 14, <i>k</i> = -18 → 18, <i>l</i> = -23 → 32
Refinement		
<i>R</i> [ <i>F</i> <sup>2</sup> > 2 $\sigma$ ( <i>F</i> <sup>2</sup> )], <i>wR</i> ( <i>F</i> <sup>2</sup> ), <i>S</i>	0.0375, 0.0937, 0.938	0.0592, 0.1678, 0.942
No. of reflections	9354	17920
No. of parameters	545	1071
No. of restraints	0	0
H-atom treatment	H-atom parameters constrained	H-atom parameters constrained
$\Delta$ <sub>max</sub> , $\Delta$ <sub>min</sub> (e Å <sup>-3</sup> )	1.675, -1.267	2.818, -1.751

Computer programs for **4a** and **4b**: CrysAlisPro 1.171.38.41 (Rigaku OD, 2015), SHELXT-2014/7 (Sheldrick, 2014), SHELXL-2014/7 (Sheldrick, 2014)

**82 | V - Three-Component Self-Assembly:**  
**A Way to Overcome Simple Coordination Polymers in Favor**  
**of 3D Connected Spherical Supramolecular Aggregates**

**Table 5:** Experimental details for compounds **5** and **6a**.

Crystal data	<b>5</b>	<b>6a</b>
Chemical formula	C <sub>36</sub> H <sub>54</sub> Ag <sub>2</sub> F <sub>12</sub> Fe <sub>2</sub> N <sub>4</sub> P <sub>10</sub> Sb <sub>2</sub>	C <sub>159.70</sub> H <sub>238.40</sub> Ag <sub>11</sub> Cl <sub>3.40</sub> F <sub>66</sub> Fe <sub>9</sub> N <sub>12</sub> P <sub>45</sub> Sb <sub>11</sub>
<i>M<sub>r</sub></i>	1651.47	8123.06
Crystal system, space group	triclinic, <i>P</i> $\bar{1}$	orthorhombic, <i>Pnna</i>
Temperature (K)	90	90
<i>a</i> , <i>b</i> , <i>c</i> (Å)	8.0920 (5), 13.5264 (8), 14.1133 (9)	34.3655 (3), 31.1270 (3), 24.70440 (19)
$\alpha$ , $\beta$ , $\gamma$ (°)	70.068 (5), 75.001 (5), 79.357 (5)	90, 90, 90
<i>V</i> (Å <sup>3</sup> )	1394.83 (15)	26426.2 (4)
<i>Z</i>	1	4
<i>F</i> (000)	804	15678
<i>D<sub>x</sub></i> (Mg m <sup>-3</sup> )	1.966	2.042
Radiation type	Cu <i>K</i> α	Cu <i>K</i> α
$\mu$ (mm <sup>-1</sup> )	20.451	22.63
Crystal shape	prism	plate
Colour	green-brown	brown
Crystal size (mm)	0.16 × 0.09 × 0.06	0.195 × 0.167 × 0.084
<b>Data collection</b>		
Diffractometer	SuperNova, Titan <sup>S2</sup>	SuperNova, Titan <sup>S2</sup>
Absorption correction	Gaussian	Gaussian
<i>T<sub>min</sub></i> , <i>T<sub>max</sub></i>	0.177, 0.407	0.144, 0.354
No. of measured, independent and observed [ <i>I</i> > 2σ( <i>I</i> )] reflections	10398, 5493, 4633	73587, 26212, 20911
<i>R<sub>int</sub></i>	0.046	0.0415
(sin $\theta/\lambda$ ) <sub>max</sub> (Å <sup>-1</sup> )	0.623	0.623
Range of <i>h</i> , <i>k</i> , <i>l</i>	<i>h</i> = -10 → 8, <i>k</i> = -16 → 16, <i>l</i> = -17 → 17	<i>h</i> = -30 → 42, <i>k</i> = -32 → 38, <i>l</i> = -26 → 30
<b>Refinement</b>		
<i>R</i> [ <i>F</i> <sup>2</sup> > 2σ( <i>F</i> <sup>2</sup> )], <i>wR</i> ( <i>F</i> <sup>2</sup> ), <i>S</i>	0.0410, 0.1065, 0.981	0.0619, 0.1684, 1.017
No. of reflections	5493	26212
No. of parameters	307	1751
No. of restraints	0	34
H-atom treatment	H-atom parameters constrained	H-atom parameters constrained
$\Delta$ <sub>max</sub> , $\Delta$ <sub>min</sub> (e Å <sup>-3</sup> )	1.051, -1.419	0.0619, 0.1684, 1.017

Computer programs for **5**: CrysAlisPro 1.171.38.41 (Rigaku OD, 2015), SHELXT (Sheldrick, 2014), SHELXL-2014/7 (Sheldrick, 2014)

Computer programs for **6a**: CrysAlisPro 1.171.38.42b (Rigaku OD, 2015), SHELXS-2014/7 (Sheldrick, 2014), SHELXL-2014/7 (Sheldrick, 2014)

**Table 6:** Experimental details for compounds **6b** and **6c**.

Crystal data	<b>6b</b>	<b>6c</b>
Chemical formula	C <sub>19</sub> H <sub>29</sub> AgF <sub>6</sub> FeN <sub>2</sub> P <sub>5</sub> Sb	C <sub>28</sub> H <sub>43</sub> Ag <sub>2</sub> FeN <sub>4</sub> P <sub>5</sub> ·2(SbF <sub>6</sub> )·0.25(CH <sub>2</sub> Cl <sub>2</sub> )
<i>M<sub>r</sub></i>	839.76	1354.83
Crystal system, space group	monoclinic, <i>P</i> 2 <sub>1</sub> / <i>n</i>	tetragonal, <i>P</i> 4 <sub>3</sub> 2 <sub>1</sub> 2
Temperature (K)	123	80
<i>a</i> , <i>b</i> , <i>c</i> (Å)	8.2734 (4), 25.6048 (13), 14.3471 (7)	12.61455 (16), 12.61455 (16), 56.871 (4)
<i>β</i> (°)	105.856 (5)	90
<i>V</i> (Å <sup>3</sup> )	2923.6 (3)	9049.7 (6)
<i>Z</i>	4	8
<i>F</i> (000)	1640	5236
<i>D<sub>x</sub></i> (Mg m <sup>-3</sup> )	1.908	1.989
Radiation type	Cu <i>Kα</i>	synchrotron, λ = 0.6199 Å
μ (mm <sup>-1</sup> )	19.57	1.81
Crystal shape	polyhedron	plate
Colour	green	green
Crystal size (mm)	0.38 × 0.18 × 0.10	0.10 × 0.10 × 0.08
<b>Data collection</b>		
Diffractometer	SuperNova, Titan <sup>S2</sup>	Synchrotron, beamline P11, DESY Petra III, DECTRIS PILATUS M6
Absorption correction	Gaussian	Multi-scan
<i>T<sub>min</sub></i> , <i>T<sub>max</sub></i>	0.038, 0.354	0.011, 1.000
No. of measured, independent and observed [ <i>I</i> > 2σ( <i>I</i> )] reflections	9261, 5218, 4752	41206, 9945, 6353
<i>R<sub>int</sub></i>	0.067	0.061
(sin θ/λ) <sub>max</sub> (Å <sup>-1</sup> )	0.599	0.641
Range of <i>h</i> , <i>k</i> , <i>l</i>	<i>h</i> = -8 → 9, <i>k</i> = -22 → 30, <i>l</i> = -15 → 17	<i>h</i> = -15 → 15, <i>k</i> = -16 → 16, <i>l</i> = -58 → 72
<b>Refinement</b>		
<i>R</i> [ <i>F</i> <sup>2</sup> > 2σ( <i>F</i> <sup>2</sup> )], <i>wR</i> ( <i>F</i> <sup>2</sup> ), <i>S</i>	0.079, 0.229, 1.09	0.058, 0.160, 0.94
No. of reflections	5218	9945
No. of parameters	342	510
No. of restraints	0	8
H-atom treatment	H-atom parameters constrained	H-atom parameters constrained
Δ <sub>max</sub> , Δ <sub>min</sub> (e Å <sup>-3</sup> )	1.83, -2.56	0.75, -0.80
Absolute structure parameter	-	-0.04 (3)

Computer programs for **6b**: CrysAlis PRO 1.171.38.41 (Rigaku OD, 2015), SHELXS2014/7 (Sheldrick, 2014), SHELXL2014/7 (Sheldrick, 2014).

Computer programs for **6c**: XDS, (Kabsch, 2010), CrysAlis PRO 1.171.39.37b (Rigaku OD, 2017), SHELXT2014/7 (Sheldrick, 2014), SHELXL2014/7 (Sheldrick, 2014).

## 5.6 Author Contributions

- The synthesis and characterization of all compounds were performed by B. Hiltl, except for compounds **5** and **6a-c**, which were synthesized and characterized by B. Hiltl and K. Grill.
- The synthesis and characterization of compounds **5** and **6a-c** are also part of the Bachelor thesis of K. Grill (University of Regensburg, **2017**)
- The manuscript (introduction, results and discussions, experimental part, conclusion; including figures and graphical abstract) was written by B. Hiltl.
- The section 'crystallographic details' was written by Dr. E. Peresypkina.
- In-house X-ray structure analyses were performed by Dr. E. Peresypkina and Dr. Sc. A. V. Virovets with B. Hiltl. Synchrotron measurements including sample preparation, data reduction and all calculations were performed by Dr. E. Peresypkina and Dr. Sc. A. V. Virovets. The calculation of the topological characteristics of net and packing in **6a** was performed by Dr. Sc. A. V. Virovets.
- MAS NMR investigation of **6a** was performed by Prof. W. Kremer.

## 5.7 References

- <sup>1</sup> a) M. Albrecht, *Naturwissenschaften* **2007**, *94*, 951-966; b) J. M. Lehn, *Angew. Chem.* **1988**, *100*, 91-116.
- <sup>2</sup> a) Y. Chu, A. Saad, P. Yin, J. Wu, O. Oms, A. Dolbecq, P. Mialane, T. Liu, *Chem. Eur. J.* **2016**, *22*, 11756-11762; b) S. H. Chikkali, M. Nieger, D. Gudat, *New J. Chem.* **2010**, *34*, 1348-1354; c) K. Suzuki, M. Kawano, M. Fujita, *Angew. Chem., Int. Ed.* **2007**, *46*, 2819-2822; d) M. Scheer, J. Bai, B. P. Johnson, R. Merkle, A. V. Virovets, C. E. Anson, *Eur. J. Inorg. Chem.* **2005**, 4023-4026; e) V. Patroniak, M. Kubicki, A. Mondry, J. Lisowski, W. Radecka-Paryzek, *Dalton Trans.* **2004**, 3295-3304.
- <sup>3</sup> Q.-F. Sun, J. Iwasa, D. Ogawa, Y. Ishido, S. Sato, T. Ozeki, Y. Sei, K. Yamaguchi, M. Fujita, *Science* **2010**, *328*, 1144-1147.
- <sup>4</sup> J. Bunzen, J. Iwasa, P. Bonakdarzadeh, E. Numata, K. Rissanen, S. Sato, M. Fujita, *Angew. Chem., Int. Ed.* **2012**, *51*, 3161-3163.
- <sup>5</sup> a) A. Lennartson, P. Southon, N. F. Sciortino, C. J. Kepert, C. Frandsen, S. Morup, S. Piligkos, C. J. McKenzie, *Chem. Eur. J.* **2015**, *21*, 16066-16072; b) K. Chainok, W. Saphu, P. Khemthong, D. J. Harding, *Z. Anorg. Allg. Chem.* **2013**, *639*, 2134-2137; c) A. Westcott, N. Whitford, M. J. Hardie, *Inorg. Chem.* **2004**, *43*, 3663-3672; d) L. Carlucci, G. Ciani, D. M. Proserpio, S. Rizzato, *CrystEngComm* **2002**, *4*, 413-425.

- <sup>6</sup> M. Elsayed Moussa, S. Evariste, B. Kraemer, R. Reau, M. Scheer, C. Lescop, *Angew. Chem., Int. Ed.* **2018**, *57*, 795-799.
- <sup>7</sup> a) M. Scheer, A. Schindler, C. Groeger, A. V. Virovets, E. V. Peresypkina, *Angew. Chem., Int. Ed.* **2009**, *48*, 5046-5049; b) J. Bai, A. V. Virovets, M. Scheer, *Science* **2003**, *300*, 781-783..
- <sup>8</sup> a) C. Heindl, E. Peresypkina, A. V. Virovets, I. S. Bushmarinov, M. G. Medvedev, B. Kraemer, B. Dittrich, M. Scheer, *Angew. Chem., Int. Ed.* **2017**, *56*, 13237-13243; b) E. Peresypkina, C. Heindl, E. Madl, H. Brake, A. Virovets, M. Scheer, *Chemistry* **2017**; c) C. Heindl, E. V. Peresypkina, A. V. Virovets, W. Kremer, M. Scheer, *J. Am. Chem. Soc.* **2015**, *137*, 10938-10941; d) C. Schwarzmaier, A. Schindler, C. Heindl, S. Scheuermayer, E. V. Peresypkina, A. V. Virovets, M. Neumeier, R. Gschwind, M. Scheer, *Angew. Chem., Int. Ed.* **2013**, *52*, 10896-10899.
- <sup>9</sup> S. Heindl, E. Peresypkina, J. Sutter, M. Scheer, *Angew. Chem., Int. Ed.* **2015**, *54*, 13431-13435.
- <sup>10</sup> a) M. Elsayed Moussa, B. Attenberger, M. Seidl, A. Schreiner, M. Scheer, *Eur. J. Inorg. Chem.* **2017**, *2017*, 5616-5620; b) M. Elsayed Moussa, B. Attenberger, E. V. Peresypkina, M. Fleischmann, G. Balazs, M. Scheer, *Chem. Commun.* **2016**, *52*, 10004-10007; c) B. Attenberger, E. V. Peresypkina, M. Scheer, *Inorg. Chem.* **2015**, *54*, 7021-7029; d) B. Attenberger, S. Welsch, M. Zabel, E. Peresypkina, M. Scheer, *Angew. Chem., Int. Ed.* **2011**, *50*, 11516-11519.
- <sup>11</sup> M. Scheer, L. J. Gregoriades, A. V. Virovets, W. Kunz, R. Neueder, I. Krossing, *Angew. Chem., Int. Ed.* **2006**, *45*, 5689-5693.
- <sup>12</sup> Diameter were calculated considering the maximum distance between two F atoms plus twice the van der Waals radius of F (147 ppm, from A. Bondi, *J. Phys. Chem.* **1964**, *68*, 441-451.)
- <sup>13</sup> a) M. Fleischmann, S. Welsch, E. V. Peresypkina, A. V. Virovets, M. Scheer, *Chem. Eur. J.* **2015**, *21*, 14332-14336; b) C. Heindl, S. Heindl, D. Luedeker, G. Brunklaus, W. Kremer, M. Scheer, *Inorg. Chim. Acta* **2014**, *422*, 218-223; c) J. Bai, A. V. Virovets, M. Scheer, *Angew. Chem., Int. Ed.* **2002**, *41*, 1737-1740.
- <sup>14</sup> M. Scheer, A. Schindler, C. Groeger, A. V. Virovets, E. V. Peresypkina, *Angew. Chem., Int. Ed.* **2009**, *48*, 5046-5049.
- <sup>15</sup> L. Carlucci, G. Ciani, D. M. Proserpio, S. Rizzato, *CrystEngComm* **2002**, *4*, 413-425.
- <sup>16</sup> M. Scheer, L. J. Gregoriades, A. V. Virovets, W. Kunz, R. Neueder, I. Krossing, *Angew. Chem., Int. Ed.* **2006**, *45*, 5689-5693.
- <sup>17</sup> The interplanar distance  $d(P_5^{plane}...P_5^{plane})$  was calculated as an atom-to-plane distance from the centroid of one *cyclo*-P<sub>5</sub> ligand to the plane of the other *cyclo*-P<sub>5</sub> ligand, as the P<sub>5</sub> planes are not parallel.
- <sup>18</sup> M. E. Moussa, S. Welsch, M. Lochner, E. V. Peresypkina, A. V. Virovets, M. Scheer, *Eur. J. Inorg. Chem.* **2018**, *2018*, 2689-2694.
- <sup>19</sup> O. J. Scherer, T. Brueck, *Angew. Chem.* **1987**, *99*, 59.

- 20 Osakada *et al.*, *J. Inorg. Organomet. Polym. Mater.* **2009**, *19*, 35.
- 21 The outer diameter was calculated as the maximum distance of two H atoms situated at opposing Cp\* residues plus twice the van der Waals radius of H (110 pm, from R. S. Rowland, R. Taylor, *J. Phys. Chem.* **1996**, *100*, 7384-7391).
- 22 a) V. A. Blatov, A. P. Shevchenko, D. M. Proserpio, *Cryst. Growth Des.* **2014**, *14*, 3576–3586; b) V. A. Blatov, M. O’Keeffe, D. M. Proserpio, *CrystEngComm* **2010**, *12*, 44-48; c) <http://rcsr.net/>
- 23 M. O’Keeffe, M. A. Peskov, S. J. Ramsden, O. M. Yaghi *Accts. Chem. Res.* **2008**, *41*, 1782-1789.
- 24 M. Detzel, G. Friedrich, O. J. Scherer and G. Wolmershäuser, *Angew. Chem. Int. Ed.* **1995**, *34*, 1321.
- 25 A. Burkhardt, T. Pakendorf, B. Reime, *et al*, *Eur. Phys. J. Plus* **2016**, *131*, 56-64.
- 26 Kabsch, W. XDS. *Acta Cryst.* **2010**, D66, 125-132.
- 27 CrysAlis Pro, different versions (Rigaku OD).
- 28 G. M. Sheldrick, *Acta Cryst. sect. C* **2015**, C71, 3.

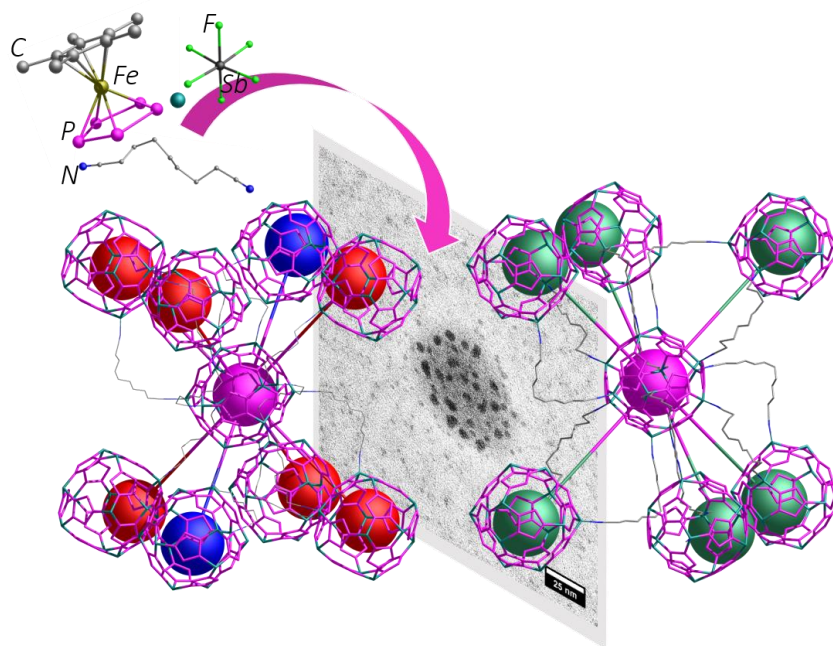




## 6. Benefitting from Flexibility: A Versatile Approach to Linked and Close-Packed Spherical Host-Guest Assemblies

B. Hiltl, E. Peresyphkina, A. V. Virovets, W. Kremer, J. Hilgert, W. Tremel, M. Scheer

### Graphical Abstract



### Abstract:

By exploring the self-assembly processes of the system of  $[\text{Cp}^R\text{Fe}(\eta^5\text{-P}_5)]$  ( $\text{Cp}^R = \text{Cp}^*$  (**1a**),  $\text{Cp}^{\text{Bn}}$  (**1b**)) and  $\text{AgSbF}_6$ , the potential of fully flexible linkers to supramolecular chemistry is reported. Dinitriles  $\text{NC}(\text{CH}_2)_x\text{CN}$  with  $x = 8 - 10$  were implemented in combination with coinage metal salts of weakly coordinating anions of different sizes ( $[\text{Cu}(\text{CH}_3\text{CN})_4]\text{BF}_4$ ,  $\text{AgSbF}_6$ ,  $\text{Ag}[\text{Al}\{\text{OC}(\text{CF}_3)_3\}_4]$ ) and the polyphosphorus complexes **1a-b**. Thus, offering free coordination sites on the metal atoms for the dinitrile linkers, in one-pot synthetic procedures 1D (**3**), 2D (**2**, **9**) and 3D (**4**, **5**) three-component coordination polymers were obtained. Moreover, three fully self-assembled compounds of linked spherical host molecules constituting a 3D polymer  $[[\text{Cp}^*\text{Fe}(\eta^5\text{-P}_5)]@[\{\text{Cp}^*\text{Fe}(\eta^{5:1:1:1}\text{-P}_5)\}_{12}\{\text{Ag}_{12}(\text{NC}(\text{CH}_2)_x\text{CN})_6\}]]_n[\text{SbF}_6]_{12n}$  (**6**, **7**, **8**) are formed. The nodes consist of fullerene-type nano-sized spherical host supramolecules. Owing to the flexibility of the linker molecules, the spheres are packed in distorted cubic close packings, showing slight differences in the connectivity of **6** – **8**. All herein presented compounds were fully characterized by X-ray structure analysis, NMR and MS spectroscopy. Furthermore, as the first polymeric self-assembly product based on **1a**, the size of the individual spheres in **6** was also characterized by transmission electron microscopy.

## 6.1 Introduction

Supramolecular host cages, reaction vessels and capsules have been investigated in detail over the past years by many groups concerning their dynamic behavior, host-guest interactions and guest uptake selectivity.<sup>1</sup> These discrete compounds are facing a large variety of polymeric MOF materials which are able to act as crystalline sponges to absorb mainly small molecules<sup>2</sup> or to be applied as gas storage<sup>3</sup> or sensing materials.<sup>4</sup> In contrast to this, interconnected spherical host-guest compounds constituting polymers remain rare. In 2010 *Fujita et al.* succeeded in the transfer of discrete molecular cages  $M_6L_4$  from solution into a polymeric framework in solid state, hereby maintaining the ability of guest uptake.<sup>5</sup> This self-assembled crystalline sponge features voids of different dimensions. By soaking these crystals with a  $C_{60}$  or  $C_{70}$  solution, the fullerenes are incorporated by the single crystals of the MOF, which retain their crystallinity.<sup>6</sup> Though the individual building blocks resemble the cage compounds in solution, a linking unit is missing as the octahedra are vertex-sharing (*Figure 1a*). In contrast to this, the approach of “large clusters and small bridges” was successfully applied by the group of *Tung et al.* obtaining 2D- and 3D-connected  $Ag_{20}$  and  $Ag_{22}$  cluster cores, interconnected by  $NO_3^-$  anions.<sup>7</sup> These building blocks even act as hosts for  $CO_3^{2-}$  and  $SO_4^{2-}$  anions (*Figure 1b*).

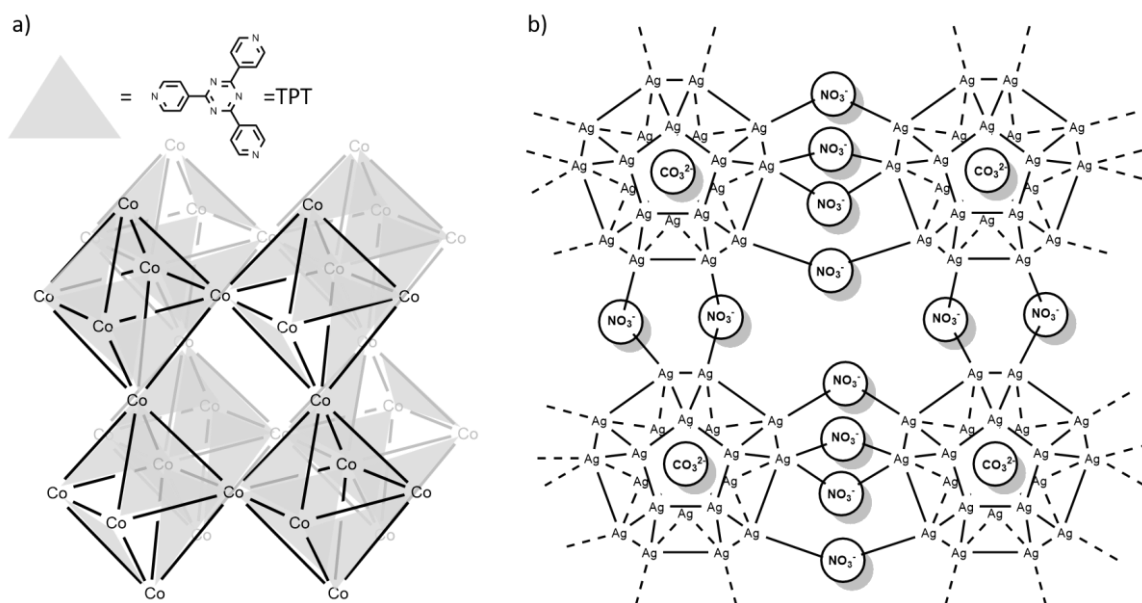


**Figure 1:** Networked a) cages  $[[Co(SCN)_2\{TPT\}_4] \cdot x(guest)_n$ ,<sup>5</sup> b)  $Ag_{20}$  cluster cores.<sup>7</sup>

Recently, our group has successfully examined the host-guest properties of spherical aggregates based on the *cyclo*- $P_5$  ligands  $[Cp^RFe(\eta^5-P_5)]$  ( $Cp^R = Cp^*$  (**1a**),  $Cp^{Bn}$  (**1b**)) and Cu halides in solid state as well as in solution.<sup>8</sup> Considering this expertise, we recently transferred our approach from

constructing discrete host cages to interconnected spherical compounds. As in the case of Cu halides or triflates (cf. *Chapter III*) the scaffold building metal atoms are saturated by the counter anions and therefore not available anymore for potential linkage, we applied the weakly coordinating anion  $\text{SbF}_6^-$  instead. The first successful examinations of the self-assembly of **1a**,  $\text{AgSbF}_6$  and fully flexible dinitriles  $\text{NC}(\text{CH}_2)_x\text{CN}$  ( $x = 5 - 7$ ) were undertaken yielding in a unprecedented 3D polymer of connected nano-sized host supramolecules (cf. *Figure 2* and *Chapter V*). The polycationic nodes consist of novel scaffolds of **1a** and Ag atoms, incorporating one  $\text{SbF}_6^-$  anion as a guest.

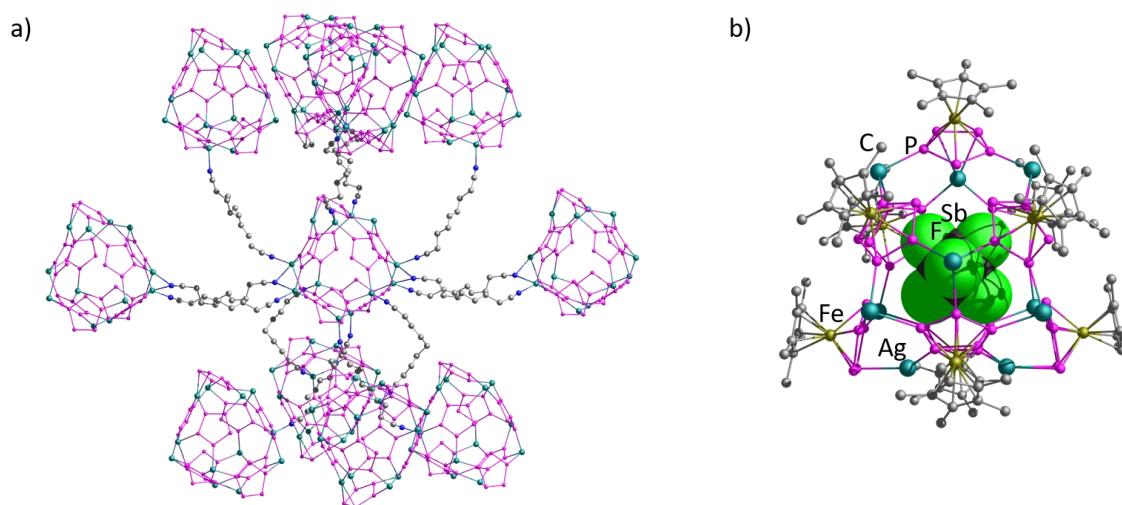


**Figure 2:** a) Section of 3D network  $[[\text{SbF}_6]@[\{\text{Cp}^*\text{Fe}(\eta^5\text{-P}_5)\}_9\{\text{Ag}_{11}(\text{NC}(\text{CH}_2)_7\text{CN})_6\}]]_n[\text{SbF}_6]_{10n}$ , b) host-guest aggregate as node (cf. *Chapter V*).

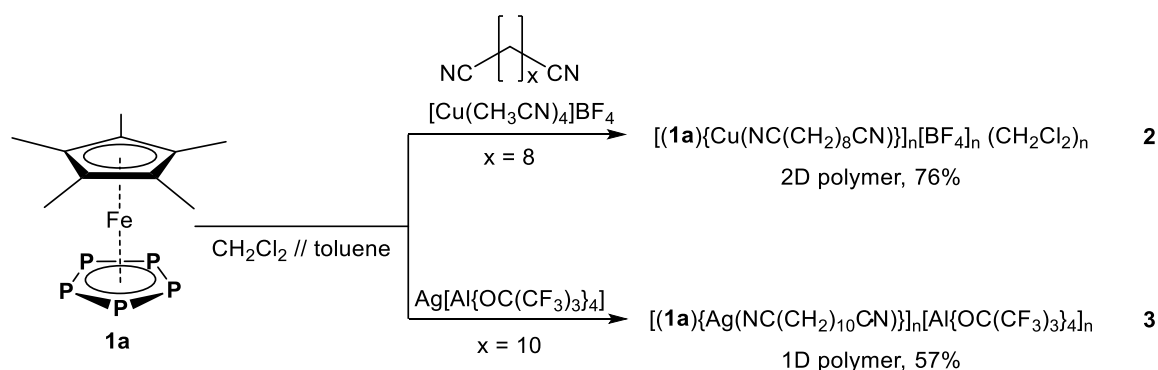
But how is this system reacting on the implementation of even longer dinitrile linking units or the change in the starting materials **1** and the coinage metal salts? This encouraged us to search for a deeper insight in this new field of supramolecular chemistry and to investigate these influences. Thus, we employed the longer dinitriles  $\text{NC}(\text{CH}_2)_x\text{CN}$  with  $x = 8 - 10$  in combination with the other coinage metal salts as  $[\text{Cu}(\text{CH}_3\text{CN})_4]\text{BF}_4$  and  $\text{Ag}[\text{Al}\{\text{OC}(\text{CF}_3)_3\}_4]$ , which would allow free coordination sites on the metal atom as well. Furthermore we applied both the  $[\text{Cp}^*\text{Fe}(\eta^5\text{-P}_5)]$  **1a** and the bulkier  $\text{Cp}^{\text{Bn}}$  derivative **1b** in one-pot self-assembly reactions with  $\text{AgSbF}_6$  and the dinitriles.

## 6.2 Results and Discussion

To obtain the compounds discussed herein, one general reaction procedure was applied, varied only marginally. A solution of the coinage metal salt in  $\text{CH}_2\text{Cl}_2$  was first layered with a mixture of  $\text{CH}_2\text{Cl}_2$  and toluene (2:1) and then with a layer of **1** together with the 10-fold excess of dinitrile  $\text{NC}(\text{CH}_2)_x\text{CN}$  in toluene. All structural discussion of the coordination products is based on the characterization by X-ray structure analysis.

### Self-Assembly of $\text{Cp}^*\text{Fe}(\eta^5\text{-P}_5)$ with $[\text{Cu}(\text{CH}_3\text{CN})_4]\text{BF}_4$ or $\text{Ag}[\text{Al}\{\text{OC}(\text{CF}_3)_3\}_4]$ and flexible dinitriles

Based on the previous self-assembly results of **1a**,  $\text{AgSbF}_6$  and the aliphatic dinitriles  $\text{NC}(\text{CH}_2)_x\text{CN}$  ( $x = 5 - 7$ , cf. Chapter V), we wanted to vary the size of the weakly coordinating anion as well as increase the length of the aliphatic backbone in the organic linking unit. Thus, a possible dependency of the obtained coordination products on the size of the counter-anion can be clarified. Decreasing the size from  $\text{SbF}_6^-$  to  $\text{BF}_4^-$  ( $\varnothing(\text{SbF}_6^-) = 6.69 \text{ \AA}$ ,  $\varnothing(\text{BF}_4^-) = 5.29 \text{ \AA}$ )<sup>9</sup> and changing the metal atom from Ag to Cu, leads with  $\text{NC}(\text{CH}_2)_8\text{CN}$  to the 2D polymer  $[(\text{Cp}^*\text{Fe}(\eta^5\text{-P}_5))\{\text{Cu}(\text{NC}(\text{CH}_2)_8\text{CN})\}]_n[\text{BF}_4]_n \cdot (\text{CH}_2\text{Cl}_2)_n$  (**2**) (Scheme 1). Contrarily, increasing the size of the counter-anion to  $[\text{Al}\{\text{OC}(\text{CF}_3)_3\}_4]^-$  ( $\varnothing([\text{Al}\{\text{OC}(\text{CF}_3)_3\}_4]^-) = 12.46 \text{ \AA}$ )<sup>9</sup> a chain length of the linker of  $x = 10$  is required for the formation of the 1D polymer  $[(\text{Cp}^*\text{Fe}(\eta^5\text{-P}_5))\{\text{Ag}(\text{NC}(\text{CH}_2)_{10}\text{CN})\}]_n[\text{Al}\{\text{OC}(\text{CF}_3)_3\}_4]_n$  (**3**). For comparison, the self-assembly reactions of **1a**,  $[\text{Ag}(\text{CH}_3\text{CN})_4]\text{BF}_4$  and the dinitrile with  $x = 8, 10$  and **1a** with  $\text{Ag}[\text{Al}\{\text{OC}(\text{CF}_3)_3\}_4]$  and  $x = 8$  did not furnish any crystalline products. Both compounds **2** and **3** could be isolated in good crystalline yields.



**Scheme 1:** One-pot self-assembly reactions of **1a** with  $[\text{Cu}(\text{CH}_3\text{CN})_4]\text{BF}_4$  and  $\text{Ag}[\text{Al}\{\text{OC}(\text{CF}_3)_3\}_4]$  and different flexible dinitrile linkers  $\text{NC}(\text{CH}_2)_x\text{CN}$ .

Compound **2** reveals a 2D polymeric structure (Figure 3a), which is similar to the Ag-containing networks  $[(\text{Cp}^*\text{Fe}(\eta^5\text{-P}_5))\{\text{Ag}(\text{NC}(\text{CH}_2)_x\text{CN})\}]_n[\text{SbF}_6]_n$  (cf. Chapter V,  $x = 6, 7$ ). The nodes consist of dimers of  $[(\text{Cp}^*\text{Fe}(\eta^5\text{-P}_5))_2\text{Cu}_2]^{2+}$  with two ligands **1a** coordinating in a 1,2 mode towards two Cu atoms, which are in turn tetrahedrally coordinated by two ligands **1a** and two dinitrile linkers. This

structural motif can also be found in the discrete dimeric  $[\{\text{Cp}^*\text{Fe}(\eta^{5:1:1}\text{-P}_5)\}\{\text{Ag}(\text{CH}_3\text{CN})_2\}]_2[\text{SbF}_6]_2$  with  $\text{CH}_3\text{CN}$  coordinating towards the coinage metal atom instead of a dinitrile linker (cf. *Chapter V*). As each linker connects a dimeric node to a neighboring one, the 2D polymeric structure of **2** is formed. In the crystal a  $\pi$ - $\pi$  stacking of the 2D layers can be observed, exhibiting short interplanar distances of 3.62 Å of two almost parallel *cyclo*- $\text{P}_5$  ligands ( $2.53^\circ$ ) (*Figure 3c*). Similar stacking behavior of *cyclo*- $\text{P}_5$  ligands is observed in the Ag-containing 2D polymers containing the dinitriles  $x = 6, 7$  mentioned above, as well as in  $[\{\text{Cp}^*\text{Fe}(\eta^5\text{-P}_5)\}_4\{\text{Ag}_4(\text{NC}(\text{CH}_2)_5\text{CN})_2\}]_n[\text{SbF}_6]_{4n}$  (cf. *Chapter V*). Thus, the rectangles in **2** formed between the nodes and the linkers are occupied by the dimeric nodes of the next layers and the small  $\text{BF}_4^-$  anions. By partial fragmentation with pyridine, in the  $^{31}\text{P}\{^1\text{H}\}$  NMR spectrum a signal at 143.5 ppm for **1a** was detected, shifted slightly to higher fields compared to the free ligand **1a**. The largest three-component fragment found in the positive-ion ESI MS spectrum was detected at  $m/z = 573.0$  and can be assigned to  $[\{\text{Cp}^*\text{Fe}(\eta^5\text{-P}_5)\}\text{Cu}(\text{CN}(\text{CH}_2)_8\text{CN})]^+$ .

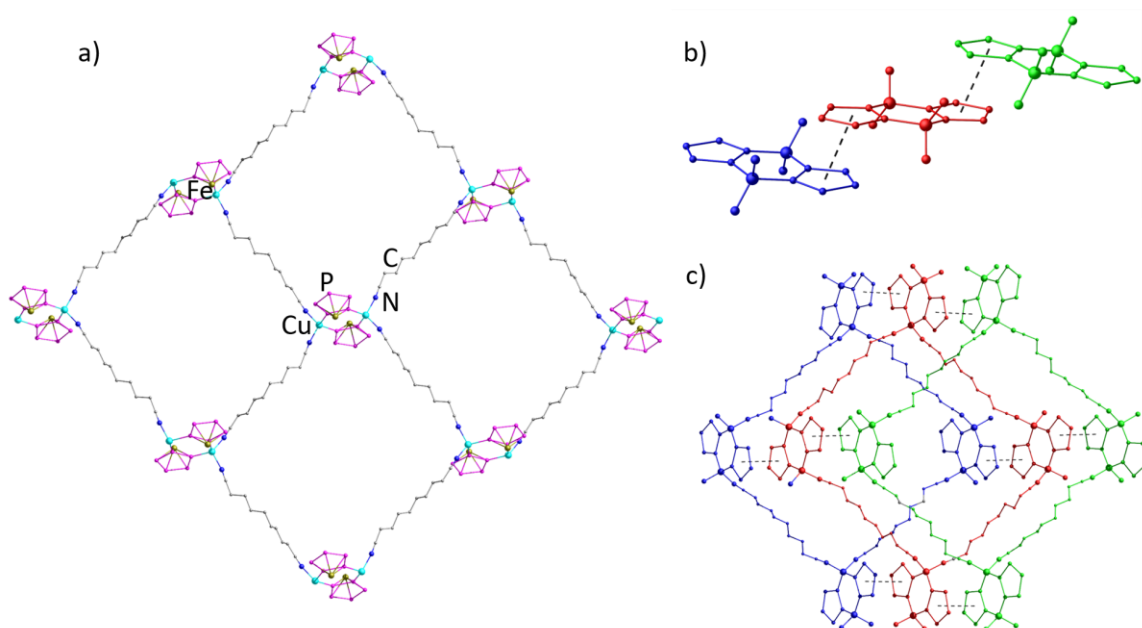


**Figure 3:** a) Section of the cationic 2D polymer **2**, b) - c) slipped  $\text{P}_5\cdots\text{P}_5$   $\pi$ -interactions between the dimeric nodes of the layers (black dashed lines). H atoms and  $[\text{Cp}^*\text{Fe}]$  units are omitted for clarity.

In contrast to that, compound **3** reveals a 1D polymeric structure containing  $[\text{Al}\{\text{OC}(\text{CF}_3)_3\}_4]^-$  (*Figure 4*). The huge size of the anions most likely prevent short contacts between the cationic polymeric parts and also decrease the dimensionality compared to **2**. However, the nodes of **3** consist of dimeric units  $[\{\text{Cp}^*\text{Fe}(\eta^5\text{-P}_5)\}_2\text{Ag}_2]^{2+}$ , similarly to the Cu-containing **2** and the examples of *Chapter V* mentioned above (*Figure 4c*). The anions isolate the 1D polymeric strands from one another, and therefore no  $\pi$ - $\pi$  stacking interactions occur, as in **2** (*Figure 4d,e*). The 1D polymeric structure of the cationic part results from a pairwise linkage of two nodes by two dinitriles. Compound **3** is

insoluble in solvents as  $\text{CH}_2\text{Cl}_2$  or toluene, but readily dissolves in  $\text{CH}_3\text{CN}$  giving a deep red solution, accompanied by partial fragmentation of the polymeric structure. Thus, in the  $^1\text{H}$  NMR spectrum in  $\text{CD}_3\text{CN}$  the expectable signals for the free dinitrile and **1a** can be observed with an integral ratio of 1 : 1 (dinitrile : **1a**). In the  $^{31}\text{P}\{^1\text{H}\}$  NMR spectrum a sharp signal at 137.42 ppm can be observed. Due to the shift to free **1a** at 153 ppm<sup>10</sup> it can be assigned to a ligand **1a** still coordinating to a certain extent to Ag atoms as an effect to incomplete coordination of  $\text{CH}_3\text{CN}$  to Ag atoms. The largest fragment detected in the positive-ion ESI MS spectrum at  $m/z = 798.75$  can be assigned to  $[\{\text{Cp}^*\text{Fe}(\eta^5\text{-P}_5)\}_2\text{Ag}]^+$ .

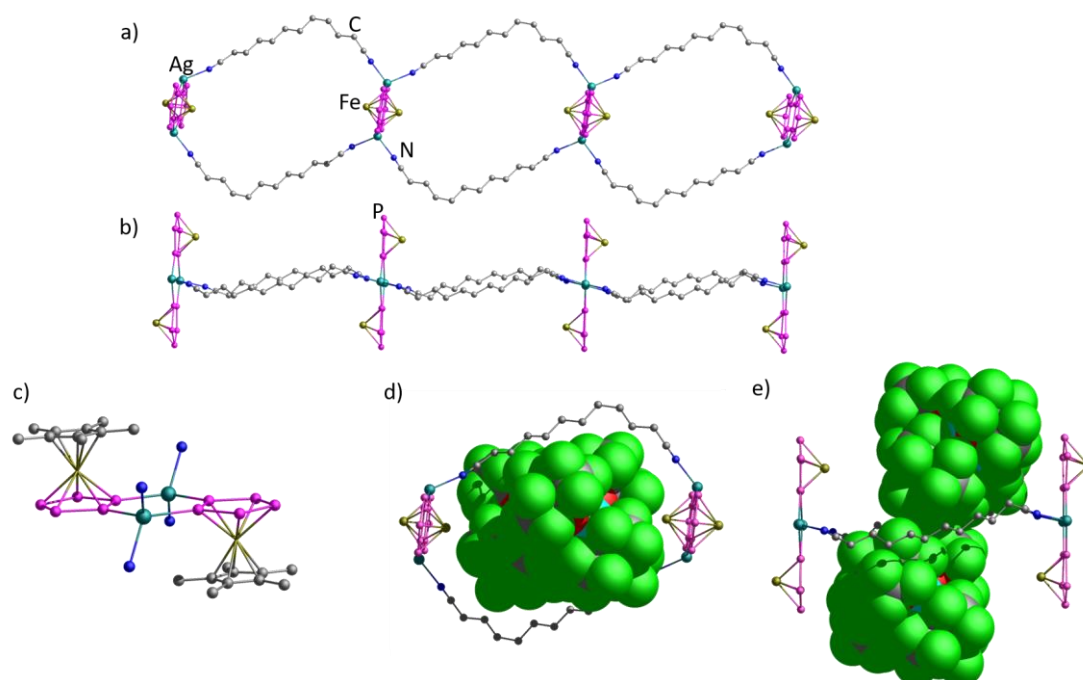
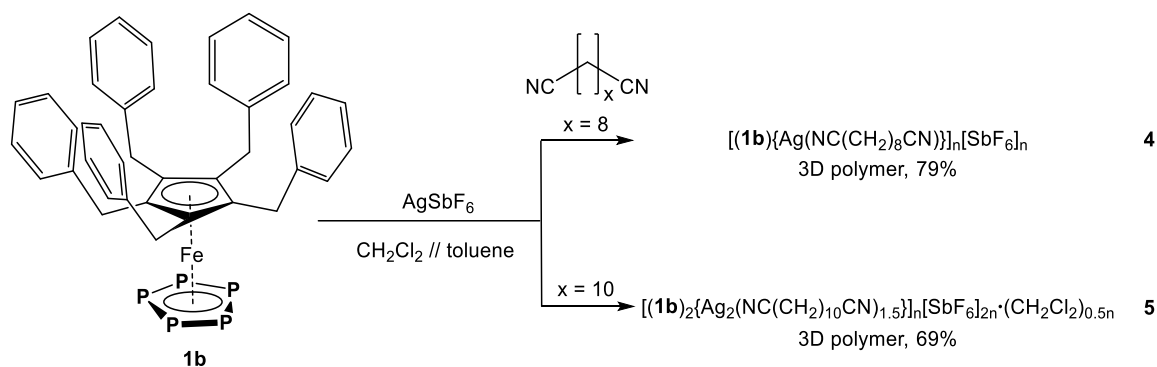


**Figure 4:** Section of the cationic 1D polymer **3** in a) top view and b) side view with c) dimeric nodes. d) and e) arrangement of the anions in the voids, highlighted by space-filling model. H atoms,  $[\text{Al}\{\text{OC}(\text{CF}_3)_3\}_4]^-$  anions, and Cp\* residues are omitted for clarity.

#### Self-Assembly of $\text{Cp}^{\text{Bn}}\text{Fe}(\eta^5\text{-P}_5)$ and $\text{AgSbF}_6$ with flexible dinitriles

Compared to **1a**, the bulkier **1b** offers interesting features to the self-assembly with coinage metal salts to give nano-sized spherical scaffolds. Due to the large organic residue it leads to an improved solubility of the coordination products. Combined with  $\text{AgSbF}_6$  and a coordinating benzonitrile, we recently observed **1b** to self-assemble into spherical scaffolds, which exhibit a novel anti-prismatic shape and act as hosts for one  $\text{SbF}_6^-$  anion, respectively (cf. *Chapter IV*). On the level of the Cp ligand, the steric properties of the complex are barely influenced by the Bn residues ( $\varnothing^{\text{Cp}}(\mathbf{1a}) = 8.20 \text{ \AA}$ ,  $\varnothing^{\text{Cp}}(\mathbf{1b}) = 8.34 \text{ \AA}$ ), although the height of **1b** is with  $10.59 \text{ \AA}$  nearly 1.5 times as

large as **1a** (7.11 Å).<sup>11</sup> To connect two nodes containing **1b** would not afford a linker of twice the length as the ligand itself, as the linker coordinates towards a metal atom next to the ligand. This could lead to the steric bulk of **1b** aligning side by side. Thus, we employed this P<sub>n</sub> complex in the self-assembly system of AgSbF<sub>6</sub> and flexible ditopic nitriles NC(CH<sub>2</sub>)<sub>x</sub>CN (x = 8 - 10) as well (Scheme 2). For all syntheses involving **1b**, the concentration was set to 10 mmol/L in the respective layers. This was found to facilitate crystallization, as the bulky Bn substituents in **1b** enhance solubility of the resulting coordination products and hence hinder crystallization in diluted solutions. Whereas together with AgSbF<sub>6</sub> and NC(CH<sub>2</sub>)<sub>9</sub>CN the self-assembly with **1b** does not lead to a characterizable product, by applying x = 8 and 10 two 3D polymeric compounds [(Cp<sup>Bn</sup>Fe(η<sup>5</sup>-P<sub>5</sub>))Ag(NC(CH<sub>2</sub>)<sub>8</sub>CN)]<sub>n</sub>[SbF<sub>6</sub>]<sub>n</sub> (**4**) and [(Cp<sup>Bn</sup>Fe(η<sup>5</sup>-P<sub>5</sub>))<sub>2</sub>{Ag<sub>2</sub>(NC(CH<sub>2</sub>)<sub>10</sub>CN)<sub>1.5</sub>}]<sub>n</sub>[SbF<sub>6</sub>]<sub>2n</sub>·(CH<sub>2</sub>Cl<sub>2</sub>)<sub>0.5n</sub> (**5**) were isolated in good crystalline yields.



**Scheme 2:** One-pot self-assembly reactions of **1b** with AgSbF<sub>6</sub> and different flexible dinitriles NC(CH<sub>2</sub>)<sub>x</sub>CN.

Compounds **4** and **5** show two structurally related 3D polymeric frameworks (Figure 5a,b). Both can be described as interconnected 1D strands of [(Cp<sup>Bn</sup>Fe(η<sup>5</sup>-P<sub>5</sub>))Ag]<sup>+</sup> (Figure 5c-f). In **4**, all *cyclo*-P<sub>5</sub> ligands coordinate in a η<sup>2:1</sup>-mode to Ag atoms (Figure 5c,e). Contrarily, in **5** the *cyclo*-P<sub>5</sub> ligands coordinate alternately in a η<sup>2:1</sup>-mode and a 1,3-fashion towards Ag atoms (Figure 5d,f). Therefore, while all Ag atoms in **4** show a pseudo-tetrahedral coordination environment of 2 × P (**1b**) and 2 × N (dinitrile), in **5** they exhibit also alternately a pseudo-trigonal (2 × P (**1b**) and 1 × N (dinitrile)) environment. Each strand is connected via the flexible linkers to four other strands and thus, a 3D network is formed. The large organic residue Cp<sup>Bn</sup> of **1b** results in a good solubility of both compounds in CH<sub>2</sub>Cl<sub>2</sub>, assumedly accompanied by partial fragmentation. The signals in the <sup>31</sup>P{<sup>1</sup>H} NMR spectra in CD<sub>2</sub>Cl<sub>2</sub> are slightly shifted upfield (145 ppm (**4**), 149 ppm (**5**)) compared to the spectra of **4** and **5** fragmented with pyridine (152 ppm (**4**), 155 ppm (**5**)) and to the signal of free **1b** (162.2 ppm in C<sub>6</sub>D<sub>6</sub>).<sup>12</sup> This indicates that the fragmentation in CH<sub>2</sub>Cl<sub>2</sub> is not as complete, as it is by addition of pyridine as a good ligand for the coordination to the Ag atoms. In the positive-ion ESI



MS spectra three-component fragments were found, whereas the largest could be attributed to  $m/z = 1340.8$   $[\{\text{Cp}^{\text{Bn}}\text{Fe}(\eta^5\text{-P}_5)\}\text{Ag}_2\text{SbF}_6(\text{NC}(\text{CH}_2)_8\text{CN})]^+$  (for **4**) and  $m/z = 1027.5$   $[\{\text{Cp}^{\text{Bn}}\text{Fe}(\eta^5\text{-P}_5)\}\text{Ag}(\text{NC}(\text{CH}_2)_{10}\text{CN})]^+$  (for **5**).

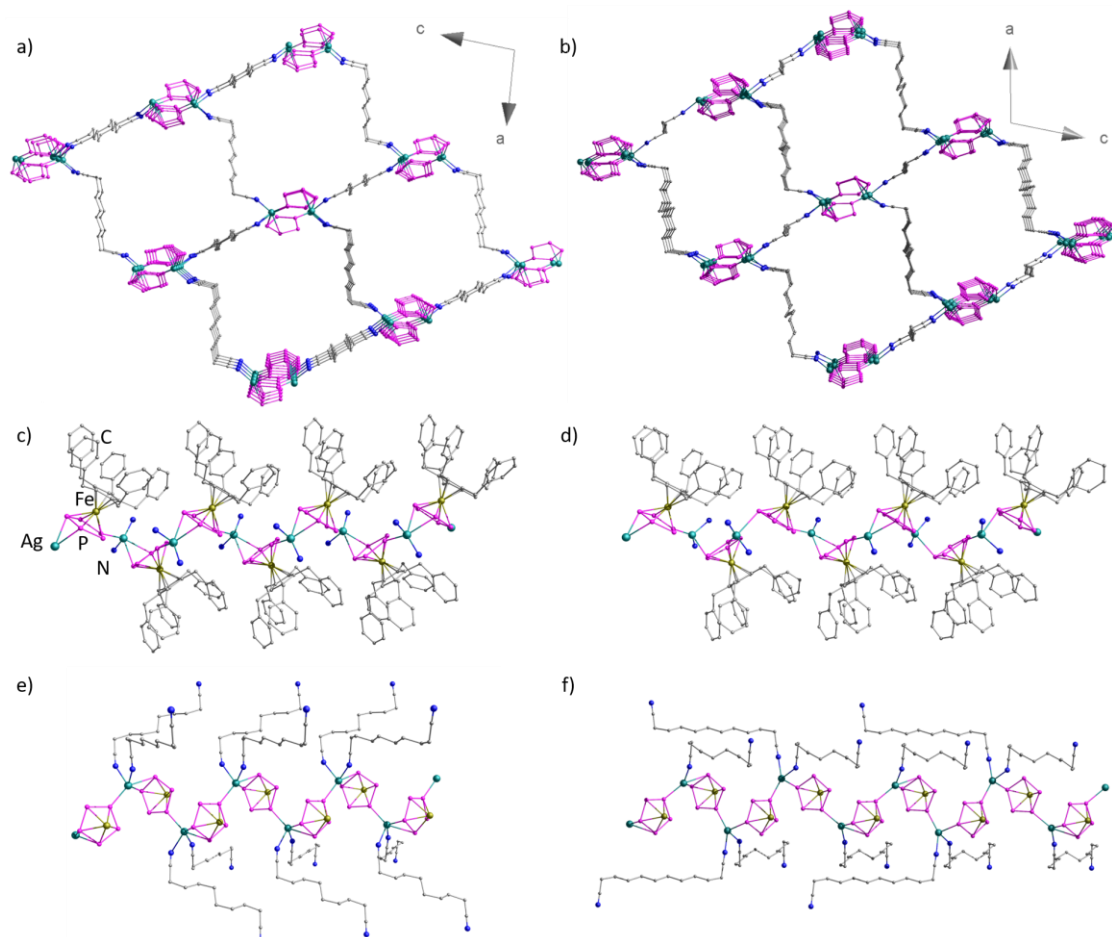
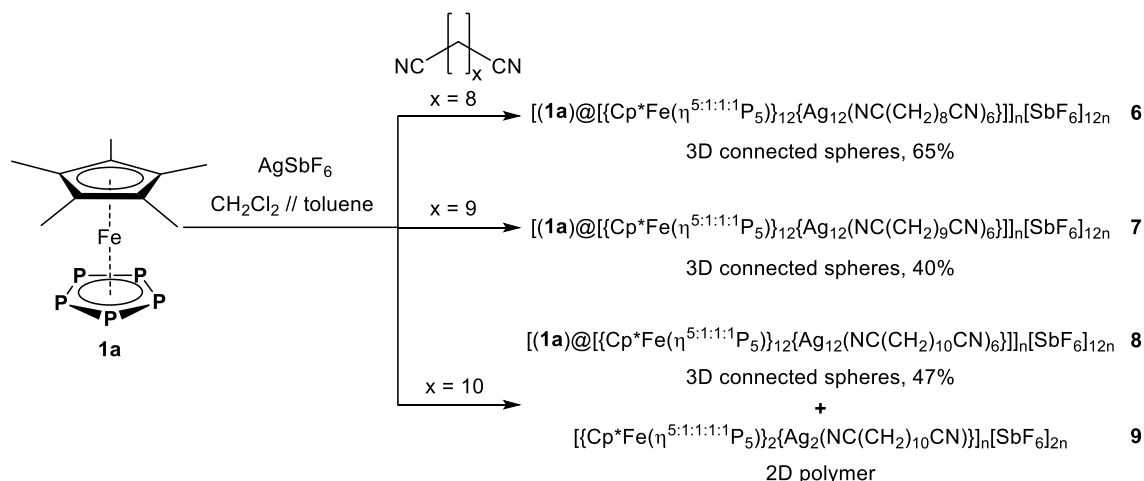


**Figure 5:** Section of the cationic 3D polymers a) **4** and b) **5**. Side view of the 1D strand in c) **4** and d) **5**. Top views of the 1D strands in e) **4** and f) **5** with linkers.  $[\text{Cp}^{\text{Bn}}\text{Fe}]$  units, H atoms, and minor parts of disordered linkers are partly omitted for clarity.

### Self-Assembly of $\text{Cp}^*\text{Fe}(\eta^5\text{-P}_5)$ and $\text{AgSbF}_6$ with flexible dinitriles

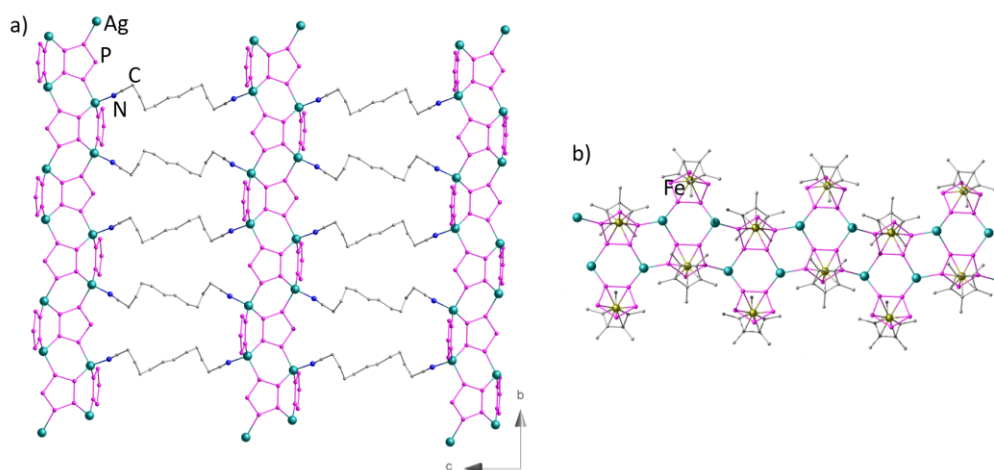
Having in mind the self-assembly of **1a**,  $\text{AgSbF}_6$  and  $\text{NC}(\text{CH}_2)_7\text{CN}$  furnishing with the formation of a 3D network of connected host scaffolds (cf. *Chapter V*) extraordinary results, the extension of the already examined lengths of the potential linker from  $\text{NC}(\text{CH}_2)_x\text{CN}$  with  $x = 5 - 7$  to  $x = 8 - 10$  promised further astonishing outcomes. Applying these combinations to the aforementioned one-pot synthetic procedure, spherical aggregates, which are interconnected to give a 3D polymeric framework of  $[\{\text{Cp}^*\text{Fe}(\eta^5\text{-P}_5)\}][\{\text{Cp}^*\text{Fe}(\eta^{5:1:1:1}\text{-P}_5)\}_{12}\{\text{Ag}_{12}(\text{NC}(\text{CH}_2)_x\text{CN})_6\}]_n[\text{SbF}_6]_{12n}$  (with  $x = 8$  (**6**), 9 (**7**), 10 (**8**)) were obtained (*Scheme 3*). A selective formation of **6** and **7** was observed, by strictly controlling the reaction conditions to an application of a concentration of 2 mmol/L in the

respective layers and an equimolar ratio of Ag : **1a**. Increasing the concentration of the building blocks or decreasing the excess of dinitrile results in the formation of the 1D polymer  $[(\text{Cp}^*\text{Fe}(\eta^{5:2:1}\text{-P}_5))_2\text{Ag}]_n[\text{SbF}_6]_n$  as a byproduct (cf. *Chapter V*). In the case of **8** the formation of the 1D polymer could not be impeded completely, along with the formation of few crystals of  $[(\text{Cp}^*\text{Fe}(\eta^5\text{-P}_5))_2\{\text{Ag}_2(\text{NC}(\text{CH}_2)_{10}\text{CN})\}]_n[\text{SbF}_6]_{2n}$  (**9**) as a second byproduct. The 3D polymers of connected spherical aggregates **6** - **8** were obtained in reasonable crystalline yields.



**Scheme 3:** Reactions of **1a** with  $\text{AgSbF}_6$  and  $\text{NC}(\text{CH}_2)_x\text{CN}$  ( $x = 8 - 10$ ).

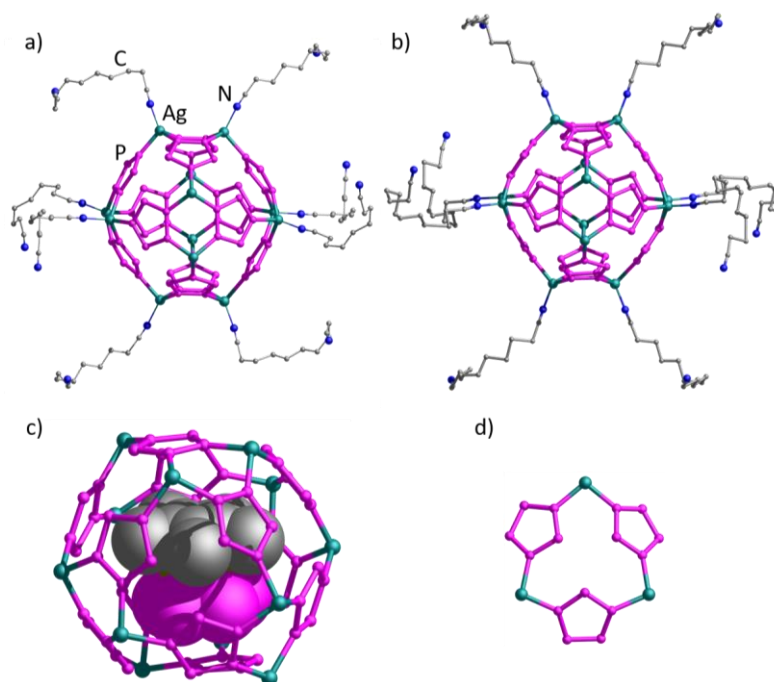
The second byproduct of the self-assembly of **1a**,  $\text{AgSbF}_6$  and the dinitrile with  $x = 10$ , compound **9** shows a 2D polymeric framework of interconnected 1D strands  $[(\text{Cp}^*\text{Fe}(\eta^5\text{-P}_5))_2\text{Ag}_2]_n^{2n+}$  (*Figure 6*). The *cyclo*- $\text{P}_5$  ligands coordinate either in a 1,2 or a 1,2,3,4 mode towards Ag atoms, which in turn are tetrahedrally coordinated by three ligands **1a** and one dinitrile linker.



**Figure 6:** a) Section of the cationic 2D polymeric structure of **9**, b) 1D strand as a substructure of **9**. H atoms and partly  $[\text{Cp}^*\text{Fe}]$  units are omitted for clarity.

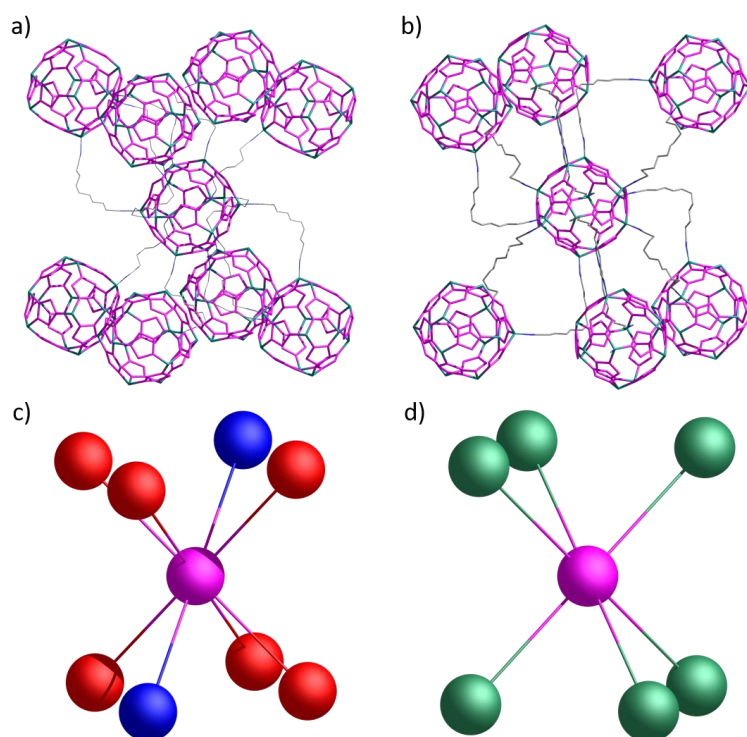
The structures of **6** - **8** derived from single crystal X-ray structure analysis show spherical scaffolds, which are connected by flexible dinitriles and act as nodes in resulting 3D polymeric networks.

Moreover, the crystal structures of **6** and **7** are isotypic. The nodes are constructed in an analogous way for **6** – **8** (Figure 7a,b). Each sphere consists of 12 molecules **1a**, positioned at the vertices of an icosahedron, and 12 Ag atoms systematically situated over 12 of the 20 available trigonal faces of the icosahedron. The pores formed in this way give rise to twelve-membered rings  $\{Ag_3P_9\}$  in the inorganic scaffold (Figure 7d). Every *cyclo*-P<sub>5</sub> ligand is coordinating in a 1,2,4-way to Ag atoms, which are in turn tetrahedrally coordinated by three ligands **1a** and one dinitrile linker connecting neighboring spheres. The sphere itself acts as a host for one molecule **1a** with a maximum diameter of 9.3 Å, which is incorporated (Figure 7c). This is possible, due to the orientation of the methyl groups of the guest either towards the  $\{Ag_3P_9\}$  rings or towards scaffold building Ag atoms, which offer corners to the inner void. In **6** - **7** the *cyclo*-P<sub>5</sub> ring of the guest shows no parallel orientation towards one *cyclo*-P<sub>5</sub> ring of the host scaffold, with minimum distances of 3.78 Å (**6**) and 3.75 Å (**7**),<sup>13</sup> which are all larger than the sum of the van der Waals radii. Together with these values, the angles between the *cyclo*-P<sub>5</sub> planes of  $\alpha(P_5^{plane}...P_5^{plane}) = 2.53^\circ$  (**6**) and  $8.39^\circ$  (**7**) suggest rather weak or no  $\pi$ - $\pi$  interactions. For **8** the preliminary model obtained from X-ray structure analysis does not allow a statement on the orientations and distances of the guest inside the host scaffold, yet. Previously observed cases of **1a** acting as a template in self-assembled spheres with distances  $d(P_5^{plane}...P_5^{plane}) = 3.86 - 4.03$  Å and angles  $\angle(P_5^{plane}...P_5^{plane}) < 0.9^\circ$  were interpreted as  $\pi$ - $\pi$  interactions enforced by encapsulation.<sup>14</sup>



**Figure 7:** Inorganic scaffolds of a) **6**, **7** and b) **8** with outgoing linkers, c) guest highlighted in space-filling model, representatively shown for **6**, d) twelve-membered ring  $\{Ag_3P_9\}$  in scaffolds of **6** - **8**. H atoms,  $[Cp^*Fe]$  fragments, and minor parts of disordering are omitted for clarity.

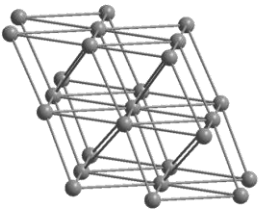
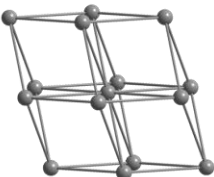
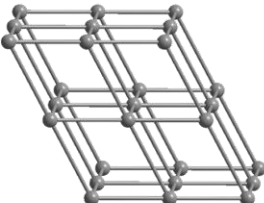
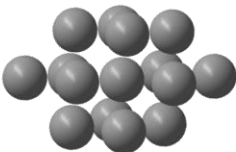
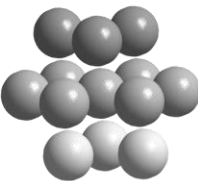
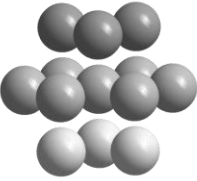
Each sphere of **6** and **7** is connected *via* 12 dinitrile ligands to 8 neighboring spheres. This implies that certain spheres are linked by more than one dinitrile. To six of them (red in *Figure 8c*) the connectivity is onefold, but to two of them (blue) it is threefold. In contrast, in **8** with a linker with  $x = 10$ , the connectivity differs to **6** and **7**. Here, each spherical node is connected to 6 others *via* 12 linkers, each pair of nodes being twofold connected (green in *Figure 8d*). Considering the similarity of the unit cell constants, the same space group and other structural features, crystal structures of **6** and **7** are isotyp. Using the program TOPOSPro,<sup>15</sup> the nets were assigned to the topologies **bccu** (body centered cubic, **6**, **7**) and **pcu** (primitive cubic packing, **8**) (*Table 1*, top).



**Figure 8:** Sections of the cationic part of the 3D polymers a) **6**, **7** and b) **8**, different connectivity types in c) **6**, **7** and d) **8**. Red: 1-, green: 2-, blue: 3-connected nodes towards central node (pink). H atoms,  $[\text{Cp}^*\text{Fe}]$  fragments, guests, and minor parts of disordering are omitted for clarity.

However, only regarding the centroids of the spherical nodes, all three 3D polymers **6** - **8** can surprisingly be described as a slightly distorted **fcc** (face centered cubic) close packing of equal spheres. In *Table 1* the 3D polymers **6** - **8** are compared to  $[\text{SbF}_6]@[\{\text{Cp}^*\text{Fe}(\eta^5\text{-P}_5)\}_9\{\text{Ag}_{11}(\text{NC}(\text{CH}_2)_7\text{CN})_6\}]_n[\text{SbF}_6]_{10n}$  (cf. *Chapter V*), which shows a more unusual topology of the net **bccu-x-10-Fmmm** and a packing of spheres which can be described as **bccu-x**.

**Table 1:** Comparison of net topologies and packings of 3D polymers of spherical nodes. The topologies were calculated using TOPOSPro.<sup>15</sup>

	$[[\text{SbF}_6]@[\{\text{Cp}^*\text{Fe}(\eta^5\text{-P}_5)\}_9\{\text{Ag}_{11}(\text{NC}(\text{CH}_2)_7\text{CN})_6\}]]_n[\text{SbF}_6]_{10n}$	<b>6, 7</b>	<b>8</b>
	Chapter V	this Chapter	this Chapter
Topologies of nets	<b>bcu-x-10-Fmmm</b> 	<b>bcu</b> 	<b>pcu</b> 
packings	<b>bcc-x</b> 	<b>fcc</b> 	<b>fcc</b> 

All three polymers **6** - **8** are insoluble in common solvents, such as hexane, toluene,  $\text{CH}_2\text{Cl}_2$ , thf and  $\text{Et}_2\text{O}$ . Only in  $\text{CH}_3\text{CN}$  or pyridine they are soluble, though accompanied by fragmentation of the coordination network. Therefore, in the  $^1\text{H}$  NMR and in the  $^{13}\text{C}$  NMR spectrum in  $\text{CD}_2\text{Cl}_2$  after fragmentation with pyridine, only signals corresponding to free **1a** and the dinitrile linker molecule are visible, whereas in the  $^{31}\text{P}\{^1\text{H}\}$  spectrum two signals for **1a** at 144.1 ppm and 144.8 ppm can be observed, most likely due to different coordination towards Ag atoms as a result of incomplete fragmentation. Due to the structural analogy of **6** – **8** in the solid state, and the therefore expectable similarity, a  $^{31}\text{P}$  MAS measurement was performed exemplarily for this class of polymers on compound **6**. A broad signal at 125 ppm with an integral intensity of 60 is observed, which can most likely be attributed to the scaffold-building P atoms. Two sharp signals at 150 ppm and 169 ppm respectively with integral intensities of 5, can be attributed to different guest molecules of **1a**, due to disorder in the host scaffold. Considering the chemical shift of free **1a** at 149 ppm, these results suggest one position of the guest showing no interaction to the scaffold, whereas the other position may show e.g.  $\pi$ -stacking interactions. **1a** incorporated in the 90-vertex sphere  $[(\mathbf{1a})_{12}(\text{CuCl})_{25}(\text{CH}_3\text{CN})_{10}]$  shows a comparable chemical shift in the  $^{31}\text{P}$  MAS spectrum at 160 ppm, downfield shifted to the signal of the free complex due to enforced  $\pi$ -interactions.<sup>14</sup> In the ESI MS spectrum oligomeric fragments can be detected, such as  $m/z = 3729$  for  $[\{\text{Cp}^*\text{Fe}(\eta^5\text{-P}_5)\}_9\text{Ag}_2(\text{NC}(\text{CH}_2)_8\text{CN})(\text{SbF}_6)]^+$  in **6**,  $m/z = 2521.98$  for  $[\{\text{Cp}^*\text{Fe}(\eta^5\text{-P}_5)\}_4\text{Ag}_4(\text{SbF}_6)_3]^+$  in **7** and  $m/z = 2522.0$  for  $[\{\text{Cp}^*\text{Fe}(\eta^5\text{-P}_5)\}_4\text{Ag}_4(\text{SbF}_6)_3]^+$  in **8**. In the IR spectrum of crystals of **6** - **8** the

stretching mode of the nitrile group could be observed at  $\tilde{\nu} = 2264 \text{ cm}^{-1}$  (**6**),  $2269 \text{ cm}^{-1}$  (**7**),  $2268 \text{ cm}^{-1}$  (**8**), which is slightly blue-shifted to those of the free dinitriles at  $\tilde{\nu} = 2247 \text{ cm}^{-1}$  due to the coordination towards the Ag atoms. Additionally, transmission electron microscopic (TEM) measurements were conducted for **6**. As the compound is not soluble, but dispersable in a  $\text{CH}_2\text{Cl}_2$  solution, the spheres visible in *Figure 9* are expected to not be distributed isotropically. Larger spherical aggregates, marked with white bars, show a mean diameter of 4.5 nm, whereas the smaller ones, marked with red bars, show a mean diameter of 3.1 nm. Both is larger than the calculated diameter of 2.3 nm for the individual spherical scaffolds, considering the distance between two opposing Cp ligands. However, according to X-ray structure analysis, these scaffolds are 12-fold positively charged, with the 12  $\text{SbF}_6^-$  counter-anions being located non-coordinatingly in the surrounding of the spheres. This explains the deviation between the size of the examined aggregates in the TEM record and the theoretical dimensions of the spherical scaffold in **6**, as 12  $\text{SbF}_6^-$  counter-anions ( $d(\text{SbF}_6^-) = 0.67 \text{ nm}$ ) and six  $\text{NC}(\text{CH}_2)_8\text{CN}$  linkers are expected to show aggregation to the inorganic cores during the preparation procedure.

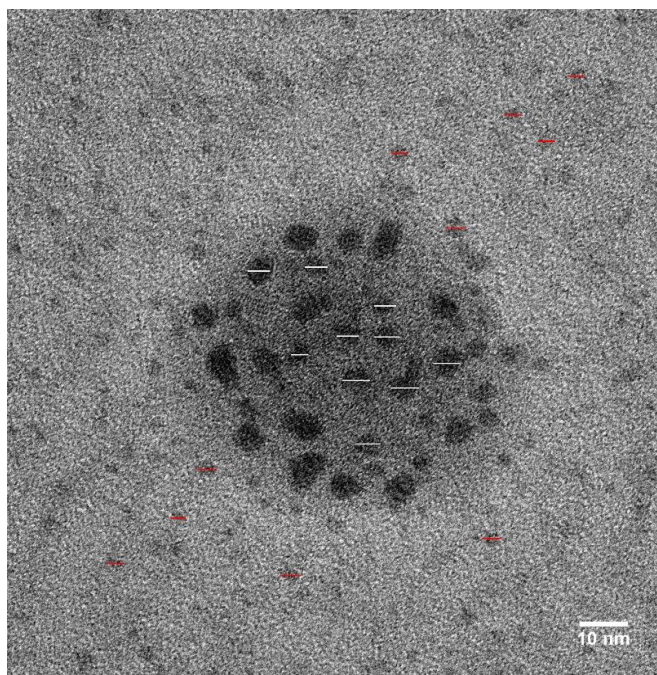


**Figure 9:** TEM record of **6** dispersed in a  $\text{CH}_2\text{Cl}_2$  on a Cu grid, coated with amorphous carbon and measured on a FEI Tecnai G2 Spirit Twin transmission electron microscope with an acceleration voltage of 120 kV.



### 6.3 Conclusion

We have shown the tremendous possibilities that arise from using fully flexible linkers in supramolecular chemistry of the five-fold symmetric polyphosphorus ferrocene  $[\text{Cp}^{\text{R}}\text{Fe}(\eta^5\text{-P}_5)]$  ( $\text{Cp}^{\text{R}} = \text{Cp}^*$  (**1a**),  $\text{Cp}^{\text{Bn}}$  (**1b**)). We presented the use of coinage metal salts of small and huge weakly coordinating anions ( $[\text{Cu}(\text{CH}_3\text{CN})_4]\text{BF}_4$  and  $\text{Ag}[\text{Al}\{\text{OC}(\text{CF}_3)_3\}_4]$ ) in a one-pot three-component self-assembly procedure together with **1a** and  $\text{NC}(\text{CH}_2)_x\text{CN}$  ( $x = 8, 10$ ) to give the coordination networks  $[\{\text{Cp}^*\text{Fe}(\eta^5\text{-P}_5)\}\{\text{Cu}(\text{NC}(\text{CH}_2)_8\text{CN})\}]_n[\text{BF}_4]_n \cdot (\text{CH}_2\text{Cl}_2)_n$  (**2**) and  $[\{\text{Cp}^*\text{Fe}(\eta^5\text{-P}_5)\}\{\text{Ag}(\text{NC}(\text{CH}_2)_{10}\text{CN})\}]_n[\text{Al}\{\text{OC}(\text{CF}_3)_3\}_4]_n$  (**3**). The small size of  $\text{BF}_4^-$  allows the cationic polymeric layers to stack in the solid state, showing  $\pi$ - $\pi$  interactions. In contrast to this, the steric bulk of  $[\text{Al}\{\text{OC}(\text{CF}_3)_3\}_4]^-$  prevents those short contacts, even along with the use of the longest linker with  $x = 10$ , and decreases the dimensionality to a 1D polymeric structure. Varying then the steric influence of the organic residue of the *cyclo*- $\text{P}_5$  complex from **1a** to **1b** and using the medium sized anion  $\text{SbF}_6^-$ , two 3D coordination networks  $[\{\text{Cp}^{\text{Bn}}\text{Fe}(\eta^5\text{-P}_5)\}\{\text{Ag}(\text{NC}(\text{CH}_2)_8\text{CN})\}]_n[\text{SbF}_6]_n$  (**4**) and  $[\{\text{Cp}^{\text{Bn}}\text{Fe}(\eta^5\text{-P}_5)\}_2\{\text{Ag}_2(\text{NC}(\text{CH}_2)_{10}\text{CN})_{1.5}\}]_n[\text{SbF}_6]_{2n} \cdot (\text{CH}_2\text{Cl}_2)_{0.5n}$  (**5**) are formed by linkers with  $x = 8$  and 10. Due to steric hinderance of either the anion or the polyphosphorus ligand, with these combinations no formation of spheres was possible. But furthermore, we presented the construction of three compounds of nano-sized spherical scaffolds, that are interconnected to form 3D polymeric frameworks, by implementing the fully flexible dinitriles together with  $\text{AgSbF}_6$  and **1a** in a three-component self-assembly. Thus, we successfully synthesized selectively and characterized  $[\{\text{Cp}^*\text{Fe}(\eta^5\text{-P}_5)\}@\{\{\text{Cp}^*\text{Fe}(\eta^{5:1:1:1}\text{-P}_5)\}_{12}\{\text{Ag}_{12}(\text{NC}(\text{CH}_2)_x\text{CN})_6\}\}]_n[\text{SbF}_6]_{12n}$  (with  $x = 8$  (**6**), 9 (**7**), 10 (**8**)). The inorganic scaffolds of the spherical nodes are identical for **6** – **8** and astonishingly very similar to the individual derivative based on a two-component self-assembly of **1a** and  $\text{AgSO}_3\text{CF}_3$   $[\{\text{Cp}^*\text{Fe}(\eta^{5:1:1:1}\text{-P}_5)\}_{12}(\text{AgSO}_3\text{CF}_3)_{10}]$  (cf. *Chapter III*). Whereas **6** and **7** represent isotypic compounds, **8** slightly differs to them with respect to the connectivity of the supramolecular nodes, which may be due to different packing effects with increasing the size of the linking unit. Surprisingly, the flexibility of the aliphatic dinitriles allows the spheres to pack in either **bcc**-x or **fcc** cubic closest packings. Moreover, despite the insolubility of the polymers **6** - **8**, we were able to characterize compound **6** exemplarily by TEM methods, visualizing for the first time the spherical structure of the subunits in these class of 3D connected spherical aggregates.

## 6.4 Experimental Part

### General Remarks

All reactions were performed under an inert atmosphere of dry nitrogen with standard vacuum, Schlenk and glove-box techniques. Solvents were purified, dried and degassed prior to use by standard procedures.  $[\text{Cp}^*\text{Fe}(\eta^5\text{-P}_5)]$ ,<sup>10</sup>  $[\text{Cp}^{\text{Bn}}\text{Fe}(\eta^5\text{-P}_5)]$ <sup>16</sup> and  $\text{Ag}[\text{Al}\{\text{OC}(\text{CF}_3)_3\}_4]$ <sup>17</sup> were synthesized following reported procedures. Commercially available chemicals ( $\text{AgSbF}_6$ ,  $[\text{Ag}(\text{CH}_3\text{CN})_4](\text{BF}_4)$ ,  $[\text{Cu}(\text{CH}_3\text{CN})_4](\text{BF}_4)$ ,  $\text{NC}(\text{CH}_2)_x\text{CN}$  ( $x = 8 - 10$ )) were used without further purification. Solution NMR spectra were recorded on a Bruker Avance 300 or 400 spectrometer. The  $^{31}\text{P}\{^1\text{H}\}$  MAS spectrum was measured on a Bruker Avance 300. The corresponding ESI-MS spectra were acquired on a ThermoQuest Finnigan MAT TSQ 7000 mass spectrometer. CHN Elemental analyses were performed on a Vario EL III apparatus, whereas all other elements were determined by the Catalysis Research Center of the Technical University Munich by photometry, atomic absorption spectroscopy or titrimetry.

The Transmission electron microscopy (TEM) measurements were carried out on a FEI Tecnai G2 Spirit Twin transmission electron microscope equipped with a field emission gun and processed with an acceleration voltage of 120 kV. The machine is fitted with a LaB6 cathode and the pictures were recorded with an Gatan US1000 CCD-camera ( $2\text{k} \times 2\text{k}$ ). The analysis of the pictures was done with the graphic software Fiji.<sup>18</sup> For the preparation of the samples the nanoparticles were dispersed in dichloromethane and 20  $\mu\text{L}$  were dropped on copper grids coated with amorphous carbon.



**Synthesis of  $[\{\text{Cp}^*\text{Fe}(\eta^5\text{-P}_5)\}\{\text{Cu}(\text{NC}(\text{CH}_2)_8\text{CN})\}]_n[\text{BF}_4]_n \cdot (\text{CH}_2\text{Cl}_2)_n$  (**2**)**

In a Schlenk tube a solution of  $\text{CuBF}_4(\text{CH}_3\text{CN})_4$  (30 mg, 0.1 mmol) in  $\text{CH}_2\text{Cl}_2$  (5 mL) is carefully layered with a green solution of  $[\text{Cp}^*\text{Fe}(\eta^5\text{-P}_5)]$  (20 mg, 0.05 mmol) and  $\text{NC}(\text{CH}_2)_8\text{CN}$  (1.3 mL, 0.5 mmol, 0.4 mmol/mL in  $\text{CH}_2\text{Cl}_2$ ) in toluene (5 mL). Thereby, the phase boundary turns red. After a few days, the formation of brown prismatic crystals of **2** at the phase boundary can be observed. After complete diffusion, the light green mother liquor is decanted, the crystals are washed with hexane (3 x 10 mL) and dried *in vacuo*.

Analytical data of **2**:

**Yield:** 20 mg (0.028 mmol, 57% based on  $[\text{Cp}^*\text{Fe}(\eta^5\text{-P}_5)]$ ).

**$^1\text{H}$  NMR** ( $\text{CD}_2\text{Cl}_2/\text{pyridine}$ ):  $\delta$  [ppm] = 1.34 (s(br), 4H,  $\text{NC}(\text{CH}_2)_8\text{CN}$ ), 1.44 (s, 15H,  $[\text{Cp}(\text{CH}_3)_5\text{Fe}(\eta^5\text{-P}_5)]$ ), 1.65 (m, 8H,  $\text{NC}(\text{CH}_2)_8\text{CN}$ ), 2.34 (t, 4H,  $\text{NC}(\text{CH}_2)_8\text{CN}$ ), 7.46 (m(br), 8H,  $\beta$ -H, pyridine), 7.88 (m(br), 4H,  $\gamma$ -H, pyridine), 8.62 (m(br), 8H,  $\alpha$ -H, pyridine).

**$^{31}\text{P}\{^1\text{H}\}$  NMR** ( $\text{CD}_2\text{Cl}_2/\text{pyridine}$ ):  $\delta$  [ppm] = 143.5 ( $[\text{Cp}^*\text{Fe}(\eta^5\text{-P}_5)]$ ).

**$^{13}\text{C}$  NMR** ( $\text{CD}_2\text{Cl}_2/\text{pyridine}$ ):  $\delta$  [ppm] = no signal was found.

**$^{19}\text{F}$  NMR** ( $\text{CD}_2\text{Cl}_2/\text{pyridine}$ ):  $\delta$  [ppm] = -151.95, -151.90, -151.65 (s(br)).

**Positive ion ESI-MS** ( $\text{CH}_3\text{CN}$ ):  $m/z$  (%) = 754.77  $[\{\text{Cp}^*\text{Fe}(\eta^5\text{-P}_5)\}_2\text{Cu}]^+$ , 572.99  $[\{\text{Cp}^*\text{Fe}(\eta^5\text{-P}_5)\}\text{Cu}(\text{NC}(\text{CH}_2)_8\text{CN})]^+$ , 449.88  $[\{\text{Cp}^*\text{Fe}(\eta^5\text{-P}_5)\}\text{Cu}(\text{CH}_3\text{CN})]^+$ , 391.19  $[\text{Cu}(\text{NC}(\text{CH}_2)_8\text{CN})_2]^+$ , 227.06 (100)  $[\text{Cu}(\text{CH}_3\text{CN})_4]^+$ .

**Negative ion ESI-MS** ( $\text{CH}_3\text{CN}$ ):  $m/z$  (%) = 87.00 (100)  $[\text{BF}_4]^-$ .

**Elemental analysis:** Calculated (%) for  $[\{\text{Cp}^*\text{Fe}(\eta^5\text{-P}_5)\}\{\text{CuBF}_4\}(\text{NC}(\text{CH}_2)_8\text{CN})](\text{CH}_2\text{Cl}_2)_{0.5}]$  (703.01 g/mol): C 35.02, H 4.59, N 3.98; found: C 34.77, H 4.60, N 4.03.

**IR:**  $\tilde{\nu}/\text{cm}^{-1}$  = 2930 (vw), 2848 (vw), 2347 (vw), 2270 (vw), 1623 (vw), 1457 (vw), 1420 (vw), 1034 (vs), 876 (m), 554 (m).

### Synthesis of $[\{\text{Cp}^*\text{Fe}(\eta^5\text{-P}_5)\}\{\text{Ag}(\text{NC}(\text{CH}_2)_{10}\text{CN})\}]_n[\text{Al}\{\text{OC}(\text{CF}_3)_3\}_4]_n$ (**3**)

In a Schlenk tube a solution of  $\text{Ag}[\text{Al}\{\text{OC}(\text{CF}_3)_3\}_4]$  (58 mg, 0.04 mmol) in  $\text{CH}_2\text{Cl}_2$  (5 mL) is carefully layered with a green solution of  $[\text{Cp}^*\text{Fe}(\eta^5\text{-P}_5)]$  (17 mg, 0.04 mmol) and  $\text{NC}(\text{CH}_2)_{10}\text{CN}$  (1 mL, 0.4 mmol, 0.4 mmol/mL in  $\text{CH}_2\text{Cl}_2$ ) in toluene (5 mL). Thereby, the phase boundary turns yellow. After a few days, the formation of green plates crystals of **3** at the phase boundary can be observed. After complete diffusion, the light green mother liquor is decanted, the crystals are washed with hexane (3 x 10 mL) and dried *in vacuo*.

Analytical data of **3**:

**Yield:** 49 mg (0.030 mmol, 76% based on  $[\text{Cp}^*\text{Fe}(\eta^5\text{-P}_5)]$ ).

**$^1\text{H}$  NMR** ( $\text{CD}_3\text{CN}$ ):  $\delta$  [ppm] = 1.31 (m, 8H,  $\text{NC}(\text{CH}_2)_8\text{CN}$ ), 1.40 (m, 4H,  $\text{NC}(\text{CH}_2)_8\text{CN}$ ), 1.47 (s, 15H,  $[\text{Cp}^*\text{Fe}(\eta^5\text{-P}_5)]$ ), 1.60 (m, 4H,  $\text{NC}(\text{CH}_2)_8\text{CN}$ ), 2.36 (t, 4H,  $\text{NC}(\text{CH}_2)_8\text{CN}$ ).

**$^{31}\text{P}\{^1\text{H}\}$  NMR** ( $\text{CD}_3\text{CN}$ ):  $\delta$  [ppm] = 137.42 ( $[\text{Cp}^*\text{Fe}(\eta^5\text{-P}_5)]$ , coordinated).

**$^{13}\text{C}$  NMR** ( $\text{CD}_3\text{CN}$ ):  $\delta$  [ppm] = 10.14 ( $[\text{Cp}(\text{CH}_3)_5\text{Fe}(\eta^5\text{-P}_5)]$ ), 16.40 (C-1,  $\text{NC}(\text{CH}_2)_8\text{CN}$ ), 25.06 (C-2,  $\text{NC}(\text{CH}_2)_8\text{CN}$ ), 28.30 (C-3,  $\text{NC}(\text{CH}_2)_8\text{CN}$ ), 28.38 (C-4,  $\text{NC}(\text{CH}_2)_8\text{CN}$ ), 28.89, (C-5,  $\text{NC}(\text{CH}_2)_8\text{CN}$ ), 93.09 ( $[\text{Al}\{\text{OC}(\text{CF}_3)_3\}_4]$ ), 119.76 ( $[\text{Al}\{\text{OC}(\text{CF}_3)_3\}_4]$ ), 122.65 ( $\text{NC}(\text{CH}_2)_8\text{CN}$ ).

**$^{19}\text{F}$  NMR** ( $\text{CD}_3\text{CN}$ ):  $\delta$  [ppm] = -74.76 ( $\text{Al}\{\text{OC}(\text{CF}_3)_3\}_4$ ).

**Positive ion ESI-MS** ( $\text{CH}_3\text{CN}$ ):  $m/z$  (%) = 798.75  $[\{\text{Cp}^*\text{Fe}(\eta^5\text{-P}_5)\}_2\text{Ag}]^+$ , 646.99  $[\{\text{Cp}^*\text{Fe}(\eta^5\text{-P}_5)\}\text{Ag}(\text{NC}(\text{CH}_2)_{10}\text{CN})]^+$ , 495.85 (100)  $[\{\text{Cp}^*\text{Fe}(\eta^5\text{-P}_5)\}\text{Ag}(\text{CH}_3\text{CN})]^+$ , 452.83  $[\{\text{Cp}^*\text{Fe}(\eta^5\text{-P}_5)\}\text{Ag}]^+$ , 299.07  $[\text{Ag}(\text{NC}(\text{CH}_2)_{10}\text{CN})]^+$ .

**Negative ion ESI-MS** ( $\text{CH}_3\text{CN}$ ):  $m/z$  (%) = 966.92 (100)  $[\text{Al}\{\text{OC}(\text{CF}_3)_3\}_4]^-$ .

**Elemental analysis:** Calculated (%) for  $[\{\text{Cp}^*\text{Fe}(\eta^5\text{-P}_5)\}\{\text{Ag}[\text{Al}\{\text{OC}(\text{CF}_3)_3\}_4]\}(\text{NC}(\text{CH}_2)_{10}\text{CN})]$  (1613.13 g/mol): C 28.29, H 2.19, N 1.74; found: C 28.26, H 2.22, N 1.61.

**IR:**  $\tilde{\nu}/\text{cm}^{-1}$  = 2928 (vw), 2275 (vw), 1353 (vw), 1297 (w), 1275 (w), 1240 (w), 1215 (s), 1164 (w), 972 (s), 726 (s).

**Synthesis of  $[\{\text{Cp}^{\text{Bn}}\text{Fe}(\eta^5\text{-P}_5)\}\{\text{Ag}(\text{NC}(\text{CH}_2)_8\text{CN})\}]_n[\text{SbF}_6]_n$  (**4**)**

In a Schlenk tube a solution of  $\text{AgSbF}_6$  (17 mg, 0.05 mmol) in  $\text{CH}_2\text{Cl}_2$  (5 mL) is carefully layered with a green solution of  $[\text{Cp}^{\text{Bn}}\text{Fe}(\eta^5\text{-P}_5)]$  (40 mg, 0.05 mmol) and  $\text{NC}(\text{CH}_2)_8\text{CN}$  (1 mL, 0.4 mmol, 0.4 mmol/mL in  $\text{CH}_2\text{Cl}_2$ ) in toluene (5 mL). Thereby, the phase boundary turns yellow. After a few days, the formation of brown-green plates of **4** at the phase boundary was observed. After complete diffusion, the light green mother liquor is decanted, the crystals are washed with hexane (3 x 10 mL) and dried *in vacuo*.

Analytical data of **4**:

**Yield:** 48 mg (0.039 mmol, 79% based on  $[\text{Cp}^{\text{Bn}}\text{Fe}(\eta^5\text{-P}_5)]$ ).

**$^1\text{H}$  NMR** ( $\text{CD}_2\text{Cl}_2$ ):  $\delta$  [ppm] = 1.39 (s(br), 4H,  $\text{NC}(\text{CH}_2)_8\text{CN}$ ), 1.49 (s(br), 4H,  $\text{NC}(\text{CH}_2)_8\text{CN}$ ), 1.73 (s(br), 4H,  $\text{NC}(\text{CH}_2)_8\text{CN}$ ), 2.79 (s(vbr), 4H,  $\text{NC}(\text{CH}_2)_8\text{CN}$ ), 3.62 (s, 10H,  $[\text{Cp}(\text{CH}_2\text{C}_6\text{H}_5)_5\text{Fe}(\eta^5\text{-P}_5)]$ ), 6.28 (d, 10H,  $[\text{Cp}(\text{CH}_2\text{C}_6\text{H}^{\text{ortho}})_5\text{Fe}(\eta^5\text{-P}_5)]$ ), 6.83 (m, 10H,  $[\text{Cp}(\text{CH}_2\text{C}_6\text{H}^{\text{meta}})_5\text{Fe}(\eta^5\text{-P}_5)]$ ), 6.97 (m, 5H,  $[\text{Cp}(\text{CH}_2\text{C}_6\text{H}^{\text{para}})_5\text{Fe}(\eta^5\text{-P}_5)]$ ).

**$^1\text{H}$  NMR** ( $\text{CD}_2\text{Cl}_2/\text{pyridine}$ ):  $\delta$  [ppm] = 1.34 (s(br), 4H,  $\text{NC}(\text{CH}_2)_8\text{CN}$ ), 1.44 (m, 4H,  $\text{NC}(\text{CH}_2)_8\text{CN}$ ), 1.65 (m, 4H,  $\text{NC}(\text{CH}_2)_8\text{CN}$ ), 2.38 (s(vbr), 4H,  $\text{NC}(\text{CH}_2)_8\text{CN}$ ), 3.63 (s, 10H,  $[\text{Cp}(\text{CH}_2\text{C}_6\text{H}_5)_5\text{Fe}(\eta^5\text{-P}_5)]$ ), 6.18 (d, 10H,  $[\text{Cp}(\text{CH}_2\text{C}_6\text{H}^{\text{ortho}})_5\text{Fe}(\eta^5\text{-P}_5)]$ ), 6.75 (m, 10H,  $[\text{Cp}(\text{CH}_2\text{C}_6\text{H}^{\text{meta}})_5\text{Fe}(\eta^5\text{-P}_5)]$ ), 6.90 (m, 5H,  $[\text{Cp}(\text{CH}_2\text{C}_6\text{H}^{\text{para}})_5\text{Fe}(\eta^5\text{-P}_5)]$ ).

**$^{13}\text{C}$  NMR** ( $\text{CD}_2\text{Cl}_2/\text{pyridine}$ ):  $\delta$  [ppm] = 25.26, 28.45, 28.51, 33.80, 96.65, 126.36, 128.04, 128.73, 137.33

**$^{31}\text{P}\{^1\text{H}\}$  NMR** ( $\text{CD}_2\text{Cl}_2$ ):  $\delta$  [ppm] = 145 (s,  $[\text{Cp}^{\text{Bn}}\text{Fe}(\eta^5\text{-P}_5)]$ ).

**$^{31}\text{P}\{^1\text{H}\}$  NMR** ( $\text{CD}_2\text{Cl}_2/\text{pyridine}$ ):  $\delta$  [ppm] = 152 (s,  $[\text{Cp}^{\text{Bn}}\text{Fe}(\eta^5\text{-P}_5)]$ ).

**$^{19}\text{F}$  NMR** ( $\text{CD}_2\text{Cl}_2$ ): no signal was detected.

**$^{19}\text{F}$  NMR** ( $\text{CD}_2\text{Cl}_2/\text{pyridine}$ ): no signal was detected.

**Positive ion ESI-MS** ( $\text{CH}_2\text{Cl}_2$ ):  $m/z$  (%) = 1560.9  $[\{\text{Cp}^{\text{Bn}}\text{Fe}(\eta^5\text{-P}_5)\}_2\text{Ag}]^+$ , 1340.8  $[\{\text{Cp}^{\text{Bn}}\text{Fe}(\eta^5\text{-P}_5)\}\text{Ag}_2\text{SbF}_6(\text{NC}(\text{CH}_2)_8\text{CN})]^+$ , 1175  $[\{\text{Cp}^{\text{Bn}}\text{Fe}(\eta^5\text{-P}_5)\}\text{Ag}_2\text{SbF}_6]^+$ , 997.0  $[\{\text{Cp}^{\text{Bn}}\text{Fe}(\eta^5\text{-P}_5)\}\text{Ag}(\text{NC}(\text{CH}_2)_8\text{CN})]^+$ , 832.9  $[\{\text{Cp}^{\text{Bn}}\text{Fe}(\eta^5\text{-P}_5)\}\text{Ag}]^+$ , 435.1 (100)  $[\text{Ag}(\text{NC}(\text{CH}_2)_8\text{CN})_2]^+$ , 271.0  $[\text{Ag}(\text{NC}(\text{CH}_2)_8\text{CN})]^+$ .

**Negative ion ESI-MS** ( $\text{CH}_2\text{Cl}_2$ ):  $m/z$  (%) = 234.7 (100)  $[\text{SbF}_6]^-$ .

**Elemental analysis:** Calculated (%) for  $[\{\text{Cp}^{\text{Bn}}\text{Fe}(\eta^5\text{-P}_5)\}\{\text{AgSbF}_6\}(\text{CN}(\text{CH}_2)_8\text{CN})]$  (1234.29 g/mol): C 48.66, H 4.16, N 2.27; found: C 48.64, H 4.19, N 2.24.

**IR:**  $\tilde{\nu}/\text{cm}^{-1}$  = 3030 (vw), 2925 (vw), 2854 (vw), 2360 (vw), 2343 (vw), 2267 (vw), 1601 (vw), 1495 (vw), 1455 (vw), 1444 (vw), 1419 (vw), 1076 (vw), 1030 (vw), 972 (vw), 847 (vw), 738 (w), 722 (vw), 715 (vw), 697 (w), 653 (s), 615 (vw).

### Synthesis of $[\{\text{Cp}^{\text{Bn}}\text{Fe}(\eta^5\text{-P}_5)\}_2\{\text{Ag}_2(\text{NC}(\text{CH}_2)_{10}\text{CN})_{1.5}\}]_n[\text{SbF}_6]_{2n}(\text{CH}_2\text{Cl}_2)_{0.5n}$ (**5**)

In a Schlenk tube a solution of  $\text{AgSbF}_6$  (17 mg, 0.05 mmol) in  $\text{CH}_2\text{Cl}_2$  (5 mL) is carefully layered with a green solution of  $[\text{Cp}^{\text{Bn}}\text{Fe}(\eta^5\text{-P}_5)]$  (40 mg, 0.05 mmol) and  $\text{NC}(\text{CH}_2)_{10}\text{CN}$  (0.625 mL, 0.25 mmol, 0.4 mmol/mL in  $\text{CH}_2\text{Cl}_2$ ) in toluene (5 mL). Thereby, the phase boundary turns yellow. After a few days, the formation of brown-green elongated plates of **5** at the phase boundary was observed. After complete diffusion, the light green mother liquor is decanted, the crystals are washed with hexane (3 x 10 mL) and dried *in vacuo*.

Analytical data of **5**:

**Yield:** 42 mg (0.017 mmol, 69% based on  $[\text{Cp}^{\text{Bn}}\text{Fe}(\eta^5\text{-P}_5)]$ ).

$^1\text{H}$  NMR ( $\text{CD}_2\text{Cl}_2$ ):  $\delta$  [ppm] = 1.30 (s(br), 8H,  $\text{NC}(\text{CH}_2)_8\text{CN}$ ), 1.40 (s(br), 4H,  $\text{NC}(\text{CH}_2)_8\text{CN}$ ), 1.62 (s(br), 4H,  $\text{NC}(\text{CH}_2)_8\text{CN}$ ), 2.44 (s(vbr), 4H,  $\text{NC}(\text{CH}_2)_8\text{CN}$ ), 3.61 (s, 13H,  $[\text{Cp}(\text{CH}_2\text{C}_6\text{H}_5)_5\text{Fe}(\eta^5\text{-P}_5)]$ ), 6.28 (d, 13H,  $[\text{Cp}(\text{CH}_2\text{C}_6\text{H}^{\text{ortho}})_5\text{Fe}(\eta^5\text{-P}_5)]$ ), 6.83 (m, 13H,  $[\text{Cp}(\text{CH}_2\text{C}_6\text{H}^{\text{meta}})_5\text{Fe}(\eta^5\text{-P}_5)]$ ), 6.97 (m, 7H,  $[\text{Cp}(\text{CH}_2\text{C}_6\text{H}^{\text{para}})_5\text{Fe}(\eta^5\text{-P}_5)]$ ).

$^1\text{H}$  NMR ( $\text{CD}_2\text{Cl}_2/\text{pyridine}$ ):  $\delta$  [ppm] = 1.30 (s(br), 8H,  $\text{NC}(\text{CH}_2)_8\text{CN}$ ), 1.42 (m, 4H,  $\text{NC}(\text{CH}_2)_8\text{CN}$ ), 1.63 (m, 4H,  $\text{NC}(\text{CH}_2)_8\text{CN}$ ), 2.32 (t, 4H,  $\text{NC}(\text{CH}_2)_8\text{CN}$ ), 3.63 (s, 12H,  $[\text{Cp}(\text{CH}_2\text{C}_6\text{H}_5)_5\text{Fe}(\eta^5\text{-P}_5)]$ ), 6.20 (d, 12H,  $[\text{Cp}(\text{CH}_2\text{C}_6\text{H}^{\text{ortho}})_5\text{Fe}(\eta^5\text{-P}_5)]$ ), 6.75 (m, 12H,  $[\text{Cp}(\text{CH}_2\text{C}_6\text{H}^{\text{meta}})_5\text{Fe}(\eta^5\text{-P}_5)]$ ), 6.90 (m, 6H,  $[\text{Cp}(\text{CH}_2\text{C}_6\text{H}^{\text{para}})_5\text{Fe}(\eta^5\text{-P}_5)]$ ), 7.48 (8H,  $\beta$ -C, pyridine), 7.89 (4H,  $\alpha$ -C, pyridine), 8.59 (8H,  $\gamma$ -C, pyridine).

$^{13}\text{C}$  NMR ( $\text{CD}_2\text{Cl}_2/\text{pyridine}$ ):  $\delta$  [ppm] = 17.01, 25.38, 28.60, 28.67, 29.13, 33.79, 96.47, 125.13, 126.31, 128.02, 128.75, 137.45, 138.39, 149.93.

$^{31}\text{P}\{^1\text{H}\}$  NMR ( $\text{CD}_2\text{Cl}_2$ ):  $\delta$  [ppm] = 149 (s,  $[\text{Cp}^{\text{Bn}}\text{Fe}(\eta^5\text{-P}_5)]$ ).

$^{31}\text{P}\{^1\text{H}\}$  NMR ( $\text{CD}_2\text{Cl}_2/\text{pyridine}$ ):  $\delta$  [ppm] = 155 (s,  $[\text{Cp}^{\text{Bn}}\text{Fe}(\eta^5\text{-P}_5)]$ ).

$^{19}\text{F}$  NMR ( $\text{CD}_2\text{Cl}_2$ ): no signal was detected.

$^{19}\text{F}$  NMR ( $\text{CD}_2\text{Cl}_2/\text{pyridine}$ ): no signal was detected.

**Positive ion ESI-MS** ( $\text{CH}_2\text{Cl}_2$ ):  $m/z$  (%) = 1561.6  $[\{\text{Cp}^{\text{Bn}}\text{Fe}(\eta^5\text{-P}_5)\}_2\text{Ag}]^+$ , 1181.3  $[\{\text{Cp}^{\text{Bn}}\text{Fe}(\eta^5\text{-P}_5)\}\text{Ag}_2\text{SbF}_6]^+$ , 1027.5  $[\{\text{Cp}^{\text{Bn}}\text{Fe}(\eta^5\text{-P}_5)\}\text{Ag}(\text{NC}(\text{CH}_2)_{10}\text{CN})]^+$ , 877  $[\text{Ag}(\text{NC}(\text{CH}_2)_{10}\text{CN})_4]^+$ , 835.2 (100)  $[\text{Cp}^{\text{Bn}}\text{Fe}(\eta^5\text{-P}_5)\text{Ag}]^+$ , 491.4  $[\text{Ag}(\text{NC}(\text{CH}_2)_{10}\text{CN})_2]^+$ , 301.1  $[\text{Ag}(\text{NC}(\text{CH}_2)_{10}\text{CN})]^+$ .

**Negative ion ESI-MS** ( $\text{CH}_2\text{Cl}_2$ ):  $m/z$  (%) = 234.7 (100)  $[\text{SbF}_6]^-$ .

**Elemental analysis:** Calculated (%) for  $[\{\text{Cp}^{\text{Bn}}\text{Fe}(\eta^5\text{-P}_5)\}_2\{\text{AgSbF}_6\}_2(\text{NC}(\text{CH}_2)_{10}\text{CN})_{1.5}(\text{CH}_2\text{Cl}_2)_{0.5}]$  (2428.93 g/mol): C 47.88, H 4.12, N 1.70; found: C 47.94, H 4.12, N 1.56.

**IR:**  $\tilde{\nu}/\text{cm}^{-1}$  = 2922 (vw), 2859 (vw), 2281 (vw), 1601 (vw), 1495 (w), 1446 (w), 1076 (vw), 1029 (vw), 973 (vw), 738 (m), 698 (m), 654 (s).

**Synthesis of  $[[\text{Cp}^*\text{Fe}(\eta^5\text{-P}_5)]@[\{\text{Cp}^*\text{Fe}(\eta^{5:1:1:1}\text{-P}_5)]_{12}\{\text{Ag}_{12}(\text{NC}(\text{CH}_2)_8\text{CN})_6\}]]_n[\text{SbF}_6]_{12n}$  (**6**)**

In a Schlenk tube a solution of  $\text{AgSbF}_6$  (17 mg, 0.05 mmol) in  $\text{CH}_2\text{Cl}_2$  (25 mL) is carefully layered first with a solvent mixture of  $\text{CH}_2\text{Cl}_2$ /toluene (10 mL, 2:1) and then with a green solution of  $[\text{Cp}^*\text{Fe}(\eta^5\text{-P}_5)]$  (20 mg, 0.05 mmol) and  $\text{NC}(\text{CH}_2)_8\text{CN}$  (1 mL, 0.4 mmol, 0.4 M in  $\text{CH}_2\text{Cl}_2$ ) in toluene (25 mL). After a few hours, the phase boundary turns yellow and after one day, the formation of dark brown-green plates of **6** at the phase boundary can be observed. Furthermore a few crystals of  $[[\text{Cp}^*\text{Fe}(\eta^{5:2:1}\text{-P}_5)]_2\text{Ag}]_n[\text{SbF}_6]_n$  appear at the phase boundary (cf. Chapter V). After complete diffusion, the light-yellow mother liquor is decanted, the crystals are washed with  $\text{CH}_2\text{Cl}_2$  (3 × 10 mL) to remove **2** and dried *in vacuo*.

Analytical data of **6**:

**Yield:** 24 mg (0.0025 mmol, 65% referred to  $[\text{Cp}^*\text{Fe}(\eta^5\text{-P}_5)]$ )

**$^1\text{H}$  NMR** (pyridine/ $\text{CD}_2\text{Cl}_2$ ):  $\delta$  [ppm] = 1.34 (m, 24 H, C-4,  $(\text{NC}(\text{CH}_2)_8\text{CN})$ ), 1.43 (s, 195 H,  $[\text{Cp}^*\text{Fe}(\eta^5\text{-P}_5)]$ ), 1.64 (m, 24 H, C-3,  $(\text{NC}(\text{CH}_2)_8\text{CN})$ ), 1.81 (m, 24 H, C-2,  $(\text{NC}(\text{CH}_2)_8\text{CN})$ ), 2.33 (t, 24 H, C-1,  $(\text{NC}(\text{CH}_2)_8\text{CN})$ ), 7.38 (m,  $\beta$ -H, pyridine), 7.79 (m,  $\gamma$ -H, pyridine), 8.58 (m,  $\alpha$ -H, pyridine).

**$^{13}\text{C}$  NMR** (pyridine/ $\text{CD}_2\text{Cl}_2$ ):  $\delta$  [ppm] = 10.64  $[\text{Cp}(\text{CH}_3)_5\text{Fe}(\eta^5\text{-P}_5)]$ , 17.00 (C-1,  $\text{NC}(\text{CH}_2)_8\text{CN}$ ), 25.33 (C-2,  $\text{NC}(\text{CH}_2)_8\text{CN}$ ), 28.46 (C-3,  $\text{NC}(\text{CH}_2)_8\text{CN}$ ), 28.5 (C-4,  $\text{NC}(\text{CH}_2)_8\text{CN}$ ), 124.3 ( $\beta$ -C, pyridine), 137.01 ( $\gamma$ -C, pyridine), 149.45 ( $\alpha$ -C, pyridine), 149.50 ( $\text{NC}(\text{CH}_2)_8\text{CN}$ ).

**$^{31}\text{P}\{^1\text{H}\}$  NMR** (pyridine/ $\text{CD}_2\text{Cl}_2$ ):  $\delta$  [ppm] = 144.14 (s, 60P,  $[\text{Cp}^*\text{Fe}(\eta^5\text{-P}_5)]$ ), 144.81 (s, 5P,  $[\text{Cp}^*\text{Fe}(\eta^5\text{-P}_5)]$ ).

**$^{31}\text{P}$  MAS NMR** :  $\delta$  [ppm] = 125.1 (m(br),  $\omega_{1/2}$  = 5000 Hz, 55 P  $[\text{Cp}^*\text{Fe}(\eta^5\text{-P}_5)]$  host), 150.23 (s, 5 P  $[\text{Cp}^*\text{Fe}(\eta^5\text{-P}_5)]$  guest), 168.63 (s(br),  $\omega_{1/2}$  = 360 Hz, 5 P  $[\text{Cp}^*\text{Fe}(\eta^5\text{-P}_5)]$  guest).

**$^{19}\text{F}$  NMR** (pyridine/ $\text{CD}_2\text{Cl}_2$ ): no signal was detected.

**Positive ion ESI-MS** ( $\text{CH}_3\text{CN}$ ):  $m/z$  (%) = 3729  $[[\text{Cp}^*\text{Fe}(\eta^5\text{-P}_5)]_9\text{Ag}_2(\text{SbF}_6)(\text{NC}(\text{CH}_2)_8\text{CN})]^+$ , 3564  $[[\text{Cp}^*\text{Fe}(\eta^5\text{-P}_5)]_9\text{Ag}_2(\text{SbF}_6)]^+$ , 3383  $[[\text{Cp}^*\text{Fe}(\eta^5\text{-P}_5)]_8\text{Ag}_2(\text{SbF}_6)(\text{NC}(\text{CH}_2)_8\text{CN})]^+$ , 3220  $[[\text{Cp}^*\text{Fe}(\eta^5\text{-P}_5)]_8\text{Ag}_2(\text{SbF}_6)]^+$ , 3037  $[[\text{Cp}^*\text{Fe}(\eta^5\text{-P}_5)]_7\text{Ag}_2(\text{SbF}_6)(\text{NC}(\text{CH}_2)_8\text{CN})]^+$ , 2867.37  $[[\text{Cp}^*\text{Fe}(\eta^5\text{-P}_5)]_7\text{Ag}_2(\text{SbF}_6)]^+$ , 2690  $[[\text{Cp}^*\text{Fe}(\eta^5\text{-P}_5)]_6\text{Ag}_2(\text{SbF}_6)(\text{NC}(\text{CH}_2)_8\text{CN})]^+$ , 2520  $[[\text{Cp}^*\text{Fe}(\eta^5\text{-P}_5)]_6\text{Ag}_2(\text{SbF}_6)]^+$ , 2340  $[[\text{Cp}^*\text{Fe}(\eta^5\text{-P}_5)]_5\text{Ag}_2(\text{SbF}_6)(\text{NC}(\text{CH}_2)_8\text{CN})]^+$ , 2177.80  $[[\text{Cp}^*\text{Fe}(\eta^5\text{-P}_5)]_5\text{Ag}_2(\text{SbF}_6)]^+$ , 1998.08  $[[\text{Cp}^*\text{Fe}(\eta^5\text{-P}_5)]_4\text{Ag}_2(\text{SbF}_6)(\text{NC}(\text{CH}_2)_8\text{CN})]^+$ , 1834.07  $[[\text{Cp}^*\text{Fe}(\eta^5\text{-P}_5)]_4\text{Ag}_2(\text{SbF}_6)]^+$ , 1650.22  $[[\text{Cp}^*\text{Fe}(\eta^5\text{-P}_5)]_3\text{Ag}_2(\text{SbF}_6)(\text{NC}(\text{CH}_2)_8\text{CN})]^+$ , 1488.25  $[[\text{Cp}^*\text{Fe}(\eta^5\text{-P}_5)]_3\text{Ag}_2(\text{SbF}_6)]^+$ , 1306.51  $[[\text{Cp}^*\text{Fe}(\eta^5\text{-P}_5)]_2\text{Ag}_2(\text{SbF}_6)(\text{NC}(\text{CH}_2)_8\text{CN})]^+$ , 1142.43  $[[\text{Cp}^*\text{Fe}(\eta^5\text{-P}_5)]_2\text{Ag}_2(\text{SbF}_6)]^+$ , 1124.74  $[[\text{Cp}^*\text{Fe}(\eta^5\text{-P}_5)]\text{Ag}_2(\text{SbF}_6)(\text{NC}(\text{CH}_2)_8\text{CN})_2]^+$ , 960.64  $[[\text{Cp}^*\text{Fe}(\eta^5\text{-P}_5)]\text{Ag}_2(\text{SbF}_6)(\text{NC}(\text{CH}_2)_8\text{CN})]^+$ , 798.58  $[[\text{Cp}^*\text{Fe}(\eta^5\text{-P}_5)]_2\text{Ag}]^+$ , 616.84  $[\text{Ag}_2(\text{CH}_3\text{CN})_4(\text{SbF}_6)]^+$ , 581  $[\text{Ag}_2(\text{CD}_3\text{CN})_3(\text{SbF}_6)]^+$ , 537.05

$[\text{Ag}_2(\text{CD}_3\text{CN})_2(\text{SbF}_6)]^+$ , 493.73 (100)  $[\{\text{Cp}^*\text{Fe}(\eta^5\text{-P}_5)\}\text{Ag}(\text{CH}_3\text{CN})]^+$ , 452.76  $[\{\text{Cp}^*\text{Fe}(\eta^5\text{-P}_5)\}\text{Ag}]^+$ , 435.10  $[\text{Ag}(\text{NC}(\text{CH}_2)_8\text{CN})_2]^+$ , 270.98  $[\text{Ag}(\text{NC}(\text{CH}_2)_8\text{CN})]^+$  or  $[\text{Ag}(\text{CH}_3\text{CN})_4]^+$ .

**Negative ion ESI-MS** ( $\text{CH}_2\text{Cl}_2/\text{CH}_3\text{CN}$ ):  $m/z$  (%) = 234.84 (100)  $[\text{SbF}_6]^-$ .

**Elemental analysis:** Calculated (%) for  $[\text{Cp}^*\text{Fe}(\eta^5\text{-P}_5)]@[\text{Cp}^*\text{Fe}(\eta^5\text{-P}_5)_{12}(\text{AgSbF}_6)_{12}(\text{NC}(\text{CH}_2)_8\text{CN})_6]$  (9606.11 g/mol): C 23.76, H 3.05, N 1.75; found: C 23.19, H 3.05, N 1.28.

**IR:**  $\tilde{\nu}/\text{cm}^{-1}$  = 2934 (vw), 2266 (vw), 1476 (w), 1424 (w), 1377 (w), 1074 (vw), 1020 (w), 655 (s).

**TEM measurements:** measured diameter of selected aggregates /nm, marked in white: 4.03, 4.27, 4.76, 4.70, 3.42, 4.40, 5.32, 5.31, 4.17, 4.58. Mean value: 4.5(5) nm; marked in red: 2.84, 2.81, 2.81, 3.05, 3.79, 2.87, 3.42, 2.57, 3.42, 2.57, 3.42, 3.60. Mean value: 3.1(4). Expected diameter ( $\text{Cp}^*\text{-Cp}^*$ ):  $\approx$  2.30 nm.

### Synthesis of $[[\text{Cp}^*\text{Fe}(\eta^5\text{-P}_5)]@[\{\text{Cp}^*\text{Fe}(\eta^{5:1:1:1}\text{-P}_5)\}_{12}\{\text{Ag}_{12}(\text{NC}(\text{CH}_2)_9\text{CN})_6\}]]_n[\text{SbF}_6]_{12n}$ (**7**)

In a Schlenk tube a solution of  $\text{AgSbF}_6$  (17 mg, 0.05 mmol) in  $\text{CH}_2\text{Cl}_2$  (25 mL) is carefully layered first with a solvent mixture of  $\text{CH}_2\text{Cl}_2$ /toluene (10 mL, 2:1) and then with a green solution of  $[\text{Cp}^*\text{Fe}(\eta^5\text{-P}_5)]$  (20 mg, 0.05 mmol) and  $\text{NC}(\text{CH}_2)_9\text{CN}$  (1 mL, 0.4 mmol, 0.4 M in  $\text{CH}_2\text{Cl}_2$ ) in toluene (25 mL). After a few hours, the phase boundary turns yellow and after one day, the formation of dark brown-green plates of **7** at the phase boundary can be observed. Furthermore a few crystals of  $[\{\text{Cp}^*\text{Fe}(\eta^{5:2:1}\text{-P}_5)\}_2\text{Ag}]_n[\text{SbF}_6]_n$  appear at the phase boundary. After complete diffusion, the light-yellow mother liquor is decanted, the crystals are washed with  $\text{CH}_2\text{Cl}_2$  ( $3 \times 10$  mL) to remove  $[\{\text{Cp}^*\text{Fe}(\eta^{5:2:1}\text{-P}_5)\}_2\text{Ag}]_n[\text{SbF}_6]_n$  and dried *in vacuo*.

Analytical data of **7**:

**Yield:** 15 mg (0.0015 mmol, 40% referred to  $[\text{Cp}^*\text{Fe}(\eta^5\text{-P}_5)]$ )

**$^1\text{H}$  NMR** ( $\text{CD}_2\text{Cl}_2$ /pyridine):  $\delta$  [ppm] = 1.33 (m, C-4/C-5/C-6/C-7/C-8,  $\text{NC}(\text{CH}_2)_9\text{CN}$ ), 1.45 (s,  $[\text{Cp}(\text{CH}_3)_5\text{Fe}(\eta^5\text{-P}_5)]$ ), 1.64 (m, C-3/C-9,  $\text{NC}(\text{CH}_2)_9\text{CN}$ ), 2.34 (m, 24H, C-2/C-10,  $\text{NC}(\text{CH}_2)_9\text{CN}$ ).

**$^{13}\text{C}$  NMR** ( $\text{CD}_2\text{Cl}_2$ /pyridine):  $\delta$  [ppm] = 10.76 ( $[\text{Cp}(\text{CH}_3)_5\text{Fe}(\eta^5\text{-P}_5)]$ ), 17.02 (C-2/C-10,  $\text{NC}(\text{CH}_2)_9\text{CN}$ ), 25.35 (C-3/C-9,  $\text{NC}(\text{CH}_2)_9\text{CN}$ ), 28.58 (C-4/C-5/C-7/C-8,  $\text{NC}(\text{CH}_2)_9\text{CN}$ ), 28.96 (C-6,  $\text{NC}(\text{CH}_2)_9\text{CN}$ ), 93.17 ( $[\text{C}_5(\text{CH}_3)_5\text{Fe}(\eta^5\text{-P}_5)]$ ), 125.59 ( $\beta$ -C, pyridine), 137.4 ( $\text{NC}(\text{CH}_2)_9\text{CN}$ ), 139.34 ( $\gamma$ -C, pyridine), 148.49 ( $\alpha$ -C, pyridine).

**$^{31}\text{P}\{^1\text{H}\}$  NMR** ( $\text{CD}_2\text{Cl}_2$ /pyridine):  $\delta$  [ppm] = 142.98 (s,  $[\text{Cp}^*\text{Fe}(\eta^5\text{-P}_5)]$ ).

**Positive ion ESI-MS** ( $\text{CH}_2\text{Cl}_2/\text{CH}_3\text{CN}$ ):  $m/z$  (%) = 2521.98  $[\{\text{Cp}^*\text{Fe}(\eta^5\text{-P}_5)\}_4\text{Ag}_4(\text{SbF}_6)_3]^+$ , 2354.21  $[\{\text{Cp}^*\text{Fe}(\eta^5\text{-P}_5)\}_3\text{Ag}_4(\text{SbF}_6)_3(\text{NC}(\text{CH}_2)_9\text{CN})]^+$ , 2178.18  $[\{\text{Cp}^*\text{Fe}(\eta^5\text{-P}_5)\}_3\text{Ag}_4(\text{SbF}_6)_3]^+$ , 1832.26  $[\{\text{Cp}^*\text{Fe}(\eta^5\text{-P}_5)\}_3\text{Ag}_3(\text{SbF}_6)_2]^+$ , 1664.49  $[\{\text{Cp}^*\text{Fe}(\eta^5\text{-P}_5)\}_3\text{Ag}_2(\text{SbF}_6)(\text{NC}(\text{CH}_2)_9\text{CN})]^+$ , 1142.54  $[\{\text{Cp}^*\text{Fe}(\eta^5\text{-P}_5)\}_2\text{Ag}(\text{NC}(\text{CH}_2)_9\text{CN})(\text{CH}_3\text{CN})_4]^+$ , 974.77  $[\{\text{Cp}^*\text{Fe}(\eta^5\text{-P}_5)\}\text{Ag}_2(\text{SbF}_6)(\text{NC}(\text{CH}_2)_9\text{CN})]^+$ , 953.14  $[\{\text{Cp}^*\text{Fe}(\eta^5\text{-P}_5)\}\text{Ag}_2(\text{SbF}_6)(\text{CH}_3\text{CN})_4]^+$ , 798.75 (100)  $[\{\text{Cp}^*\text{Fe}(\eta^5\text{-P}_5)\}\text{Ag}_2(\text{SbF}_6)]^+$ , 630.97  $[\{\text{Cp}^*\text{Fe}(\eta^5\text{-P}_5)\}\text{Ag}(\text{NC}(\text{CH}_2)_9\text{CN})]^+$ , 493.85  $[\{\text{Cp}^*\text{Fe}(\eta^5\text{-P}_5)\}\text{Ag}(\text{CH}_3\text{CN})]^+$ , 452.8  $[\{\text{Cp}^*\text{Fe}(\eta^5\text{-P}_5)\}\text{Ag}]^+$ , 285.05  $[\text{Ag}(\text{NC}(\text{CH}_2)_9\text{CN})]^+$ , 188.96  $[\text{Ag}(\text{CH}_3\text{CN})_2]^+$ , 147.93  $[\text{Ag}(\text{CH}_3\text{CN})]^+$ , 106.90  $[\text{Ag}]^+$ .

**Negative ion ESI-MS** ( $\text{CH}_2\text{Cl}_2/\text{CH}_3\text{CN}$ ):  $m/z$  (%) = 2648  $[\{\text{Cp}^*\text{Fe}(\eta^5\text{-P}_5)\}_4\text{Ag}_3(\text{SbF}_6)_4]^-$ , 1958.14  $[\{\{\text{Cp}^*\text{Fe}(\eta^5\text{-P}_5)\}_3\text{Ag}_2(\text{SbF}_6)_3\}]^-$ , 234.89 (100)  $[\text{SbF}_6]^-$ .

**Elemental analysis:** Calculated (%) for  $[\text{Cp}^*\text{Fe}(\eta^5\text{-P}_5)]@[\{\text{Cp}^*\text{Fe}(\eta^5\text{-P}_5)\}_{12}(\text{AgSbF}_6)_{12}(\text{NC}(\text{CH}_2)_9\text{CN})_6]$  (825.75 g/mol): C 24.29, H 3.15, N 1.73; found: C 24.54, H 3.24, N 1.66.

**IR:**  $\tilde{\nu}/\text{cm}^{-1}$  = 2928 (vw), 2269 (vw), 1476 (vw), 1427 (vw), 1377 (w), 1020 (w), 656 (vs).

**Synthesis of  $[\text{Cp}^*\text{Fe}(\eta^5\text{-P}_5)]@[\{\text{Cp}^*\text{Fe}(\eta^{5:1:1:1}\text{-P}_5)\}_{12}\{\text{Ag}_{12}(\text{NC}(\text{CH}_2)_{10}\text{CN})_6\}]_n[\text{SbF}_6]_{12n}$  (**8**) and  $[\{\text{Cp}^*\text{Fe}(\eta^5\text{-P}_5)\}_2\{\text{Ag}_2(\text{NC}(\text{CH}_2)_{10}\text{CN})\}]_n[\text{SbF}_6]_{2n}$  (**9**)**

In a Schlenk tube a solution of  $\text{AgSbF}_6$  (34 mg, 0.1 mmol) in  $\text{CH}_2\text{Cl}_2$  (25 mL) is carefully layered first with a solvent mixture of  $\text{CH}_2\text{Cl}_2$ /toluene (10 mL, 2:1) and then with a green solution of  $[\text{Cp}^*\text{Fe}(\eta^5\text{-P}_5)]$  (40 mg, 0.1 mmol) and  $\text{NC}(\text{CH}_2)_{10}\text{CN}$  (2 mL, 0.8 mmol, 0.4 M in  $\text{CH}_2\text{Cl}_2$ ) in toluene (25 mL). After a few hours, the phase boundary turns yellow and after one day, the formation of brown-green plates of **8** at the phase boundary can be observed. Furthermore a few crystals of  $[\{\text{Cp}^*\text{Fe}(\eta^{5:2:1}\text{-P}_5)\}_2\text{Ag}]_n[\text{SbF}_6]_n$  appear at the phase boundary. Occasionally the formation of **9** was observed. After complete diffusion, the light yellow mother liquor is decanted, the crystals are washed with  $\text{CH}_2\text{Cl}_2$  (3 × 10 mL) to remove  $[\{\text{Cp}^*\text{Fe}(\eta^{5:2:1}\text{-P}_5)\}_2\text{Ag}]_n[\text{SbF}_6]_n$  and dried *in vacuo*.

Analytical data of **8**:

**Yield:** 71 mg (0.00726 mmol, 47.2 % referred to  $[\text{Cp}^*\text{Fe}(\eta^5\text{-P}_5)]$ )

**$^1\text{H}$  NMR** ( $\text{CD}_2\text{Cl}_2$ /pyridine):  $\delta$  [ppm] = 1.31 (s, 48H, C-5/C-6/C-7/C-8,  $\text{NC}(\text{CH}_2)_{10}\text{CN}$ ), 1.41 (s, 24H, C-4/C-9,  $\text{NC}(\text{CH}_2)_{10}\text{CN}$ ), 1.44 (s, 195H,  $[\text{Cp}^*\text{Fe}(\eta^5\text{-P}_5)]$ ), 1.64 (m, 24H, C-3/C-10,  $\text{NC}(\text{CH}_2)_{10}\text{CN}$ ), 2.33 (t, 24H, C-2/C-11,  $\text{NC}(\text{CH}_2)_{10}\text{CN}$ ), 7.37 (m,  $\beta$ -H, pyridine), 7.77 (m,  $\gamma$ -H, pyridine), 8.59 (m,  $\alpha$ -H, pyridine).

**$^{13}\text{C}$  NMR** ( $\text{CD}_2\text{Cl}_2$ /pyridine):  $\delta$  [ppm] = 10.63 ( $\text{Cp}(\text{CH}_3)_5\text{Fe}(\eta^5\text{-P}_5)$ ), 17.01 (C-2/C-11,  $\text{NC}(\text{CH}_2)_8\text{CN}$ ), 25.34 (C-3/C-10,  $\text{NC}(\text{CH}_2)_8\text{CN}$ ), 28.6 (C-4/C-9,  $\text{NC}(\text{CH}_2)_8\text{CN}$ ), 28.67 (C-5/C-8,  $\text{NC}(\text{CH}_2)_8\text{CN}$ ), 29.14 (C-6/C-7,  $\text{NC}(\text{CH}_2)_8\text{CN}$ ), 124.19 ( $\beta$ -C, pyridine), 136.85 ( $\gamma$ -C, pyridine), 146.45 ( $\alpha$ -C, pyridine). No signal for ( $\text{NC}(\text{CH}_2)_8\text{CN}$ ) was found.

**$^{31}\text{P}\{^1\text{H}\}$  NMR** ( $\text{CD}_2\text{Cl}_2$ /pyridine):  $\delta$  [ppm] = 145.15 (s (br),  $[\text{Cp}^*\text{Fe}(\eta^5\text{-P}_5)]$ ), 145.57 (s (vbr),  $[\text{Cp}^*\text{Fe}(\eta^5\text{-P}_5)]$ ).

**$^{19}\text{F}$  NMR** ( $\text{CD}_2\text{Cl}_2$ /pyridine): no signal was detected.

**Positive ion ESI-MS** ( $\text{CH}_2\text{Cl}_2/\text{CH}_3\text{CN}$  (1:1)):  $m/z$  (%) = 2522.0  $[\{\text{Cp}^*\text{Fe}(\eta^5\text{-P}_5)\}_4\text{Ag}_4(\text{SbF}_6)_3]^+$ , 2178.2  $[\{\text{Cp}^*\text{Fe}(\eta^5\text{-P}_5)\}_4\text{Ag}_3(\text{SbF}_6)_2]^+$ , 1832.3  $[\{\text{Cp}^*\text{Fe}(\eta^5\text{-P}_5)\}_3\text{Ag}_3(\text{SbF}_6)_2]^+$ , 1678.5  $[\{\text{Cp}^*\text{Fe}(\eta^5\text{-P}_5)\}_2\text{Ag}_3(\text{SbF}_6)_2(\text{NC}(\text{CH}_2)_{10}\text{CN})]^+$ , 798.7  $[\{\text{Cp}^*\text{Fe}(\eta^5\text{-P}_5)\}_2\text{Ag}]^+$ , 645.0  $[\{\text{Cp}^*\text{Fe}(\eta^5\text{-P}_5)\}\text{Ag}(\text{NC}(\text{CH}_2)_{10}\text{CN})]^+$ , 493.9 (100)  $[\{\text{Cp}^*\text{Fe}(\eta^5\text{-P}_5)\}\text{Ag}(\text{CH}_3\text{CN})]^+$ , 452.8  $[\{\text{Cp}^*\text{Fe}(\eta^5\text{-P}_5)\}\text{Ag}]^+$ .

**Negative ion ESI-MS** ( $\text{CH}_2\text{Cl}_2/\text{CH}_3\text{CN}$  (1:1)):  $m/z$  (%) = 2647.9  $[\{\text{Cp}^*\text{Fe}(\eta^5\text{-P}_5)\}_4\text{Ag}_3(\text{SbF}_6)_4]^-$ , 1958.1  $[\{\text{Cp}^*\text{Fe}(\eta^5\text{-P}_5)\}_3\text{Ag}_2(\text{SbF}_6)_3]^-$ , 234.9 (100)  $[\text{SbF}_6]^-$ .

**Elemental analysis:** Calculated (%) for  $[\text{Cp}^*\text{Fe}(\eta^5\text{-P}_5)]@[\{\text{Cp}^*\text{Fe}(\eta^5\text{-P}_5)\}_{12}(\text{AgSbF}_6)_{12}(\text{NC}(\text{CH}_2)_{10}\text{CN})_6(\text{C}_7\text{H}_8)]$  (9866.57 g/mol): C 25.44, H 3.30, N 1.70; found: C 25.47, H 3.28, N 1.73.

**IR:**  $\tilde{\nu}/\text{cm}^{-1}$  = 2930 (vw), 2268 (vw), 1476 (w), 1425 (w), 1378 (w), 1075 (vw), 1020 (w), 656 (s).



## 6.5 Crystallographic Details

Crystals of **2-5** were taken from a Schlenk flask under a stream of argon and immediately covered with perfluorinated Fomblin® mineral oil to prevent both, decomposition and a loss of solvent. The quickly chosen single crystals covered by a drop of the oil were directly placed into a stream of cold nitrogen with the pre-centered goniometer head with CryoMount® and attached to the goniometer of a diffractometer.

The data for **2-5** were collected on an Agilent Technologies diffractometer equipped with a Titan<sup>S2</sup> CCD detector and a SuperNova Cu K $\alpha$  microfocus source using either 1° (**3-5**) or 0.5° (**2**)  $\omega$  scans depending on the unit cell constants. Analytical absorption correction for **2-5** was applied based on crystal faces. Crystallographic data and further details of the diffraction experiments are given in *Tables 2-5*.

The structures were solved by direct methods with *SHELXT*<sup>[19]</sup> and were refined by full-matrix least-squares method against  $F^2$  in anisotropic approximation using multiprocessor variable memory versions of *SHELXL* (2014-2015).

In **4** and **5** the  $\text{SbF}_6^-$  counter-anions are disordered over two or more close positions. The occupation factors for disordered positions of Sb atoms were refined with fixed isotropic  $U_{\text{iso}}$  similar to the average  $U_{\text{iso}}$  (usually 0.025-0.035 Å<sup>2</sup>) for the fully occupied heavy atoms in the corresponding structure. In **3**, a strong tendency for disorder of the  $[\text{Al}\{\text{OC}(\text{CF}_3)_3\}_4]^-$  anion was partly suppressed by using lower temperature,  $T = 90\text{K}$ . At the same time weak superstructural reflections appeared in the diffraction pattern suggesting a twice as large unit cell,  $a = 14.5454(4)$ ,  $b = 17.0363(4)$ ,  $c = 24.6987(4)$  Å,  $\alpha = 94.7898(17)$ ,  $\beta = 99.0389(19)$ ,  $\gamma = 101.822(2)^\circ$ ,  $V = 5873.6(2)$  Å<sup>3</sup> (*cf.* Table 5). The temperature-induced superstructural ordering was traced back to the ordering process of the  $[\text{Al}\{\text{OC}(\text{CF}_3)_3\}_4]^-$  anions; however, doubled structural model in the larger unit cell returned higher  $R_1 = 0.11$  and other quality factors, due to rather small impact of the ordering. Obviously, to consider the superstructural model, one needs to perform a diffraction experiment at deeper temperatures unavailable in-house. Therefore, the model in the small unit cell was preferred resulting in reasonable well-modeled re-orientation of the eight  $\text{CF}_3$  groups and two close positions one  $\text{C}(\text{CF}_3)_3$  group. All other structural fragments stay ordered in both structural models. The final results of the refinement are shown in *Table 5*.

The flexible linker molecules also showed a strong tendency for disorder. In **2** the dinitrile molecules were disordered typically over two close positions with different occupancies. Their molecular site

occupancy factors (equal s.o.f.'s for all atoms of a molecule) were refined using the FVAR instruction of SHELX with isotropic displacement parameters fixed at  $U_{iso} = 0.05 \text{ \AA}^{-2}$ . The resulting occupancies were fixed and the C and N atoms with occupancies of more than 0.5 were refined in anisotropic approximation. Some minor positions of the linker molecules were refined with restraint geometry. The restraints were removed at the final stage of the refinement when possible. The disorder of the solvent molecules ( $\text{CH}_2\text{Cl}_2$ ) was treated in a similar way.

In **4**, an unusual type of positional disorder takes place. One unique position of a Ag atom (Ag1 and Ag1a) is split into two close ones in a refined ratio of 1 : 1, followed by one of two unique positions of flexible dinitrile ligands overlapping with partly occupied solvent  $\text{CH}_2\text{Cl}_2$  molecule in the same ratio. The resulting coordination environment of the Ag1a position is trigonal with one  $\sigma$ -coordinating *cyclo*-P<sub>5</sub> ligand and two N of the dinitrile linkers; whereas that of Ag1 is pseudo-tetrahedral with one linker molecule, one  $\eta^2$ -coordinating and one  $\sigma$ -coordinating *cyclo*-P<sub>5</sub> ligand.

In crystals of **8**, weak superstructural reflections appeared in the diffraction pattern suggesting a three times as large unit cell as preliminary found unit cell with  $c = 22.41 \text{ \AA}$  (*cf.* Table 5). To collect diffraction data for the weak superstructural reflections, the crystals of **8** were carefully selected, mounted on a magnetic holder, checked for quality and placed into a Dewar vessel with liquid nitrogen using standard cryocrystallography tools. After a few weeks it was taken to the DESY PETRA III synchrotron. Using standard procedures it was placed into a special Dewar vessel filled with liquid nitrogen among other crystals. A robotic mounting/demounting was used for further manipulations in the P11 beamline hutch.<sup>16</sup> X-ray diffraction experiment for **8** were measured at 10 K using robotic mounting.<sup>20</sup> The data collection was acquired by  $360^\circ$   $\phi$ -rotation with  $0.3^\circ$  scan width and exposure 0.3 s per frame at wavelength  $\lambda = 0.6702 \text{ \AA}$  (18.5 keV). Data reduction for all data sets was performed with CrysAlis software.<sup>21</sup> Due to partial radiolysis only those frames were taken into integration, which were not affected by decomposition of the crystal. Empirical absorption correction using equivalent reflections was used.

For supramolecular compounds **6-8**, the refinement of the structural models is not finished. The refinement is complicated by disorder of the silver atoms and in some cases of also pentaphosphaferrocene building blocks in the inorganic cores of the supramolecular nodes, by severe disorder of the guest molecules of pentaphosphaferrocene, dinitrile linkers, counter-anions  $\text{SbF}_6^-$  and solvent molecules. Therefore, only up-to-date stage of the refinement is presented in Tables 4 and 5.

**Table 2:** Experimental details for compound **2** and **3**.

Crystal data	<b>2</b>	<b>3</b>
Chemical formula	C <sub>20</sub> H <sub>31</sub> CuFeN <sub>2</sub> P <sub>5</sub> ·BF <sub>4</sub> ·CH <sub>2</sub> Cl <sub>2</sub>	C <sub>22</sub> H <sub>35</sub> AgFeN <sub>2</sub> P <sub>5</sub> ·AlO <sub>4</sub> C <sub>16</sub> F <sub>36</sub>
<i>M<sub>r</sub></i>	745.44	1613.23
Crystal system, space group	monoclinic, <i>P</i> 2 <sub>1</sub> / <i>n</i>	triclinic, <i>P</i> $\bar{1}$
Temperature (K)	123	90
<i>a</i> , <i>b</i> , <i>c</i> (Å)	13.8554 (4), 29.4734 (6), 16.2907 (4)	14.3748 (4), 14.5419 (3), 17.0377 (4)
$\alpha$ , $\beta$ , $\gamma$ (°)	90, 111.967 (3), 90	101.7960 (19), 114.678 (2), 104.408 (2)
<i>V</i> (Å <sup>3</sup> )	6169.6 (3)	2935.83 (13)
<i>Z</i>	8	2
<i>F</i> (000)	3024	1588
<i>D<sub>x</sub></i> (Mg m <sup>-3</sup> )	1.605	1.825
Radiation type	Cu K $\alpha$	Cu K $\alpha$
$\mu$ (mm <sup>-1</sup> )	9.01	7.53
Crystal shape	prism	plate
Colour	brown	green
Crystal size (mm)	0.37 × 0.25 × 0.11	0.22 × 0.16 × 0.14
Data collection		
Diffractionmeter	SuperNova, Titan <sup>S2</sup>	SuperNova, Titan <sup>S2</sup>
Absorption correction	Gaussian	Gaussian
<i>T<sub>min</sub></i> , <i>T<sub>max</sub></i>	0.177, 0.467	0.398, 0.663
No. of measured, independent and observed [ <i>I</i> > 2 $\sigma$ ( <i>I</i> )] reflections	36724, 12270, 10021	20956, 11710, 10941
<i>R<sub>int</sub></i>	0.035	0.052
(sin $\theta$ / $\lambda$ ) <sub>max</sub> (Å <sup>-1</sup> )	0.624	0.628
Range of <i>h</i> , <i>k</i> , <i>l</i>	<i>h</i> = -16 → 17, <i>k</i> = -36 → 33, <i>l</i> = -20 → 14	<i>h</i> = -17 → 16, <i>k</i> = -16 → 17, <i>l</i> = -19 → 21
Refinement		
<i>R</i> [ <i>F</i> <sup>2</sup> > 2 $\sigma$ ( <i>F</i> <sup>2</sup> )], <i>wR</i> ( <i>F</i> <sup>2</sup> ), <i>S</i>	0.041, 0.113, 1.04	0.067, 0.200, 1.06
No. of reflections	12268	11710
No. of parameters	733	1091
No. of restraints	0	60
H-atom treatment	H-atom parameters constrained	H-atom parameters constrained
$\Delta$ <sub>max</sub> , $\Delta$ <sub>min</sub> (e Å <sup>-3</sup> )	0.79, -0.77	1.51, -2.58

Computer programs for **2**: CrysAlis PRO 1.171.38.41 (Rigaku OD, 2015), SHELXT2014/7 (Sheldrick, 2014), SHELXL2014/7 (Sheldrick, 2014).

Computer programs for **3**: CrysAlis PRO 1.171.39.45g (Rigaku OD, 2018), SHELXT2014/7 (Sheldrick, 2014), SHELXL2014/7 (Sheldrick, 2014).

**Table 3:** Experimental details for compounds **4** and **5**.

Crystal data	<b>4</b>	<b>5</b>
Chemical formula	C <sub>50</sub> H <sub>51</sub> AgFeN <sub>2</sub> P <sub>5</sub> ·F <sub>6</sub> Sb	C <sub>196</sub> H <sub>200</sub> N <sub>6</sub> Ag <sub>4</sub> Fe <sub>4</sub> P <sub>20</sub> ·4(F <sub>6</sub> Sb)·2(CH <sub>2</sub> Cl <sub>2</sub> )
<i>M<sub>r</sub></i>	1234.24	4941.81
Crystal system, space group	monoclinic, <i>P</i> <sub>2</sub> <sub>1</sub> / <i>n</i>	monoclinic, <i>P</i> <sub>2</sub> <sub>1</sub> / <i>n</i>
Temperature (K)	123	123
<i>a</i> , <i>b</i> , <i>c</i> (Å)	18.2093 (3), 9.5766 (2), 28.3305 (5)	18.0693 (7), 10.2568 (4), 26.9826 (10)
<i>β</i> (°)	95.8409 (18)	101.848 (4)
<i>V</i> (Å <sup>3</sup> )	4914.71 (17)	4894.2 (3)
<i>Z</i>	4	1
<i>F</i> (000)	2472	2472
<i>D<sub>x</sub></i> (Mg m <sup>-3</sup> )	1.668	1.677
Radiation type	Cu Kα	Cu Kα
<i>μ</i> (mm <sup>-1</sup> )	11.86	12.16
Crystal shape	plate	elongated plate
Colour	brown-green	brown-green
Crystal size (mm)	0.72 × 0.33 × 0.06	1.08 × 0.15 × 0.02
<b>Data collection</b>		
Diffractometer	SuperNova, Titan <sup>S2</sup>	SuperNova, Titan <sup>S2</sup>
Absorption correction	Gaussian	Gaussian
<i>T<sub>min</sub></i> , <i>T<sub>max</sub></i>	0.029, 0.514	0.069, 0.793
No. of measured, independent and observed [ <i>I</i> > 2σ( <i>I</i> )] reflections	22717, 9531, 8185	20020, 9587, 7407
<i>R<sub>int</sub></i>	0.056	0.032
(sin <i>θ</i> /λ) <sub>max</sub> (Å <sup>-1</sup> )	0.622	0.623
Range of <i>h</i> , <i>k</i> , <i>l</i>	<i>h</i> = -22 → 17, <i>k</i> = -11 → 10, <i>l</i> = -30 → 34	<i>h</i> = -22 → 22, <i>k</i> = -8 → 12, <i>l</i> = -33 → 24
<b>Refinement</b>		
<i>R</i> [ <i>F</i> <sup>2</sup> > 2σ( <i>F</i> <sup>2</sup> )], <i>wR</i> ( <i>F</i> <sup>2</sup> ), <i>S</i>	0.040, 0.103, 0.98	0.036, 0.093, 0.97
No. of reflections	9531	9587
No. of parameters	595	723
No. of restraints	0	0
H-atom treatment	H-atom parameters constrained	H-atom parameters constrained
Δ <sub>max</sub> , Δ <sub>min</sub> (e Å <sup>-3</sup> )	1.52, -1.41	0.58, -0.73

Computer programs for **4**: CrysAlis PRO 1.171.38.41 (Rigaku OD, 2015), SHELXT2014 (Sheldrick, 2014), SHELXL2014/7 (Sheldrick, 2014).

Computer programs for **5**: CrysAlis PRO 1.171.38.41 (Rigaku OD, 2015), SHELXT2014/7 (Sheldrick, 2014), SHELXL2014/7 (Sheldrick, 2014).

**Table 4:** Experimental details for compounds **6** and **7**, (\*) preliminary data.

Crystal data	6	7
Chemical formula	C <sub>190</sub> H <sub>291</sub> Ag <sub>12</sub> F <sub>72</sub> Fe <sub>13</sub> N <sub>12</sub> P <sub>65</sub> Sb <sub>12</sub> (*)	C <sub>196</sub> H <sub>303</sub> Ag <sub>12</sub> F <sub>72</sub> Fe <sub>13</sub> N <sub>12</sub> P <sub>65</sub> Sb <sub>12</sub> (*)
$M_r$	9606.11 (*)	9690.27 (*)
Crystal system, space group	orthorhombic, <i>Pccn</i>	orthorhombic, <i>Pccn</i>
Temperature (K)	100	100
$a, b, c$ (Å)	30.9896(3), 34.8444(3), 32.1679(3)	31.49535(16), 35.1511(2), 32.1736(2)
$\alpha, \beta, \gamma$ (°)	90, 90, 90	90, 90, 90
$V$ (Å <sup>3</sup> )	34735.3(5)	35619.3(3)
$Z$	4	4
Radiation type	Cu $K\alpha$	Cu $K\alpha$
Crystal shape	plate	prism
Colour	green-brown	green-brown
Crystal size (mm)	0.29 × 0.23 × 0.09	0.42 × 0.34 × 0.23
<b>Data collection</b>		
Diffractometer	SuperNova, Titan <sup>S2</sup>	SuperNova, Titan <sup>S2</sup>
Absorption correction	Gaussian	Gaussian
No. of measured, independent and observed [ $I > 2\sigma(I)$ ] reflections	120036, 34786, 26176	180408, 35894, 29158
$R_{\text{int}}$	0.0564	0.0767
Range of $h, k, l$	$h = -37 \rightarrow 38, k = -43 \rightarrow 41, l = -30 \rightarrow 39$	$h = -39 \rightarrow 43, k = -38 \rightarrow 39, l = -38 \rightarrow 39$
<b>Refinement</b>		
$R[F^2 > 2\sigma(F^2)], wR(F^2), S$	0.0644, 0.1838, 1.006	0.0775, 0.2181, 1.030
No. of reflections	34786	35894
No. of parameters	2089	2146
No. of restraints	0	9
H-atom treatment	H atoms constrained	H atoms constrained
$\Delta_{\text{max}}, \Delta_{\text{min}}$ (e Å <sup>-3</sup> )	1.39, -2.82	2.17, -2.58

**Table 5:** Experimental details for compounds **8** and **9**, (\*) preliminary data.

Crystal data	<b>8</b>	<b>9</b>
Chemical formula	C <sub>202</sub> H <sub>315</sub> Ag <sub>12</sub> F <sub>72</sub> Fe <sub>13</sub> N <sub>12</sub> P <sub>65</sub> Sb <sub>12</sub> (*)	C <sub>32</sub> H <sub>50</sub> Ag <sub>2</sub> Fe <sub>2</sub> N <sub>2</sub> P <sub>10</sub> ·2(SbF <sub>6</sub> )·CH <sub>2</sub> Cl <sub>2</sub>
<i>M<sub>r</sub></i>	9774.43 (*)	1656.30
Crystal system, space group	monoclinic, <i>P</i> 2 <sub>1</sub>	Monoclinic, <i>P</i> 2 <sub>1</sub> / <i>m</i>
Temperature (K)	10	123
<i>a</i> , <i>b</i> , <i>c</i> (Å)	23.87241(6), 34.13292(7), 67.2276(2)	11.7403 (2), 12.5880 (2), 19.0497 (4)
<i>α</i> , <i>β</i> , <i>γ</i> (°)	90, 93.3919(2), 90	105.899 (2)
<i>V</i> (Å <sup>3</sup> )	54683.4(2)	2707.60 (9)
<i>Z</i>	8	2
<i>F</i> (000)		1608
<i>D<sub>x</sub></i> (Mg m <sup>-3</sup> )		2.032
Radiation type	synchrotron	Cu <i>Kα</i>
<i>μ</i> (mm <sup>-1</sup> )		21.64
Crystal shape	prism	Block
Colour	green-brown	Green
Crystal size (mm)	0.10 × 0.10 × 0.06	0.20 × 0.17 × 0.08
<b>Data collection</b>		
Diffractometer	synchrotron, 1-axis goniostat	SuperNova, TitanS2
Absorption correction	empirical	Gaussian
<i>T<sub>min</sub></i> , <i>T<sub>max</sub></i>		0.088, 0.345
No. of measured, independent and observed [ <i>I</i> > 2σ( <i>I</i> )] reflections	860861, 110760, 63320	10544, 5533, 4662
<i>R<sub>int</sub></i>	0.0682	0.039
(sin <i>θ</i> /λ) <sub>max</sub> (Å <sup>-1</sup> )	0.676	0.623
Range of <i>h</i> , <i>k</i> , <i>l</i>	<i>h</i> = -32→32, <i>k</i> = -46→46, <i>l</i> = -88→88	<i>h</i> = -14→11, <i>k</i> = -15→11, <i>l</i> = -23→19
<b>Refinement</b>		
<i>Refinement on</i>	0.2021, 0.6503, 2.693	<i>F</i> <sup>2</sup>
<i>R</i> [ <i>F</i> <sup>2</sup> > 2σ( <i>F</i> <sup>2</sup> )], <i>wR</i> ( <i>F</i> <sup>2</sup> ), <i>S</i>	110760	0.040, 0.104, 0.99
No. of reflections	3970	5533
No. of parameters	0	328
No. of restraints	-	0
H-atom treatment	7.09, -2.76	H-atom parameters constrained
Δ <sub>max</sub> , Δ <sub>min</sub> (e Å <sup>-3</sup> )	0.2021, 0.6503, 2.693	0.90, -1.79

Computer programs for **9**: CrysAlis PRO 1.171.38.42b (Rigaku OD, 2015), SHELXS2013 (Sheldrick, 2013), SHELXL2013 (Sheldrick, 2013).

## 6.6 Author Contributions

- The synthesis and characterization of all compounds were performed by B. Hiltl.
- The manuscript (introduction, results and discussions, experimental part, conclusion; including figures and graphical abstract) was written by B. Hiltl.
- The section 'crystallographic details' was written by Dr. E. Peresypkina.
- In-house X-ray structure analyses were performed by Dr. E. Peresypkina and Dr. Sc. A. V. Virovets with B. Hiltl.
- Synchrotron measurements including sample preparation, data reduction and all calculations were performed by Dr. E. Peresypkina and Dr. Sc. A. V. Virovets.
- MAS NMR investigation of E was performed by Prof. W. Kremer.
- TEM measurements were performed by J. Hilgert.

## 6.7 References

- <sup>1</sup> a) M. Otte, *ACS Catal.* **2016**, *6*, 6491-6510; b) S. Zarra, D. M. Wood, D. A. Roberts, J. R. Nitschke, *Chem. Soc. Rev.* **2015**, *44*, 419-432; c) D. Ajami, L. Liu, J. Rebek, Jr., *Chem. Soc. Rev.* **2015**, *44*, 490-499; d) P. Ballester, M. Fujita, J. Rebek, Jr., *Chem. Soc. Rev.* **2015**, *44*, 392-393; e) W. Meng, A. B. League, T. K. Ronson, J. K. Clegg, W. C. Isley, D. Semrouni, L. Gagliardi, C. J. Cramer, J. R. Nitschke, *J. Am. Chem. Soc.* **2014**, *136*, 3972-3980; f) Y. Inokuma, M. Kawano, M. Fujita, *Nat. Chem.* **2011**, *3*, 349-358; g) C. J. Hastings, M. D. Pluth, R. G. Bergman, K. N. Raymond, *J. Am. Chem. Soc.* **2010**, *132*, 6938-6940.
- <sup>2</sup> a) K. Rissanen, *Chem Soc Rev* **2017**, *46*, 2638-2648.; b) Y. Inokuma, S. Yoshioka, J. Ariyoshi, T. Arai, Y. Hitora, K. Takada, S. Matsunaga, K. Rissanen, M. Fujita, *Nature* **2013**, *495*, 461-466.
- <sup>3</sup> a) X. Yang, Q. Xu, *Cryst. Growth Des.* **2017**, *17*, 1450-1455; b) K. Sumida, D. L. Rogow, J. A. Mason, T. M. McDonald, E. D. Bloch, Z. R. Herm, T.-H. Bae, J. R. Long, *Chem. Rev.* **2012**, *112*, 724-781; c) M. P. Suh, H. J. Park, T. K. Prasad, D.-W. Lim, *Chem. Rev.* **2012**, *112*, 782-835; d) J.-R. Li, R. J. Kuppler, H.-C. Zhou, *Chem. Soc. Rev.* **2009**, *38*, 1477-1504.
- <sup>4</sup> a) G. Ji, J. Liu, X. Gao, W. Sun, J. Wang, S. Zhao, Z. Liu, *J. Mater. Chem. A* **2017**, *5*, 10200-10205; b) Y. Yu, J.-P. Ma, C.-W. Zhao, J. Yang, X.-M. Zhang, Q.-K. Liu, Y.-B. Dong, *Inorg. Chem.* **2015**, *54*, 11590-11592; c) L. E. Kreno, K. Leong, O. K. Farha, M. Allendorf, R. P. Van Duyne, J. T. Hupp, *Chem. Rev.* **2012**, *112*, 1105-1125.
- <sup>5</sup> a) Y. Inokuma, T. Arai, M. Fujita, *Nat. Chem.* **2010**, *2*, 780-783; b) S. Matsuzaki, T. Arai, K. Ikemoto, Y. Inokuma, M. Fujita, *J. Am. Chem. Soc.* **2014**, *136*, 17899-17901.

- 6 a) M. Yoshizawa, J. K. Klosterman, M. Fujita, *Angew. Chem. Int. Ed.* **2009**, *48*, 3418-3438, b) M. Fujita, D. Oguro, M. Miyazawa, H. Oka, K. Yamaguchi, K. Ogura, *Nature* **1995**, *378*, 469-471.
- 7 Z. Wang, X.-Y. Li, L.-W. Liu, S.-Q. Yu, Z.-Y. Feng, C.-H. Tung, D. Sun, *Chem. Eur. J.* **2016**, *22*, 6830-6836.
- 8 a) E. Peresypkina, C. Heindl, A. Virovets, H. Brake, E. Maedl, M. Scheer, *Chem. Eur. J.* **2018**, *24*, 2503-2508; b) F. Dielmann, M. Fleischmann, C. Heindl, E. V. Peresypkina, A. V. Virovets, R. M. Gschwind, M. Scheer, *Chem. Eur. J.* **2015**, *21*, 6208-6214; c) C. Schwarzmaier, A. Schindler, C. Heindl, S. Scheuermayer, E. V. Peresypkina, A. V. Virovets, M. Neumeier, R. Gschwind, M. Scheer, *Angew. Chem., Int. Ed.* **2013**, *52*, 10896-10899; d) A. Schindler, C. Heindl, G. Balazs, C. Groeger, A. V. Virovets, E. V. Peresypkina, M. Scheer, *Chem. Eur. J.* **2012**, *18*, 829-835; e) M. Scheer, A. Schindler, R. Merkle, B. P. Johnson, M. Linseis, R. Winter, C. E. Anson, A. V. Virovets, *J. Am. Chem. Soc.* **2007**, *129*, 13386-13387; f) J. Bai, A. V. Virovets, M. Scheer, *Science* **2003**, *300*, 781-783.
- 9 Diameter were calculated considering the maximum distance between two F atoms plus twice the van der Waals radius of F (147 ppm from A. Bondi, *J. Phys. Chem.* **1964**, *68*, 441-451).
- 10 M. Detzel, G. Friedrich, O. J. Scherer and G. Wolmershäuser, *Angew. Chem. Int. Ed.* **1995**, *34*, 1321.
- 11 The diameter on the level of the Cp residues were calculated as the distance of one H atom of one methylene group to the center of the H atoms of two opposing methylene groups plus twice the van der Waals radius of C (170 pm). The length of the complexes **1** were calculated as the atom-to-plane distance of the centroids of the *cyclo*-P<sub>5</sub> residues to the planes through the most distant H atoms of the Cp<sup>R</sup> residue plus the van der Waals radii of P (180 pm) and H (110 pm). Van der Waals radii were used according to A. Bondi, *J. Phys. Chem.* **1964**, *68*, 441-451.
- 12 F. Dielmann, R. Merkle, S. Heindl, M. Scheer, *Z. Naturforsch.* **2009**, *64*, 3.
- 13 The distances between the *cyclo*-P<sub>5</sub> rings of host and scaffold were calculated as the distance of the centroid of the *cyclo*-P<sub>5</sub> ring of the host scaffold to the plane through the five P atoms of the guest.
- 14 M. Scheer, A. Schindler, J. Bai, B. P. Johnson, R. Merkle, R. Winter, A. V. Virovets, E. V. Peresypkina, V. A. Blatov, M. Sierka, H. Eckert, *Chem. Eur. J.* **2010**, *16*, 2092-2107.
- 15 a) V. A. Blatov, A. P. Shevchenko, D. M. Proserpio, *Cryst. Growth Des.* **2014**, *14*, 3576-3586; b) V. A. Blatov, M. O'Keeffe, D. M. Proserpio, *CrystEngComm* **2010**, *12*, 44-48; c) <http://rcsr.net/>
- 16 F. Dielmann, R. Merkle, S. Heindl, M. Scheer, *Z. Naturforsch.* **2009**, *64*, 3.
- 17 I. Krossing, *Chem. Eur. J.* **2001**, *7*, 490-502.
- 18 a) C. T. Rueden, J. Schindelin, M. C. Hiner, et al. *BMC Bioinformatics* **2017**, *18*, 529; b) C. A. Schneider, W. S. Rasband, K. W. Eliceiri, *Nature methods* **2012**, *9*, 7, 671-675; c) J. Schindelin, I. Arganda-Carreras, E. Frise, et al. *Nature methods* **2012**, *9*, 7, 676-682.
- 19 G. M. Sheldrick, *Acta Cryst. sect. C* **2015**, *C71*, 3.
- 20 A. Burkhardt, T. Pakendorf, B. Reime, et al, *Eur. Phys. J. Plus* **2016**, *131*, 56-64.
- 21 CrysAlis Pro. Different versions (Rigaku OD).

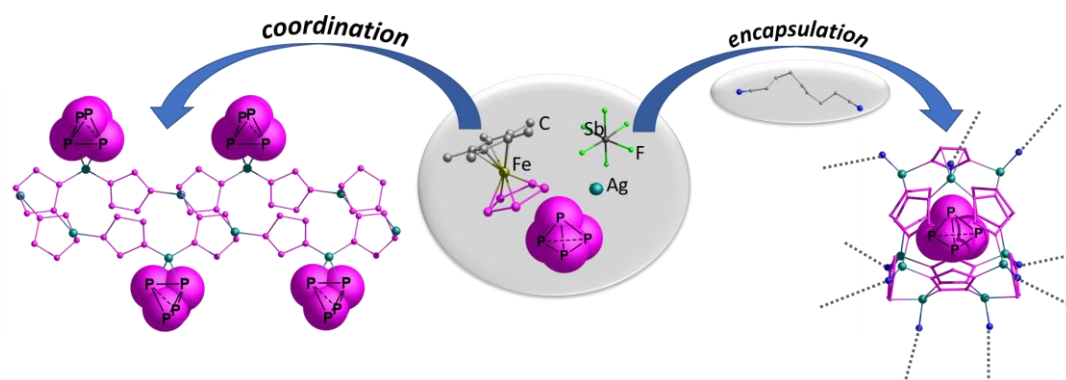




## 7. Polymeric Supramolecular Assemblies: Encapsulation or Coordination of White Phosphorus

B. Hiltl, E. Peresyphkina, A. V. Virovets, G. Balász, W. Kremer, M. Scheer

### Graphical Abstract



### Abstract:

By adding white phosphorus to the self-assembly system of  $[\text{Cp}^*\text{Fe}(\eta^5\text{-P}_5)]$  (**1**) and  $\text{AgSbF}_6$ , a 1D coordination polymer  $[\{\text{Cp}^*\text{Fe}(\eta^5\text{-P}_5)\}_2\{\text{Ag}_2(\eta^2\text{-P}_4)\}_n[\text{SbF}_6]_{2n}$  (**3c**) was obtained, with  $\text{P}_4$  tetrahedra acting as ligands towards Ag atoms. Furthermore, as a rare example of a four-component self-assembly a series of novel networked polycationic supramolecular assemblies **4a-c** are formed in the presence of a flexible dinitrile  $\text{NC}(\text{CH}_2)_{10}\text{CN}$  as a linker, all featuring similar supramolecular host-guest aggregates templated by  $\text{P}_4$  molecules with a sum formula of  $[\text{P}_4@[\{\text{Cp}^*\text{Fe}(\eta^5\text{-P}_5)\}_9\text{Ag}_x]]^{11+}$  ( $x = 8 - 10$ ) as nodes. All these compounds can easily release either coordinated (**3c**) or encapsulated (**4a-c**)  $\text{P}_4$  upon losing their polymeric structure. In addition to X-ray structure analysis, the intact tetrahedral structure and the bonding situation of the coordinated  $\text{P}_4$  in **3c** were investigated by single point DFT calculations. Furthermore, crystalline material of both reactions was characterized by  $^{31}\text{P}$  MAS NMR and Raman spectroscopy.

## 7.1 Introduction

Host molecules can be a powerful tool for different purposes. Besides catalytic improvement<sup>1</sup> and drug delivery,<sup>2</sup> the storage and stabilization of labile molecules<sup>3</sup> is a top goal in supramolecular chemistry and has already furnished various achievements. White phosphorus ( $P_4$ ) being an extremely reactive and metastable molecule is needed as a starting material in both, academic research and industry. The interests in activation of the tetrahedral molecule<sup>4</sup> and the attractive synthetic way to generate pure phosphoric acid and organophosphorus compounds make  $P_4$  indispensable. Its use, though, goes along with severe restrictions concerning handling and shipping, due to its toxicity, high reactivity and its metastability to light. By involving supramolecular cage compounds, several approaches were developed to stabilize  $P_4$ , as e.g. by the incorporation in a matrix of a coordination polymer,<sup>5</sup> in self-assembled discrete capsules<sup>5,6</sup> or in porous material.<sup>7</sup> Thus, *Nitschke* et al. reported on a water-soluble tetrahedral shaped Fe-based capsule, incorporating  $P_4$  (*Figure 1a*).<sup>6b</sup> Therein enclosed, white phosphorus is air-stable and can be extracted by appropriate solvents. A facile and efficient way to store and release white phosphorus and yellow arsenic recently was presented by our group.<sup>7b</sup> By adsorption of the dissolved starting materials on the activated porous carbon material, an air- and light-stable material results (*Figure 1a*). It can be used for storage as well as a convenient source for subsequent reactions due to its high loading capacities of 36 (weight) %.

Our interests lie also in supramolecular compounds based on the polyphosphorus complex  $[Cp^RFe(\eta^5-P_5)]$  ( $Cp^R = Cp^*$  (**1**),  $Cp^{Bn}$ ) and copper halides, which can form diverse coordination polymers or spherical aggregates acting as hosts for a wide range of guest molecules, irrespective of their size, symmetry and charge.<sup>8</sup> Thus, also  $P_4$  and  $As_4$  were successfully incorporated in both, a 1D coordination polymer acting as a matrix for the small molecules, or in the inner void of the capsule  $[(Cp^*Fe(\eta^5-P_5))_{10}Cu_{30}I_{30}(CH_3CN)_6]$  (*Figure 1b*).<sup>6a</sup> Besides copper halides, silver salts ( $AgOTf$ ,  $AgSbF_6$ ) can provide suitable building blocks to form supramolecular host scaffolds, which can incorporate **1** itself (cf. *Chapter III, VI*) or the  $SbF_6^-$  anion (cf. *Chapter IV and V*). The use of  $SbF_6^-$  as a weakly coordinating anion provides free coordination sites on the scaffold building  $Ag^+$  cations. When flexible ditopic nitriles are introduced in this system as donating linkers, 3D coordination networks of connected spherical host scaffolds can be formed *in situ* by a complete self-assembly (*Figure 1c*, cf. *Chapter V, VI*).

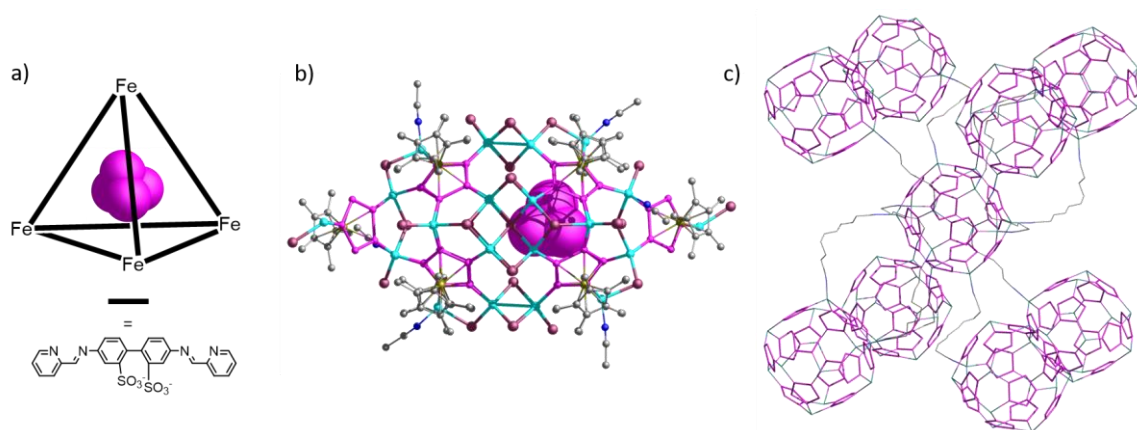
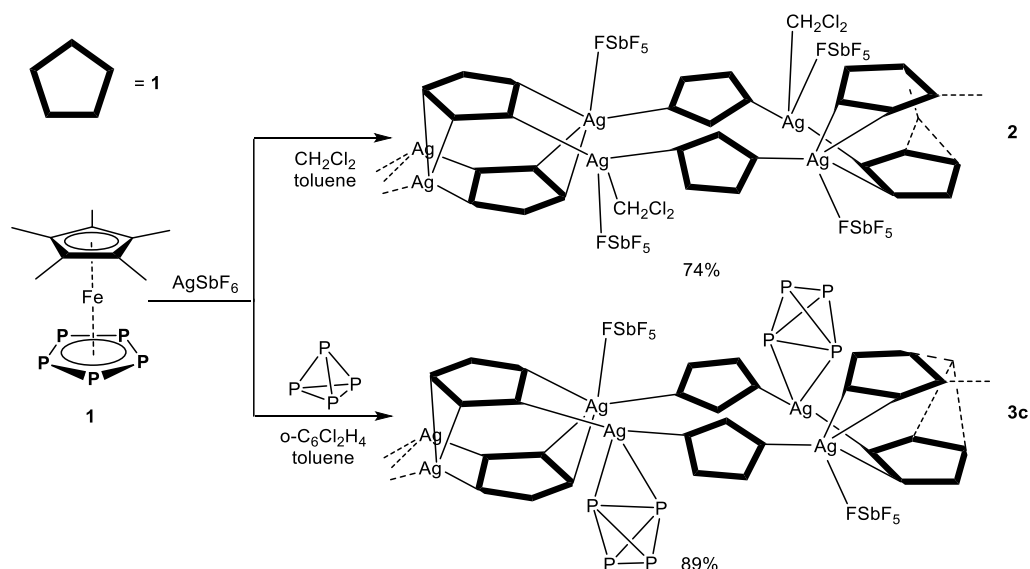


**Figure 1:** Stabilization of P<sub>4</sub> in a capsule based on a) Fe<sup>2+</sup> and a N-donor linker,<sup>6b</sup> b) **1** and CuI,<sup>6a</sup> c) 3D coordination network of spherical host aggregates based on **1**, AgSbF<sub>6</sub> and NC(CH<sub>2</sub>)<sub>x</sub>CN (x = 8, 9) (cf. Chapter V).

Encouraged by the excellent up-take abilities of Cu based polymers and spherical aggregates, together with the possibility of establishing a network of host-guest aggregates by implementing linkers in the self-assembly, the question arose as to whether white phosphorus could be introduced as a template to a system of linked supramolecular aggregates, or a coordination towards the metal atoms occurs instead. By featuring a tetrahedral symmetry, this guest molecule could affect the shape of the host scaffolds and thus create novel supramolecular assemblies.

## 7.2 Results and Discussion

When **1** is reacted with AgSbF<sub>6</sub> in a 1:1 stoichiometric ratio (**1** : AgSbF<sub>6</sub>) in a self-assembly layering set-up, the formation of [{Cp\*Fe(η<sup>5</sup>-P<sub>5</sub>)}<sub>2</sub>{Ag<sub>2</sub>(CH<sub>2</sub>Cl<sub>2</sub>)}]<sub>n</sub>[SbF<sub>6</sub>]<sub>2n</sub> (**2**) is observed. By using a 1 : 2 stoichiometric ratio a different 1D polymer [{Cp\*Fe(η<sup>5:2:1</sup>-P<sub>5</sub>)}<sub>2</sub>Ag]<sub>n</sub>[SbF<sub>6</sub>]<sub>n</sub> is obtained (see Chapter V). To test the effect of P<sub>4</sub> on the coordination chemistry of **1** and AgSbF<sub>6</sub>, a three-component self-assembly was also examined. By layering AgSbF<sub>6</sub> in CH<sub>2</sub>Cl<sub>2</sub> with a mixture of **1** and P<sub>4</sub> in toluene, crystals of [{Cp\*Fe(η<sup>5</sup>-P<sub>5</sub>)}<sub>2</sub>{Ag<sub>2</sub>(η<sup>2</sup>-P<sub>4</sub>)<sub>m</sub>(CH<sub>2</sub>Cl<sub>2</sub>)<sub>1-m</sub>}]<sub>n</sub>[SbF<sub>6</sub>]<sub>2n</sub> (**3**; m = 0.75 (**3a**), 0.67 (**3b**), 1 (**3c**)) are formed, depending on the reaction conditions. In this synthesis, the 1D coordination polymer **2** is sometimes obtained as a minor byproduct. Compounds **2** and **3** could be isolated in good yields (Scheme 1).



**Scheme 1:** Self-assembly reactions of **1** with AgSbF<sub>6</sub> (**2**) and in the presence of P<sub>4</sub> (**3**).

The X-ray crystal structure analysis of **2** and **3** reveals related 1D polymeric structures of  $[\{\text{Cp}^*\text{Fe}(\eta^5\text{-P}_5)\}_2\{\text{Ag}_2(\text{CH}_2\text{Cl}_2)\}]_n[\text{SbF}_6]_{2n}$  (**2**) and an isostructural series of  $[\{\text{Cp}^*\text{Fe}(\eta^5\text{-P}_5)\}_2\{\text{Ag}_2(\eta^2\text{-P}_4)_m(\text{CH}_2\text{Cl}_2)_{1-m}\}]_n[\text{SbF}_6]_{2n}$  (**3**, cf. Figure 2). The *cyclo*-P<sub>5</sub> ligands either coordinate in a 1,3- or in a 1,2,3,4-fashion with one side-on and two end-on coordination modes per ligand. The Ag<sup>+</sup> cations are coordinated in a trigonal or pseudo-tetrahedral way by three ligands **1** and one or two additional small molecules. In **2**, the Ag<sup>+</sup> cations are saturated by either one SbF<sub>6</sub><sup>-</sup> anion or one end-on coordinating CH<sub>2</sub>Cl<sub>2</sub> molecule. In **3**, the Ag<sup>+</sup> cations are also partly saturated by either one CH<sub>2</sub>Cl<sub>2</sub> molecule or one P<sub>4</sub> tetrahedron, both acting as a η<sup>2</sup>-coordinating ligands. The content of coordinated P<sub>4</sub> tetrahedra depends on the stoichiometric amount of added white phosphorus as well as on the solvents used. In **3a** a 1 : 1 : 2 ratio (**1** : AgSbF<sub>6</sub> : P<sub>4</sub>) in CH<sub>2</sub>Cl<sub>2</sub> leads to P<sub>4</sub> tetrahedra occupied to 75 %, the remaining 25 % are occupied by coordinating dichloromethane molecules similar to **2**. Interestingly, by increasing the excess of white phosphorus in **3b** to 1 : 1 : 4 the occupancy of P<sub>4</sub> slightly decreases to 66 % and therefore the pure P<sub>4</sub>-containing compound **3c** cannot be obtained in this way. To avoid a coordination of the Ag<sup>+</sup> atoms by dichloromethane non-coordinating *o*-dichlorobenzene was used in **3c** as a solvent for AgSbF<sub>6</sub>. In this way, **3c** was synthesized selectively.

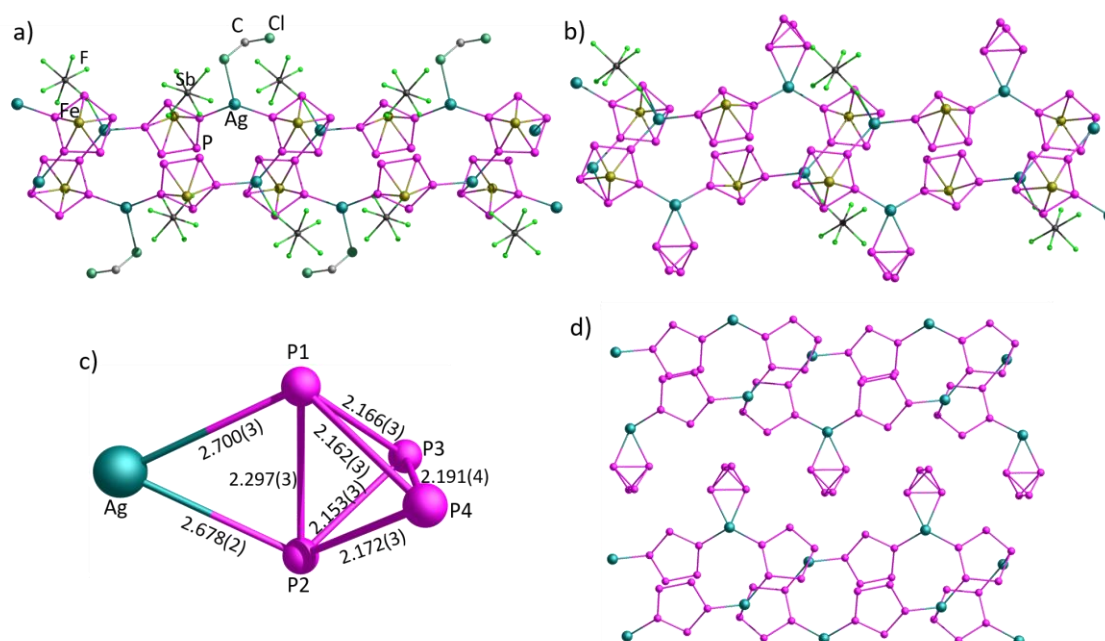


**Figure 2:** Section of the 1D polymers a) **2** and b) **3c**, c)  $\eta^2$ -coordinated  $P_4$  tetrahedron with bond lengths, d) orientation of two polymeric strands of **3c** in the crystal lattice. H, Fe atoms, and  $Cp^*$  ligands are partly omitted for clarity.

The P-P bond lengths in the coordinated  $P_4$  tetrahedra of **3** as well as their coordinating Ag-P bonds are comparable to compounds, in which the  $P_4$  tetrahedron coordinates in a  $\eta^2$ -mode towards a coinage metal cation (Table 1).<sup>9,10</sup> Moreover the P-P bond distances are in agreement with those found in free tetrahedral  $P_4$  molecule (2.1994(3) Å - 2.2228(5) Å).<sup>11,12</sup> Furthermore, single point DFT computations on the experimental geometry of **3** at the D3<sup>13</sup>-B3LYP/def2-TZVPP level of theory confirmed an elongated but intact nature of the coordinating P1-P2 bond (cf. Figure 3).

**Table 1:** Selected interatomic distances in **3c** and comparable coordination products of coinage metals.<sup>9,10</sup>

	<b>3c</b>	$[LCu(\eta^2-P_4)]^{9c}$	$[(\eta^2-P_4)AgAl\{OC(CH_3)(CF_3)_2\}_4]^{10b}$	$[iPrAuP_4]^+[SbF_6]^{-9d}$
$d_{av}(M...P)$ [Å]	2.689(3)	2.280(3)	2.5268(9)	2.4343(7)
$d(P_M...P_M)$ [Å]	2.297(3)	2.386(4)	2.3076(12)	2.3571(10)
$d_{av}(P_M...P_P)$ [Å]	2.163(3)	2.186(4)	2.159(1)	2.1678(11)
$d(P_P...P_P)$ [Å]	2.191(4)	2.141(6)	2.188(2)	2.194111

$L = [N(C_6H_3iPr_{2-2,6})C(Me)]_2CH^-$

Both **2** and **3**, are insoluble in common solvents, such as hexane, toluene or  $CH_2Cl_2$ . Upon addition of  $CH_3CN$  or pyridine, they give an orange solution while undergoing fragmentation. Therefore, in the  $^1H$  NMR and in the  $^{31}P$  NMR spectrum in  $CD_2Cl_2$  of a fragmented solution of **2** or **3**, only signals corresponding to the free starting materials are detected. For **2** in the  $^1H$  NMR spectrum the signals of **1** and a signal of the coordinating  $CH_2Cl_2$  molecule are visible in the expected ratio, whereas the  $^{31}P$  NMR spectrum only shows a broad signal at 138 ppm corresponding to Ag- and **1**-containing fragments. In the  $^{31}P$  NMR spectrum of **3**, additionally to a similar signal for **1** at 136 ppm, a weak

singlet at -525 ppm can be observed, which can be attributed to free  $P_4$  molecules. White phosphorus is also released from the polymer by grinding crystalline **3**, readily reacting with oxygen when exposed to air. The  $^{31}\text{P}\{^1\text{H}\}$  MAS NMR spectrum of crystalline **3** is in agreement with the data of X-ray structure analysis (Figure 3). Thus, at 150.2 ppm a sharp and at 133.4 ppm a small broad signal is detected, which can most probably be attributed to the different coordination modes of the P atoms in **1**. At -495.4 ppm a singlet can be attributed to the coordinated intact  $P_4$  tetrahedra and is in agreement to that in similar compounds like  $[\text{Ag}(\eta^2\text{-}P_4)\{\text{Al}[\text{OC}(\text{CF}_3)_2\text{Cl}_2]_3\}_4]$  (-497 ppm).<sup>10b</sup> The Raman spectra of solid **3** reveal bands similar to those found for free **1** and for solid  $P_4$  (Table 2). In the ESI MS spectrum for **2** and **3** in  $\text{CH}_3\text{CN}/\text{CH}_2\text{Cl}_2$ , peaks for oligomeric fragments can be detected. In both cases the peak with the highest mass can be attributed to  $[\{\text{Cp}^*\text{Fe}(\eta^5\text{-}P_5)\}_4\text{Ag}_4(\text{SbF}_6)_3]^+$  at  $m/z = 2521.98$ .

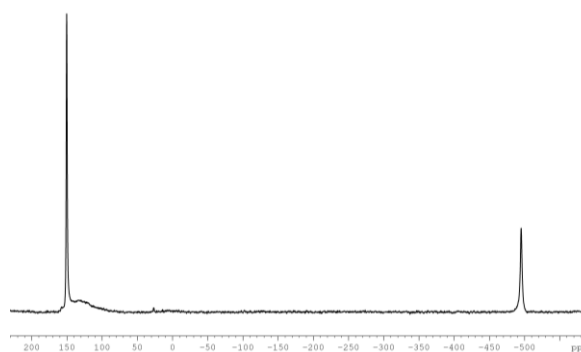


Figure 3:  $^{31}\text{P}\{^1\text{H}\}$  MAS NMR spectrum of **3c**.

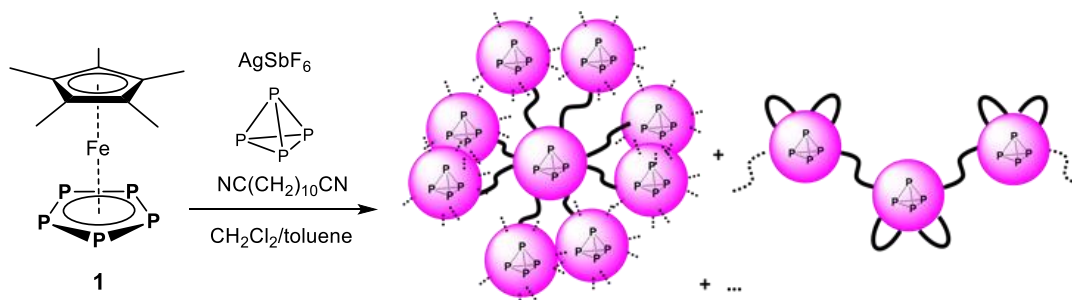
Table 2: Comparison of Raman modes observed in **1**, **3**, solid  $P_4$ , and  $(\eta^2\text{-}P_4)\text{AgAl}[\text{OC}(\text{CH}_3)(\text{CF}_3)_2]_4$ <sup>10b</sup>

<b>1</b> <sup>[a]</sup>	<b>3</b> <sup>[a]</sup>	solid $P_4$ <sup>[b]</sup>	$(\eta^2\text{-}P_4)\text{AgAl}[\text{OC}(\text{CH}_3)(\text{CF}_3)_2]_4$ <sup>10b</sup>
1017.15	1015.86	597.89 ( $A_1$ )	589
592.32	637.52	456.98 ( $T_2$ )	469
485.76	599.07	356.16 ( $E$ )	457
441.18	591.21		414
353.47	498.48		371
301.23	454.81		358
264.09	446.40		
190.65	343.56		
	325.13		
	297.70		
	267.50		
	187.41		

[a]  $\lambda_{\text{exc}} = 780 \text{ nm}$ ; [b]  $\lambda_{\text{exc}} = 532 \text{ nm}$

By introducing a fourth component to the self-assembly system and adding the flexible dinitrile  $\text{NC}(\text{CH}_2)_{10}\text{CN}$  to the mixture of **1** and  $P_4$ , the one-pot layering experiment with  $\text{AgSbF}_6$  furnished several crystalline phases with a general formula of  $[P_4@[\{\text{Cp}^*\text{Fe}(\eta^5\text{-}P_5)\}_9\{\text{Ag}_x(\text{NC}(\text{CH}_2)_{10}\text{CN})_y\}]]_n$

[SbF<sub>6</sub>]<sub>xn</sub> (**4a-c**) as the major product along with [{Cp\*Fe(η<sup>5:2:1</sup>-P<sub>5</sub>)}<sub>2</sub>Ag]<sub>n</sub>[SbF<sub>6</sub>]<sub>n</sub> (cf. *Chapter V*) as a minor product.



**Scheme 2:** Four-component self-assembly reaction of **1**, AgSbF<sub>6</sub>, NC(CH<sub>2</sub>)<sub>10</sub>CN and P<sub>4</sub>.

Preliminary X-ray structure analysis of the products of the four-component self-assembly reaction reveal triclinic (**4a**), monoclinic (**4b**), and orthorhombic (**4c**, minor) crystals, featuring a general formula of [P<sub>4</sub>@{[Cp\*Fe(η<sup>5</sup>-P<sub>5</sub>)]<sub>9</sub>[Ag<sub>x</sub>(NC(CH<sub>2</sub>)<sub>10</sub>CN)<sub>y</sub>]}]<sub>n</sub>[SbF<sub>6</sub>]<sub>xn</sub> (**4a**: x = 9, y = 4, **4b**: x = 9, y = 4.5, **4c**: x = 10 y = 4.5). All compounds feature similar polycationic supramolecular host-guest assemblies, which are interconnected by the fully flexible dinitrile linkers to networks of different dimensionality. Thus, the preliminary data on the triclinic phase (**4a**) indicates a 3D extended network, whereas the topology of the polymer cannot be determined at the current stage of structure refinement, due to disorder of the flexible linkers and their partly overlapping positions with SbF<sub>6</sub><sup>-</sup> counter-anions. The monoclinic phase (**4b**) proved to be incommensurate, according to the diffractions pattern, showing non-Bragg satellite reflections. A structure solution, using only Bragg reflections, was performed to obtain a preliminary structural model, so called ‘average structure’, which reveals the type of the host-guest assemblies, but does not allow exact statements concerning the dimensionality of the compound or accurate bond lengths. However, these first evidences indicate that most of the linkers connect two Ag atoms of the same scaffold, thus forming intramolecular bridges. Therefore, a low-dimensional structure is formed, in which the host-guest assemblies could be connected by one linker in an oligomeric or 1D fashion, depending on the partial or full occupancy of the linker. A hypothetical 1D polymeric structure based on these evidences is shown in *Scheme 2*. A 1D polymeric network of the supramolecular nodes is also suggested by the preliminary data on the orthorhombic phase (**4c**). The inorganic scaffolds of the host-guest assemblies consist in each case of nine units **1**, whereas the exact number of scaffold-building Ag atoms, varies in each crystalline phase (*Figure 4*). The data on **4a** show at least two different scaffolds with a ratio of about 90 : 10% in one position for one of two crystallographically unique supramolecular nodes. Thus, the presence of at least three different supramolecular nodes in **4a** is assumed, containing 8, 9 or 10 scaffold-building Ag atoms, while those on **4b** and **4c** reveal 9 and 10 Ag atoms, respectively. The Ag atoms are in all cases



tetrahedrally or pseudo-tetrahedrally coordinated by three ligands of **1** and either one nitrile group of a linker or, in the case of **4c**, one  $\text{SbF}_6^-$  counter-anion. Only one Ag atom in the scaffold with an occupancy of 10% in **4a** shows a pseudo-trigonal coordination environment of three ligands **1**. The nine *cyclo*- $\text{P}_5$  ligands are arranged to a capped tetragonal antiprism (*Figure 4k-l*) and coordinate in diverse coordination modes from 1,2- to 1,2,3,4,5-fashion towards the Ag cations. An overview of the architectures of the scaffolds in **4a-c** is given in *Table 3*. Some architectures arise from different positions of building blocks **1** showing disordering within the scaffolds. All non-coordinating  $\text{SbF}_6^-$  counter-anions are located in the outer sphere of the networked scaffolds, except for that mentioned for **4c**. Moreover, each supramolecular host aggregate in **4a-c** is templated by one tetrahedral molecule  $\text{P}_4$ , showing disorder over at least four close positions inside the scaffold. Considering these structural characteristics, a similarity of **4a-c** with the scaffolds in the 3D network of host-guest assemblies  $[[\text{SbF}_6]@\{[\text{Cp}^*\text{Fe}(\eta^5\text{-P}_5)]_9\{\text{Ag}_{11}(\text{NC}(\text{CH}_2)_7\text{CN})_6\}]]_n[\text{SbF}_6]_{10n}$  can be stated (cf. *Table 3, Chapter V*).

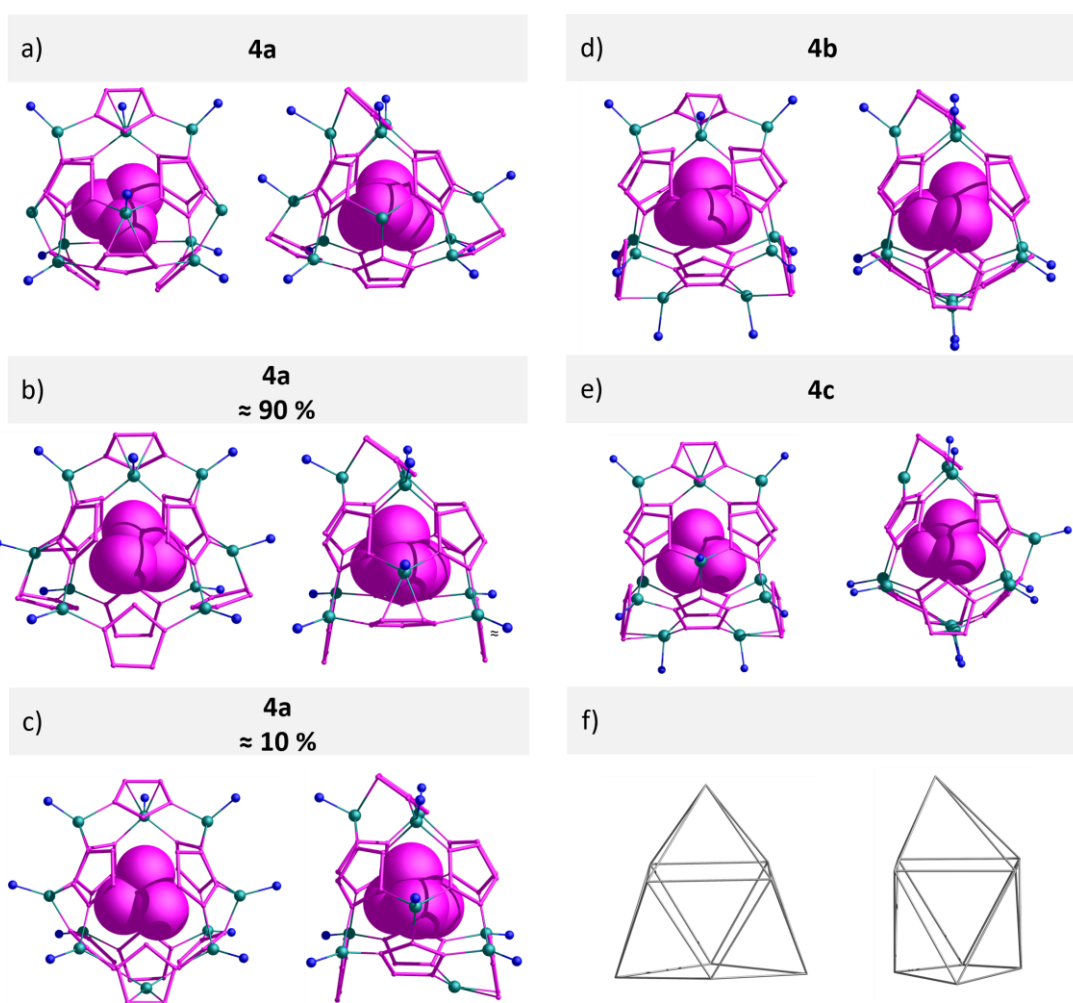


**Figure 4:** Front and side view of the scaffolds of **4a-c** with  $\text{P}_4$  as guest molecule shown in space-filling model.  
 f) capped tetragonal antiprism formed by ligands of **1**.

**Table 3:** Scaffold-building units and the coordination modes of **1** in the supramolecular nodes of **4a-c** and  $[[\text{SbF}_6]@[\{\text{Cp}^*\text{Fe}(\eta^5\text{-P}_5)\}_9\text{Ag}_{11}]]_n[\text{SbF}_6]$  (cf. Chapter V).

	scaffold-building unit		coordination modes of <b>1</b>						reference
	Ag cations	ligands <b>1</b>	1,2	1,3	1,2,4	1,2,3	1,2,3,4	1,2,3,4,5	
<b>4a</b>	1 x 8	9				2	7		Figure 5a,b
	1 x 9 ( $\approx 90\%$ )	9		3	4		2		Figure 5c,d
	1 x 10 ( $\approx 10\%$ )	9		1		2	6		Figure 5e,f
<b>4b</b>	9	9		2	2		5		Figure 5g,h
<b>4c</b>	10	9	1		4		3	1	Figure 5i,j
$[[\text{SbF}_6]@[\{\text{Cp}^*\text{Fe}(\eta^5\text{-P}_5)\}_9\text{Ag}_{11}]]$ $[\text{SbF}_6]_{10}$	11	9			2		5	2	Chapter V, Figure 7-8

The polymeric products **4a-c** are insoluble in all common solvents, and show no degradation exposed to air. However, grinding of crystalline **4a-c** destroys their polymeric structure and the guest  $\text{P}_4$  is released, readily reacting with oxygen in air.  $\text{P}_4$  also can be partially released by stirring washed crystals of **4** for a minimum of 1h in  $\text{CS}_2$  and can be detected by  $^{31}\text{P}$  NMR spectroscopy in the supernatant solution at -510 ppm, while the degraded polymer remains undissolved as a brown powder. Thereby, traces of free **1** can also be found in the  $^{31}\text{P}$  NMR spectrum as a sharp singlet at 156.2 ppm and an integral ratio of 12 P : 4 P (**1** :  $\text{P}_4$  = 2.5 : 1), meaning more favoured extraction of white phosphorus from the crystalline material to the  $\text{CS}_2$  solution, compared to the ratio in the solid state of 9 : 1 (**1** :  $\text{P}_4$ , providing that  $\text{P}_4$  is fully occupied). Fragmentation of the polymer and release of white phosphorus can also be reached by adding pyridine or  $\text{CH}_3\text{CN}$  to solid **4**. Moreover, direct subsequent reactions with released  $\text{P}_4$  can be carried out using solid **4**. To fundamentally prove this possibility on a small scale, solid **4** was refluxed with a red-brown solution of  $[\text{Cp}^{\text{Bn}}\text{Fe}(\text{CO})_2]_2$  in decalin (190°C) for 17h, in order to extract white phosphorus and involve it in a reaction of a typical thermolysis to synthesize the benzyl-substituted pentaphosphaferrocene  $[\text{Cp}^{\text{Bn}}\text{Fe}(\eta^5\text{-P}_5)]$ .<sup>14</sup> After 2h of heating the solution turned to bright green, typical for free dissolved pentaphosphaferrocenes, **1** and  $[\text{Cp}^{\text{Bn}}\text{Fe}(\eta^5\text{-P}_5)]$ . After cooling to room temperature, the solvent of the supernatant solution was removed, and the residue dissolved in  $\text{CD}_2\text{Cl}_2$ . In the  $^{31}\text{P}$  NMR spectrum of this reaction solution a signal at 161.9 ppm can be assigned to free  $[\text{Cp}^{\text{Bn}}\text{Fe}(\eta^5\text{-P}_5)]$ , besides a signal for free **1** at 152.4 ppm, arising from the fragmented supramolecular hosts. Furthermore,  $^{31}\text{P}\{^1\text{H}\}$  MAS NMR spectroscopy was conducted for crystalline **4** and showed a broad singlet at -469.2 ppm for white phosphorus as well as a broad signal at 128.8 ppm for the P atoms of the *cyclo*- $\text{P}_5$  ligand of **1**, clearly upfield-shifted with respect to the signal in **3c** (150 ppm, cf. Figure

2). The integral ratio of these signals corresponds to  $1 \times P_4 : 9 \times \mathbf{1}$ , and is in agreement with the ratio in the solid state, derived from the X-ray structure analysis.

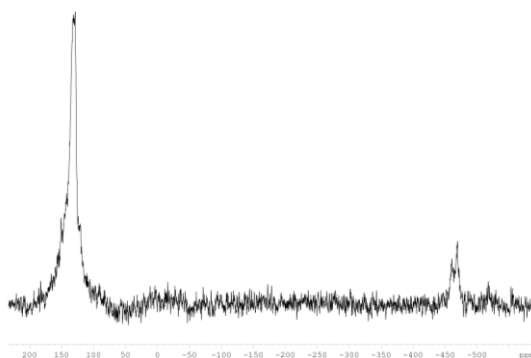


Figure 5:  $^{31}\text{P}\{^1\text{H}\}$  MAS NMR spectrum of **4**.

ESI MS spectroscopy was carried out for a fragmented solution of **4** in  $\text{CH}_3\text{CN}$ . The positive mode of the ESI MS spectrum showed the largest peak at  $m/z = 2712$ , which can be assigned to  $[\{\text{Cp}^*\text{Fe}(\eta^5\text{-P}_5)\}_3\text{Ag}_5(\text{SbF}_6)_4(\text{NC}(\text{CH}_2)_{10}\text{CN})]^+$ , whereas the negative mode of the ESI MS shows its largest peak at  $m/z = 2647.86$  for  $[\{\text{Cp}^*\text{Fe}(\eta^5\text{-P}_5)\}_4\text{Ag}_3(\text{SbF}_6)_4]^-$ . Due to intense photobleaching and fluorescence effects of the sample, no signals could be detected in the Raman spectrum.

Furthermore, current investigations involving other linkers, as the  $\text{NC}(\text{CH}_2)_8\text{CN}$  instead of  $\text{NC}(\text{CH}_2)_{10}\text{CN}$ , also indicate the formation of networked supramolecular host-guest assemblies incorporating intact  $P_4$  molecules. Due to promising preliminary experimental results, the topic of a selective incorporation of small molecules into connected supramolecular scaffolds by a four-component self-assembly will be examined in detail in the future.

### 7.3 Conclusion

In summary, we have shown that the self-assembly of  $[\text{Cp}^*\text{Fe}(\eta^5\text{-P}_5)]$  with  $\text{AgSbF}_6$  and the flexible dinitrile linker  $\text{NC}(\text{CH}_2)_{10}\text{CN}$  can be used to create supramolecular assemblies, acting as nodes in a network and offering their inner void for the selective encapsulation of small molecules as the tetrahedral  $P_4$ . By a four-component self-assembly reaction conducted in a layering experiment, the networked supramolecular host-guest assemblies  $[P_4@[\{\text{Cp}^*\text{Fe}(\eta^5\text{-P}_5)\}_9\{\text{Ag}_x(\text{NC}(\text{CH}_2)_{10}\text{CN})_y\}]]_n[\text{SbF}_6]_{xn}$  (**4a**:  $x = 9$ ,  $y = 4$ , **4b**:  $x = 9$ ,  $y = 4.5$ , **4c**:  $x = 10$ ,  $y = 4.5$ ) are formed. The connectivity of these could not be explicitly established by now, but preliminary data suggest polymers of different dimensionality, with similar supramolecular host-guest assemblies acting as nodes. From a three-component self-assembly of **1**,  $\text{AgSbF}_6$  and  $P_4$ , a series of 1D coordination polymers  $[\{\text{Cp}^*\text{Fe}(\eta^5\text{-P}_5)\}_2\{\text{Ag}_2(\eta^2\text{-P}_4)_m(\text{CH}_2\text{Cl}_2)_{1-m}\}]_n[\text{SbF}_6]_{2n}$  (**3**;  $m = 0.75$  (**3a**),  $0.67$  (**3b**),  $1$  (**3c**)) is formed, with

the  $P_4$  tetrahedron coordinating in a side-on fashion towards a  $Ag^+$  cation. The coordination of the competing solvent molecules  $CH_2Cl_2$  can be completely avoided by using a non-coordinating solvent, like *ortho*-dichlorobenzene. Furthermore, DFT computations underlined the intact although slightly distorted tetrahedral structure of the  $P_4$  ligand. A similar 1D polymer  $[[Cp^*Fe(\eta^5-P_5)]_2\{Ag_2(CH_2Cl_2)\}]_n[SbF_6]_{2n}$  (**2**) can also be obtained from the direct two-component reaction of  $[Cp^*Fe(\eta^5-P_5)]$  with  $AgSbF_6$  in a 1 : 1 stoichiometric ratio. Both compounds involving  $P_4$ , either in coordinated (**3**) or incorporated (**4**) form, can release intact white phosphorus by degradation of the structure upon grinding of crystalline **4a-c** or adding coordinating solvents as  $CH_3CN$  or pyridine. Furthermore, the release of  $P_4$  from the polymeric structures **3** and **4** can be used for subsequent reactions, by exposing the solid material to a dissolved reaction partner of  $P_4$ .

## 7.4 Experimental Part

### General Remarks

All reactions were performed under an inert atmosphere of dry nitrogen with standard vacuum, Schlenk and glove-box techniques. Solvents were purified, dried and degassed prior to use by standard procedures.  $[\text{Cp}^*\text{Fe}(\eta^5\text{-P}_5)]^{15}$  was synthesized following reported procedures. Commercially available chemicals ( $\text{AgSbF}_6$ ,  $\text{NC}(\text{CH}_2)_{10}\text{CN}$ ) were used without further purification. Solution NMR spectra were recorded on a Bruker Avance 300 or 400 spectrometer. The  $^{31}\text{P}\{^1\text{H}\}$  MAS spectrum was measured on a Bruker Avance 300. The corresponding ESI MS spectra were acquired on a ThermoQuest Finnigan MAT TSQ 7000 mass spectrometer. CHN Elemental analyses were performed on a Vario EL III apparatus. Raman spectra were recorded in solid state at a DXR Raman Microscope (Thermo Fischer Scientific™) using excitation sources  $\lambda_{\text{exc}} = 780 \text{ nm}$  and  $\lambda_{\text{exc}} = 532 \text{ nm}$ , a laser power of 10mV and exposure times of 10 seconds.

### Synthesis of $[\{\text{Cp}^*\text{Fe}(\eta^5\text{-P}_5)\}_2\{\text{Ag}_2(\text{CH}_2\text{Cl}_2)\}]_n[\text{SbF}_6]_{2n}$ (**2**)

In a Schlenk tube a solution of  $\text{AgSbF}_6$  (28 mg, 0.08 mmol) in  $\text{CH}_2\text{Cl}_2$  (8 mL) is carefully layered with a green solution of  $[\text{Cp}^*\text{Fe}(\eta^5\text{-P}_5)]$  (28 mg, 0.08 mmol) in toluene (8 mL). Thereby, the phase boundary turns yellow turbid. After one day, the formation of red rod-like crystals of  $[\{\text{Cp}^*\text{Fe}(\eta^{5:2:1}\text{-P}_5)\}_2\text{Ag}]_n[\text{SbF}_6]_n$  at the phase boundary can be observed. After complete diffusion, the red rod-like crystals could not be observed anymore but very thin greenish needles. The light green mother liquor is decanted, the crystals are washed with pentane ( $3 \times 5 \text{ mL}$ ) and dried *in vacuo*.

Analytical data of **2**:

**Yield:** 52 mg (0.0356 mmol, 89% referred to  $[\text{Cp}^*\text{Fe}(\eta^5\text{-P}_5)]$ )

$^1\text{H}$  NMR ( $\text{CD}_3\text{CN}$ ):  $\delta$  [ppm] = 1.47 (s, 15H,  $[\text{Cp}(\text{CH}_3)_5\text{Fe}(\eta^5\text{-P}_5)]$ ), 5.45 (s, 1H,  $\text{CH}_2\text{Cl}_2$ ).

$^{31}\text{P}\{^1\text{H}\}$  NMR ( $\text{CD}_3\text{CN}$ ):  $\delta$  [ppm] = 137.98 (m (br),  $[\text{Cp}^*\text{Fe}(\eta^5\text{-P}_5)]$ ), 140.19 (s,  $[\text{Cp}^*\text{Fe}(\eta^5\text{-P}_5)]$ )

$^{13}\text{C}$  NMR ( $\text{CD}_3\text{CN}$ ):  $\delta$  [ppm] = 10.11 ( $[\text{Cp}(\text{CH}_3)_5\text{Fe}(\eta^5\text{-P}_5)]$ )

$^{19}\text{F}$  NMR ( $\text{CD}_3\text{CN}$ ):  $\delta$  [ppm] = -124.49 (m,  $\text{SbF}_6$ )

**Positive ion ESI-MS** ( $\text{CH}_3\text{CN}/\text{CH}_2\text{Cl}_2$ ):  $m/z$  (%) = 2521.98  $[\{\text{Cp}^*\text{Fe}(\eta^5\text{-P}_5)\}_4\text{Ag}_4(\text{SbF}_6)_3]^+$ , 2178.18  $[\{\text{Cp}^*\text{Fe}(\eta^5\text{-P}_5)\}_4\text{Ag}_3(\text{SbF}_6)_2]^+$ , 2176  $[\{\text{Cp}^*\text{Fe}(\eta^5\text{-P}_5)\}_3\text{Ag}_4(\text{SbF}_6)_3]^+$ , 1832.26  $[\{\text{Cp}^*\text{Fe}(\eta^5\text{-P}_5)\}_3\text{Ag}_3(\text{SbF}_6)_2]^+$ , 1142.54  $[\{\text{Cp}^*\text{Fe}(\eta^5\text{-P}_5)\}_2\text{Ag}_2(\text{SbF}_6)]^+$ , 798.75  $[\{\text{Cp}^*\text{Fe}(\eta^5\text{-P}_5)\}\text{Ag}_2(\text{SbF}_6)]^+$ , 493.85 (100)  $[\{\text{Cp}^*\text{Fe}(\eta^5\text{-P}_5)\}\text{Ag}(\text{CH}_3\text{CN})]^+$ , 452.83  $[\{\text{Cp}^*\text{Fe}(\eta^5\text{-P}_5)\}\text{Ag}]^+$ , 188.96  $[\text{Ag}(\text{CH}_3\text{CN})_2]^+$ , 147.93  $[\text{Ag}(\text{CH}_3\text{CN})]^+$ .

**Negative ion ESI-MS** ( $\text{CH}_3\text{CN}/\text{CH}_2\text{Cl}_2$ ):  $m/z$  (%) = 234.90  $[\text{SbF}_6]^-$ .

**Elemental analysis:** Calculated (%) for  $[(\text{Cp}^*\text{Fe}(\eta^5\text{-P}_5))_2(\text{AgSbF}_6)_2(\text{CH}_2\text{Cl}_2)]$  (1464.04 g/mol): C 17.23, H 2.20; found: C 16.96, H 2.18.

### Synthesis of $[(\text{Cp}^*\text{Fe}(\eta^5\text{-P}_5))_2(\text{Ag}_2(\eta^2\text{-P}_4)_m(\text{CH}_2\text{Cl}_2)_{1-m})_n(\text{SbF}_6)_{2n}]$ (**3**; $m = 0.75$ (**3a**), $0.67$ (**3b**), $1$ (**3c**))

In a Schlenk tube a solution of  $\text{AgSbF}_6$  (28 mg, 0.08 mmol) in  $\text{CH}_2\text{Cl}_2$  (for **3a**, **b**) or *o*-dichlorobenzene (for **3c**) (8 mL) is carefully layered with a green solution of  $[\text{Cp}^*\text{Fe}(\eta^5\text{-P}_5)]$  (28 mg, 0.08 mmol) and  $\text{P}_4$  (20 mg (**3a**) or 40 mg (**3b**, **c**), 0.16 mmol or 0.38 mmol) in toluene (8 mL). Thereby, the colour at the phase boundary turns to a turbid yellow. After one day, the formation of red rod-like crystals of  $[(\text{Cp}^*\text{Fe}(\eta^{5:2:1}\text{-P}_5))_2\text{Ag}]_n(\text{SbF}_6)_n$  at the phase boundary can be observed. After complete diffusion, the red rod-like crystals could not be observed anymore but very thin yellow-brown needles of **3**. The light green mother liquor is decanted, the crystals are washed with toluene ( $3 \times 5$  mL) to remove free  $\text{P}_4$  and dried *in vacuo*.

Analytical data of **3c**:

**Yield:** 44 mg (0.015 mmol, 74 % referred to  $[\text{Cp}^*\text{Fe}(\eta^5\text{-P}_5)]$ )

$^1\text{H}$  NMR ( $\text{CD}_3\text{CN}$ ):  $\delta$  [ppm] = 1.47 (s, 10 H,  $[\text{Cp}^*\text{Fe}(\eta^5\text{-P}_5)]$ ), 5.43 (s, 1 H,  $\text{CH}_2\text{Cl}_2$ )

$^{31}\text{P}\{^1\text{H}\}$  NMR ( $\text{CD}_3\text{CN}$ ):  $\delta$  [ppm] = -525.07 (s, 0.07 P,  $\text{P}_4$ ), 136.11 (s, 10 P,  $[\text{Cp}^*\text{Fe}(\eta^5\text{-P}_5)]$ )

$^{31}\text{P}\{^1\text{H}\}$  MAS NMR:  $\delta$  [ppm] = -495.39 (s, 4 P,  $\text{P}_4$ ), 133.41 (s(br), 5 P,  $[\text{Cp}^*\text{Fe}(\eta^5\text{-P}_5)]$ ), 150.22 (s, 10 P,  $[\text{Cp}^*\text{Fe}(\eta^5\text{-P}_5)]$ )

**Positive ion ESI-MS** ( $\text{CH}_3\text{CN}/\text{CH}_2\text{Cl}_2$ ):  $m/z$  (%) = 2521.98  $[(\text{Cp}^*\text{Fe}(\eta^5\text{-P}_5))_4\text{Ag}_4(\text{SbF}_6)_3]^+$ , 2178.18  $[(\text{Cp}^*\text{Fe}(\eta^5\text{-P}_5))_4\text{Ag}_3(\text{SbF}_6)_2]^+$ , 2176  $[(\text{Cp}^*\text{Fe}(\eta^5\text{-P}_5))_3\text{Ag}_4(\text{SbF}_6)_3]^+$ , 1832.26  $[(\text{Cp}^*\text{Fe}(\eta^5\text{-P}_5))_3\text{Ag}_3(\text{SbF}_6)_2]^+$ , 1486.34  $[(\text{Cp}^*\text{Fe}(\eta^5\text{-P}_5))_2\text{Ag}_3(\text{SbF}_6)_2]^+$ , 1142.54  $[(\text{Cp}^*\text{Fe}(\eta^5\text{-P}_5))_2\text{Ag}_2(\text{SbF}_6)]^+$ , 798.75  $[(\text{Cp}^*\text{Fe}(\eta^5\text{-P}_5))\text{Ag}_2(\text{SbF}_6)]^+$ , 493.85 (100)  $[(\text{Cp}^*\text{Fe}(\eta^5\text{-P}_5))\text{Ag}(\text{CH}_3\text{CN})]^+$ , 452.8  $[(\text{Cp}^*\text{Fe}(\eta^5\text{-P}_5))\text{Ag}]^+$ , 188.96  $[\text{Ag}(\text{CH}_3\text{CN})_2]^+$ , 147.93  $[\text{Ag}(\text{CH}_3\text{CN})]^+$ .

**Negative ion ESI-MS** ( $\text{CH}_3\text{CN}/\text{CH}_2\text{Cl}_2$ ):  $m/z$  (%) = 1958.14  $[(\text{Cp}^*\text{Fe}(\eta^5\text{-P}_5))_2\text{Ag}_3(\text{SbF}_6)_4]^-$ , 1612.98  $[(\text{Cp}^*\text{Fe}(\eta^5\text{-P}_5))_2\text{Ag}_2(\text{SbF}_6)_3]^-$ , 234.90 (100)  $[\text{SbF}_6]^-$ .

**Elemental analysis:** Calculated (%) for  $[(\text{Cp}^*\text{Fe}(\eta^5\text{-P}_5))_4(\text{AgSbF}_6)_4(\text{CH}_2\text{Cl}_2)(\text{P}_4)]$  (2967.05 g/mol): C 16.6, H 2.11; found: C 16.78, H 2.21.

**Raman:**  $\tilde{\nu}/\text{cm}^{-1}$  = 1015.86, 637.52, 599.07, 591.21, 498.48, 454.81, 446.40, 343.56, 325.13, 297.70, 267.50, 187.41.

**Synthesis of  $[P_4@[\{Cp^*Fe(\eta^5-P_5)\}_9\{Ag_x(NC(CH_2)_{10}CN)_y\}]]_n[SbF_6]_{11n}$  (4a:  $x = 9$ ,  $y = 4$ ; 4b:  $x = 9$ ,  $y = 4.5$ ; 4c:  $x = 10$ ,  $y = 4.5$ )**

In a Schlenk tube a solution of  $AgSbF_6$  (34 mg, 0.1 mmol) in  $CH_2Cl_2$  (25 mL) is carefully layered first with a solvent mixture of  $CH_2Cl_2$ /toluene (10 mL, 2:1) and then with a green solution of  $[Cp^*Fe(\eta^5-P_5)]$  (40 mg, 0.1 mmol),  $P_4$  (40 mg, 0.32 mmol) and  $NC(CH_2)_{10}CN$  (2 mL, 0.8 mmol, 0.4 M in  $CH_2Cl_2$ ) in toluene (25 mL). After a few hours, the phase boundary turns yellow and after one day, the formation of dark plates of **4** at the phase boundary can be observed. Furthermore a few crystals of  $[\{Cp^*Fe(\eta^{5:2:1}-P_5)\}_2Ag]_n[SbF_6]_n$  are appearing at the phase boundary as a byproduct. After complete diffusion, the light-yellow mother liquor is decanted, the crystals are washed with  $CH_2Cl_2$  and toluene ( $3 \times 10$  mL) to remove the byproduct and free  $P_4$  and dried *in vacuo*.

Analytical data of **4**:

**Yield:** due to different undistinguishable crystalline phases no exact yield can be given.

**$^1H$  NMR** ( $CD_2Cl_2$ /pyridine):  $\delta$  [ppm] = 1.31 (s, C-5/C-6/C-7/C-8,  $NC(CH_2)_{10}CN$ ), 1.41 (s, C-4/C-9,  $NC(CH_2)_{10}CN$ ), 1.45 (s,  $[Cp^*Fe(\eta^5-P_5)]$ ), 1.63 (m, C-3/C-10,  $NC(CH_2)_{10}CN$ ), 2.33 (t, C-2/C-11,  $NC(CH_2)_{10}CN$ ), 7.56 (m,  $\beta$ -H, pyridine), 7.94 (m,  $\gamma$ -H, pyridine), 8.64 (m,  $\alpha$ -H, pyridine).

**$^{31}P\{^1H\}$  NMR** ( $CD_2Cl_2$ /pyridine):  $\delta$  [ppm] = -522.72 (s,  $P_4$ ), 146.74 (m (br),  $[Cp^*Fe(\eta^5-P_5)]$ ).

**$^{31}P\{^1H\}$  MAS NMR:**  $\delta$  [ppm] = -469.16 (s(br), 4 P,  $P_4$ ), 128.77 (s(br), 45 P,  $[Cp^*Fe(\eta^5-P_5)]$ )

**$^{13}C$  NMR** ( $CD_2Cl_2$ /pyridine):  $\delta$  [ppm] = 11.02 ( $Cp(CH_3)_5Fe(\eta^5-P_5)$ ), 17.39 (C-2/C-11,  $NC(CH_2)_8CN$ ), 25.77 (C-3/C-10,  $NC(CH_2)_8CN$ ), 28.98 (C-4/C-9,  $NC(CH_2)_8CN$ ), 29.05 (C-5/C-8,  $NC(CH_2)_8CN$ ), 29.51 (C-6/C-7,  $NC(CH_2)_8CN$ ), 91.83 ( $C_5(CH_3)_5Fe(\eta^5-P_5)$ ), 125.60 ( $\beta$ -C, pyridine), 140.30 ( $\gamma$ -C, pyridine), 147.39 ( $\alpha$ -C, pyridine).

**Positive ion ESI-MS** ( $CH_3CN$ ):  $m/z$  (%) = ( $CH_2Cl_2/CH_3CN$  (1:1)):  $m/z$  (%) = 2712  $[\{Cp^*Fe(\eta^5-P_5)\}_3Ag_5(SbF_6)_4(NC(CH_2)_{10}CN)]^+$ , 2521.98  $[\{Cp^*Fe(\eta^5-P_5)\}_4Ag_4(SbF_6)_3]^+$ , 2368.23  $[\{Cp^*Fe(\eta^5-P_5)\}_3Ag_4(SbF_6)_3(NC(CH_2)_{10}CN)]^+$ , 2178.18  $[\{Cp^*Fe(\eta^5-P_5)\}_3Ag_4(SbF_6)_3]^+$ , 2176  $[\{Cp^*Fe(\eta^5-P_5)\}_4Ag_3(SbF_6)_2]^+$ , 1832.26  $[\{Cp^*Fe(\eta^5-P_5)\}_3Ag_3(SbF_6)_2]^+$ , 1678.51  $[\{Cp^*Fe(\eta^5-P_5)\}_2Ag_3(SbF_6)_2(NC(CH_2)_{10}CN)]^+$ , 1142.55  $[\{Cp^*Fe(\eta^5-P_5)\}_2Ag_2(SbF_6)]^+$ , 988.79  $[\{Cp^*Fe(\eta^5-P_5)\}_2Ag(NC(CH_2)_{10}CN)]^+$ , 798.75  $[\{Cp^*Fe(\eta^5-P_5)\}_2Ag]^+$ , 644.99  $[\{Cp^*Fe(\eta^5-P_5)\}Ag(NC(CH_2)_{10}CN)]^+$ , 493.85 (100)  $[\{Cp^*Fe(\eta^5-P_5)\}Ag(CH_3CN)]^+$ , 452.83  $[\{Cp^*Fe(\eta^5-P_5)\}Ag]^+$ , 299.07  $[Ag(NC(CH_2)_{10}CN)]^+$ , 188.96  $[Ag(CH_3CN)_2]^+$ , 147.93  $[Ag(CH_3CN)]^+$ , 106.90  $[Ag]^+$ .

**Negative ion ESI-MS** ( $CH_3CN$ ):  $m/z$  (%) = 2647.86  $[\{Cp^*Fe(\eta^5-P_5)\}_4Ag_3(SbF_6)_4]^-$ , 1958.14  $[\{Cp^*Fe(\eta^5-P_5)\}_3Ag_2(SbF_6)_3]^-$ , 1804.38  $[\{Cp^*Fe(\eta^5-P_5)\}_2Ag_2(SbF_6)_3(NC(CH_2)_{10}CN)]^-$ , 1612.98  $[\{Cp^*Fe(\eta^5-P_5)\}_2Ag_2(SbF_6)_3]^-$ , 234.90 (100)  $[SbF_6]^-$ .

**Elemental analysis:** Calculated (%) for  $[P_4@[\{Cp^*Fe(\eta^5-P_5)\}_9\{Ag_9(NC(CH_2)_{10}CN)_{4.5}\}]]_n[SbF_6]_9$  (7195.26 g/mol): C 24.04, H 3.15, N 1.75; found: C 24.68, H 3.41, N 1.87.

## 7.5 Crystallographic Details

Crystals of **2**, **3a-c**, **4a-c** were taken from a Schlenk flask under a stream of argon and immediately covered with perfluorinated Fomblin® mineral oil to prevent possible loss of solvent and/or decomposition. The single crystals were quickly chosen under the microscope with CryoMount® mounted on the magnetic base so that they were covered by a drop of the oil. They the crystals were immediately placed into a stream of cold nitrogen to the pre-centered goniometer head of a diffractometer.

The crystals of **4a-c** were carefully selected, mounted on a magnetic holder, checked for quality and placed into a Dewar vessel with liquid nitrogen using standard cryocrystallography tools. After a few weeks, it was taken to the DESY PETRA III synchrotron. Using standard procedures, the crystals were placed into a special Dewar vessel filled with liquid nitrogen among other crystals. A robotic mounting/demounting was used for further manipulations in the P11 beamline hutch.<sup>16</sup>

The data for **2-3** and **4a** were collected on an Agilent Technologies diffractometer equipped with a Titan<sup>S2</sup> CCD detector and a SuperNova Cu K $\alpha$  microfocus source using either 0.5°  $\omega$  scans at T = 90 K. Analytical absorption correction for **2-3** was applied based on crystal faces. For **4a-c**, different kinds of experimental complications did not allow in-house data collections suitable for complete structure refinement.

Crystals of **4a** from different samples showed weak non-Bragg reflections (*Figure 6*). For this reason, only trial experiment was measured, which allowed to solve the structure and roughly determine an average model. The intensities of the satellite reflections were quite low, and  $q$ -vector for first-order satellites was preliminary determined as {0.227, 0, -0.222}. However, still many reflections are not explained in this model, which suggests that more complex model should be derived. Crystals of **4b** could not be measured in-house due to malfunctioning of the LT system and icing of the crystals during required measurement time of more than 4 days. Crystals of **4c** were too small and did not possess required scattering power. However, preliminary structural models were obtained for all **4a-4c**. Further attempts to collect the datasets with better signal-to-noise  $I/\sigma$  ratio were performed at DESY synchrotron (Hamburg, Germany).

X-ray diffraction experiments for **4a-c** were measured at 80 K at the DESY PETRA III synchrotron (beamline P11) using robotic mounting.<sup>16</sup> Data collection for **4a** was performed by a shutterless 360°  $\phi$ -rotation with 0.1° scan width and exposure 0.08 s per frame at wavelength  $\lambda = 0.6199$  Å (20 keV). Data collections for **4b** and **4c** were acquired by 360°  $\phi$ -rotation with 0.2° and 0.1° scan width, respectively, and exposure 0.05 s per frame at wavelength  $\lambda = 0.7085$  Å (17.5 keV). Data reduction



for all data sets was performed with CrysAlis Pro software.<sup>17</sup> In all cases, **4a-c** radiolysis took place to some extent; therefore, only those frames not affected by decomposition of the crystal were taken into integration. Analytical absorption correction was applied for **2** and series of **3** based on crystal faces; whereas empirical absorption correction using equivalent reflections was used for **4a-c**. Crystallographic data and further details of the diffraction experiments are given in *Tables 4-6*.

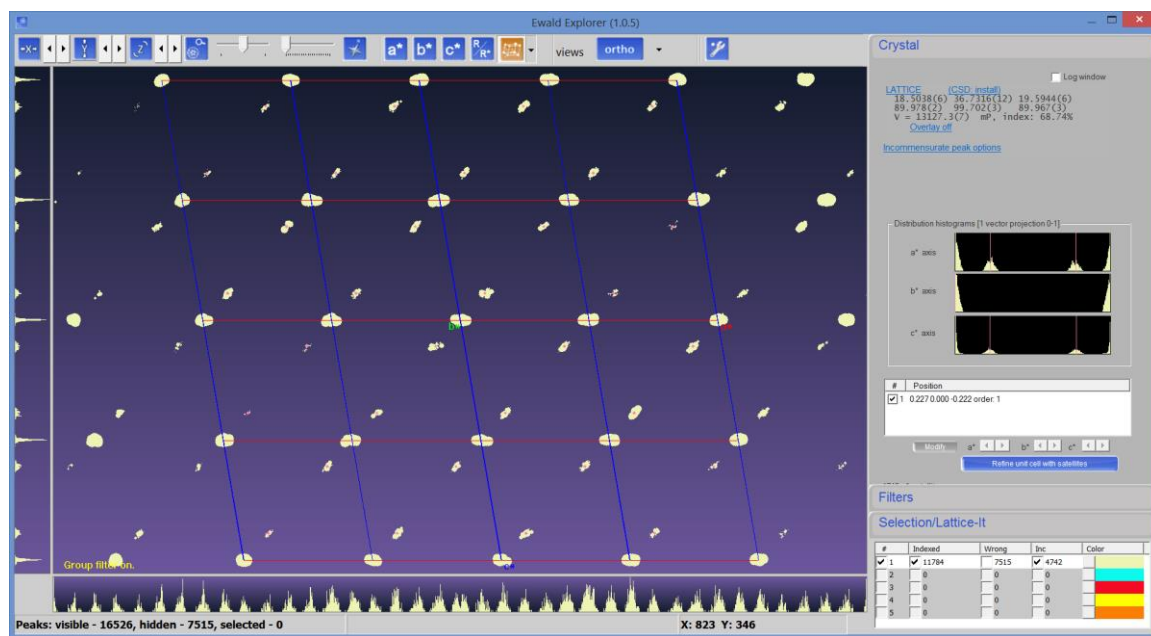


**Figure 6:** Bragg and first-order satellite reflections for incommensurate structure **4b**, projection along  $b^*$ .<sup>17</sup>

The structures were solved by direct methods with *SHELXT*<sup>18</sup> and were refined by full-matrix least-squares method against  $F^2$  in anisotropic approximation using multiprocessor variable memory versions of *SHELXL* (2014-2015). Crystallographic data and further details of the diffraction experiments are given in *Tables 4-6*.

The refinement of crystal structures **2-3** is finished, for series **4** it is under way. The refinement is complicated by disorder of the silver atoms and, in some cases, also by disorder of pentaphosphaferrocene building blocks in the supramolecular scaffolds, by severe disorder of linkers, counter-anions and  $\text{CH}_2\text{Cl}_2$  solvent molecules.

**Table 4:** Experimental details for compounds **2** and **3a**.

Crystal data	<b>2</b>	<b>3a</b>
Chemical formula	C <sub>21</sub> H <sub>32</sub> Ag <sub>2</sub> Cl <sub>2</sub> F <sub>6</sub> Fe <sub>2</sub> P <sub>10</sub> Sb·F <sub>6</sub> Sb	C <sub>20.33</sub> H <sub>30.67</sub> Ag <sub>2</sub> Cl <sub>0.67</sub> F <sub>6</sub> Fe <sub>2</sub> P <sub>13</sub> Sb·(F <sub>6</sub> Sb)
<i>M<sub>r</sub></i>	1464.00	1490.02
Crystal system, space group	Triclinic, <i>P</i> $\bar{1}$	Monoclinic, <i>P</i> 2 <sub>1</sub> / <i>n</i>
Temperature (K)	90	90
<i>a</i> , <i>b</i> , <i>c</i> (Å)	12.71926 (17), 13.1631 (2), 24.9754 (4)	13.3509 (5), 12.6976 (5), 24.6201 (12)
$\alpha$ , $\beta$ , $\gamma$ (°)	90.3811 (13), 95.6898 (13), 96.3651 (13)	90.030 (4)
<i>V</i> (Å <sup>3</sup> )	4134.60 (11)	4173.7 (3)
<i>Z</i>	4	4
<i>F</i> (000)	2792	2840
<i>D<sub>x</sub></i> (Mg m <sup>-3</sup> )	2.352	2.371
Radiation type	Cu K $\alpha$	Cu K $\alpha$
$\mu$ (mm <sup>-1</sup> )	28.69	28.60
Crystal shape	needle	needle
Colour	green	brown
Crystal size (mm)	0.30 × 0.02 × 0.01	0.13 × 0.01 × 0.01
<b>Data collection</b>		
Diffractometer	SuperNova, Titan <sup>S2</sup>	SuperNova, Titan <sup>S2</sup>
Absorption correction	Gaussian	Gaussian
<i>T<sub>min</sub></i> , <i>T<sub>max</sub></i>	0.082, 0.888	0.282, 0.804
No. of measured, independent and observed [ <i>I</i> > 2 $\sigma$ ( <i>I</i> )] reflections	29264, 16136, 12402	14382, 7413, 4342
<i>R<sub>int</sub></i>	0.037	0.083
(sin $\theta$ / $\lambda$ ) <sub>max</sub> (Å <sup>-1</sup> )	0.623	0.599
Range of <i>h</i> , <i>k</i> , <i>l</i>	<i>h</i> = -12 → 15, <i>k</i> = -16 → 15, <i>l</i> = -31 → 29	<i>h</i> = -15 → 15, <i>k</i> = -15 → 12, <i>l</i> = -22 → 29
<b>Refinement</b>		
<i>R</i> [ <i>F</i> <sup>2</sup> > 2 $\sigma$ ( <i>F</i> <sup>2</sup> )], <i>wR</i> ( <i>F</i> <sup>2</sup> ), <i>S</i>	0.036, 0.087, 0.91	0.055, 0.116, 0.84
No. of reflections	16133	7413
No. of parameters	939	507
No. of restraints	0	126
H-atom treatment	H-atom parameters constrained	H-atom parameters constrained
$\Delta$ <sub>max</sub> , $\Delta$ <sub>min</sub> (e Å <sup>-3</sup> )	1.60, -1.59	1.61, -1.51
Computer programs for <b>2</b> : CrysAlis PRO 1.171.38.46 (Rigaku OD, 2015), SHELXT2014/7 (Sheldrick, 2014), SHELXL2014/7 (Sheldrick, 2014).		
Computer programs for <b>3a</b> : CrysAlis PRO 1.171.38.41 (Rigaku OD, 2015), SHELXT2014/7 (Sheldrick, 2014), SHELXL2014/7 (Sheldrick, 2014).		

**Table 5:** Experimental details for compounds **3b** and **3c**.

Crystal data	<b>3b</b>	<b>3c</b>
Chemical formula	C <sub>20.25</sub> H <sub>30.5</sub> Ag <sub>2</sub> Cl <sub>0.5</sub> F <sub>12</sub> Fe <sub>2</sub> P <sub>13</sub> Sb <sub>2</sub>	C <sub>20</sub> H <sub>30</sub> Ag <sub>2</sub> F <sub>6</sub> Fe <sub>2</sub> P <sub>10</sub> Sb·F <sub>6</sub> Sb
<i>M<sub>r</sub></i>	1493.22	1502.96
Crystal system, space group	monoclinic, <i>P</i> 2 <sub>1</sub> / <i>n</i>	monoclinic, <i>P</i> 2 <sub>1</sub> / <i>n</i>
Temperature (K)	90	90
<i>a</i> , <i>b</i> , <i>c</i> (Å)	13.3439 (3), 12.7104 (3), 24.6189 (6)	13.3701 (3), 12.6877 (3), 24.6806 (6)
$\alpha$ , $\beta$ , $\gamma$ (°)	90.234 (2)	90.411 (2)
<i>V</i> (Å <sup>3</sup> )	4175.49 (16)	4186.59 (16)
<i>Z</i>	4	4
<i>F</i> (000)	2846	2864
<i>D<sub>x</sub></i> (Mg m <sup>-3</sup> )	2.375	2.384
Radiation type	Cu K $\alpha$	Cu K $\alpha$
$\mu$ (mm <sup>-1</sup> )	28.62	28.62
Crystal shape	needle	needle
Colour	brown	brown
Crystal size (mm)	0.28 × 0.03 × 0.02	0.24 × 0.01 × 0.01
<b>Data collection</b>		
Diffractometer	SuperNova, Titan <sup>S2</sup>	SuperNova, Titan <sup>S2</sup>
Absorption correction	Gaussian	Gaussian
<i>T<sub>min</sub></i> , <i>T<sub>max</sub></i>	0.046, 0.612	0.149, 0.935
No. of measured, independent and observed [ <i>I</i> > 2 $\sigma$ ( <i>I</i> )] reflections	15588, 8096, 7200	15491, 8151, 6014
<i>R<sub>int</sub></i>	0.032	0.038
(sin $\theta$ / $\lambda$ ) <sub>max</sub> (Å <sup>-1</sup> )	0.622	0.623
Range of <i>h</i> , <i>k</i> , <i>l</i>	<i>h</i> = -16 → 12, <i>k</i> = -15 → 11, <i>l</i> = -23 → 30	<i>h</i> = -16 → 15, <i>k</i> = -15 → 10, <i>l</i> = -30 → 26
<b>Refinement</b>		
<i>R</i> [ <i>F</i> <sup>2</sup> > 2 $\sigma$ ( <i>F</i> <sup>2</sup> )], <i>wR</i> ( <i>F</i> <sup>2</sup> ), <i>S</i>	0.045, 0.118, 1.06	0.039, 0.090, 0.91
No. of reflections	8096	8151
No. of parameters	502	480
No. of restraints	0	0
H-atom treatment	H-atom parameters constrained	H-atom parameters constrained
$\Delta$ <sub>max</sub> , $\Delta$ <sub>min</sub> (e Å <sup>-3</sup> )	1.8, -1.71	1.48, -1.55
Computer programs for <b>3b</b> : CrysAlisPro 1.171.38.46 (Rigaku OD, 2015), SHELXS-2014/7 (Sheldrick, 2014), SHELXL-2014/7 (Sheldrick, 2014).		
Computer programs for <b>3c</b> : CrysAlis PRO 1.171.38.46 (Rigaku OD, 2015), SHELXT2014/7 (Sheldrick, 2014), SHELXL2014/7 (Sheldrick, 2014).		

**Table 6:** Experimental details for compounds **4a-c**.\*.

Crystal data	<b>4a</b>	<b>4b</b>	<b>4c</b>
Tentative chemical formula based on the major component of the disorder	$[P_4@[\{Cp^*Fe(\eta^5-P_5)\}_9\{Ag_9(NC(CH_2)_{10}CN)_4\}][SbF_6]_9]$	$[P_4@[\{Cp^*Fe(\eta^5-P_5)\}_9\{Ag_9(NC(CH_2)_{10}CN)_{4.5}\}][SbF_6]_9]$	$[P_4@[\{Cp^*Fe(\eta^5-P_5)\}_9\{Ag_{10}(NC(CH_2)_{10}CN)_{4.5}\}][SbF_6]_{10}]$
$M_r$	9527.82	9623.97	9967.58
Crystal system, space group	monoclinic, $P2_1/n$	triclinic, $P\bar{1}$	orthorhombic, $Pnma$
Temperature (K)	80	80	80
$a, b, c$ (Å)	18.46130(11), 36.6790(2), 19.57988(8) **	21.36744(15), 34.85953(17), 35.8131(3)	35.89982(12), 37.19465(14), 21.50881(13)
$\alpha, \beta, \gamma$ (°)	90, 99.5000(4), 90	82.8241(5), 78.2185(6), 83.4991(5)	90, 90, 90
$V$ (Å <sup>3</sup> )	13076.53(12)	25803.3(3)	28720.3(2)
$Z$	2	4	4
Radiation type	synchrotron, 1-axis goniostat, Dectris Pilatus 6M	synchrotron, 1-axis goniostat, Dectris Pilatus 6M	synchrotron, 1-axis goniostat, Dectris Pilatus 6M
Crystal shape	plate	rod	prism
Colour	green brown	green brown	green brown
<b>Preliminary refinement</b>			
No. of reflections	24806	60883	25644
No. of parameters	1796	4966	1330
No. of restraints	3	0	0
$R[F^2 > 2\sigma(F^2)], wR(F^2), S$	0.0849, 0.3122, 1.494	0.1103, 0.3368, 2.151	0.1109, 0.3304, 1.059

\* preliminary data;

\*\* preliminary  $q$ -vector was roughly determined with *CrysAlis PRO* program as {0.265, 0, 0.443}.

## 7.6 Computational Details on 3c

All calculations have been performed with the TURBOMOLE program package.<sup>19</sup> The geometry of a  $[(\text{Cp}^*\text{Fe}(\eta^5\text{-P}_5))_2(\eta^2\text{-P}_4)\text{Ag}]^+$  unit, as a section of the polymeric structure **3c**, has been optimised using the RI<sup>[20]</sup>-B3LYP<sup>[21]</sup> functional together with the def2-TZVP<sup>[22]</sup> basis set. To speed up the geometry optimization the Resolution of Identity and the Multipole Accelerated Resolution-of-the-Identity (MARI-J)<sup>[23]</sup> approximations has been used.

In the gas phase optimised geometry of a fragment of **3c**, the Ag-P distances to  $\text{P}_4$  are longer while the coordinating P-P bond in  $\text{P}_4$  is shorter than determined experimentally by X-ray structure analysis (Ag-P: 3.057, 3.063 Å and 2.67(5), 2.717(4) Å, respectively; P-P: 2.244 and 2.307(6) Å, respectively). Additionally, the  $\text{P}_4$  ligand rotates leading to a tetrahedral like coordination around the silver. Based on this discrepancies between the gas phase optimised and experimental geometry, we performed single point calculations on the experimental geometry at the D3<sup>13</sup>-B3LYP/def2-TZVPP level. The Wiberg Bond Indices (WBI) of the coordinating P-P bond is 0.86, which is lower than the WBI of the other P-P bonds in  $\text{P}_4$  (1.02 to 1.04) indicating that the coordinating P-P bond is weakened, but still intact. The WBI of the P-P bonds in the  $\text{P}_5$  units vary from 1.28 to 1.30 reflecting the multiple bond character of these bonds. The localised molecular orbital describing the Ag- $\text{P}_4$  bonding is depicted in *Figure 7*. It shows a high orbital contribution from the  $\text{P}_4$  ligand (90%) and only a minor contribution from Ag (10%). The tendential activation of the coordinating P-P bond of  $\text{P}_4$  is also obvious from the natural charge distribution. While the coordinating P atoms in  $\text{P}_4$  ligand are slightly negatively charged (−0.05e), the other two P atoms are slightly positively charged (0.08e). The silver ion bears a positive charge of 0.65e.

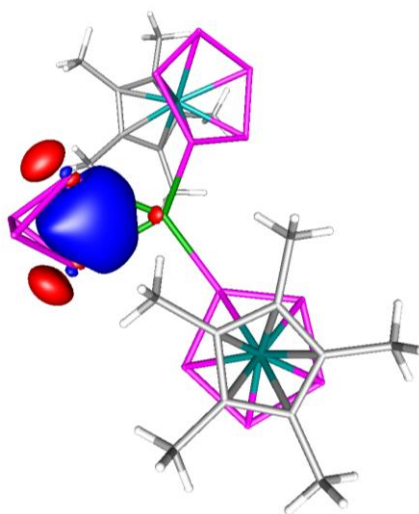
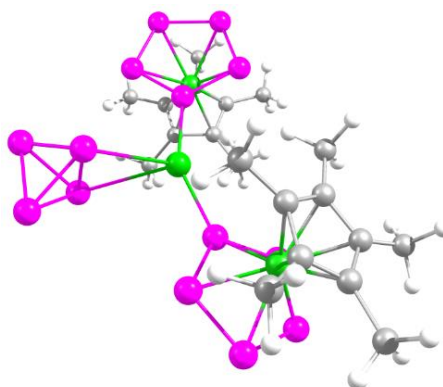


**Figure 7:** Localized Molecular Orbital representing the Ag- $\text{P}_4$  bonding in  $[(\text{Cp}^*\text{Fe}(\text{P}_5))_2(\eta^2\text{-P}_4)]$  at the RI-B3LYP/def2-TZVP level of theory.

**Table 7:** Cartesian coordinates of the gas phase optimized geometry of  $[(\text{Cp}^*\text{Fe}(\text{P}_5))_2(\eta^2\text{-P}_4)]$  at the RI-B3LYP/def2-TZVP level of theory.

Atom	x	y	z
P	-4.4900679	-0.1528151	-1.0109752
P	-4.4364036	0.5077351	1.1329440
P	-5.9541008	1.2962698	-0.2454066
P	-6.0242940	-0.8277148	0.4086988
P	-0.9340215	5.5560436	-1.5524996
P	0.9983579	5.1177179	-0.7766450
P	1.0470130	3.0986379	-0.1328377
P	-0.9165994	2.3729837	-0.4743203
P	-2.1477606	3.8244671	-1.4081106
P	-1.3018496	-5.4721971	1.5490760
P	-2.3950368	-3.6602580	1.4280880
P	-1.0782252	-2.2917624	0.4860191
P	0.8267245	-3.1488915	0.1174747
P	0.6467449	-5.1635324	0.7515594
Ag	-1.6189352	0.0642905	0.0169402
Fe	0.0744075	3.4884226	-2.3159493
Fe	-0.1443911	-3.4835955	2.3096305
C	-0.2945376	2.2092065	-3.9652399
C	1.0213931	1.9736765	-3.4568072
C	1.7626388	3.1906460	-3.5705994
C	0.9055602	4.1779985	-4.1490454
C	-0.3659262	3.5713669	-4.3927848
C	-1.3681239	1.1836181	-4.1390700
H	-1.2944552	0.3879295	-3.3983970
H	-1.2849609	0.7187279	-5.1263302
H	-2.3633478	1.6208159	-4.0666308
C	1.5678193	0.6581422	-3.0026140
H	0.7923355	0.0165405	-2.5857922
H	2.3437502	0.7798901	-2.2479142
H	2.0124402	0.1258188	-3.8491495
C	3.2123664	3.3683390	-3.2511903
H	3.4416904	4.3917139	-2.9572603
H	3.8183771	3.1353446	-4.1322076
H	3.5357528	2.7085199	-2.4470375
C	1.3054862	5.5643870	-4.5404755
H	0.4630668	6.2541654	-4.5144652
H	1.6981125	5.5620769	-5.5620760
H	2.0842934	5.9620205	-3.8911731
C	-1.5252618	4.2167766	-5.0818737
H	-1.5663518	5.2883736	-4.8911266
H	-2.4759536	3.7846847	-4.7718085
H	-1.4382402	4.0787681	-6.1640766
C	1.5793992	-3.2771577	3.5339412
C	0.6921807	-4.2354553	4.1156022
C	-0.5469025	-3.5785774	4.3936050
C	-0.4253548	-2.2144324	3.9840586
C	0.8891981	-2.0280615	3.4522993
C	3.0135802	-3.5111001	3.1825232
H	3.3477008	-2.8553035	2.3794391
H	3.1944236	-4.5394264	2.8724420
H	3.6464453	-3.3140678	4.0533894
C	1.0385950	-5.6436081	4.4792314
H	0.1671587	-6.2965376	4.4556768
H	1.4459737	-5.6744159	5.4945522
H	1.7898710	-6.0633623	3.8117484
C	-1.7195053	-4.1835285	5.0967789
H	-2.6564591	-3.7070146	4.8108246
H	-1.6062830	-4.0641361	6.1787706
H	-1.8102572	-5.2496528	4.8930143
C	-1.4504466	-1.1467825	4.1941435
H	-1.3572868	-0.3437976	3.4636575
H	-1.3282805	-0.7010524	5.1861456
H	-2.4645437	-1.5403227	4.1351613
C	1.4840364	-0.7309755	3.0058192
H	0.7272855	-0.0440545	2.6290191
H	2.2277532	-0.8734609	2.2226643
H	1.9822321	-0.2390648	3.8469517



## 7.7 Spectra

### NMR spectra

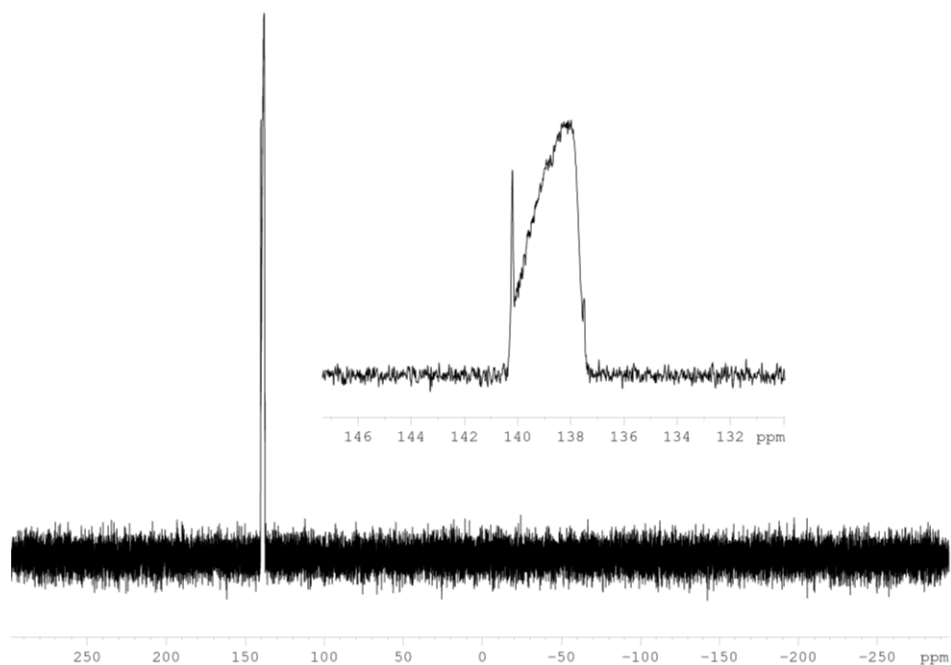


Figure 7:  $^{31}\text{P}$  NMR spectrum of **2** in  $\text{CD}_3\text{CN}$ .

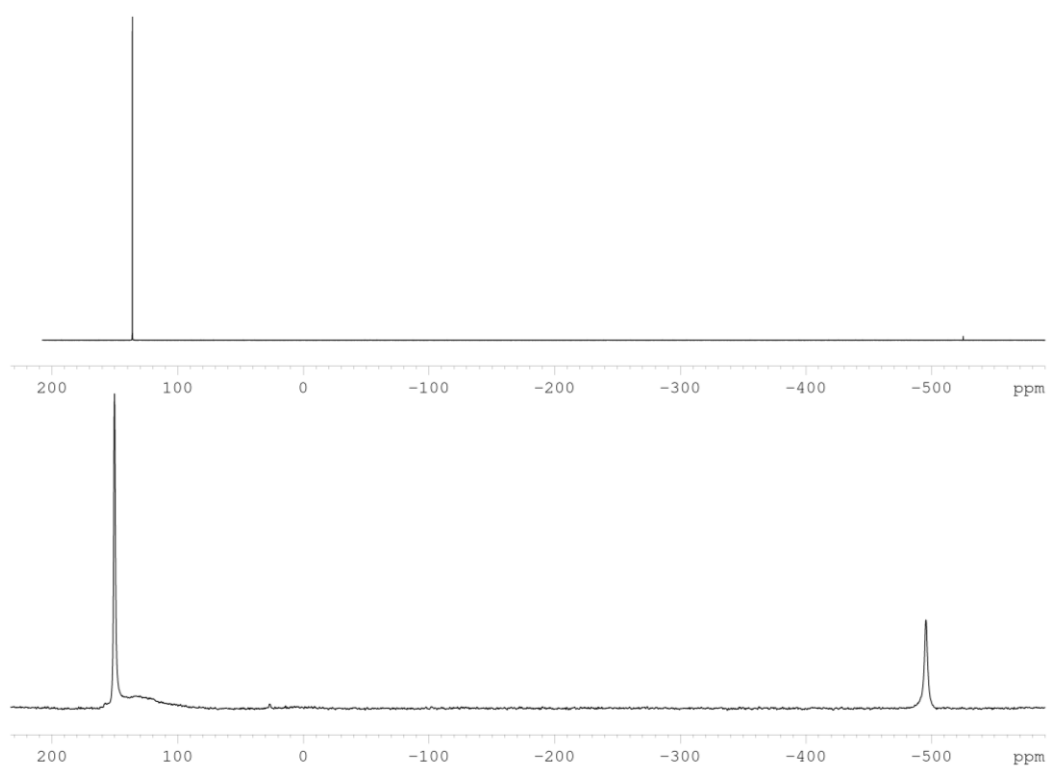


Figure 8:  $^{31}\text{P}$  NMR spectrum of **3c** in  $\text{CD}_3\text{CN}$  (top) and in solid state ( $^{31}\text{P}\{^1\text{H}\}$  MAS NMR, bottom).

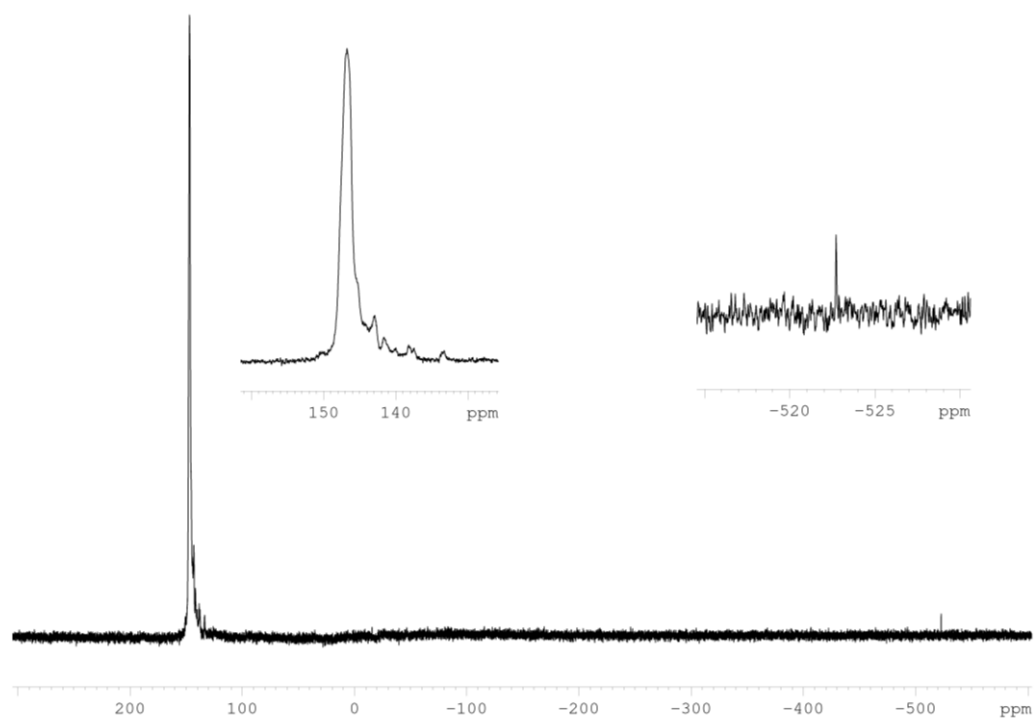


Figure 9:  $^{31}\text{P}$  NMR spectrum of **4** in  $\text{CD}_2\text{Cl}_2$  with pyridine.

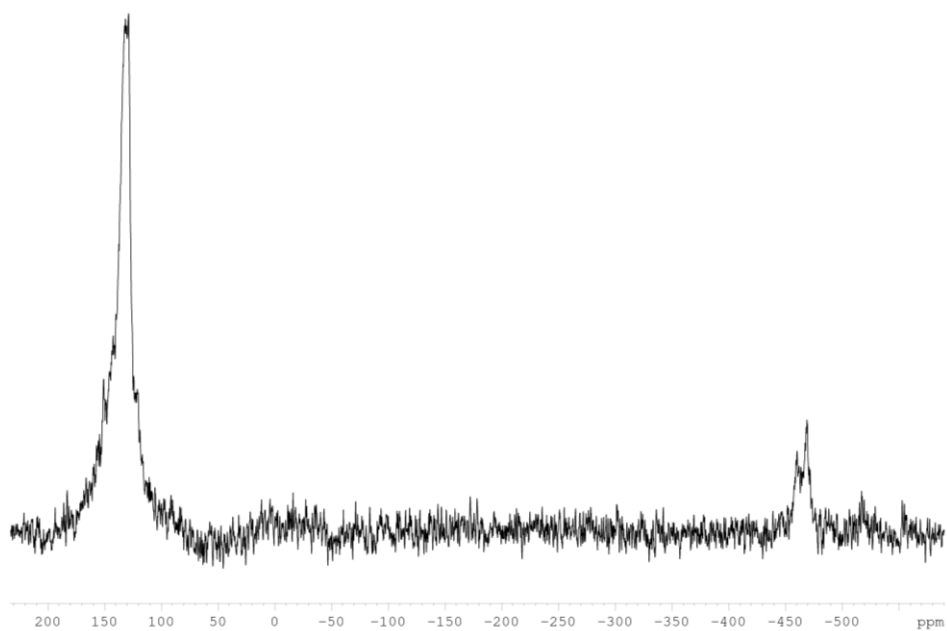
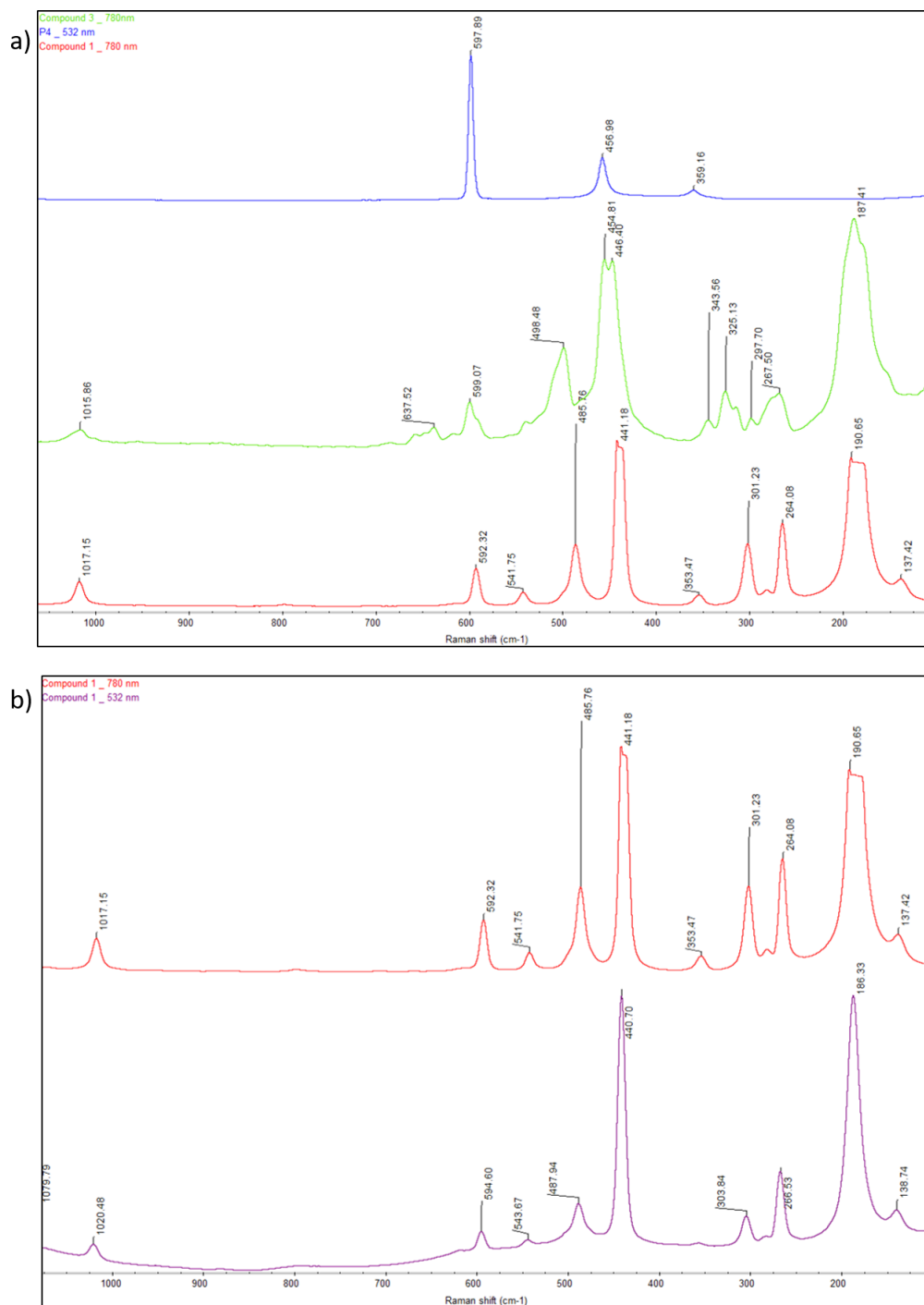


Figure 10:  $^{31}\text{P}\{^1\text{H}\}$  MAS NMR spectrum of **4**.



## Raman spectra



**Figure 11:** Comparison of Raman spectra of a) P<sub>4</sub> (532 nm, blue), **3** (780 nm, green) and **1** (780 nm, red); b) **1**, recorded at 780 nm (red) and 532 nm (violet).

## 7.8 Author Contributions

- The synthesis and characterization of all compounds were performed by B. Hiltl.
- The manuscript (introduction, results and discussions, experimental part, conclusion; including figures and graphical abstract) was written by B. Hiltl.
- The section ‘crystallographic details’ was written by Dr. E. Peresyphkina.
- All X-ray structural investigations were performed by Dr. E. Peresyphkina and Dr. Sc. A. V. Virovets.
- MAS NMR investigations were performed by Prof. W. Kremer.
- DFT computations were performed by Dr. Gábor Balász.

## 7.9 References

- <sup>1</sup> a) C. J. Brown, F. D. Toste, R. G. Bergman, K. N. Raymond, *Chem. Rev.* **2015**, *115*, 3012-3035; b) S. H. A. M. Leenders, R. Gramage-Doria, B. de Bruin, J. N. H. Reek, *Chem. Soc. Rev.* **2015**, *44*, 433-448.
- <sup>2</sup> N. Ahmad, H. A. Younus, A. H. Chughtai, F. Verpoort, *Chem. Soc. Rev.* **2015**, *44*, 9-25.
- <sup>3</sup> a) J. L. Brumaghim, M. Michels, D. Pagliero, K. N. Raymond, *Eur. J. Org. Chem.* **2004**, 5115-5118; b) D. Fiedler, R. G. Bergman, K. N. Raymond, *Angew. Chem., Int. Ed.* **2006**, *45*, 745-748; c) S. Horiuchi, T. Murase, M. Fujita, *J. Am. Chem. Soc.* **2011**, *133*, 12445-12447;
- <sup>4</sup> a) M. Caporali, L. Gonsalvi, A. Rossin, M. Peruzzini, *Chem. Rev.* **2010**, *110*, 4178-4235; b) B. M. Cossairt, N. A. Piro, C. C. Cummins, *Chem. Rev.* **2010**, *110*, 4164-4177; c) M. Scheer, G. Balazs, A. Seitz, *Chem. Rev.* **2010**, *110*, 4236-4256.
- <sup>5</sup> C. Schwarmaier, A. Schindler, C. Heindl, S. Scheuermayer, E. V. Peresyphkina, A. V. Virovets, M. Neumeier, R. Gschwind, M. Scheer, *Angew. Chem., Int. Ed.* **2013**, *52*, 10896-10899.
- <sup>6</sup> a) D. Yang, J. Zhao, L. Yu, X. Lin, W. Zhang, H. Ma, A. Gogoll, Z. Zhang, Y. Wang, X.-J. Yang, B. Wu, *J. Am. Chem. Soc.* **2017**, *139*, 5946-5951; b) P. Mal, B. Breiner, K. Rissanen, J. R. Nitschke, *Science* **2009**, *324*, 1697-1699.
- <sup>7</sup> a) W. Choi, H. Ohtsu, Y. Matsushita, M. Kawano, *Dalton Trans.* **2016**, *45*, 6357-6360; b) A. E. Seitz, M. Scheer, F. Hippauf, S. Kaskel, W. Kremer, *Nat Commun* **2018**, *9*, 361;
- <sup>8</sup> a) M. Scheer, A. Schindler, R. Merkle, B. P. Johnson, M. Linseis, R. Winter, C. E. Anson, A. V. Virovets, *J. Am. Chem. Soc.* **2007**, *129*, 13386-13387; b) M. Scheer, A. Schindler, C. Groeger, A. V. Virovets, E. V. Peresyphkina, *Angew. Chem., Int. Ed.* **2009**, *48*, 5046-5049; c) A. Schindler, C. Heindl, G. Balazs, C. Groeger, A. V. Virovets, E. V. Peresyphkina, M. Scheer, *Chem. Eur. J.* **2012**, *18*, 829-835; d) E. Peresyphkina, C. Heindl, A. Virovets, H. Brake, E. Maedl, M. Scheer, *Chem. Eur. J.* **2018**, *24*, 2503-2508.
- <sup>9</sup> a) G. Santiso-Quinones, A. Reisinger, J. Slattery, I. Krossing, *Chem. Commun.* **2007**, 5046-5048; b) L. C. Forfar, T. J. Clark, M. Green, S. M. Mansell, C. A. Russell, R. A. Sanguramath, J. M. Slattery, *Chem.*

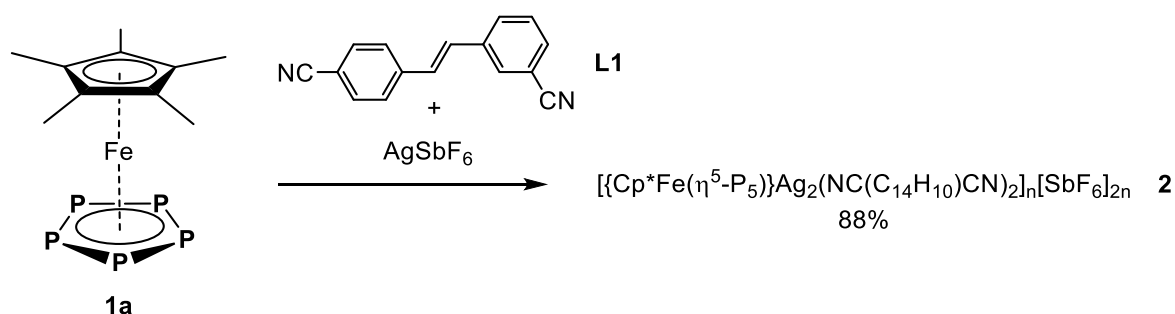
- Commun.* **2012**, *48*, 1970-1972; c) F. Spitzer, M. Sierka, M. Latronico, P. Mastorilli, A. V. Virovets, M. Scheer, *Angew. Chem., Int. Ed.* **2015**, *54*, 4392-4396; d) L. C. Forfar, D. Zeng, M. Green, J. E. McGrady, C. A. Russell, *Chem. Eur. J.* **2016**, *22*, 5397-5403.
- <sup>10</sup> a) A. Bihlmeier, M. Gonsior, I. Raabe, N. Trapp, I. Krossing, *Chem. Eur. J.* **2004**, *10*, 5041-5051; b) I. Krossing, L. Van Wullen, *Chem. Eur. J.* **2002**, *8*, 700-711; c) L. C. Forfar, T. J. Clark, M. Green, S. M. Mansell, C. A. Russell, R. A. Sanguramath, J. M. Slattery, *Chem. Commun.* **2012**, *48*, 1970-1972.
- <sup>11</sup> B. M. Cossairt, C. C. Cummins, A. R. Head, D. L. Lichtenberger, R. J. F. Berger, S. A. Hayes, N. W. Mitzel, G. Wu, *J. Am. Chem. Soc.* **2010**, *132*, 8459-8465.
- <sup>12</sup> N. J. Brassington, H. G. M. Edwards, D. A. Long, *J. Raman Spectrosc.* **1981**, *11*, 346-348.
- <sup>13</sup> S. Grimme; J. Antony; S. Ehrlich; H. Krieg. *J. Chem. Phys.*, **2010**. *132*, 154104.
- <sup>14</sup> F. Dielmann, R. Merkle, S. Heinel, M. Scheer, *Z. Naturforsch.* **2009**, *64*, 3.
- <sup>15</sup> M. Detzel, G. Friedrich, O. J. Scherer and G. Wolmershäuser, *Angew. Chem. Int. Ed.* **1995**, *34*, 1321.
- <sup>16</sup> A. Burkhardt, T. Pakendorf, B. Reime, et al, *Eur. Phys. J. Plus* **2016**, *131*, 56-64.
- <sup>17</sup> CrysAlis Pro. Different versions (Rigaku OD).
- <sup>18</sup> G. M. Sheldrick, *Acta Cryst. sect. C* **2015**, C71, 3.
- <sup>19</sup> a) R. Ahlrichs, M. Bär, M. Häser, H. Horn, C. Kölmel, *Chem. Phys. Lett.* **1989**, *162*, 165-169; b) O. Treutler, R. Ahlrichs, *J. Chem. Phys.* **1995**, *102*, 346-354.
- <sup>20</sup> a) K. Eichkorn, O. Treutler, H. Oehm, M. Häser, R. Ahlrichs, *Chem. Phys. Lett.* **1995**, *242*, 652-660; b) K. Eichkorn, F. Weigend, O. Treutler, R. Ahlrichs, *Theor. Chem. Acc.* **1997**, *97*, 119.
- <sup>21</sup> a) A. D. Becke, *J. Chem. Phys.* **1993**, *98*, 5648-5652, b) C. Lee, W. Yang, R. G. Parr, *Phys. Rev. B* **1988**, *37*, 785-789, c) A. D. Becke, *Phys. Rev. A* **1988**, *38*, 3098-3100, d) S. H. Vosko, L. Wilk, M. Nusair, *Can. J. Phys.* **1980**, *58*, 1200-1211, e) J. C. Slater, *Phys. Rev.* **1951**, *81*, 385-390, f) P. A. M. Dirac, *Proc. Royal Soc. A* **1929**, *123*, 714-733.
- <sup>22</sup> a) A. Schäfer, C. Huber, R. Ahlrichs, *J. Chem. Phys.* **1994**, *100*, 5829; b) K. Eichkorn, F. Weigend, O. Treutler, R. Ahlrichs, *Theor. Chem. Acc.* **1997**, *97*, 119.
- <sup>23</sup> a) M. Sierka, A. Hogekamp, R. Ahlrichs, *J. Chem. Phys.* **2003**, *118*, 9136. b) K. Eichkorn, O. Treutler, H. Oehm, M. Häser, R. Ahlrichs, *Chem. Phys. Lett.* **1995**, *242*, 652-660. c) K. Eichkorn, F. Weigend, O. Treutler, R. Ahlrichs, *Theor. Chem. Acc.* **1997**, *97*, 119.

## 8. Thesis Treasury

The following chapter presents preliminary results, which can provide a basis for future research efforts. The obtained compounds could not be fully characterized, however, all data and knowledge that was acquired about the described coordination products and reactions will be presented.

### 8.1 Three-component self-assembly of $[\text{Cp}^*\text{Fe}(\eta^5\text{-P}_5)]$ with $\text{AgSbF}_6$ and $\text{NC}(\text{C}_{14}\text{H}_{10})\text{CN}$ (**L1**)

The combination of  $[\text{Cp}^R\text{Fe}(\eta^5\text{-P}_5)]$  ( $\text{Cp}^R = \text{Cp}^*$  (**1a**),  $\text{Cp}^{\text{Bn}}$  (**1b**)) with Ag salts of weakly coordinating anions and ditopic nitriles in self-assembly brought various stunning coordination products ranging from 1D - 3D polymers and further on to three dimensionally linked spherical host assemblies (cf. *Chapters 5-7*). These results were all obtained by using  $\text{NC}(\text{CH}_2)_x\text{CN}$  ( $x = 5 - 10$ ) as fully flexible linking units. Previously reported coordination networks of  $[\{\text{Cp}^*(\text{CO})_2\text{Mo}\}_2(\eta^2\text{-P}_2)]$ , however, also use rigid or semi-rigid ditopic nitriles or pyridines as linkers.<sup>1</sup> To see in which extent linkers with limited flexibility give polymeric coordination products with **1a** and  $\text{AgSbF}_6$ ,  $\text{NC}(\text{C}_{14}\text{H}_{10})\text{CN}$  (**L1**) was applied in a reaction setup proven for flexible ditopic nitriles for a first trial. Thus, layering of  $\text{AgSbF}_6$  with **1a** and **L1** yielded the 2D coordination polymer  $[\{\text{Cp}^*\text{Fe}(\eta^5\text{-P}_5)\}\{\text{Ag}(\text{C}_{16}\text{H}_{10}\text{N}_2)\}_2(\text{C}_7\text{H}_8)]_n[\text{SbF}_6]_{2n}$  (**2**) in good yields (*Scheme 1*).



**Scheme 1:** Reaction of **1a** with  $\text{AgSbF}_6$  and **L1**.

Preliminary results from X-ray structure analysis show a 2D polymeric structure, built up by strands of  $[\{\text{Cp}^*\text{Fe}(\eta^5\text{-P}_5)\}\text{Ag}_2]_n$  which are linked by **L1** (*Figure 1*). All *cyclo*- $\text{P}_5$  ligands are coordinating in a 1,2,3,4 mode towards Ag atoms, which are in turn tetrahedrally coordinated by two *cyclo*- $\text{P}_5$  ligands and two linkers **L1**. All anions are non-coordinating and located the pores of the cationic coordination polymer. These structural features strongly remind of the 3D polymers  $[\{\text{Cp}^*\text{Fe}(\eta^5\text{-P}_5)\}\{\text{Ag}(\text{NC}(\text{CH}_2)_5\text{CN})\}_2]_n[\text{SbF}_6]_n$  and  $[\{\text{Cp}^*\text{Fe}(\eta^5\text{-P}_5)\}\{\text{Ag}_2(\text{NC}(\text{CH}_2)_7\text{CN})\}]_n[\text{SbF}_6]_{2n}$  (cf. *Chapter V*), which also consist of these 1D strands linked by  $\text{NC}(\text{CH}_2)_x\text{CN}$  ( $x = 5, 7$ ). The separate 2D

layers are oriented towards each other, directed by the aromatic parts of the linkers (*Figure 1b*). **2** is insoluble in organic solvents as  $\text{CH}_2\text{Cl}_2$  or toluene and shows fragmentation in  $\text{CH}_3\text{CN}$ .

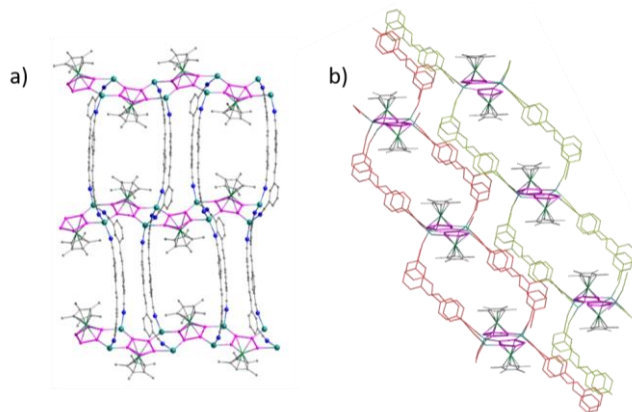
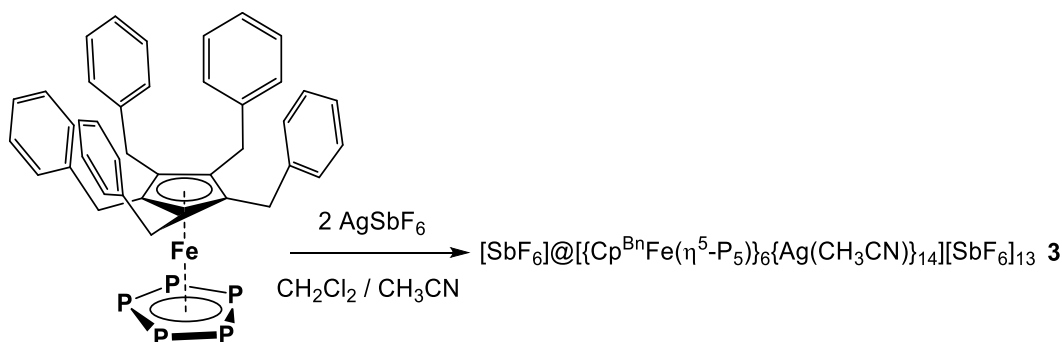


**Figure 1:** a) 2D polymeric **2**; b) Orientation of 2D layers. H atoms and anions are omitted for clarity.

With this result it can be stated that also linkers with a limited flexibility are suitable for constructing polymeric coordination products along with **1a** and  $\text{AgSbF}_6$ . As this is only a first trial to extend the field of linkers from fully flexible to rigid or semi-rigid linkers, a whole variety of designed ditopic nitriles and benzonitriles with special features of length and flexibility can be investigated in future.

## 8.2 Self-assembly of $[\text{Cp}^{\text{Bn}}\text{Fe}(\eta^5\text{-P}_5)]$ with $\text{AgSbF}_6$ in the presence of $\text{CH}_3\text{CN}$

In the course of the studies presented in *Chapter IV*, the coordination and self-assembly products of **1b**,  $\text{AgSbF}_6$  and a benzonitrile were considered. Regarding the results of this three-component self-assembly, namely the formation of the pentanuclear  $\{[\text{Cp}^{\text{Bn}}\text{Fe}(\eta^5\text{-P}_5)]_4[\text{Ag}(\text{CN}(\text{C}_6\text{H}_4)\text{Cl})]_5\}[\text{SbF}_6]_5 \cdot (\text{CH}_2\text{Cl}_2)$  and the trigonal anti-prismatic shaped sphere  $[\text{SbF}_6]^- @ \{[\text{Cp}^{\text{Bn}}\text{Fe}(\eta^5\text{-P}_5)]_6\}[\text{Ag}(\text{NC}(\text{C}_6\text{H}_4)\text{Cl})]_{9.55}[\text{SbF}_6]_{8.55}$ , the idea came to mind to also try the smaller  $\text{CH}_3\text{CN}$  as coordinating solvent to saturate the free coordination sites at the Ag atoms of the supramolecular assemblies. For this purpose, a solution of  $[\text{Cp}^{\text{Bn}}\text{Fe}(\eta^5\text{-P}_5)]$  and  $\text{AgSbF}_6$  in a mixture of  $\text{CH}_2\text{Cl}_2$  and  $\text{CH}_3\text{CN}$  was stirred. The olive crystalline product with an assumed sum formula of  $[\text{SbF}_6]^- @ \{[\text{Cp}^{\text{Bn}}\text{Fe}(\eta^5\text{-P}_5)]_6\}[\text{Ag}(\text{CH}_3\text{CN})]_{14}[\text{SbF}_6]_{13}$  (**3**) was obtained by layering a  $\text{CH}_2\text{Cl}_2$  solution with pentane in moderate yield of 65 %.



**Scheme 2:** Reaction of **1b** with  $\text{AgSbF}_6$  in the presence of  $\text{CH}_3\text{CN}$ .

The molecular structure was elucidated by X-ray structure analysis, for which however only could obtain preliminary results, due to a limited quality of the obtained crystals. The poor crystallinity led to a low-angle diffraction pattern. The absence of high-angle data did not allow to perform an adequate structure refinement and to establish a reliable composition of this compound. The therefore supposed structure of **3** consists of discrete polycationic spherical assemblies of six *cyclo*-P<sub>5</sub> ligands and 14 positions for Ag atoms (*Figure 2*). Each, but two, Ag atoms are coordinatively saturated by CH<sub>3</sub>CN ligands. The sphere acts as a host for one SbF<sub>6</sub><sup>-</sup> anion, whereas the remaining ones are located non-coordinating in the surrounding of the assembly. The centroids of the *cyclo*-P<sub>5</sub> ligands form a trigonal antiprism with an inner diameter of about 12.6 Å. The exact composition and occupancy of the Ag atoms could not be determined so far, due to very low scattering behaviour of the crystals and severe disordering of the SbF<sub>6</sub><sup>-</sup> anions and the Bn residues of **1b**. Furthermore, the elemental analysis did not furnish reliable results, due to the possibility of intercalating solvent molecules between the Bn residues. Considering the structural similarities with [SbF<sub>6</sub><sup>-</sup>][{Cp<sup>Bn</sup>Fe(η<sup>5</sup>-P<sub>5</sub>)}<sub>6</sub>{Ag(CN(C<sub>6</sub>H<sub>4</sub>)Cl)}<sub>9.55</sub>] [SbF<sub>6</sub>]<sub>8.55</sub> (cf. *Chapter IV*), assumedly not all positions of Ag atoms are fully occupied. Whereas in the <sup>1</sup>H NMR spectrum very broad signals for the Bn residues suggest larger aggregates in solution, from the DOSY measurements only an estimated diameter of 1.8 nm could be derived, being only 62 % of the 2.9 nm, expected for the size of the sphere from the preliminary X-ray data, indicating a limited stability of the spherical aggregates in solution.

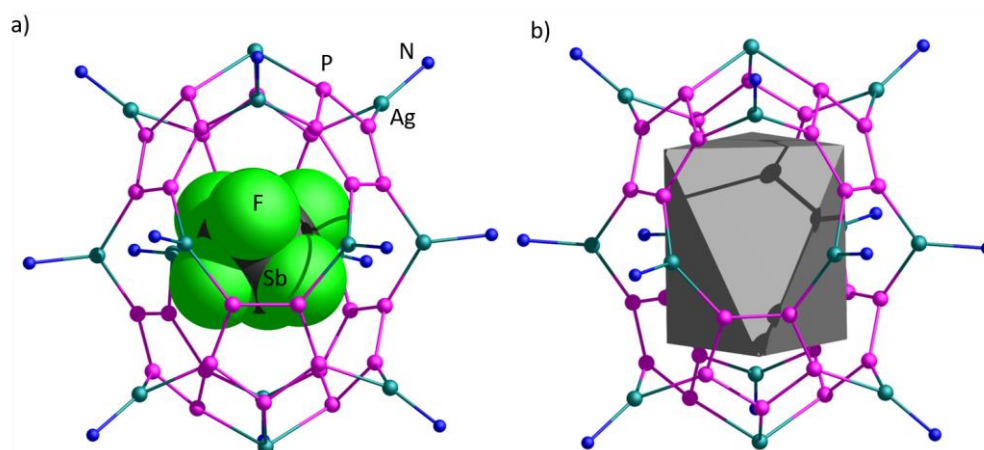
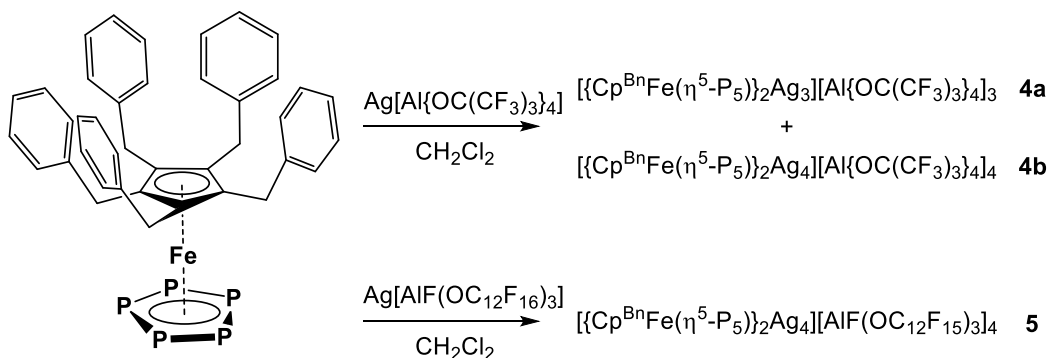


**Figure 2:** Spherical scaffold of **3** with a) SbF<sub>6</sub><sup>-</sup> as a template; b) units of **1b** forming a trigonal antiprism. [Cp<sup>Bn</sup>Fe] units, CCH<sub>3</sub> residues of CH<sub>3</sub>CN ligands and anions are partly omitted for clarity.

### 8.3 Self-assembly of $[\text{Cp}^{\text{Bn}}\text{Fe}(\eta^5\text{-P}_5)]$ with Ag salts of the huge weakly coordinating anions $[\text{Al}\{\text{OC}(\text{CF}_3)_3\}_4]^-$ and $[\text{AlF}(\text{OC}_{12}\text{F}_{15})_3]^-$

Having in mind the promising results of the reactions of the pentaphosphaferrocene derivatives with the Ag salts of the weakly coordinating anion  $\text{SbF}_6^-$ , we also wanted to examine other Ag salts of weakly coordinating anions. As the probability of coordination decreases with increasing possibility of charge distribution over the volume of an anion, the two huge perfluorinated aluminate anions  $[\text{Al}\{\text{OC}(\text{CF}_3)_3\}_4]^-$  (TEF<sup>-</sup>) and  $[\text{AlF}(\text{OC}_{12}\text{F}_{15})_3]^-$  (FAl<sup>-</sup>) are known to be very weakly coordinating.<sup>2</sup> As described in *Chapter VI* AgTEF was tested in a three-component self-assembly with **1a** and the long flexible  $\text{NC}(\text{CH}_2)_{10}\text{CN}$  in order to possibly form connected spherical aggregates. However, the size of the anions prevent a polycationic assembly as their dense arrangement in the surrounding is not favoured due to repulsion forces of their negative charges. Although we also wanted to investigate the two-component self-assembly of these weakly coordinating anions with **1b** without an additional coordinating building block such as nitriles. Thus, a solution of both starting materials was stirred in  $\text{CH}_2\text{Cl}_2$ , whereas crystals of  $[\{\text{Cp}^{\text{Bn}}\text{Fe}(\eta^5\text{-P}_5)\}_2\text{Ag}_3][\text{Al}\{\text{OC}(\text{CF}_3)_3\}_4]_3 \cdot (\text{CH}_2\text{Cl}_2)$  (**4a**),  $[\{\text{Cp}^{\text{Bn}}\text{Fe}(\eta^5\text{-P}_5)\}_2\text{Ag}_4][\text{Al}\{\text{OC}(\text{CF}_3)_3\}_4]_4 \cdot (\text{CH}_2\text{Cl}_2)_2$  (**4b**) and  $[\{\text{Cp}^{\text{Bn}}\text{Fe}(\eta^5\text{-P}_5)\}_2\text{Ag}_4][\text{AlF}(\text{OC}_{12}\text{F}_{15})_3]_4$  (**5**) were obtained upon layering with *n*-hexane. For **4a,b** no yield can be given, as an exact ratio of the built dimers was not identified. **5** was only obtained as few crystals among a red oil, therefore no yield can be given as well.



**Scheme 3:** Reaction of **1b** with AgTEF (top) and AgFAl (bottom).

From the reaction of **1b** and AgTEF two different dimers were characterized by X-ray structure analysis, differing in the geometrical arrangement as well as in their composition. Whereas in **4a** the two *cyclo*-P<sub>5</sub> ligands are oriented almost perpendicular towards each other, in **4b** they form one plane together with the two bridging Ag atoms. In both cases the *cyclo*-P<sub>5</sub> ligands coordinate in a 1,2 mode towards the Ag atoms, whereas in **4b** one *cyclo*-P<sub>5</sub> unit coordinates in a 1,2,3 mode with two P atoms coordinating in a  $\eta^2$  mode towards one Ag atom. Those are each pseudo-tetrahedrally coordinated by two *cyclo*-P<sub>5</sub> ligands and one Bn residue of ligand **1b**. One (in **4a**) or two additional

Ag atoms (in **4b**) are intercalated between Bn residues of **1b**, coordinatively saturated each by one  $\text{CH}_2\text{Cl}_2$  molecule. In **5** the dimeric structure is comparable to **4a,b**, but with the two *cyclo*- $\text{P}_5$  ligands facing each other and connected by two Ag atoms, which are saturated by Bn residues. In contrast to **4a** and **4b** both *cyclo*- $\text{P}_5$  ligands in **5** are coordinating in a 1,2,4 mode with two P atoms in a  $\eta^2$ -coordination mode. Like in **4b**, two additional Ag atoms are intercalated between the Bn residues of **5**, although saturating  $\text{CH}_2\text{Cl}_2$  molecules are missing. All  $\text{TEF}^-$  and  $\text{FAl}^-$  anions are located around the dimers, showing no interaction.

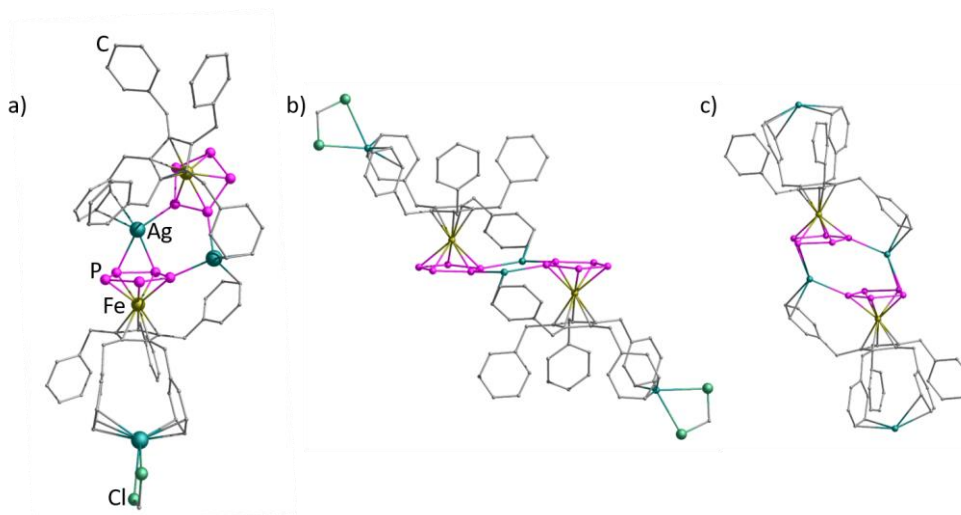
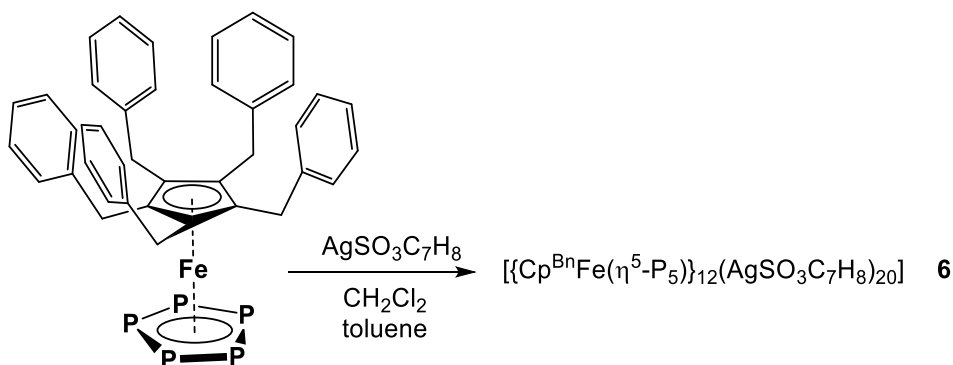


**Figure 3:** Dimers consisting of **1b** and AgTEF a) **4a**, b) **4b**, or AgFAl c) **5**. H atoms and anions are omitted for clarity.

#### 8.4 Self-assembly of $[\text{Cp}^{\text{Bn}}\text{Fe}(\eta^5\text{-P}_5)]$ with $\text{AgSO}_3\text{C}_7\text{H}_7$

In the course of the examinations regarding *Chapter III*, the self-assembly of **1b** and  $\text{AgSO}_3\text{C}_7\text{H}_7$  (AgTos) was conducted as well. These building blocks promise to assemble to desired spherical scaffolds, having the related combination of building blocks **1a** + AgTos and **1b** +  $\text{AgSO}_3\text{CF}_3$  in mind, both furnishing spherical supramolecules. The reaction was carried out in accordance to that of  $[\{\text{Cp}^{\text{Bn}}\text{Fe}(\eta^5\text{-P}_5)\}_{12}(\text{AgSO}_3\text{CF}_3)_{20-n}]$  (cf. *Chapter III*).



**Scheme 4:** Reaction of **1b** with AgTos.



Thus, large dark red rhombohedral crystals were obtained with a crystalline yield of 92 %, unfortunately showing very low scattering power, most probably due to low crystallinity. Considering the quality of the obtained X-ray data, unfortunately no reasonable refinement was possible. However, the positions of the heaviest atoms Ag, P and S could be roughly located, indicating the formation of a spherical scaffold, similar to that of  $[\{\text{Cp}^{\text{Bn}}\text{Fe}(\eta^5\text{-P}_5)\}_{12}(\text{AgSO}_3\text{CF}_3)_{20}]$  and  $[\{\text{Cp}^{\text{Bn}}\text{Fe}(\eta^5\text{-P}_5)\}_{12}(\text{CuSO}_3\text{CF}_3)_{19.4}]$ .<sup>3</sup> Thus, 12 units of **1b** assemble together with 30 positions for  $\text{Ag}^+$  in an idealized 90-vertex sphere with an assumed sum formula of  $[\{\text{Cp}^{\text{Bn}}\text{Fe}(\eta^5\text{-P}_5)\}_{12}(\text{AgSO}_3\text{C}_7\text{H}_7)_{20}]$  (**6**). Due to the similarity to AgOTf-containing compound and the preliminary localization of 20 Tos<sup>-</sup> in **6**, which are coordinating to the Ag atoms of the scaffold, assumedly the Ag positions in **6** are not fully occupied. Charge balance could possibly be reached by a disordered arrangement of about 20  $\text{Ag}^+$  over all 30 Ag positions, similar to that in  $[\{\text{Cp}^{\text{Bn}}\text{Fe}(\eta^5\text{-P}_5)\}_{12}(\text{AgSO}_3\text{CF}_3)_{20}]$  (cf. *Chapter III*).

The nature of the coordinating counter anion shows a remarkable influence on the solubility of the crystalline **6**, compared to  $[\{\text{Cp}^{\text{Bn}}\text{Fe}(\eta^5\text{-P}_5)\}_{12}(\text{AgSO}_3\text{CF}_3)_{20-n}]$ . Whereas the latter compound is well soluble in  $\text{CH}_2\text{Cl}_2$  or toluene, **6** only shows a moderate solubility in toluene and a poor solubility in  $\text{CH}_2\text{Cl}_2$ . Fragmentation of the assembly is observed upon addition of either pyridine or  $\text{CH}_3\text{CN}$ . In the  $^1\text{H}$  NMR spectrum of **6** in toluene- $d_8$ , a set of four broad signals is visible, which can be assigned to the  $\text{Cp}^{\text{Bn}}$  ligands of **1b** (4.78, 6.11 to 6.75 ppm). In the  $^{31}\text{P}\{^1\text{H}\}$  NMR spectrum of **6** in toluene- $d_8$  at room temperature only a sharp singlet of the complex **1b** occurs, which disappears upon cooling to 203 K, with broad signals at  $\delta = -49$  and 79 ppm emerging instead. These spectroscopic characteristics are in good accordance to those observed for  $[\{\text{Cp}^{\text{Bn}}\text{Fe}(\eta^5\text{-P}_5)\}_{12}(\text{AgSO}_3\text{CF}_3)_{20-n}]$  and are also reminiscent of the obtained spectra for porous 80-vertex derivatives  $[(\mathbf{1b})_{12}(\text{CuX})_{20-n}]$  ( $\text{X} = \text{Cl, Br; } n \leq 4.6$ ).<sup>4</sup> Furthermore, to prove the existence of spherical assemblies, TEM measurements were conducted along with  $[\{\text{Cp}^{\text{Bn}}\text{Fe}(\eta^5\text{-P}_5)\}_{12}(\text{AgSO}_3\text{CF}_3)_{20-n}]$ . Therefore, crystals of **6** were suspended in  $\text{CH}_2\text{Cl}_2$  and dropped on a copper grid coated with amorphous carbon. The average diameter of the particles showed to be 2.7 nm, whereas the expected outer diameter can only be estimated to be about 3.3 nm, from available X-ray data of limited quality. The inner scaffold of the comparable  $[\{\text{Cp}^{\text{Bn}}\text{Fe}(\eta^5\text{-P}_5)\}_{12}(\text{AgSO}_3\text{CF}_3)_{20-n}]$  (*Chapter III*) based on the heavy atoms Ag and P measures about 2.0 nm. The difference can be explained by the fact that the lighter atoms H and C in the outer shell of the sphere are hardly visible due to the contrast to the grid.

## 8.5 Experimental Part

### General Remarks

All reactions were performed under an inert atmosphere of dry nitrogen with standard vacuum, Schlenk and glove-box techniques. Solvents were purified, dried and degassed prior to use by standard procedures.  $[\text{Cp}^*\text{Fe}(\eta^5\text{-P}_5)]$ ,<sup>5</sup>  $[\text{Cp}^{\text{Bn}}\text{Fe}(\eta^5\text{-P}_5)]$ <sup>6</sup> and  $\text{Ag}[\text{Al}\{\text{OC}(\text{CF}_3)_3\}_4]$ <sup>7</sup> were synthesized following reported procedures. Commercially available  $\text{AgSbF}_6$  was used without further purification.  $\text{NC}(\text{C}_{14}\text{H}_{10})\text{CN}$  (**L1**) was provided by Dr. Christophe Lescope from INSA Rennes (France) and  $\text{Ag}(\text{AlF}(\text{OC}_{12}\text{F}_{15})_3)_3$  was provided by Dr. Martin Fleischmann. Solution NMR spectra were recorded on a Bruker Avance 300 or 400 spectrometer. The  $^{31}\text{P}\{^1\text{H}\}$  MAS spectrum was measured on a Bruker Avance 300. The corresponding ESI-MS spectra were acquired on a ThermoQuest Finnigan MAT TSQ 7000 mass spectrometer. CHN Elemental analyses were performed on a Vario EL III apparatus.

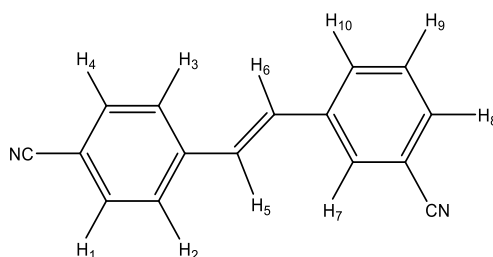
The Transmission electron microscopy (TEM) measurement were carried out on a FEI Tecnai G2 Spirit Twin transmission electron microscope equipped with a field emission gun and processed with an acceleration voltage of 120 kV. The machine is fitted with a LaB6 cathode and the pictures were recorded with an Gatan US1000 CCD-camera (2k × 2k). The analysis of the pictures was done with the graphic software Fiji.<sup>8</sup> For the preparation of the samples were the nanoparticles dispersed in dichloromethane and 20  $\mu\text{L}$  were dropped on copper grids coated with amorphous carbon

### Synthesis of $[\{\text{Cp}^*\text{Fe}(\eta^5\text{-P}_5)\}\{\text{Ag}(\text{C}_{16}\text{H}_{10}\text{N}_2)\}_2(\text{C}_7\text{H}_7)]_n[\text{SbF}_6]_{2n}$ (**2**)

In a thin Schlenk tube to a solution of  $\text{AgSbF}_6$  (41 mg, 0.12 mmol) in  $\text{CH}_2\text{Cl}_2$  (5 mL) was layered with a green solution of  $[\text{Cp}^*\text{Fe}(\eta^5\text{-P}_5)]$  (14 mg, 0.04 mmol) and **L1** (46 mg, 0.2 mmol) in toluene (5 mL). Thereby the phase boundary turns yellow. After diffusion, the formation of green plates (**2**) and some crystals of  $[\{\text{Cp}^*\text{Fe}(\eta^{5:2:1}\text{-P}_5)\}_2\text{Ag}]_n[\text{SbF}_6]_n$  can be observed. After complete diffusion, the mother liquor is decanted, the crystals are selected manually, washed with pentane (3 × 5 mL) and dried *in vacuo*.

Analytical data of **2**:

**Yield:** 57 mg (0.038 mmol, 88 % referred to  $[\text{Cp}^*\text{Fe}(\eta^5\text{-P}_5)]$ )



**$^1\text{H}$  NMR** ( $\text{CD}_3\text{CN}$ ):  $\delta$  [ppm] = 1.46 (s, 15H,  $[\text{Cp}^*\text{Fe}(\eta^5\text{-P}_5)]$ ), 7.35 (s(br), 4H,  $\text{H}_{5-6}$ ), 7.56 (t, 2H,  $J = 7.8\text{ Hz}$ ,  $\text{H}_9$ ), 7.66 (dt, 2H,  $J^1 = 7.7\text{ Hz}$ ,  $J^2 = 1.3\text{ Hz}$ ,  $\text{H}_8$ ), 7.73 (m, 8H,  $\text{H}_{1-4}$ ), 7.86 (dt, 2H,  $J^1 = 7.7\text{ Hz}$ ,  $J^2 = 1.3\text{ Hz}$ ,  $\text{H}_{10}$ ), 7.96 (m, 2H,  $\text{H}_7$ ).

**$^{31}\text{P}\{^1\text{H}\}$  NMR** ( $\text{CD}_3\text{CN}$ ):  $\delta$  [ppm] = 138.47 ( $[\text{Cp}^*\text{Fe}(\eta^5\text{-P}_5)]$ )

**Positive ion ESI-MS** ( $\text{CH}_2\text{Cl}_2/\text{CD}_3\text{CN}$ ):  $m/z$  (%) = 195.0 (100)  $[\text{Ag}(\text{CD}_3\text{CN})_2]^+$ , 452.8  $[[\text{Cp}^*\text{Fe}(\eta^5\text{-P}_5)]\text{Ag}]^+$ , 493.8  $[[\text{Cp}^*\text{Fe}(\eta^5\text{-P}_5)]\text{Ag}(\text{CH}_3\text{CN})]^+$ , 496.9  $[[\text{Cp}^*\text{Fe}(\eta^5\text{-P}_5)]\text{Ag}(\text{CD}_3\text{CN})]^+$ , 796.7  $[[\text{Cp}^*\text{Fe}(\eta^5\text{-P}_5)]\text{Ag}_2(\text{SbF}_6)]^+$ , 798.7  $[[\text{Cp}^*\text{Fe}(\eta^5\text{-P}_5)]\text{Ag}_2]^+$ , 912.9  $[[\text{Cp}^*\text{Fe}(\eta^5\text{-P}_5)]\text{Ag}(\text{C}_{16}\text{H}_{10}\text{N}_2)]^+$ , 1028.7  $[[\text{Cp}^*\text{Fe}(\eta^5\text{-P}_5)]\text{Ag}_2(\text{SbF}_6)(\text{C}_{16}\text{H}_{10}\text{N}_2)]^+$ , 1142.9  $[[\text{Cp}^*\text{Fe}(\eta^5\text{-P}_5)]\text{Ag}_2(\text{SbF}_6)(\text{C}_{16}\text{H}_{10}\text{N}_2)_2]^+$ , 1486.9  $[[\text{Cp}^*\text{Fe}(\eta^5\text{-P}_5)]\text{Ag}_2(\text{SbF}_6)(\text{C}_{16}\text{H}_{10}\text{N}_2)_3]^+$ , 1718  $[[\text{Cp}^*\text{Fe}(\eta^5\text{-P}_5)]\text{Ag}_2(\text{SbF}_6)(\text{C}_{16}\text{H}_{10}\text{N}_2)_4]^+$ , 1832.6  $[[\text{Cp}^*\text{Fe}(\eta^5\text{-P}_5)]_2\text{Ag}_2(\text{SbF}_6)(\text{C}_{16}\text{H}_{10}\text{N}_2)_3]^+$ ,

**Negative ion ESI-MS** ( $\text{CH}_2\text{Cl}_2/\text{CD}_3\text{CN}$ ):  $m/z$  (%) = 234.9 (100)  $[\text{SbF}_6]^-$

**Elemental analysis:** Calculated (%) for  $[[\text{Cp}^*\text{Fe}(\eta^5\text{-P}_5)]\{\text{Ag}(\text{C}_{16}\text{H}_{10}\text{N}_2)\}_2(\text{C}_7\text{H}_8)]_n[\text{SbF}_6]_{2n}$  (1585.84 g/mol): C 37.11, H 2.73, N 3.53; found: C 37.47, H 2.56, N 3.76.

**IR**  $\tilde{\nu}/\text{cm}^{-1}$  = 2248.6 (m), 1598.1 (m), 1475.3 (w), 1423.8 (w), 1374.0 (w), 1177.20 (w), 1016.1 (w), 956.84 (w), 864.6 (w), 822.5 (m), 794.0 (w), 751.1 (w), 651.2 (s), 548.3 (m).

### Synthesis of $[\text{SbF}_6]@[(\text{Cp}^{\text{Bn}}\text{Fe}(\eta^5\text{-P}_5))_6(\text{AgCH}_3\text{CN})_{14}][\text{SbF}_6]_{13}$ (**3**)

In a Schlenk tube to a solution of  $\text{AgSbF}_6$  (41 mg, 0.12 mmol) in  $\text{CH}_3\text{CN}$  (5 mL) was added a green solution of  $[\text{Cp}^*\text{Fe}(\eta^5\text{-P}_5)]$  (14 mg, 0.04 mmol)  $\text{CH}_2\text{Cl}_2$  (5 mL) and stirred for 1h. The solvent was removed and the residues dissolved in  $\text{CH}_2\text{Cl}_2$  and layered with hexane. At the phase boundary, the formation of brown polyhedra (**3**) can be observed. After complete diffusion, the mother liquor is decanted, the crystals are selected manually, washed with hexane (3 x 5 mL) and dried *in vacuo*.

Analytical data of **3**:

**Yield:** 25 mg (0.0026 mmol, 65 % for a assumed composition of  $(\text{C}_{40}\text{H}_{35}\text{FeP}_5)_6(\text{AgSbF}_6)_{14}(\text{CH}_3\text{CN})_{14}$ , 9743.9 g/mol)

**$^1\text{H}$  NMR** ( $\text{CD}_2\text{Cl}_2$ ):  $\delta$  [ppm] = 2.24 (s(br),  $\text{CH}_3\text{CN}$ ), 3.65 – 3.88 (m(br), 60 H,  $[\text{Cp}^{\text{Bn}}\text{Fe}(\eta^5\text{-P}_5)]$ ), 6.66 – 7.20 (m(br), 150 H,  $[\text{Cp}^{\text{Bn}}\text{Fe}(\eta^5\text{-P}_5)]$ ).

**$^{31}\text{P}\{^1\text{H}\}$  NMR** ( $\text{CD}_2\text{Cl}_2$ ):  $\delta$  [ppm] = 128.16 (s,  $[\text{Cp}^{\text{Bn}}\text{Fe}(\eta^5\text{-P}_5)]$ ).

**$^{19}\text{F}$  NMR** ( $\text{CD}_2\text{Cl}_2$ ):  $\delta$  [ppm] = -110 (m(br),  $[\text{SbF}_6]^-$ ).

**DOSY** from dissolved, stirred educts:  $M = 988\text{ g/mol}$ ,  $\varnothing = 1.8\text{ nm}$ , calculated for  $[[\text{Cp}^{\text{Bn}}\text{Fe}(\eta^5\text{-P}_5)]_6(\text{AgSbF}_6)_{14}(\text{CH}_3\text{CN})_{10}]$ :  $M = 9579\text{ g/mol}$ ,  $\varnothing = 2.9\text{ nm}$ .

**Positive ion ESI-MS** ( $\text{CH}_2\text{Cl}_2/\text{CH}_3\text{CN}$ ):  $m/z$  (%) = 2247.5  $[[\text{Cp}^{\text{Bn}}\text{Fe}(\eta^5\text{-P}_5)]_2\text{Ag}_3(\text{SbF}_6)_2]^+$ , 1903  $[[\text{Cp}^{\text{Bn}}\text{Fe}(\eta^5\text{-P}_5)]_2\text{Ag}_2(\text{SbF}_6)]^+$ , 1561.4  $[[\text{Cp}^{\text{Bn}}\text{Fe}(\eta^5\text{-P}_5)]_2\text{Ag}]^+$ , 1218.0  $[[\text{Cp}^{\text{Bn}}\text{Fe}(\eta^5\text{-P}_5)]\text{Ag}_2(\text{SbF}_6)(\text{CH}_3\text{CN})]^+$ ,

1177.0  $[\{\text{Cp}^{\text{Bn}}\text{Fe}(\eta^5\text{-P}_5)\}\text{Ag}_2(\text{SbF}_6)]^+$ , 874.1  $[\{\text{Cp}^{\text{Bn}}\text{Fe}(\eta^5\text{-P}_5)\}_2\text{Ag}(\text{CH}_3\text{CN})]^+$ , 833.1 (100)  $[\{\text{Cp}^{\text{Bn}}\text{Fe}(\eta^5\text{-P}_5)\}\text{Ag}]^+$ ,

**Negative ion ESI-MS** ( $\text{CH}_2\text{Cl}_2/\text{CH}_3\text{CN}$ ):  $m/z$  (%) = 234.7 (100)  $[\text{SbF}_6]^-$

**Elemental analysis:** Calculated (%) for  $[(\text{Cp}^{\text{Bn}}\text{Fe}(\eta^5\text{-P}_5))_6(\text{AgCH}_3\text{CN})_{14}][\text{SbF}_6]_{14}$  (9743.9 g/mol): C 33.04, H 2.61, N 2.01; found: C 31.15, H 2.92, N 1.81.

**X-ray data:** Unit cell parameters:  $a = 20.9503(6)$  Å,  $b = 21.8709(5)$  Å,  $c = 22.3401(5)$  Å,  $\alpha = 117.924(2)^\circ$ ,  $\beta = 99.563(2)^\circ$ ,  $\gamma = 91.398(2)^\circ$ ,  $V = 8857.2(4)$  Å<sup>3</sup>.

### Synthesis of $[\{\text{Cp}^{\text{Bn}}\text{Fe}(\eta^5\text{-P}_5)\}_2\{\text{Ag}(\text{Al}(\text{O}(\text{C}(\text{CF}_3)_3)_4)_3)\cdot(\text{CH}_2\text{Cl}_2)\} (4a)$ and $[\{\text{Cp}^{\text{Bn}}\text{Fe}(\eta^5\text{-P}_5)\}_2\{\text{Ag}(\text{Al}(\text{O}(\text{C}(\text{CF}_3)_3)_4)_4)\cdot(\text{CH}_2\text{Cl}_2)_2\} (4b)$

A solution of AgTEF (95 mg, 0.08 mmol) in 5 mL  $\text{CH}_2\text{Cl}_2$  was stirred with a solution of  $[\text{Cp}^{\text{Bn}}\text{Fe}(\eta^5\text{-P}_5)]$  (30 mg, 0.04 mmol) in 5 mL  $\text{CH}_2\text{Cl}_2$  for 17 h. A colour change from a bright green to olive brown was observed. The solution was layered with hexane. After diffusion the formation of a dark red oil and green crystals of **4a** and some of **4b** was observed, which were washed with hexane (3 x 5 mL) and dried *in vacuo*.

Analytical data of **4**:

**Yield:** 35 mg

**<sup>1</sup>H NMR** ( $\text{CD}_2\text{Cl}_2$ ):  $\delta$  [ppm] = 3.57 (s, 2H,  $\text{Cp}^{\text{Bn}}$ ), 6.61 (d, 2H,  $\text{Cp}^{\text{Bn}}$ ), 7.05 – 7.14 (m, 3H,  $\text{Cp}^{\text{Bn}}$ ).

**<sup>31</sup>P{<sup>1</sup>H} NMR** ( $\text{CD}_2\text{Cl}_2$ ):  $\delta$  [ppm] = 147.89 (s,  $[\text{Cp}^{\text{Bn}}\text{Fe}(\eta^5\text{-P}_5)]$ ).

**<sup>19</sup>F NMR** ( $\text{CD}_2\text{Cl}_2$ ):  $\delta$  [ppm] = -75.52 (s,  $[\text{Al}(\text{O}(\text{C}(\text{CF}_3)_3)_4)]^-$ ).

**Positive ion ESI-MS** ( $\text{CH}_2\text{Cl}_2$ ):  $m/z$  (%) = 833.1  $[\{\text{Cp}^{\text{Bn}}\text{Fe}(\eta^5\text{-P}_5)\}\text{Ag}]^+$ , 1561.5  $[\{\text{Cp}^{\text{Bn}}\text{Fe}(\eta^5\text{-P}_5)\}_2\text{Ag}]^+$ .

**Negative ion ESI-MS** ( $\text{CH}_2\text{Cl}_2$ ):  $m/z$  (%) = 967.1 (100)  $[\text{Al}(\text{O}(\text{C}(\text{CF}_3)_3)_4)]^-$

**Elemental analysis:** Calculated (%) for  $[\{\text{Cp}^{\text{Bn}}\text{Fe}(\eta^5\text{-P}_5)\}_2\{\text{Ag}(\text{Al}(\text{O}(\text{C}(\text{CF}_3)_3)_4)_3)(\text{CH}_2\text{Cl}_2)\} (4762.7 \text{ g/mol})$ : C 32.53, H 1.52; found: C 31.93, H 1.64.

### Synthesis of $[\{\text{Cp}^{\text{Bn}}\text{Fe}(\eta^5\text{-P}_5)\}_2\{\text{Ag}(\text{AlF}(\text{OC}_{12}\text{F}_{15})_3)_3\}_4] (5)$

A solution of AgFAI (210 mg, 0.14 mmol) in 5 mL  $\text{CH}_2\text{Cl}_2$  was stirred with a solution of  $[\text{Cp}^{\text{Bn}}\text{Fe}(\eta^5\text{-P}_5)]$  (50 mg, 0.07 mmol) in 5 mL  $\text{CH}_2\text{Cl}_2$  for 17 h. A colour change from a bright green to olive brown was observed. The solution was layered with hexane. After diffusion the formation of a dark red oil and a few green crystals of **5** was observed, which were washed with hexane (3 x 5 mL) and dried *in vacuo*.

Analytical data of **5**:

**$^1\text{H}$  NMR** ( $\text{CD}_2\text{Cl}_2$ ):  $\delta$  [ppm] = 3.51 (s, 2H,  $\text{Cp}^{\text{Bn}}$ ), 6.50 (d, 2H,  $\text{Cp}^{\text{Bn}}$ ), 6.98 – 7.10 (m, 3H,  $\text{Cp}^{\text{Bn}}$ ).

**$^{31}\text{P}\{^1\text{H}\}$  NMR** ( $\text{CD}_2\text{Cl}_2$ ):  $\delta$  [ppm] = 151.34 (s, [ $\text{Cp}^{\text{Bn}}\text{Fe}(\eta^5\text{-P}_5)$ ]).

**Positive ion ESI-MS** ( $\text{CH}_2\text{Cl}_2$ ):  $m/z$  (%) = 833.1 (100) [ $\{\text{Cp}^{\text{Bn}}\text{Fe}(\eta^5\text{-P}_5)\}\text{Ag}\}^+$ , 1561.4 [ $\{\text{Cp}^{\text{Bn}}\text{Fe}(\eta^5\text{-P}_5)\}_2\text{Ag}\}^+$ , 3050 [ $\{\text{Cp}^{\text{Bn}}\text{Fe}(\eta^5\text{-P}_5)\}_2\text{Ag}_2(\text{AlF}(\text{OC}_{12}\text{F}_{15})_3)\}^+$ .

**Negative ion ESI-MS** ( $\text{CH}_2\text{Cl}_2$ ):  $m/z$  (%) = 1381.2 (100) [ $\text{AlF}(\text{OC}_{12}\text{F}_{15})_3\}^-$

**Elemental analysis:** Calculated (%) for [ $\{\text{Cp}^{\text{Bn}}\text{Fe}(\eta^5\text{-P}_5)\}_2\{\text{Ag}(\text{AlF}(\text{OC}_{12}\text{F}_{15})_3)\}_3\}_4$ ] (4762.7 g/mol): C 36.31, H 0.95; found: C 37.10, H 1.44.

### Synthesis of [ $\{\text{Cp}^{\text{Bn}}\text{Fe}(\eta^5\text{-P}_5)\}_{12}\{\text{Ag}(\text{SO}_3\text{C}_7\text{H}_7)\}_{20\text{-n}}\}$ (**6**)

A solution of  $\text{AgSO}_3\text{C}_7\text{H}_7$  (50 mg, 0.18 mmol) in  $\text{CH}_2\text{Cl}_2$  (4 mL) is added dropwise to a solution of [ $\text{Cp}^{\text{Bn}}\text{Fe}(\eta^5\text{-P}_5)$ ] (50 mg, 0.07 mmol) in  $\text{CH}_2\text{Cl}_2$  (4 mL) and stirred for 3 h. After 30 minutes, the reaction mixture turned to a deep red. The solution was filtered and layered with a mixture of pentane/toluene (1:1). A few hours later, the growth of deep red-brown crystals of **6** can be observed at the phase boundary. After complete diffusion, the mother liquor was decanted, the crystals were washed with pentane (3  $\times$  5 mL) and dried *in vacuo*.

Analytical data of **6**:

**Yield:** 76 mg (5.36  $\mu\text{mol}$ , 92 % referred to [ $\text{Cp}^{\text{Bn}}\text{Fe}(\eta^5\text{-P}_5)$ ])

**$^1\text{H}$  NMR** (tol- $d_8$ , 300K):  $\delta$  [ppm] = 1.77 (s(br), 60 H, [ $\text{CH}_3\text{C}_6\text{H}_4\text{SO}_3\}^-$ ), 4.78 (s(br), 120 H, [ $\text{Cp}^{\text{Bn}}\text{Fe}(\eta^5\text{-P}_5)$ ]), 6.11 -6.75 (m(br), 380 H, [ $\text{CH}_3\text{C}_6\text{H}_4\text{SO}_3\}^-$ , [ $\text{Cp}^{\text{Bn}}\text{Fe}(\eta^5\text{-P}_5)$ ]).

**$^{31}\text{P}\{^1\text{H}\}$  NMR** (tol- $d_8$ , 300K):  $\delta$  [ppm] = 161.36 ([ $\text{Cp}^{\text{Bn}}\text{Fe}(\eta^5\text{-P}_5)$ ])

**$^{31}\text{P}\{^1\text{H}\}$  NMR** (tol- $d_8$ , 203K):  $\delta$  [ppm] = -48.90 (m(br),  $\omega_{1/2}$  = 15769 Hz, 1 P, [ $\text{Cp}^{\text{Bn}}\text{Fe}(\eta^5\text{-P}_5)$ ]), 78.70 (m(br),  $\omega_{1/2}$  = 6591 Hz, 1.2 P, [ $\text{Cp}^{\text{Bn}}\text{Fe}(\eta^5\text{-P}_5)$ ]).

**Elemental analysis:** Calculated (%) for [ $\{\text{Cp}^{\text{Bn}}\text{Fe}(\eta^5\text{-P}_5)\}_{12}\{\text{Ag}(\text{SO}_3\text{C}_7\text{H}_7)\}_{20}(\text{CH}_2\text{Cl}_2)_{15}\}$ ] (15572.5 g/mol): C 48.98, H 3.82, S 4.12, Ag 13.85, Fe 4.30, P 11.93; found: C 48.98, H 3.82, S 4.12, Ag 13.85, Fe 4.30, P 11.93.

**TEM measurements:** measured diameter of selected aggregates /nm: 1.78, 2.04, 2.10, 2.18, 2.22, 2.29, 2.33, 2.51, 2.57, 2.84, 2.86, 2.96, 2.96, 2.97, 3.18, 3.18, 3.29, 3.29, 3.44, 3.65. Mean value: 3.73 nm; standard deviation: 0.54. Expected diameter:  $\approx 3.30$  nm.

**X-ray data:** Unit cell parameters:  $a = 59.1008(16)$  Å,  $b = 59.1008(16)$  Å,  $c = 72.766(2)$  Å,  $\alpha = 90^\circ$ ,  $\beta = 90^\circ$ ,  $\gamma = 120^\circ$ ,  $V = 220113(10)$  Å<sup>3</sup>

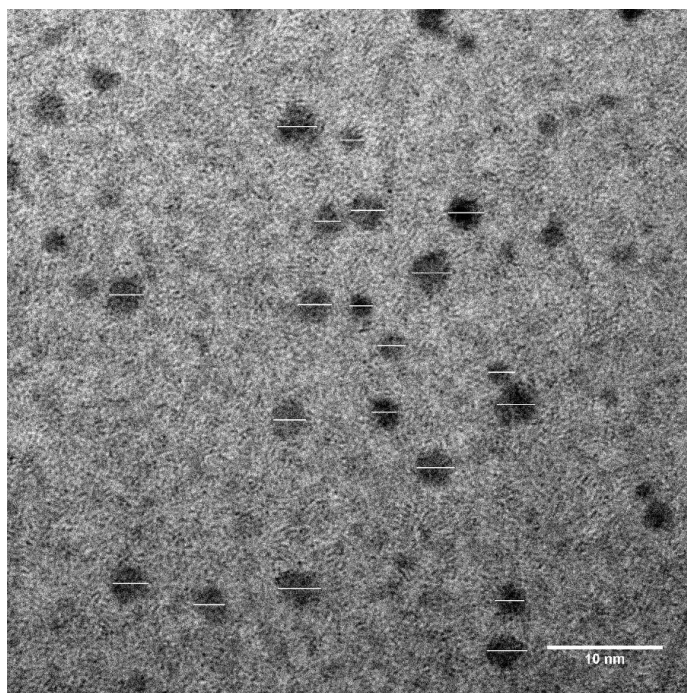


Figure 4: TEM record for **6**.

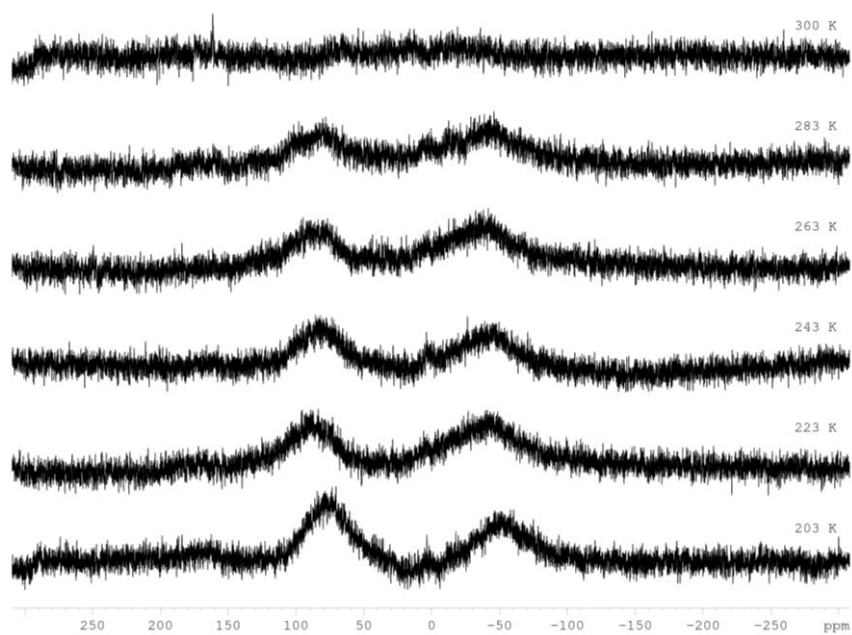


Figure 5:  $^{31}\text{P}\{^1\text{H}\}$  NMR spectra of **6** in  $\text{tol-d}_8$  at variable temperatures.

## 8.6 Crystallographic Details

**Table 1:** Experimental details for compounds **2**.

Compound	<b>2</b> (preliminary data)
Formula	C <sub>42</sub> H <sub>35</sub> Ag <sub>2</sub> F <sub>12</sub> FeN <sub>4</sub> P <sub>5</sub> Sb <sub>2</sub>
$D_{calc.}/\text{g cm}^{-3}$	1.870
$m/\text{mm}^{-1}$	18.037
Formula Weight	1493.68
Colour	green
Shape	needle
Size/mm <sup>3</sup>	0.63 × 0.11 × 0.05
$T/\text{K}$	123.01(10)
Crystal System	monoclinic
Space Group	$P2_1/n$
$\alpha/^\circ$	19.4340(6)
$\beta/^\circ$	13.1511(3)
$\gamma/^\circ$	21.2812(6)
$a/^\circ$	90
$b/^\circ$	102.693(3)
$g/^\circ$	90
$V/\text{\AA}^3$	5306.1(3)
$Z$	4
$Z'$	1
Wavelength/ $\text{\AA}$	1.54184
Radiation type	CuK $\alpha$
$Q_{min}/^\circ$	3.485
$Q_{max}/^\circ$	74.022
Measured Refl.	18582
Independent Refl.	10276
Reflections with $I > 2(I)$	8772
$R_{int}$	0.0355
Parameters	688
Restraints	142

Computer programs for **2**: 1.171.39.37b (Rigaku Oxford Diffraction, 2017), SHELXT 2014/5 (Sheldrick, 2014).

**Table 2:** Experimental details for compounds **4a-b**.

Compound	4a	4b
Formula	Ag <sub>3</sub> Al <sub>3</sub> C <sub>129.75</sub> Cl <sub>3.5</sub> F <sub>108</sub> Fe <sub>2</sub> H <sub>73.5</sub> O <sub>12</sub> P <sub>10</sub>	C <sub>152</sub> H <sub>86</sub> Ag <sub>4</sub> Al <sub>4</sub> Cl <sub>16</sub> F <sub>144</sub> Fe <sub>2</sub> O <sub>16</sub> P <sub>10</sub>
$D_{calc.}/\text{g cm}^{-3}$	1.954	2.010
$m/\text{mm}^{-1}$	7.488	8.405
Formula Weight	4826.41	6432.20
Colour	green	green
Shape	plate	block
Size/ $\text{mm}^3$	$0.60 \times 0.40 \times 0.07$	$0.54 \times 0.31 \times 0.22$
$T/\text{K}$	123.01(10)	122.97(10)
Crystal System	triclinic	triclinic
Space Group	$P\bar{1}$	$P\bar{1}$
$a/\text{\AA}$	15.8271(3)	15.4007(3)
$b/\text{\AA}$	16.9522(3)	18.1539(3)
$c/\text{\AA}$	31.6093(5)	39.2022(4)
$\alpha/^\circ$	93.7140(10)	84.4500(10)
$\beta/^\circ$	102.927(2)	80.9820(10)
$\gamma/^\circ$	95.131(2)	79.8190(10)
$V/\text{\AA}^3$	8201.4(3)	10627.5(3)
$Z$	2	2
$Z'$	1	1
Wavelength/ $\text{\AA}$	1.54184	1.54184
Radiation type	CuK $_{\alpha}$	CuK $_{\alpha}$
$Q_{min}/^\circ$	3.51	2.288
$Q_{max}/^\circ$	73.89	74.469
Measured Refl.	52874	83164
Independent Refl.	31519	40586
Reflections with $I > 2(I)$	27063	37873
$R_{int}$	0.0466	0.0439
Parameters	2541	3959
Restraints	339	2652
Largest Peak	1.230	1.505
Deepest Hole	-0.605	-1.188
GooF	1.025	1.032
$wR_2$ (all data)	0.1194	0.1570
$wR_2$	0.1126	0.1536
$R_1$ (all data)	0.0533	0.0605
$R_1$	0.0453	0.0582

Computer programs for **4a-b**: CrysAlisPro 1.171.39.37b (Rigaku Oxford Diffraction, 2017), ShelXL (Sheldrick, 2015).

For **4a** a solvent mask was calculated and 66 electrons were found in a volume of  $343 \text{ \AA}^3$  in 2 voids. This is consistent with the presence of 0.75  $[\text{CH}_2\text{Cl}_2]$  per formula unit which account for 63 electrons.



**Table 3:** Experimental details for compounds **5**.

Compound	5
Formula	C <sub>119.01</sub> H <sub>45.2</sub> Ag <sub>2</sub> Al <sub>2</sub> Cl <sub>5.09</sub> F <sub>92</sub> FeO <sub>6</sub> P <sub>5</sub>
$D_{calc.}/\text{g cm}^{-3}$	1.962
$m/\text{mm}^{-1}$	6.481
Formula Weight	3979.32
Colour	green
Shape	plate
Size/ $\text{mm}^3$	$0.57 \times 0.37 \times 0.19$
$T/\text{K}$	122.8(8)
Crystal System	triclinic
Space Group	$P\bar{1}$
$a/\text{\AA}$	18.0639(4)
$b/\text{\AA}$	18.5849(5)
$c/\text{\AA}$	21.6053(7)
$\alpha/^\circ$	83.110(2)
$\beta/^\circ$	76.625(2)
$\gamma/^\circ$	72.942(2)
$V/\text{\AA}^3$	6735.5(3)
$Z$	2
$Z'$	1
Wavelength/ $\text{\AA}$	1.54184
Radiation type	CuK $\alpha$
$Q_{min}/^\circ$	3.351
$Q_{max}/^\circ$	66.978
Measured Refl.	83445
Independent Refl.	23610
Reflections with $I > 2(I)$	21772
$R_{int}$	0.0480
Parameters	2284
Restraints	325
Largest Peak	0.686
Deepest Hole	-0.461
GooF	1.024
$wR_2$ (all data)	0.1041
$wR_2$	0.1014
$R_1$ (all data)	0.0427
$R_1$	0.0396

Computer programs for **5**: CrysAlisPro 1.171.39.37b (Rigaku Oxford Diffraction, 2017), ShelXL (Sheldrick, 2015).

## 8.7 Author Contributions

- Syntheses and characterization of all compounds was done by B. Hiltl.
- The manuscript, figures and tables were made by B. Hiltl.
- The X-ray measurements of **2**, **4** - **5** were performed by B. Hiltl and Dr. M. Seidl, those of **3** and **6** were performed by B. Hiltl, Dr. E. Peresyphkina and Dr. Sc. A. V. Virovets.
- TEM measurements were performed by J. Hilgert (University of Mainz)

## 8.8 References

- <sup>1</sup> a) M. E. Moussa, M. Seidl, G. Balazs, M. Zabel, A. V. Virovets, B. Attenberger, A. Schreiner, M. Scheer, *Chem. Eur. J.* **2017**, *23*, 16199-16203; b) M. Elsayed Moussa, B. Attenberger, M. Seidl, A. Schreiner, M. Scheer, *Eur. J. Inorg. Chem.* **2017**, *2017*, 5616-5620; c) M. Elsayed Moussa, B. Attenberger, E. V. Peresyphkina, M. Fleischmann, G. Balazs, M. Scheer, *Chem. Commun.* **2016**, *52*, 10004-10007; d) B. Attenberger, E. V. Peresyphkina, M. Scheer, *Inorg. Chem.* **2015**, *54*, 7021-7029; e) B. Attenberger, S. Welsch, M. Zabel, E. Peresyphkina, M. Scheer, *Angew. Chem., Int. Ed.* **2011**, *50*, 11516-11519.
- <sup>2</sup> I. Krossing, I. Raabe, *Angew Chem Int Ed Engl* **2004**, *43*, 2066-2090.
- <sup>3</sup> C. Heindl, E. Peresyphkina, A. V. Virovets, I. S. Bushmarinov, M. G. Medvedev, B. Kraemer, B. Dittrich, M. Scheer, *Angew. Chem., Int. Ed.* **2017**, *56*, 13237-13243.
- <sup>4</sup> F. Dielmann, M. Fleischmann, C. Heindl, E. V. Peresyphkina, A. V. Virovets, R. M. Gschwind, M. Scheer, *Chem. Eur. J.* **2015**, *21*, 6208-6214.
- <sup>5</sup> M. Detzel, G. Friedrich, O. J. Scherer and G. Wolmershäuser, *Angew. Chem. Int. Ed.* **1995**, *34*, 1321.
- <sup>6</sup> F. Dielmann, R. Merkle, S. Heint, M. Scheer, *Z. Naturforsch.* **2009**, *64*, 3.
- <sup>7</sup> I. Krossing, *Chem. Eur. J.* **2001**, *7*, 490-502.
- <sup>8</sup> a) C. T. Rueden, J. Schindelin, M. C. Hiner, et al. *BMC Bioinformatics* **2017**, *18*, 529; b) C. A. Schneider, W. S. Rasband, K. W. Eliceiri, *Nature methods* **2012**, *9*, 7, 671-675; c) J. Schindelin, I. Arganda-Carreras, E. Frise, et al. *Nature methods* **2012**, *9*, 7, 676-682.



## 9. Conclusion

This thesis addresses in its first part (*Chapters III-IV*) the coordinative self-assembly of the  $P_n$  complexes  $[Cp^RFe(\eta^5-P_5)]$  ( $Cp^R = Cp^*$  (**1a**),  $Cp^{Bn}$  (**1b**)) with coinage metal salts of weakly coordinating anions to construct novel spherical supramolecules. In a second part (*Chapters V-VIII*) three- and four-component self-assembly processes are investigated, which take place upon extending the system by organic dinitriles as potential linkers and  $P_4$  as a small guest molecule. The introductory part (*Chapter I*) briefly shows the ensemble of the general aspects and terms concerning Supramolecular Chemistry and outlines the significance of results based on  $P_n$  ligands with respect to other discrete assemblies. The importance of the research objectives is given in *Chapter II*. All results obtained in the course of this thesis are presented in self-contained *Chapters III – VII* as well as in the Thesis Treasury (*Chapter VIII*).

### Ag salts of functionalized or weakly coordinating anions applied in the self-assembly with $[Cp^RFe(\eta^5-P_5)]$ ( $Cp^R = Cp^*, Cp^{Bn}$ )

The pentaphosphaferrocene derivatives **1a,b** proved to be versatile building blocks for the formation of self-assembled spherical supramolecular aggregates due to their coordination behaviour towards Cu halides. This approach could not successfully be transferred from Cu to Ag as the halide salts are very poorly soluble in the required organic solvents. The use of  $CuSO_3CF_3$  in combination with **1b** yielded an icosidodecahedral scaffold (*Figure 1*) with  $SO_3CF_3$  acting as additional scaffold building unit. This result brought the idea to mind that a transfer to Ag-based spherical supramolecules may be possible by involving soluble salts of functionalized or weakly coordinating anions. As described in *Chapter III* the coordination behaviour of **1a,b** towards the salts  $AgSO_3CF_3$  and  $AgSO_3C_7H_7$  was investigated in cooperation with Dr. Claudia Heindl. Due to the sulfonyl group,  $SO_3CF_3^-$  and  $SO_3C_7H_7^-$  show remarkable versatility: these anions can either act as end-on, bridging or tri-podal coordinating anions.

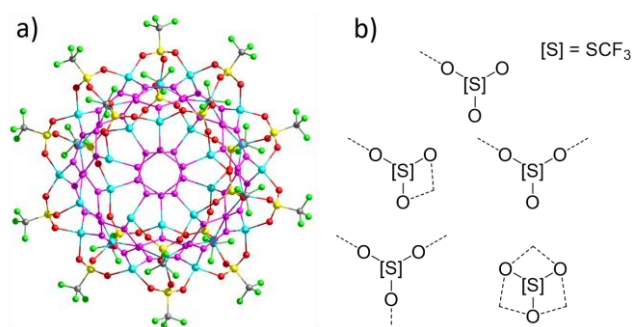
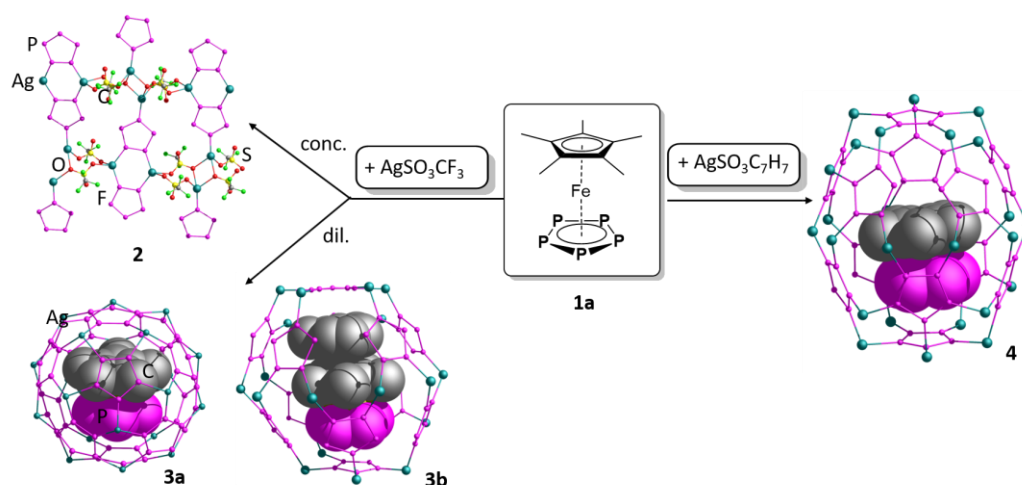


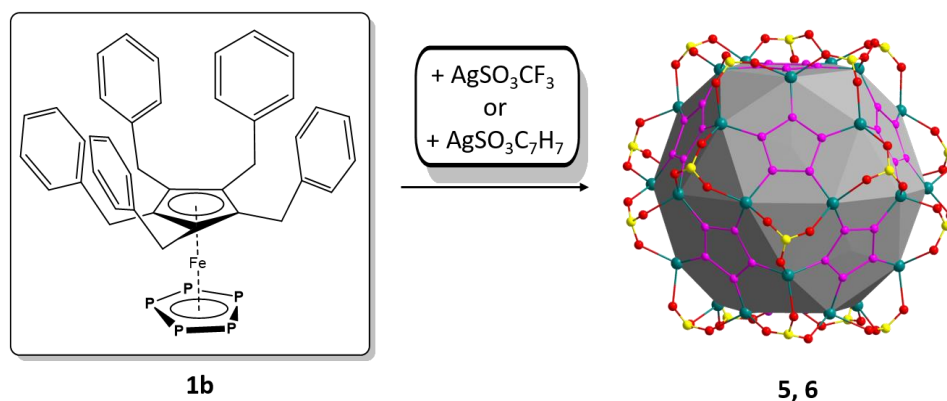
**Figure 1:** a) Average scaffold of  $[(Cp^{Bn}Fe(\eta^5-P_5))_{12}(CuSO_3CF_3)_{19.66}]$ , b) selected possible coordination modes of  $SO_3CF_3^-$ .

Upon combination of  $\text{AgSO}_3\text{CF}_3$  with **1a** either a 2D coordination polymer  $\{[\text{Cp}^*\text{Fe}(\mu_4, \eta^{5:1:1:1}-\text{P}_5)](\text{AgSO}_3\text{CF}_3)_2\}_n$  (**2**) or the discrete spherical host guest assemblies  $[\text{Cp}^*\text{Fe}(\eta^5-\text{P}_5)]@[\{\text{Cp}^*\text{Fe}(\eta^5-\text{P}_5)\}_{12}(\text{AgSO}_3\text{CF}_3)_{20-n}]$  (**3a**,  $n \approx 10$ ) and  $[\{\text{Cp}^*\text{Fe}(\eta^5-\text{P}_5)\}(\text{toluene})]@[\{\text{Cp}^*\text{Fe}(\eta^5-\text{P}_5)\}_{12}(\text{AgSO}_3\text{CF}_3)_{20-n}]$  (**3b**) are formed, depending on the concentration of the respective building blocks in solution (*Scheme 1*). The discrete supramolecules can be obtained selectively by using more diluted reaction layers as for the coordination polymer. Though the scaffolds of **3a,b** reveal topological similarities to the icosahedral symmetric compound  $[\{\text{Cp}^*\text{Fe}(\eta^5-\text{P}_5)\}_{12}(\text{CuX})_{20}]$  or to the icosidodecahedral scaffold of the Cu-containing  $[\{\text{Cp}^{\text{Bn}}\text{Fe}(\eta^5-\text{P}_5)\}_{12}(\text{CuSO}_3\text{CF}_3)_{19.66}]$  (previously reported by our group), they also feature unprecedented structural characteristics. **3a** shows an average structure with 20 positions for  $\{\text{AgOSO}_2\text{CF}_3\}$  units with occupancies  $<1$ , leading to about ten intrinsic 14-membered  $\{\text{Ag}_4\text{P}_{10}\}$  rings in the actual scaffolds. The framework of **3b** however, reveals an ordered scaffold with 20  $\text{Ag}^+$  and ten  $\{\text{Ag}_4\text{P}_{10}\}$  rings. With this, **3b** is analogue to the theoretically deduced  $D_2$  symmetric isomer of  $[\{\text{Cp}^{\text{Bn}}\text{Fe}(\eta^5-\text{P}_5)\}_{12}(\text{CuSO}_3\text{CF}_3)_{19.66}]$ . The anions show in these cases either end-on (**3a**) or bridging and tri-podal (**3b**) coordination modes towards the scaffold building Ag atoms. Moreover, in both supramolecules one complex **1a** is encapsulated, which leads to a distortion of the scaffold, due to the size of guest. Furthermore, **3a** is the first example of a polyphosphorus ligand-based host to enclose not only a molecular guest, but a supramolecular assembly, as one molecule toluene stacks on to the  $\text{Cp}^*$  residue of the incorporated complex **1a**. To increase the steric hinderance of the anion also  $\text{AgSO}_3\text{C}_7\text{H}_7$  was implemented and the reaction yielded the spherical supramolecule  $[\text{Cp}^*\text{Fe}(\eta^5-\text{P}_5)]@[\{\text{Cp}^*\text{Fe}(\eta^5-\text{P}_5)\}_{12}(\text{AgSO}_3\text{C}_7\text{H}_7)_{26-n}]$  (**4**, *Scheme 1*). The scaffold consists of 12 units **1a**, 26 Ag atoms and 20  $\text{SO}_3\text{C}_7\text{H}_7^-$  scaffold-building anions. Six additional anions, located non-coordinatingly in the outer sphere, fulfill the charge balance. Furthermore, four 14-membered  $\{\text{Ag}_4\text{P}_{10}\}$  rings cause different coordination modes of the ligands **1a** and the scaffold-building anion, similar to in **3a,b**.



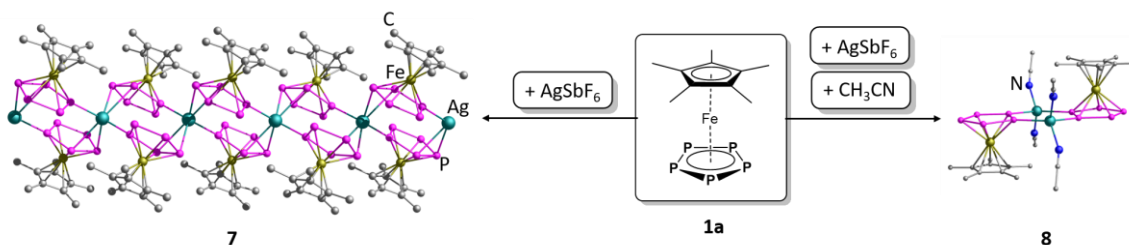
**Scheme 1:** Coordination products based on **1a** and  $\text{AgSO}_3\text{CF}_3$  or  $\text{AgSO}_3\text{C}_7\text{H}_7$ .

Upon combining the Ag sulfonyl salts with **1b** the two analogous spherical supramolecules  $[\{\text{Cp}^{\text{Bn}}\text{Fe}(\eta^5\text{-P}_5)\}_{12}\{\text{Ag}(\text{SO}_3\text{CF}_3)\}_{20-n}]$  (**5**) and  $[\{\text{Cp}^{\text{Bn}}\text{Fe}(\eta^5\text{-P}_5)\}_{12}\{\text{Ag}(\text{SO}_3\text{C}_7\text{H}_7)\}_{20-n}]$  (**6**) are formed (Scheme 2, cf. Chapter III for **5** and Chapter VIII for **6**). Like **3b** and  $[\{\text{Cp}^{\text{Bn}}\text{Fe}(\eta^5\text{-P}_5)\}_{12}(\text{CuSO}_3\text{CF}_3)_{19.66}]$  their average scaffolds feature, 30 positions for  $\text{Ag}^+$ , which show only occupancies of about 2/3. Thus, besides **3b**, compounds **5** and **6** can also be classified as (90-10)-vertex spheres. Generally, **3a,b**, **5** and **6** are the first representatives of Ag-containing spherical assemblies, based on pentaphosphaferrocene derivatives.



**Scheme 2:** Coordination products based on **1b** and  $\text{AgSO}_3\text{CF}_3$  or  $\text{AgSO}_3\text{C}_7\text{H}_7$ .

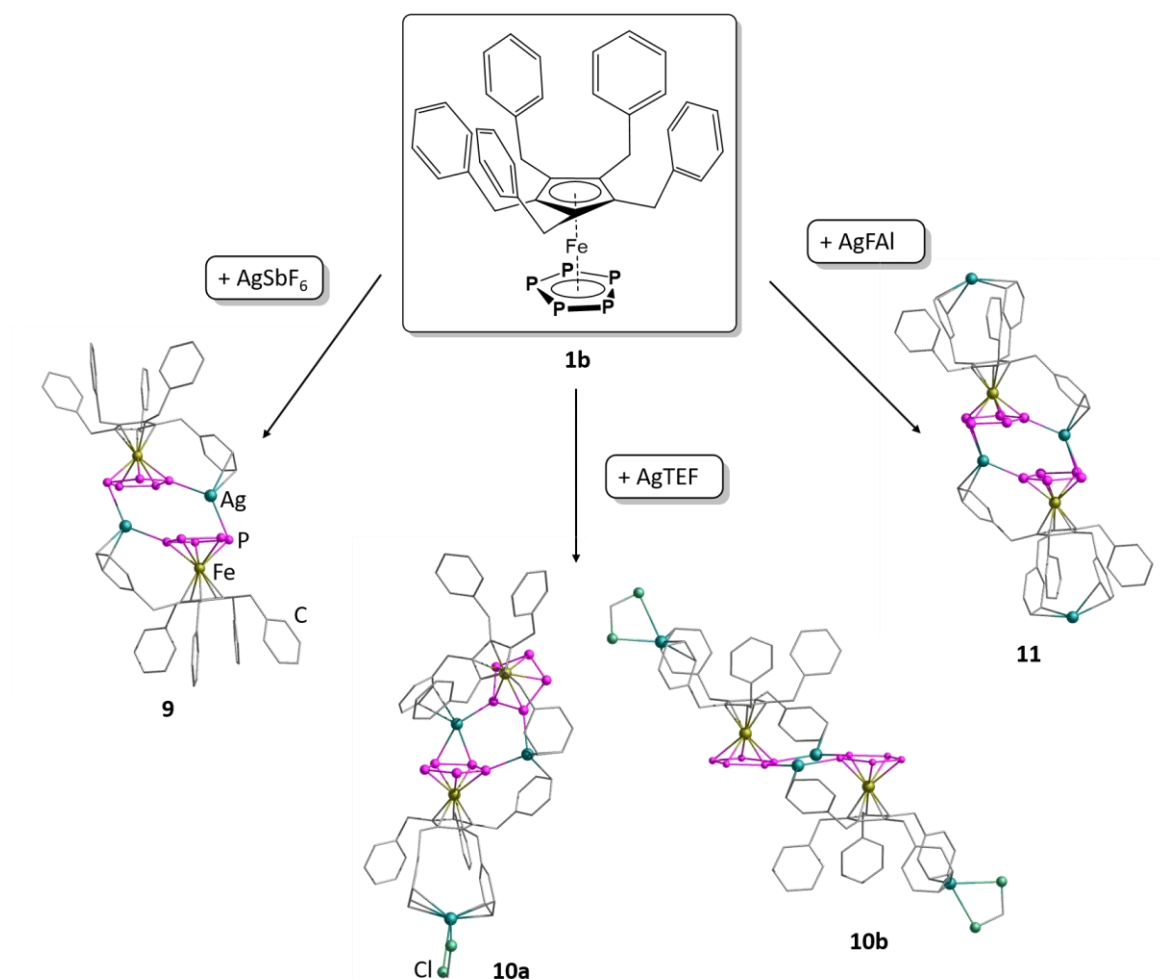
Besides functional anions, the focus of Chapters IV - VII lay on the use of the weakly coordinating anions. With this class of anions, free coordination sites on the metal atom are implemented which enabled new pathways of self-assembly. Thus three-component reactions with additional coordinating building blocks were possible. For a simple examination of coordination behaviour **1a** was first reacted with  $\text{AgSbF}_6$  in a two-component reaction to assemble to 1D polymeric  $[\{\text{Cp}^*\text{Fe}(\eta^{5:2:1}\text{-P}_5)\}_2\text{Ag}]_n[\text{SbF}_6]_n$  (**7**) or, in the presence of the coordinating solvent  $\text{CH}_3\text{CN}$ , to the dimeric  $[\{\text{Cp}^*\text{Fe}(\eta^{5:1:1}\text{-P}_5)\}\{\text{Ag}(\text{CH}_3\text{CN})_2\}]_2[\text{SbF}_6]_2$  (**8**, Scheme 3, cf. Chapter V).



**Scheme 3:** Coordination products based on **1a** and  $\text{AgSbF}_6$ .

Upon reacting **1b** with  $\text{AgSbF}_6$  also a dimeric aggregate  $[\{\text{Cp}^{\text{Bn}}\text{Fe}(\eta^{5:1:1}\text{-P}_5)\}_2\text{Ag}]_2[\text{SbF}_6]_2$  (**9**) is obtained, whereas in this case the Bn substituted  $\text{Cp}^{\text{R}}$  derivative stabilize the free coordination sites on the Ag atoms (cf. Chapter IV). With **1b** also the Ag salts of the large and very weak coordinating anions

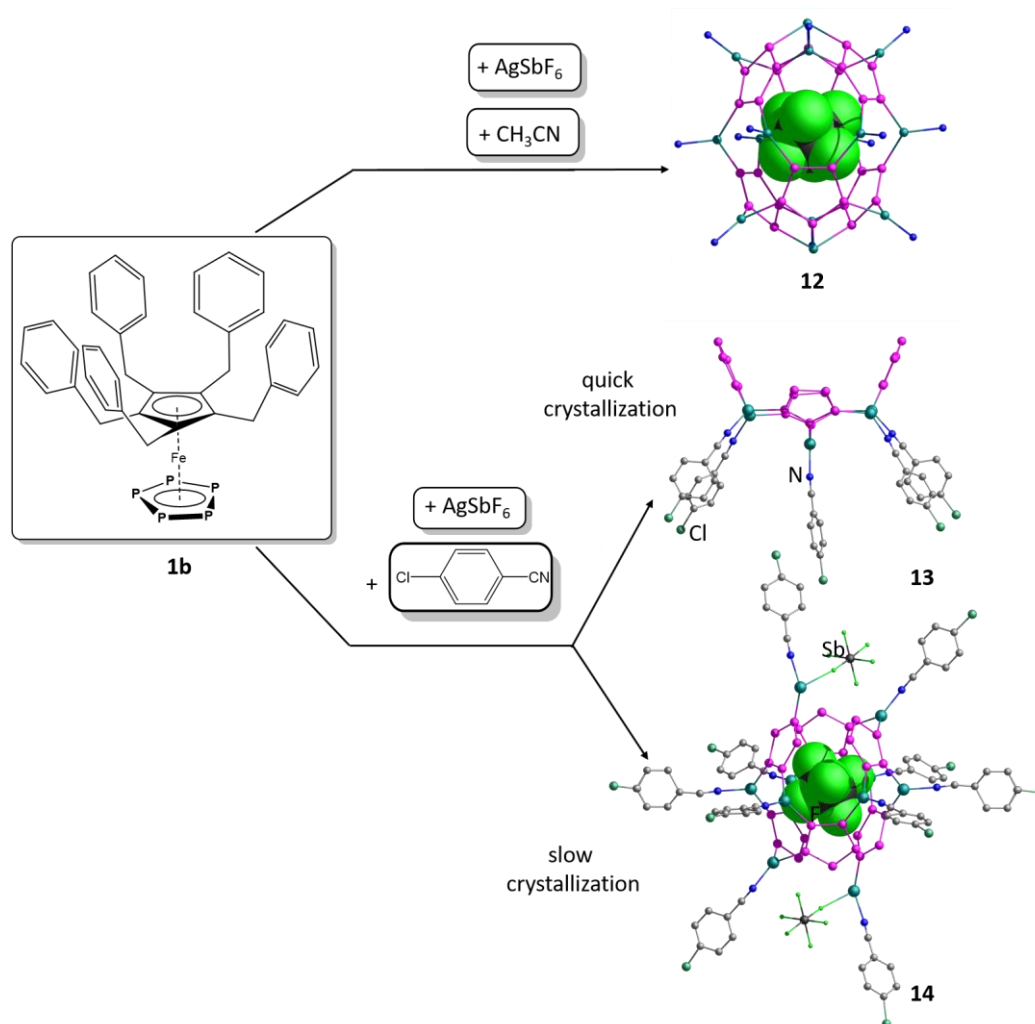
$[\text{Al}\{\text{OC}(\text{CF}_3)_3\}_4]^-$  (TEF<sup>-</sup>) and  $[\text{AlF}(\text{OC}_{12}\text{F}_{15})_3]^-$  (FAI<sup>-</sup>) were used (cf. *Chapter VIII*) to yield three different dimeric compounds:  $[\{\text{Cp}^{\text{Bn}}\text{Fe}(\eta^5\text{-P}_5)\}_2\text{Ag}_3][\text{Al}\{\text{OC}(\text{CF}_3)_3\}_4]_3\cdot(\text{CH}_2\text{Cl}_2)$  (**10a**),  $[\{\text{Cp}^{\text{Bn}}\text{Fe}(\eta^5\text{-P}_5)\}_2\text{Ag}_4][\text{Al}\{\text{OC}(\text{CF}_3)_3\}_4]_4\cdot(\text{CH}_2\text{Cl}_2)_2$  (**10b**) and  $[\{\text{Cp}^{\text{Bn}}\text{Fe}(\eta^5\text{-P}_5)\}_2\text{Ag}_4][\text{AlF}(\text{O}_{12}\text{F}_{15})_3]_4$  (**11**, *Scheme 4*). Whereas they differ in the geometrical arrangement of the *cyclo*-P<sub>5</sub> ligands towards each other, they have in common the saturation of the free coordination sites at the Ag atoms by Bn residues, as well as the additional coordination of one (**10a**) or two (**10b**, **11**) Ag atoms between the remaining Bn moieties.



**Scheme 4:** Coordination products based on **1b** and  $\text{AgSbF}_6$ ,  $\text{AgTEF}$  or  $\text{AgFAI}$ .

To use the free coordination sites on the Ag atoms for further bonding to ligands,  $\text{CH}_3\text{CN}$  was added to test the affinity of nitriles towards the Ag atoms in these self-assembly systems and to investigate if a formation of spherical aggregates is possible under these conditions (cf. *Chapter VIII*). As a result, crystals were obtained, for which a trigonal anti-prismatic host supramolecular structure  $[\text{SbF}_6^-]@[\{\text{Cp}^{\text{Bn}}\text{Fe}(\eta^5\text{-P}_5)\}_6(\text{AgCH}_3\text{CN})_{14}][\text{SbF}_6]_{13}$  (**12**) was revealed (*Scheme 5*). Six *cyclo*-P<sub>5</sub> ligands **1b** form together with up to 14 Ag atoms a novel host scaffold, enclosing one  $\text{SbF}_6^-$  counter-anion. All other counter-anions are located in the outer sphere of the positively charged host-guest assembly,

whereas the scaffold-building Ag atoms show coordination of either  $\text{CH}_3\text{CN}$  ligands or bent Bn residues of **1b**. The 14 positions for Ag atoms are assumed to be partly occupied, whereas a final sum formula could not be resolved within this thesis, due to preliminary data. When to the system of **1b** and  $\text{AgSbF}_6$  with  $\text{NC}(\text{C}_6\text{H}_4)\text{Cl}$  a potentially coordinating nitrile ligand is added as a third component to saturate the free coordination sites on the Ag atoms instead of  $\text{CH}_3\text{CN}$ , a strong dependency of the formed products on the reaction conditions is observed (cf. *Chapter IV*). The half-shell shaped  $[\{\text{Cp}^{\text{Bn}}\text{Fe}(\eta^5\text{-P}_5)\}_4\{\text{Ag}(\text{CN}(\text{C}_6\text{H}_4)\text{Cl})\}_5][\text{SbF}_6]_5$  (**13**) crystallizes using short reaction times, concentrated solutions and/or quick crystallization methods. Giving the building blocks more time to arrange in a favorable way, the supramolecule  $[\text{SbF}_6]@[\{\text{Cp}^{\text{Bn}}\text{Fe}(\eta^5\text{-P}_5)\}_6\{\text{Ag}(\text{CN}(\text{C}_6\text{H}_4)\text{Cl})\}_{10}][\text{SbF}_6]_9$  (**14**) is formed (*Scheme 5*). Similar to **12**, it's scaffold shows a trigonal anti-prismatic arrangement of the ligands **1b**, and with 6 scaffold building units of *cyclo*- $\text{P}_5$  ligands **12** and **14** represent the smallest spherical supramolecules constructed of pentaphosphaferrocene derivatives, so far. All Ag atoms are saturated with nitrile ligands, which results in the supramolecule being ten-fold positively charged. Moreover, **14** hosts in its inner void one counter-anion  $\text{SbF}_6^-$ .

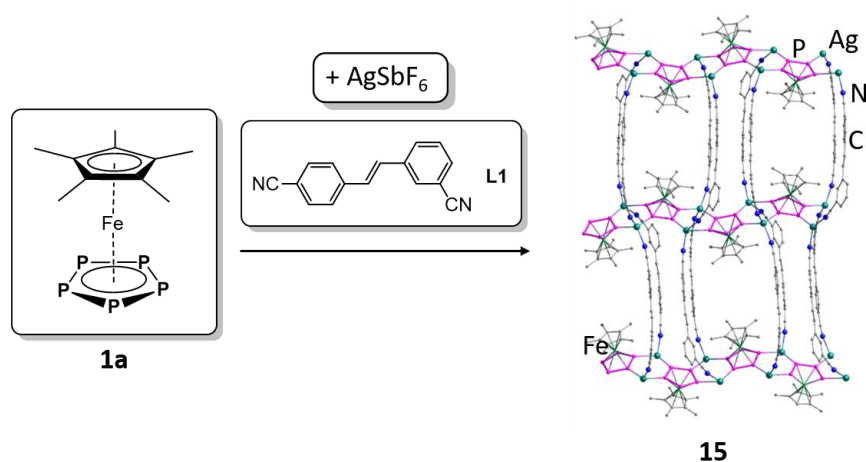


**Scheme 5:** Spherical and Half-shell assemblies based on **1b**,  $\text{AgSbF}_6$  and  $\text{CH}_3\text{CN}$  or  $\text{NC}(\text{C}_6\text{H}_4)\text{Cl}$ .



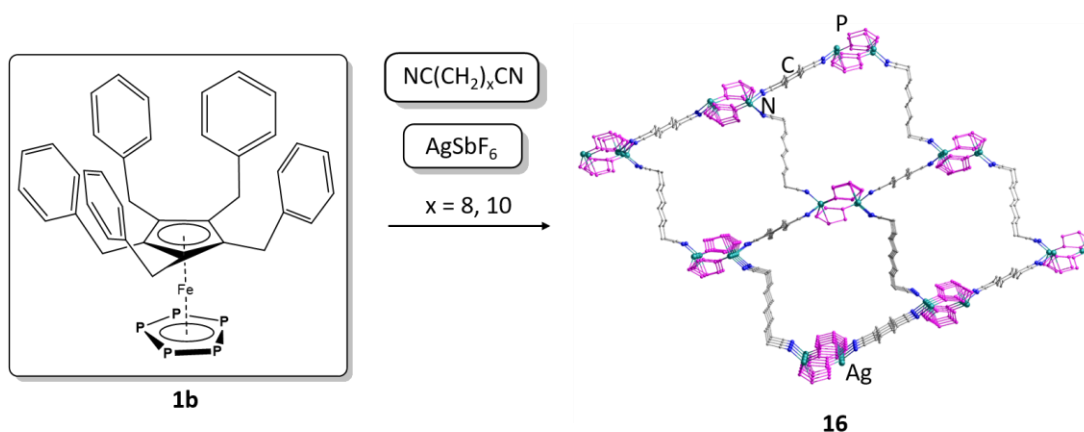
### Three-component self-assembly of $[\text{Cp}^{\text{R}}\text{Fe}(\eta^5\text{-P}_5)]$ ( $\text{Cp}^{\text{R}} = \text{Cp}^*, \text{Cp}^{\text{Bn}}$ ), coinage metal salts and dinitriles

The formation of **14** (Scheme 5) clearly shows that a three-component self-assembly of **1** and  $\text{AgSbF}_6$  can lead to spherical supramolecular aggregates with larger nitriles acting as saturating ligands for the scaffold building Ag atoms. One can therefore imagine the use of a bidentate nitrile leading to interconnected spheres. With this in mind, the choice for the linking unit first fell on a semi-rigid ditopic benzonitrile  $\text{NC}(\text{C}_6\text{H}_4)(\text{C}_2\text{H}_2)(\text{C}_6\text{H}_4)\text{CN}$  (L1). By combining it with **1a** and  $\text{AgSbF}_6$ , a 2D coordination polymer  $[\{\text{Cp}^*\text{Fe}(\eta^5\text{-P}_5)\}\{\text{Ag}(\text{C}_{16}\text{H}_{10}\text{N}_2)\}_2(\text{C}_7\text{H}_8)]_n[\text{SbF}_6]_{2n}$  (**15**) is formed, with 1D strands  $[\{\text{Cp}^*\text{Fe}(\eta^5\text{-P}_5)\}\text{Ag}_2]_n$  connected by the linkers (Scheme 6, cf. Chapter VIII). Each Ag atom in **15** is tetrahedrally coordinated by two units **1a** and two di-benzonitriles.



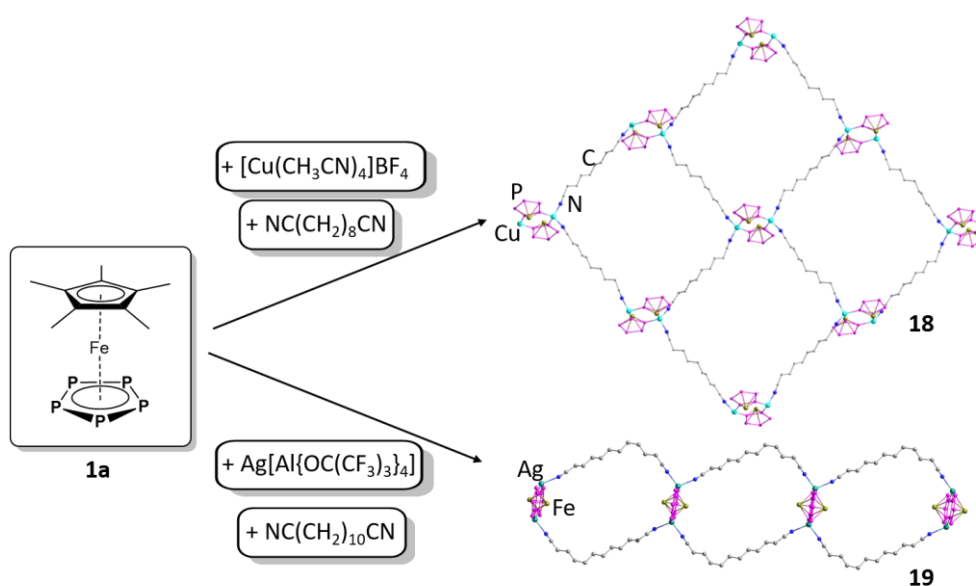
**Scheme 6:** Coordination polymer based on **1a**,  $\text{AgSbF}_6$  and L1.

As with this combination no spheres based on **1a** and Ag atoms are formed, we supposed changing the flexibility and the length of the linker to be promising for reaching the goal of connected spherical assemblies. Thus, fully flexible aliphatic dinitriles were combined with **1a** and **1b**. With this, the solubility and therefore the flexibility that is needed to arrange a spherical assembly in solution, would increase especially for combinations involving **1b**. However, when **1b** is combined with  $\text{AgSbF}_6$  and the long dinitriles  $\text{NC}(\text{CH}_2)_x\text{CN}$  ( $x = 8, 10$ ), two structurally related 3D polymers  $[\{\text{Cp}^{\text{Bn}}\text{Fe}(\eta^5\text{-P}_5)\}\{\text{Ag}(\text{NC}(\text{CH}_2)_8\text{CN})\}]_n[\text{SbF}_6]_n$  (**16**) and  $[\{\text{Cp}^{\text{Bn}}\text{Fe}(\eta^5\text{-P}_5)\}_2\{\text{Ag}_2(\text{NC}(\text{CH}_2)_{10}\text{CN})_{1.5}\}]_n[\text{SbF}_6]_{2n} \cdot (\text{CH}_2\text{Cl}_2)_{0.5n}$  (**17**) are formed (Scheme 7, cf. Chapter VI). All anions are non-coordinating and located the pores of the cationic coordination polymer.



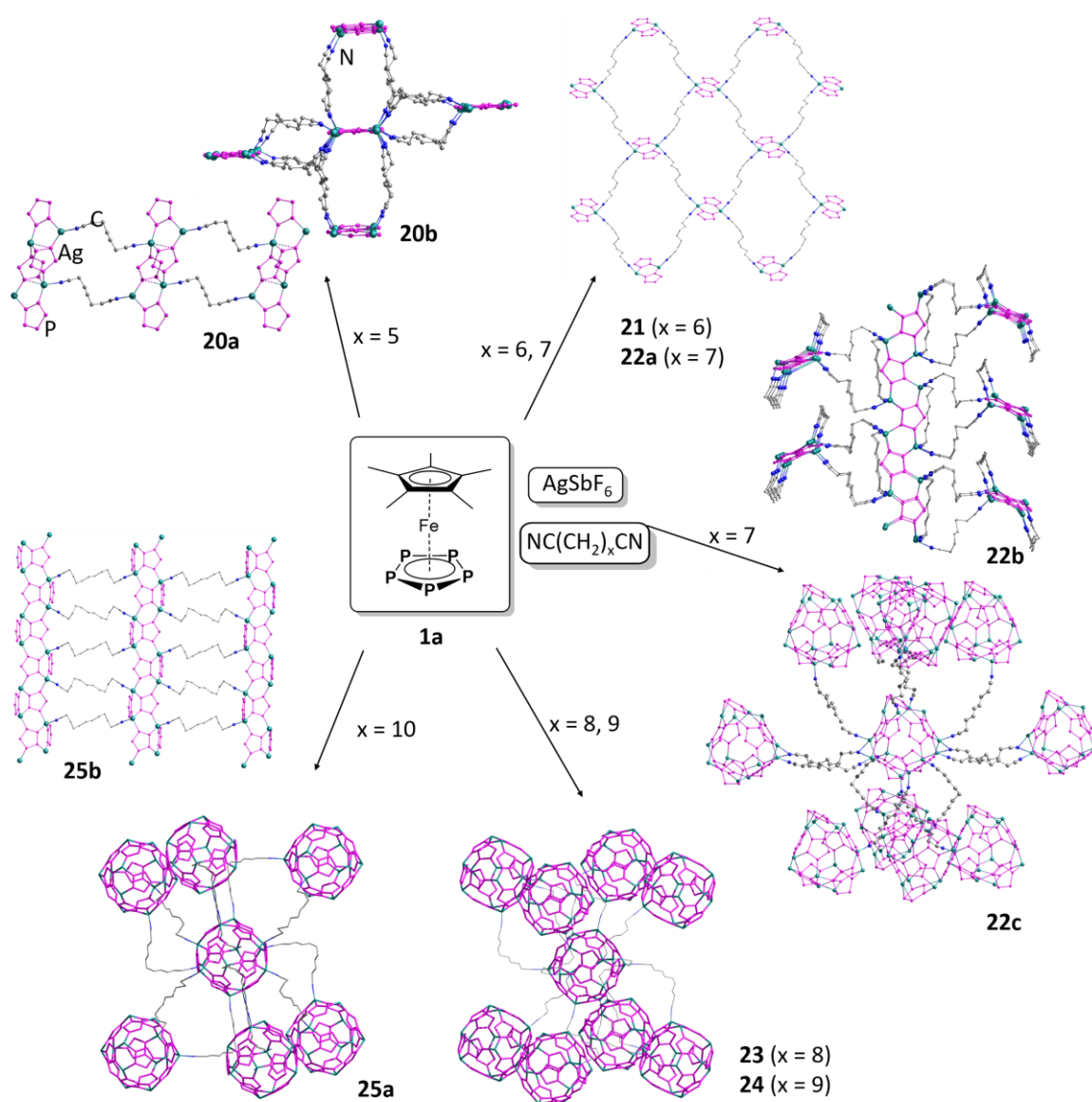
**Scheme 7:** Coordination products based on a three-component self-assembly of **1b**,  $\text{AgSbF}_6$  and flexible dinitriles. Only **16** is depicted exemplarily.

To also investigate anions of smaller and larger size than  $\text{SbF}_6^-$  in this three-component self-assembly reactions together with flexible dinitriles, in Chapter VI  $[\text{Cu}(\text{CH}_3\text{CN})_4]\text{BF}_4$  or  $\text{Ag}[\text{Al}\{\text{OC}(\text{CF}_3)_3\}_4]$  were combined with the smaller **1a** and the dinitriles with chain lengths of  $x = 8$  and 10, to yield the 2D  $[\{\text{Cp}^*\text{Fe}(\eta^5\text{-P}_5)\}\{\text{Cu}(\text{NC}(\text{CH}_2)_8\text{CN})\}]_n[\text{BF}_4]_n \cdot (\text{CH}_2\text{Cl}_2)_n$  (**18**) and the 1D ladder-like polymer  $[\{\text{Cp}^*\text{Fe}(\eta^5\text{-P}_5)\}\{\text{Ag}(\text{NC}(\text{CH}_2)_{10}\text{CN})\}]_n[\text{Al}\{\text{OC}(\text{CF}_3)_3\}_4]_n$  (**19**, Scheme 8). All anions are non-coordinating and located between the layers of the cationic coordination polymers. The absence of spherical aggregates in **16** - **19** can most likely be explained by packing effects: Whereas **1b** is assumedly too sterically demanding for a linkage *via* dinitriles with 8 or 10  $\text{CH}_2$  groups in their backbone,  $\text{BF}_4^-$  is possibly too small to fill the spaces between the potentially linked spheres adequately. Furthermore,  $[\text{Al}\{\text{OC}(\text{CF}_3)_3\}_4]^-$  seems to be too large to arrange in a higher number around a polycationic node based on **1** and Ag.



**Scheme 8:** Coordination products based on a three-component self-assembly of **1a**,  $[\text{Cu}(\text{CH}_3\text{CN})_4]\text{BF}_4$  or  $\text{Ag}[\text{Al}\{\text{OC}(\text{CF}_3)_3\}_4]$  and flexible dinitriles.

Changing to **1a** and  $\text{AgSbF}_6$ , the system becomes astonishingly versatile. Diverse coordination polymers are obtained in *Chapter V* and *VI*, applying dinitriles with  $x = 5 - 10$ . Special highlights are the cases of  $x = 7 - 10$ , which indeed enable the formation of an unprecedented novel class of compounds: Supramolecular spherical assemblies interlinked and acting as nodes in a 3D frameworks. Applying the shorter dinitriles with  $x = 5$  and  $6$ , the 1D ladder-like  $[\{\text{Cp}^*\text{Fe}(\eta^5\text{-P}_5)\}_4\{\text{Ag}_4(\text{NC}(\text{CH}_2)_5\text{CN})_2\}]_n[\text{SbF}_6]_{4n}$  (**20a**), 3D  $[\{\text{Cp}^*\text{Fe}(\eta^5\text{-P}_5)\}\{\text{Ag}(\text{NC}(\text{CH}_2)_5\text{CN})\}_2]_n[\text{SbF}_6]_n$  (**20b**) and 2D coordination polymers  $[\{\text{Cp}^*\text{Fe}(\eta^5\text{-P}_5)\}\{\text{Ag}(\text{NC}(\text{CH}_2)_6\text{CN})\}]_n[\text{SbF}_6]_n$  (**21**) are formed (*Scheme 9*). Involving a linker length of  $x = 7$ , the system becomes flexible enough to either form 2D  $[\{\text{Cp}^*\text{Fe}(\eta^5\text{-P}_5)\}\{\text{Ag}(\text{NC}(\text{CH}_2)_7\text{CN})\}]_n[\text{SbF}_6]_n$  (**22a**) or 3D polymeric frameworks  $[\{\text{Cp}^*\text{Fe}(\eta^5\text{-P}_5)\}\{\text{Ag}_2(\text{NC}(\text{CH}_2)_7\text{CN})\}]_n[\text{SbF}_6]_{2n}$  (**22b**), as well as 3D connected spherical host assemblies  $[\text{SbF}_6]@[\{\text{Cp}^*\text{Fe}(\eta^5\text{-P}_5)\}_9\{\text{Ag}_{11}(\text{NC}(\text{CH}_2)_7\text{CN})_6\}]_n[\text{SbF}_6]_{10n}$  (**22c**, *Scheme 9*). The nodes of **22c** consist of novel polycationic spherical scaffolds, which each incorporate one  $\text{SbF}_6^-$  anion and are connected towards each other by the dinitrile linkers. The *cyclo*- $\text{P}_5$  ligands show a capped tetragonal antiprismatic arrangement. With the longer dinitriles offering  $x = 8 - 10$ , a 2D polymeric  $[\{\text{Cp}^*\text{Fe}(\eta^5\text{-P}_5)\}_2\text{Ag}_2]_n[\text{SbF}_6]_{2n}$  (**25b**) and further spherical scaffolds, which are interconnected to 3D networks crystallize:  $[\{\text{Cp}^*\text{Fe}(\eta^5\text{-P}_5)\}]@[\{\text{Cp}^*\text{Fe}(\eta^{5:1:1:1:1}\text{-P}_5)\}_{12}\{\text{Ag}_{12}(\text{NC}(\text{CH}_2)_x\text{CN})_6\}]_n[\text{SbF}_6]_{12n}$  (with  $x = 8$  (**23**),  $9$  (**24**),  $10$  (**25a**), *Scheme 9*). Compounds **23 – 25a** consist of icosahedral shaped scaffolds as nodes, based on twelve ligands **1a** and twelve Ag atoms and interconnecting nitriles. Interestingly, the architecture of the nodes is similar to the discrete 80-vertex analogue **3a**, which also incorporates one complex **1a**. Due to **23** and **24** not only showing an analogous architecture of the nodes, but also the same net topology, unit cell constants and space group, they are isotypic structures. However, the network of **25a** reveals a different connection pattern. Unexpectedly, all investigated 3D networks of connected spheres in **22c** and **23 – 25a** show an arrangement of the spherical nodes derived from cubic packings: **bcu-x** for **22c** and **fcc** for **23 – 25a**.

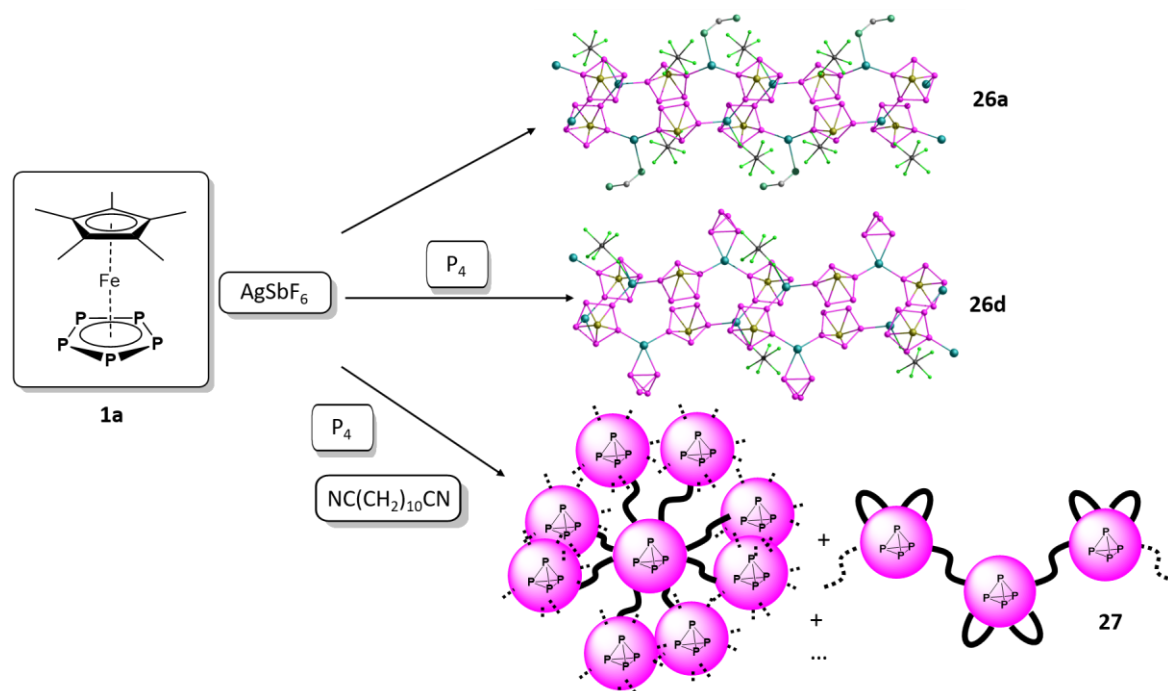


**Scheme 9:** Coordination products based on a three-component self-assembly of **1a**,  $\text{AgSbF}_6$  and flexible dinitriles.

### Four-component self-assembly of $[\text{Cp}^R\text{Fe}(\eta^5\text{-P}_5)]$ ( $\text{Cp}^R = \text{Cp}^*, \text{Cp}^{\text{Bn}}$ ), $\text{AgSbF}_6$ , flexible dinitriles $\text{NC}(\text{CH}_2)_x\text{CN}$ and white phosphorus

The above mentioned results show a remarkable versatility of the shape of the scaffold: capped tetragonal antiprismatic  $[\{\text{Cp}^*\text{Fe}(\eta^5\text{-P}_5)\}_9(\text{Ag}_{11})]$  **22c** and icosahedral symmetric  $[\{\text{Cp}^*\text{Fe}(\eta^{5:1:1:1}\text{-P}_5)\}_{12}(\text{Ag}_{12})]$  **23-25a** were observed, all acting as hosts either for one  $\text{SbF}_6^-$  counter-anion, or for the complex **1a** itself. Together with the excellent host-guest properties of the related Cu-based spherical supramolecules, like the 80-vertex  $[\{\text{Cp}^*\text{Fe}(\eta^5\text{-P}_5)\}_{12}(\text{CuX})_{20}]$  or the 90-vertex  $[\{\text{Cp}^*\text{Fe}(\eta^5\text{-P}_5)\}_{12}(\text{CuCl})_{25}(\text{CH}_3\text{CN})_{10}]$ , these findings encouraged to examine the possibility to incorporate small guest molecules in interconnected spherical assemblies. For this purpose, **1a** was reacted in a four component reaction together with  $\text{AgSbF}_6$ ,  $\text{NC}(\text{CH}_2)_{10}\text{CN}$  and white phosphorus  $\text{P}_4$  to yield a 1D coordination polymer  $[\{\text{Cp}^*\text{Fe}(\eta^5\text{-P}_5)\}_2\{\text{Ag}_2(\eta^2\text{-P}_4)_m(\text{CH}_2\text{Cl}_2)_{1-m}\}]_n[\text{SbF}_6]_{2n}$  (**26**;  $m = 0$  (**26a**), 0.67 (**26b**), 0.75 (**26c**), 1 (**26d**)) and astonishingly different spherical assemblies, incorporating each one molecule of  $\text{P}_4$  and interlinked *via* the flexible dinitriles  $[\text{P}_4@[\{\text{Cp}^*\text{Fe}(\eta^5\text{-P}_5)\}_9\{\text{Ag}_x(\text{NC}(\text{CH}_2)_{10}\text{CN})_y\}]]_n[\text{SbF}_6]_{xn}$  (**27a**:  $x = 9$ ,  $y = 4$ , **27b**:  $x = 9$ ,  $y = 4.5$ , **27c**:  $x = 10$ ,  $y = 4.5$ ). (**27**, Scheme 10, cf. Chapter VIII). The coordination polymer **26** can be obtained selectively by using a three-component reaction of **1a**,  $\text{AgSbF}_6$  and  $\text{P}_4$  and without applying the dinitrile. Furthermore, due to the competition of  $\text{CH}_2\text{Cl}_2$  and  $\text{P}_4$  over the free coordination site on the  $\text{Ag}^+$  atoms, the content of coordinating  $\text{P}_4$  can be regulated by either reducing its content to 0 equivalents (**26a**), applying a 1 : 1 : 2 stoichiometric ratio (**26c**, **1a** :  $\text{AgSbF}_6$  :  $\text{P}_4$ ) or avoiding  $\text{CH}_2\text{Cl}_2$  completely by using a non-coordinating solvent as *o*-dichlorobenzene (**26d**). Raman spectroscopy, NMR studies as well as theoretical calculations underlined the intact tetrahedral structure of the coordinating  $\text{P}_4$ . In contrast to this, **27** constitutes a rare example of a four-component self-assembly product. Three different crystalline phases were characterized, containing at least four similar host scaffolds, each consisting of 9 units **1a** and either 8, 9 or 10 Ag atoms. Though not all dinitrile linkers could be absolutely localized, the obtained data give evidences for a 1D, one 2D and one 3D network of linked host-guest assemblies. Furthermore, some dinitriles are assumed to act not as intermolecular connection but as intramolecular linker between two Ag atoms of the same supramolecular scaffold. The incorporation of  $\text{P}_4$  was furthermore verified by  $^{31}\{\text{^1H}\}$  NMR MAS measurements, which show a down-field shift for white phosphorus in comparison to free  $\text{P}_4$ . Additionally,  $\text{P}_4$  can be released by degradation of the framework upon addition of pyridine or stirring for longer times in solvents like  $\text{CH}_2\text{Cl}_2$  or toluene. Thus, subsequent reactions succeed, like

the reaction of  $P_4$  in suspended **27** with  $[Cp^{Bn}Fe(CO)_2]_2$  to yield  $[Cp^{Bn}Fe(\eta^5-P_5)]$ , which can be detected in the  $^{31}P$  NMR spectra of the reaction solution.



**Scheme 10:** Coordination products based on a three- or four-component self-assembly of **1a**,  $AgSbF_6$  and flexible dinitriles.

The results presented herein show the versatility of the self-assembly system of **1**,  $AgSbF_6$  and flexible dinitriles. By a sensible choice of starting materials the three- and even a four-component self-assembly succeeded to yield linked spherical host aggregates. The diversity of the obtained compounds promises the way for many further variations of the building blocks: varying the *cyclo*- $P_n$  complex to others, which are known to form spherical aggregates, as the  $[Cp''Ta(CO)_2P_4]$ , the nature of the linking units from fully flexible to semi-flexible or the size and the nature of the guest molecule.

## 10. Appendices

### 10.1 Alphabetic List of Abbreviations

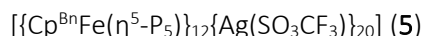
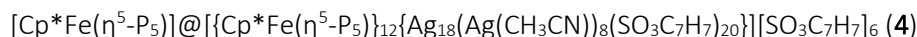
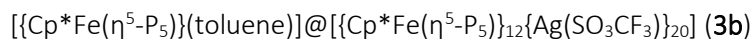
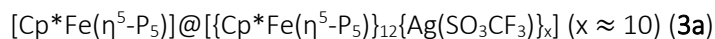
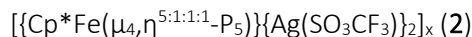
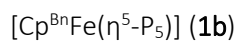
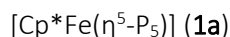
∠	angle
∅	diameter
Å	Angström, 1 Å = 1·10 <sup>-10</sup> m
°C	degree Celsius
1D	one-dimensional
2D	two-dimensional
3D	three-dimensional
<b>bcc</b>	body centered cubic
Bn	benzyl
br (NMR)	broad
<i>n</i> Bu	<i>n</i> -butyl
<i>t</i> Bu	<i>tert</i> -butyl
Cp	cyclopentadienyl, C <sub>5</sub> H <sub>5</sub>
Cp''	1,3-di- <i>tert</i> -butylcyclopentadienyl, C <sub>5</sub> H <sub>3</sub> tBu <sub>2</sub>
Cp'''	1,2,4-tris- <i>tert</i> -butylcyclopentadienyl, C <sub>5</sub> H <sub>2</sub> tBu <sub>3</sub>
Cp*	pentamethylcyclopentadienyl, C <sub>5</sub> (CH <sub>3</sub> ) <sub>5</sub>
Cp <sup>BIG</sup>	pentakis-4- <i>n</i> butylphenylcyclopentadienyl, C <sub>5</sub> ( <i>n</i> BuC <sub>6</sub> H <sub>4</sub> ) <sub>5</sub>
Cp <sup>Bn</sup>	pentabenzylcyclopentadienyl, C <sub>5</sub> (CH <sub>2</sub> C <sub>6</sub> H <sub>5</sub> )
Cp <sup>Et</sup>	tetramethyl-ethylcyclopentadienyl, C <sub>5</sub> (CH <sub>3</sub> ) <sub>4</sub> Et
Cp <sup>R</sup>	substituted cyclopentadienyl ligand
d	day(s) or distance
d (NMR)	dublet
δ	chemical shift
DFT	density functional theory
DIB	1,3-diisopropylbenzene
DOSY	diffusion ordered spectroscopy
ESI MS	electron spray ionization mass spectrometry
<b>fcc</b>	face centered cubic
h	hour(s)
Hz	Hertz
IR	infrared
J (NMR)	coupling constant
m (NMR)	multiplet
<i>m</i> -CH (NMR)	meta-CH group
m (IR)	medium
M	metal
<i>m/z</i>	mass to charge ratio
MAS	magic angle spinning
min	minutes or minimum
max	maximum
MOF	Metal-Organic Framework
MOP	Metal-Organic Polyhedron
NMR	nuclear magnetic resonance

$\nu$	frequency
$\tilde{\nu}$	wavenumber
$\omega_{1/2}$	half width
<i>o</i> -CH (NMR)	ortho-CH group
<i>p</i> -CH (NMR)	para-CH group
<b>pcu</b>	primitive cubic
POM	polyoxometallate
ppm	parts per million
q (NMR)	quartet
R	organic substituent
r.t.	room temperature
s (IR)	strong
s (NMR)	singlet
sept (NMR)	septet
t (NMR)	triplet
TEM	transmission electron microscopy
thf	tetrahydrofurane
vdW	van der Waals
VT	various temperatures
vs (IR)	very strong
vw (IR)	very weak
w (IR)	weak
X	any halide (Cl, Br, I)

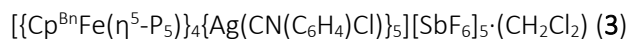
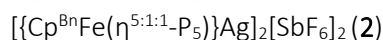
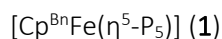


## 10.2 List of Numbered Compounds

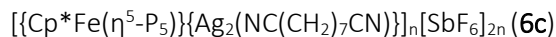
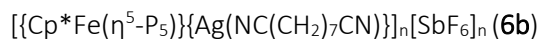
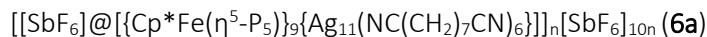
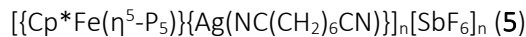
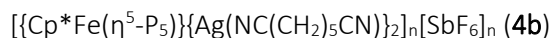
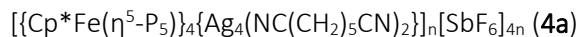
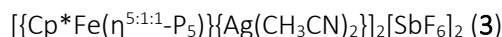
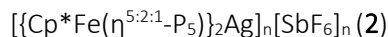
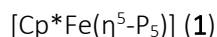
### Chapter III



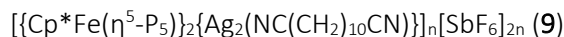
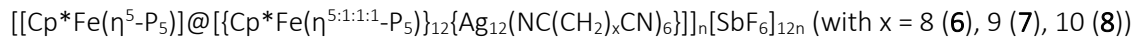
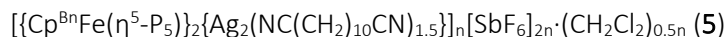
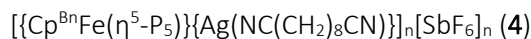
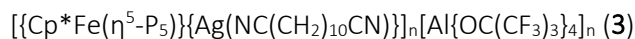
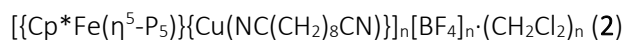
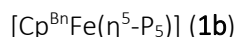
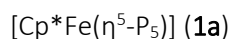
### Chapter IV



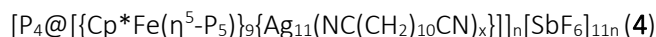
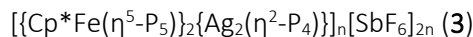
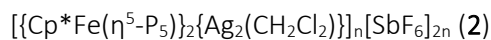
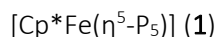
### Chapter V



### Chapter VI



### Chapter VII



## Chapter VIII – Thesis Treasury

[Cp\*Fe( $\eta^5$ -P<sub>5</sub>)] (1a)[Cp<sup>Bn</sup>Fe( $\eta^5$ -P<sub>5</sub>)] (1b)[{Cp\*Fe( $\eta^5$ -P<sub>5</sub>)}{Ag(C<sub>16</sub>H<sub>10</sub>N<sub>2</sub>)}<sub>2</sub>(C<sub>7</sub>H<sub>7</sub>)]<sub>n</sub>[SbF<sub>6</sub>]<sub>2n</sub> (2)[SbF<sub>6</sub>]@[{Cp<sup>Bn</sup>Fe( $\eta^5$ -P<sub>5</sub>)}<sub>6</sub>(AgCH<sub>3</sub>CN)<sub>14</sub>][SbF<sub>6</sub>]<sub>13</sub> (3)[{Cp<sup>Bn</sup>Fe( $\eta^5$ -P<sub>5</sub>)}<sub>2</sub>{Ag(Al(O(CF<sub>3</sub>)<sub>3</sub>)<sub>4</sub>)<sub>3</sub>·(CH<sub>2</sub>Cl<sub>2</sub>)} (4a)[{Cp<sup>Bn</sup>Fe( $\eta^5$ -P<sub>5</sub>)}<sub>2</sub>{Ag(Al(O(CF<sub>3</sub>)<sub>3</sub>)<sub>4</sub>)<sub>4</sub>·(CH<sub>2</sub>Cl<sub>2</sub>)<sub>2</sub>} (4b)[{Cp<sup>Bn</sup>Fe( $\eta^5$ -P<sub>5</sub>)}<sub>2</sub>{Ag(AlF(OC<sub>12</sub>F<sub>15</sub>)<sub>3</sub>)<sub>4</sub>} (5)[{Cp<sup>Bn</sup>Fe( $\eta^5$ -P<sub>5</sub>)}<sub>12</sub>(AgSO<sub>3</sub>C<sub>7</sub>H<sub>7</sub>)<sub>20</sub>] (6)

## Chapter IX – Conclusion

[Cp\*Fe( $\eta^5$ -P<sub>5</sub>)] (1a)[Cp<sup>Bn</sup>Fe( $\eta^5$ -P<sub>5</sub>)] (1b)[{Cp\*Fe( $\mu_4$ , $\eta^{5:1:1:1}$ -P<sub>5</sub>)}{Ag(SO<sub>3</sub>CF<sub>3</sub>)}<sub>2</sub>]<sub>x</sub> (2)[Cp\*Fe( $\eta^5$ -P<sub>5</sub>)]@[{Cp\*Fe( $\eta^5$ -P<sub>5</sub>)}<sub>12</sub>{Ag(SO<sub>3</sub>CF<sub>3</sub>)}<sub>10</sub>] (3a)[{Cp\*Fe( $\eta^5$ -P<sub>5</sub>)}(toluene)]@[{Cp\*Fe( $\eta^5$ -P<sub>5</sub>)}<sub>12</sub>{Ag(SO<sub>3</sub>CF<sub>3</sub>)}<sub>20</sub>] (3b)[Cp\*Fe( $\eta^5$ -P<sub>5</sub>)]@[{Cp\*Fe( $\eta^5$ -P<sub>5</sub>)}<sub>12</sub>{Ag<sub>18</sub>(Ag(CH<sub>3</sub>CN))<sub>8</sub>(SO<sub>3</sub>C<sub>7</sub>H<sub>7</sub>)<sub>20</sub>}] [SO<sub>3</sub>C<sub>7</sub>H<sub>7</sub>]<sub>6</sub> (4)[{Cp<sup>Bn</sup>Fe( $\eta^5$ -P<sub>5</sub>)}<sub>12</sub>{Ag(SO<sub>3</sub>CF<sub>3</sub>)}<sub>20</sub>] (5)[{Cp<sup>Bn</sup>Fe( $\eta^5$ -P<sub>5</sub>)}<sub>12</sub>{Ag(SO<sub>3</sub>C<sub>7</sub>H<sub>7</sub>)<sub>20</sub>] (6)[{Cp\*Fe( $\eta^{5:2:1}$ -P<sub>5</sub>)}<sub>2</sub>Ag]<sub>n</sub>[SbF<sub>6</sub>]<sub>n</sub> (7)[{Cp\*Fe( $\eta^{5:1:1}$ -P<sub>5</sub>)}{Ag(CH<sub>3</sub>CN)<sub>2</sub>}]<sub>2</sub>[SbF<sub>6</sub>]<sub>2</sub> (8)[{Cp<sup>Bn</sup>Fe( $\eta^{5:1:1}$ -P<sub>5</sub>)}Ag]<sub>2</sub>[SbF<sub>6</sub>]<sub>2</sub> (9)[{Cp<sup>Bn</sup>Fe( $\eta^5$ -P<sub>5</sub>)}<sub>2</sub>Ag<sub>3</sub>][Al{OC(CF<sub>3</sub>)<sub>3</sub>}<sub>4</sub>]<sub>3</sub>·(CH<sub>2</sub>Cl<sub>2</sub>) (10a)[{Cp<sup>Bn</sup>Fe( $\eta^5$ -P<sub>5</sub>)}<sub>2</sub>Ag<sub>4</sub>][Al{OC(CF<sub>3</sub>)<sub>3</sub>}<sub>4</sub>]<sub>4</sub>·(CH<sub>2</sub>Cl<sub>2</sub>)<sub>2</sub> (10b)[{Cp<sup>Bn</sup>Fe( $\eta^5$ -P<sub>5</sub>)}<sub>2</sub>Ag<sub>4</sub>][AlF(O<sub>12</sub>F<sub>15</sub>)<sub>3</sub>]<sub>4</sub> (11)[SbF<sub>6</sub>]@[{Cp<sup>Bn</sup>Fe( $\eta^5$ -P<sub>5</sub>)}<sub>6</sub>(AgCH<sub>3</sub>CN)<sub>14</sub>][SbF<sub>6</sub>]<sub>13</sub> (12)[{Cp<sup>Bn</sup>Fe( $\eta^5$ -P<sub>5</sub>)}<sub>4</sub>{Ag(CN(C<sub>6</sub>H<sub>4</sub>)Cl)}<sub>5</sub>][SbF<sub>6</sub>]<sub>5</sub>·(CH<sub>2</sub>Cl<sub>2</sub>) (13)[SbF<sub>6</sub>]@[{Cp<sup>Bn</sup>Fe( $\eta^5$ -P<sub>5</sub>)}<sub>6</sub>{Ag(CN(C<sub>6</sub>H<sub>4</sub>)Cl)}<sub>10</sub>][SbF<sub>6</sub>]<sub>9</sub> (14)[{Cp\*Fe( $\eta^5$ -P<sub>5</sub>)}{Ag(C<sub>16</sub>H<sub>10</sub>N<sub>2</sub>)}<sub>2</sub>(C<sub>7</sub>H<sub>7</sub>)]<sub>n</sub>[SbF<sub>6</sub>]<sub>2n</sub> (15)[{Cp<sup>Bn</sup>Fe( $\eta^5$ -P<sub>5</sub>)}{Ag(NC(CH<sub>2</sub>)<sub>8</sub>CN)}]<sub>n</sub>[SbF<sub>6</sub>]<sub>n</sub> (16)[{Cp<sup>Bn</sup>Fe( $\eta^5$ -P<sub>5</sub>)}<sub>2</sub>{Ag<sub>2</sub>(NC(CH<sub>2</sub>)<sub>10</sub>CN)<sub>1.5</sub>}]<sub>n</sub>[SbF<sub>6</sub>]<sub>2n</sub>·(CH<sub>2</sub>Cl<sub>2</sub>)<sub>0.5n</sub> (17)[{Cp\*Fe( $\eta^5$ -P<sub>5</sub>)}{Cu(NC(CH<sub>2</sub>)<sub>8</sub>CN)}]<sub>n</sub>[BF<sub>4</sub>]<sub>n</sub>·(CH<sub>2</sub>Cl<sub>2</sub>)<sub>n</sub> (18)[{Cp\*Fe( $\eta^5$ -P<sub>5</sub>)}{Ag(NC(CH<sub>2</sub>)<sub>10</sub>CN)}]<sub>n</sub>[Al{OC(CF<sub>3</sub>)<sub>3</sub>}<sub>4</sub>]<sub>n</sub> (19)[{Cp\*Fe( $\eta^5$ -P<sub>5</sub>)}<sub>4</sub>{Ag<sub>4</sub>(NC(CH<sub>2</sub>)<sub>5</sub>CN)<sub>2</sub>}]<sub>n</sub>[SbF<sub>6</sub>]<sub>4n</sub> (20a)[{Cp\*Fe( $\eta^5$ -P<sub>5</sub>)}{Ag(NC(CH<sub>2</sub>)<sub>5</sub>CN)}<sub>2</sub>]<sub>n</sub>[SbF<sub>6</sub>]<sub>n</sub> (20b)[{Cp\*Fe( $\eta^5$ -P<sub>5</sub>)}{Ag(NC(CH<sub>2</sub>)<sub>6</sub>CN)}]<sub>n</sub>[SbF<sub>6</sub>]<sub>n</sub> (21)[{Cp\*Fe( $\eta^5$ -P<sub>5</sub>)}{Ag(NC(CH<sub>2</sub>)<sub>7</sub>CN)}]<sub>n</sub>[SbF<sub>6</sub>]<sub>n</sub> (22a)[{Cp\*Fe( $\eta^5$ -P<sub>5</sub>)}{Ag<sub>2</sub>(NC(CH<sub>2</sub>)<sub>7</sub>CN)}]<sub>n</sub>[SbF<sub>6</sub>]<sub>2n</sub> (22b)[SbF<sub>6</sub>]@[{Cp\*Fe( $\eta^5$ -P<sub>5</sub>)}<sub>9</sub>{Ag<sub>11</sub>(NC(CH<sub>2</sub>)<sub>7</sub>CN)<sub>6</sub>}]<sub>n</sub>[SbF<sub>6</sub>]<sub>10n</sub> (22c)[[Cp\*Fe( $\eta^5$ -P<sub>5</sub>)]@[{Cp\*Fe( $\eta^{5:1:1:1}$ -P<sub>5</sub>)}<sub>12</sub>{Ag<sub>12</sub>(NC(CH<sub>2</sub>)<sub>x</sub>CN)<sub>6</sub>}]<sub>n</sub>[SbF<sub>6</sub>]<sub>12n</sub> (with x = 8 (23), 9 (24), 10 (25a))[{Cp\*Fe( $\eta^5$ -P<sub>5</sub>)}<sub>2</sub>{Ag<sub>2</sub>(NC(CH<sub>2</sub>)<sub>10</sub>CN)}]<sub>n</sub>[SbF<sub>6</sub>]<sub>2n</sub> (25b)[{Cp\*Fe( $\eta^5$ -P<sub>5</sub>)}<sub>2</sub>{Ag<sub>2</sub>( $\eta^2$ -P<sub>4</sub>)<sub>m</sub>(CH<sub>2</sub>Cl<sub>2</sub>)<sub>1-m</sub>}]<sub>n</sub>[SbF<sub>6</sub>]<sub>2n</sub> (26; m = 0 (26a), 0.67 (26b), 0.75 (26c), 1 (26d))[P<sub>4</sub>@[{Cp\*Fe( $\eta^5$ -P<sub>5</sub>)}<sub>9</sub>{Ag<sub>x</sub>(NC(CH<sub>2</sub>)<sub>10</sub>CN)<sub>y</sub>}]<sub>n</sub>[SbF<sub>6</sub>]<sub>xn</sub> (27a: x = 9, y = 4, b: x = 9, y = 4.5, c: x = 10 y = 4.5)

### 10.3 Acknowledgements

During four years of intense work on the topics of this thesis, many challenges, difficulties and chances, failures and successes crossed my path and had to be discussed, solved and of course, celebrated. Luckily, amazing colleagues, co-workers, friends and family were sharing this period and accompanying the way. Therefore, I want to express my gratitude to:

- Prof. Dr. Manfred Scheer, for giving me the opportunity to work on such an interesting and versatile topic, providing excellent working conditions, but also for the chances to attend interesting conferences and giving me plenty of rope in research and finding an own scientific way.
- Dr. Gábor Balázs for helpful and encouraging discussions and advices and lending an ear on every possible need.
- Dr. Eugenia Peresyphkina and Dr. Sc. Alexander Virovets for steady help and advice, not only on crystallography, and for untiring proof-reading.
- Dr. Christophe Lescop for the chance to gather precious experiences in Rennes.
- the collaboration partners, enabling diversified analytical examinations: Prof. Dr. Werner Kremer ( $^{31}\text{P}$  MAS NMR), Florian Hastreiter (DOSY NMR), and Jan Hilgert (transmission electron microscopy).
- the staff of the central analytical services, glass-blowing, and electronic and mechanic facilities of the University Regensburg.
- The incredible colleagues of the Scheer group for the Eispausen, Stammtischabende, Hirschegg hiking tours, and overall the great and unforgettable time:  
First of all, my Mädels-Labor partners Claudi, Dani, Helena and Rebecca, but also: Andi, Andrea, Anna, Bin, Claudia, Eric, Eva, Fabi, Felix S., Felix L., Jana, Jens, Julian, Christian G., Christian M., Lena, Liese, Luis, Maria, Martin B., Martin F., Martin W., Martina, Matthias A., Matthias H., Mehdi, Michi S., Michi W., Moni, Moritz, Olli, Petra, Reini, Rudi, Schotti, Sebi, Stephan, Susanne, Tobi, Vroni.
- my friends, for suffering and laughing together and knowing each other for more than (or almost) ten years: Kathi, Nadja, Anja, Annette, Anna, Babi, Marlene, Vroni K., and Vroni P.
- my family, for total support and encouragement under any circumstances.
- Basti, for all the loving and laughing and being thus a wonderful perfect match!